**UNIVERSITA' VITA-SALUTE SAN RAFFAELE**

**CORSO DI DOTTORATO DI RICERCA INTERNAZIONALE IN MEDICINA MOLECOLARE**

**CURRICULUM IN**
**Neuroscienze e Neurologia Sperimentale**

# Axonal mRNA dysregulation in a cellular model of TDP-43 proteinopathy: a functional and -omic analysis

DoS: Prof. Giacomo Consalez

Second Supervisor: Prof. Giampietro Schiavo

Tesi di DOTTORATO di RICERCA di Alessandra Pisciottani

matr. 013918

Ciclo di dottorato XXXIV

SSD BIO/13, BIO/16, MED/26

Anno Accademico 2020/2021

**CONSULTAZIONE TESI DI DOTTORATO DI RICERCA**

| | |
|---|---|
| La sottoscritta | Alessandra Pisciottani |
| Matricola / *registration number* | 013918 |
| nata a/ *born at* | Castellana Grotte (BA) |
| il/*on* | 01/01/1994 |

autrice della tesi di Dottorato di ricerca dal titolo / *author of the PhD Thesis titled*

Axonal mRNA dysregulation in a cellular model of TDP-43 proteinopathy: a functional and -omic analysis

- AUTORIZZA la Consultazione della tesi / AUTHORIZES *the public release of the thesis*

X NON AUTORIZZA la Consultazione della tesi per 12 mesi /DOES NOT AUTHORIZE *the public release of the thesis for 12 months*

a partire dalla data di conseguimento del titolo e precisamente / *from the PhD defence date, specifically*

Dal / *from* 08/04/2022 Al / *to* 07/04/2023 Poiché /*because*:

□ l'intera ricerca o parti di essa sono potenzialmente soggette a brevettabilità/ *The whole project or part of it might be subject to patentability;*

X ci sono parti di tesi che sono già state sottoposte a un editore o sono in attesa di pubblicazione/ *Parts of the thesis have been or are being submitted to a publisher or are in press;*

□ la tesi è finanziata da enti esterni che vantano dei diritti su di esse e sulla loro pubblicazione/ *the thesis project is financed by external bodies that have rights over it and on its publication.*



Data /Date 15/03/2022 Firma /Signature Alessandra Pisciottani

## DECLARATION

This thesis has been composed by myself and has not been used in any previous application for a degree. Throughout the text I use both 'I' and 'We' interchangeably.

All the results presented here were obtained by myself, except for:

1) *Polysome profiling, RNA-sequencing and initial bioinformatic analysis (Results, chapter 5.2, figure 5.20-22), and RT-qPCR (Results, chapter 5.2, figure 5.31, 5.34) were obtained by Dr. Gabriella Viero , Institute of Biophysics, National Council Research, Povo, Trento, Italy*
2) *Mouse motor tests (Results, chapter 5.1, figure 5.15) were performed by the Mouse Behavior Facility of San Raffaele Scientific Institute, Milan, Italy.*
3) *Puromycylation assay (Results, chapter 5.2, figure 5.24) was performed in collaboration with Dr. J-M. Cioni, Division of Neuroscience, San Raffaele Scientific Institute, Milan, Italy.*
4) *Oxidative stress analysis (Results, chapter 5.2, figure 5.26), FM1-43 assay (Results, chapter 5.2, figure 5.28) and calcium imaging studies (Results, chapter 5.3, figure 5.39) were obtained in collaboration with Prof. F. Codazzi, Division of Neuroscience, San Raffaele Scientific Institute, Milan, Italy.*
5) *Electrophysiological analysis (Results, chapter 5.3, figure 5.37-38; 5.40-41), was performed with Dr. S.Taverna, Division of Neuroscience, San Raffaele Scientific Institute, Milan, Italy.*
6) *Figure 3.2 (Introduction, chapter 3.1) is reused from Heimer, 1994 and Figure 5.35 (Results, chapter 5.2) from Kandel et al., 2021 according to Fair use principle of Italian legislation (legislative decree n. 68 09/04/2003).*

All sources of information are acknowledged by means of bibliographic references.

## ACKNOWLEDGEMENTS

I would like to thank Dr Jean-Michel Cioni, Division of Neuroscience, San Raffaele Scientific Institute for critical discussion of my data, and for generously sharing reagents and equipment. I am grateful to Dr. Elisa Savino for training me in the use of the Nikon Spinning Disk inverted microscope and for her precious help in image analysis.

Prof. Franca Codazzi, Dr. Stefano Taverna, Dr. Laura Croci and all members of the Consalez lab are gratefully acknowledged for helpful discussion of the results reported in this thesis.

I would like to thank Dr. Gabriella Viero and the members of her lab, Fabio Lauria and Federica Maniscalco, for their precious collaboration.

My deepest gratitude goes to the Fronzaroli family for their generous donation to Fondazione Centro San Raffaele of my PhD bursary.

## ABSTRACT

Amyotrophic lateral sclerosis (ALS) is an incurable neurodegenerative disease that mainly affects upper and lower motor neurons. Only 10% of cases are familial, while the majority are sporadic. TDP-43, encoded by the *TARDBP* gene, is an RNA-binding protein that plays essential regulatory roles in RNA metabolism, from transcription and splicing to transport and translation. While *TARDBP* mutations are only found in 2-5% of ALS cases, 97% of patients, both sporadic and familial, show nuclear TDP-43 depletion as well as its cytoplasmic accumulation and aggregate formation, known as TDP-43 proteinopathy. Several lines of evidence suggest that ALS is a distal axonopathy in which axonal degeneration precedes motor neuron death. Since axonal translation is essential for the development, maintenance and function of this subcellular compartment, we hypothesized that altered axonal mRNA levels resulting from TDP-43 deregulation may severely affect axonal biology in motor neurons, a cell type whose axon accounts for over 99% of the total cellular volume. In this project we characterized highly enriched cultures of mouse cortical motor neurons overexpressing wt TDP-43 (wtTDP) or carrying a familial ALS mutation, A315T (mutTDP). Both models exhibit cytoplasmic accumulation of TDP-43-positive aggregates, accompanied by reduced axonal mRNA translation, increased oxidative stress, impaired exocytosis and changes in $Ca^{2+}$ homeostasis. Thanks to microfluidic chambers, wt- and mutTDP axons and cell bodies were physically separated, permitting the unbiased RNA-seq analysis of both subcellular territories. Through a miniaturized sucrose gradient protocol developed by Gabriella Viero's lab, polysome-engaged and subpolysomal mRNAs were analyzed separately in comparison to control neurons. I focused on translatome and transcriptome changes related to the functional alterations observed by our group. Both wtTDP and mutTDP axons show a marked deregulation of polysomal transcripts involved in mRNA translation, the response to oxidative stress and presynaptic function, underlining the importance of axonal translation in key functional and homeostatic processes. Finally, electrophysiological recordings of wt- and mutTDP neurons revealed a significantly increase in electrical synapses. While potentially serving as a compensatory mechanism for the reduced connectivity of wt- and mutTDP neurons, gap junctions and hemichannels may contribute to the spread of toxic small molecules and to the maladaptive dissemination of neuronal damage from its focal origin.

## Table of contents

## 1. Acronyms and abbreviation

ADD2: Adducin 2

AEP: Asparaginyl endo-peptidase

ALS: Amyotrophic Lateral Sclerosis

AMPA: α-amino-3-hydroxy-5-methyl-4-isoxazolepropionic acid receptors

ANXA11: Annexin A11

AP: Action Potential

BAX: BCL2 Associated X

BDNF: Brain-derived neurotrophic factor

CBP: Creb-binding protein

CD206: Mannose Receptor C-Type 1

CDC7: Cell Division Cycle 7

CFTR: CF Transmembrane Conductance Regulator

CN: Cortical Neurons

CNS: Central Nervous System

CTD: C-terminal domain

CTF: C-terminal fragment

CTIP2: COUP-TF-interacting protein 2

Cx36: Connexin 36

DCN1: Dynactin1

DIV: Days In Vitro

DLP: Dally-like protein

DRG: Dorsal Root Ganglia

DRP1: Dynamin related protein 1

EAAT2: Excitatory amino acid transporter 2

eIF3: Eukaryotic Translation Initiation Factor 3

EPSC: Excitatory Postsynaptic Current

ER: Endoplasmic Reticulum

ERAD: Endoplasmic reticulum (ER)-associated protein degradation

fALS: familial ALS

FMRP: Fragile X mental retardation 1

FRAP: Fluorescence Recovery After Photobleaching

FTD: Frontotemporal dementia

FTLD: Frontotemporal lobar degeneration

FUS: Fused in Sarcoma/Translocated in Liposarcoma

G3BP1: G3BP Stress Granule Assembly Factor 1

GAD65: glutamic acid decarboxylase-65

GAPDH: Glyceraldehyde-3-Phosphate Dehydrogenase

GFAP: Glial fibrillary acidic protein

GJ: Gap junction

GluR2: Glutamate receptor 2

GRN: Granulin Precursor

H2DCFDA: 2',7'-dichlorodihydrofluorescein diacetate

HA: Hemagglutinin

HDAC1: Histone Deacetylase 1

HuC or ELAVL3: ELAV Like RNA Binding Protein 3

HuD or ELAVL4: ELAV Like RNA Binding Protein 3

IBA1: Ionized calcium binding adaptor molecule 1

IL-1: Interleukin-1

IL-6: Interleukin-6

IPSC: Induced Pluripotent Stem Cell

KD: Knockdown

KIF5A: kinesin family member 5A

KO: Knockout

KPNA: Karyopherin Subunit Alpha

LCD: Low Complexity Domain

LLPS: Liquid-Liquid Phase Separation

MAP1B: Microtubule Associated Protein 1B

MAP2: Microtubule Associated Protein 2

mEPSC: mini Excitatory Postsynaptic Current

mRNP: messenger ribonucleoprotein particle

mutTDP: tRFP-hTDP-43 (A315T)

NES: Nuclear Export Sequence

NFLH: Neurofilament Light Chain

NLS: Nuclear Localization Sequence

NMDA: N-methyl-D-aspartate receptors

NMJ: Neuromuscular junctions

NOX2: NADPH oxidase 2

NRF2: NF-E2–related factor 2

O4: Oligodendrocyte Marker O4

PARK7: Parkinson disease protein 7

PFN1: Profilin1

PP1: Protein phosphatase 1

Pum2: Pumilio2

Rab1a: Ras-related protein Rab-1A

Rab7a: Ras Associated Protein Rab7

RACK1: Receptor Activated C Kinase 1

RanGAP : Ras-related nuclear protein GTPase activating protein

RanGTP: Ras-related nuclear protein GTP

RBP: RNA binding protein

RGC: Retinal Ganglion Cells

ROS: Reactive Oxygen species

Rpl22: Ribosomal protein 22

RPL26: Ribosomal Protein L26

RPS6: Ribosomal Protein S6

RRM1/2: RNA Recognition Motif 1/2

S6K1: Ribosomal protein S6 kinase 1

sALS: sporadic ALS

SER: Smooth Endoplasmic Reticulum

SG: Stress granule

SKAR: Aly/REF-like target

SLC16A1: Solute Carrier Family 16 Member 1

SLC16A4: Solute Carrier Family 16 Member 4

SNAP25: Synaptosomal-Associated Protein, 25kDa

SOD1: Superoxide dismutase 1

SYNJ1: Synaptojanin 1

TBR1: T-Box Brain Transcription Factor 1

TCA: Tricarboxylic Acid Cycle

THY1: Thy-1 Cell Surface Antigen

TIA1: Cytotoxic Granule Associated RNA Binding Protein

TNF-α: Tumor Necrosis Factor alpha

TRAP: translating ribosome affinity purification

tRFP: turbo Red Fluorescent Protein

TTBK1/2: Tau tubulin kinases 1 and 2

TTX: Tetrodotoxin

TUBA4A: Tubulin alpha 4A

UBQLN2: Ubiquilin 2

ULK1: Unc-51 Like Autophagy Activating Kinase 1

UPS: Ubiquitin-Proteasome System

VCP: Valosin-containing protein

VEGF: Vascular Endothelial Growth Factor A

wtTDP: tRFP-hTDP-43 wt

YM1: Beta-N-acetylhexosaminidase

## 2. List of figures and tables

# 3. Introduction

## 3.1 Amyotrophic lateral sclerosis

Amyotrophic lateral sclerosis (ALS) is a progressive lethal neurodegenerative disease affecting people around 60 years of age. The most common clinical signs are muscular weakness, spasticity, fasciculations and dysphagia, culminating in progressive paralysis and death (reviewed in Brown & Al-Chalabi, 2017; reviewed in Hardiman *et al*, 2017).

The most frequent cause of death is respiratory failure (i.e. terminal respiratory insufficiency, pneumonia, asphyxia due to a foreign body and pulmonary embolism), followed by cardiac causes, suicide and undetermined causes (Gil *et al*, 2008). Respiratory failure is mainly due to the loss of phrenic nerve causing diaphragm weakness, which results in dyspnea and hypoventilation. Generally ALS patients die within 3-5 years after diagnosis, unless they undergo tracheostomy, which extends their survival to another 2 years. However, several patients choose not to undergo tracheostomy (reviewed in Niedermeyer *et al*, 2019). ALS is characterized by degeneration of upper and lower motor neurons. Upper motor neurons are those neurons projecting mainly from the fifth layer of the brain motor cortex to the brainstem or spinal cord, while lower motor neurons project from brainstem or spinal cord to skeletal muscles.

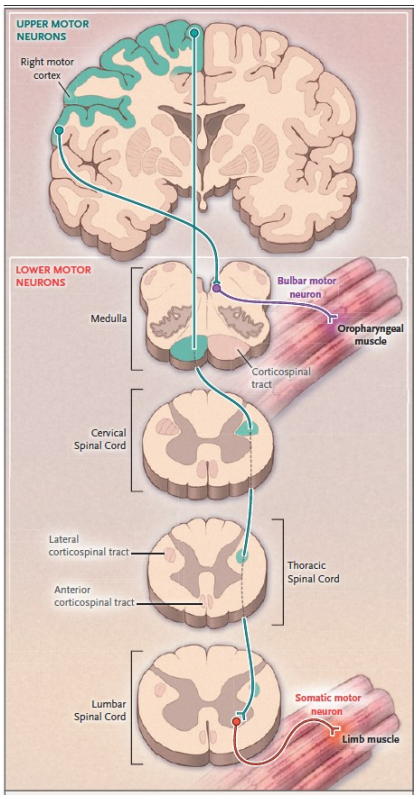


***Figure 3.1. ALS is characterized by the degeneration of upper and lower motor neurons.*** *Schematic representation of neurons mainly affected by ALS: upper motor neurons, which project from the fifth layer of brain cortex to brainstem or spinal cord (in green), and lower motor neurons, which innervate skeletal muscles from brainstem (in purple) or spinal cord (in red). Reproduced with permission (from Brown & Al-Chalabi, 2017), Copyright Massachusetts Medical Society.*

ALS has very heterogeneous manifestations in different patients, thus various classifications have been developed (reviewed in Hardiman *et al.*, 2017). One classification method considers the site of onset of the disease:

- Spinal-onset disease: the onset of the disease of these patients is the muscular weakness of the limbs.
- Bulbar-onset disease: these patients show dysarthria (difficulty with speech) and dysphagia (difficulty with swallowing).

Moreover, patients may have:

- Predominant upper motor neuron dysfunction: characterized by spasticity and weakness.
- Predominant lower motor neuron dysfunction: characterized by fasciculations, cramps and muscle wasting.

It has been reported that about 10% of ALS patients show also cognitive impairment consistent with fronto-temporal dementia (FTD) which is characterized by degeneration of neurons of frontal and temporal lobes, although up to 50% of patients develop cognitive and/or behavioral impairment during the course of disease (reviewed in Brown & Al-Chalabi, 2017). For these reasons, it is appropriate to consider ALS and FTD as the two extremities of the same disease spectrum.

### *3.1.1 Upper motor neurons resides in the fifth layer of the brain cortex*

As mentioned in the previous paragraph, ALS mainly affects upper and lower motor neurons, however in this thesis we are focusing on upper motor neurons.

The brain neocortex is divided into six layers, each one contains different neurons. Starting from the pia mater to the white matter, the brain cortex consists of:

- Layer I or molecular layer: which does not contain cells but only dendrites of the deeper layers.
- Layer II or external granular layer: which contains spherical shaped neurons.
- Layer III or external pyramidal layer: contains small pyramidal shaped neurons. Layers II and III connect neurons of the same cortical area or with other areas, thus mediating intracortical communication.
- Layer IV or internal granular layer: contains spherical shaped neurons that receive input from the thalamus. Thus, this layer is very large in primary sensory areas, such as the visual cortex, while in the primary motor cortex it is very thin; for this reason the primary motor cortex is also called agranular frontal cortex.
- Layer V or internal pyramidal layer: contains pyramidal shaped neurons larger than those of layer III. These neurons project to other cortical areas or to subcortical regions such as the spinal cord or brainstem. Indeed, in the primary motor cortex, this layer contains very large pyramidal neurons, named Betz cells, which project to the brainstem and spinal cord. These neurons are also named upper motor neurons or corticospinal motor neurons, which are the preferred target of neurodegeneration in ALS.
- Layer VI or multiform layer: which contains an heterogenous neuronal population, these neurons also project to subcortical regions (Kandel *et al*, 2021).

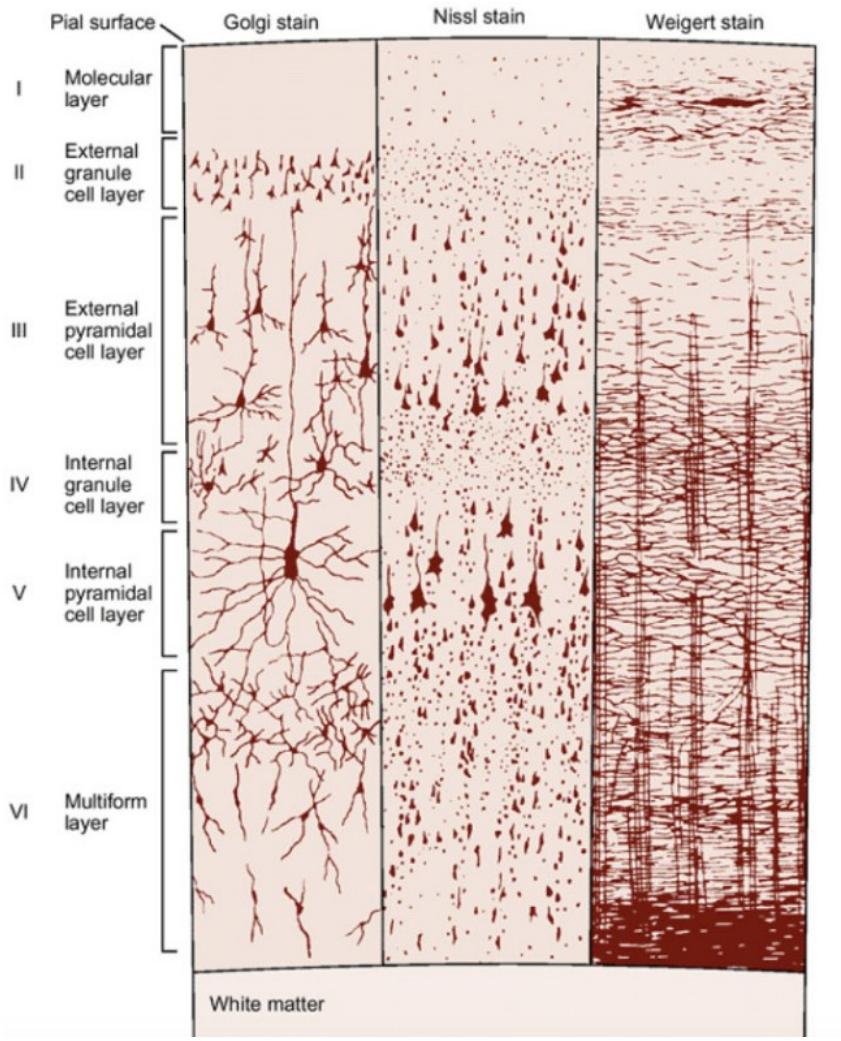


***Figure 3.2. Brain cortex contains different neurons subdivided into six layers.*** *Schematic representation of the six layers of the brain cortex: layer I or molecular layer, layer II or external granular layer, layer III or external pyramidal layer, layer IV or internal granular layer, layer V or internal pyramidal layer which contains upper motor neurons, layer VI or multiform layer. Fair use (from Heimer, 1994) according to Italian legislation (legislative decree n. 68 09/04/2003).*

In early development, the telencephalic cortex consists of undifferentiated progenitors named neuroepithelial cells, which differentiate into radial glia, generating the ventricular zone. Radial glia also generate two different progenitors: outer radial glia and intermediate progenitors, which make up the subventricular zone. Radial glia divide asymmetrically giving rise to several generations of precursors called intermediate progenitors, while maintaining the neural stem cell pool. In turn, intermediate progenitors divide symmetrically and generate two daughter neurons each in the preplate. In mice, neuronal progenitors generate projection neurons starting from E10.5 (10.5 days post

conception) and migrate from the ventricular zone to the preplate. Subsequently, later born neurons migrate in the preplate which is now divided into the marginal zone and the subplate; the cortical plate starts forming between these two layers. Newly born neurons organize into cortical layers following an “inside-out” progression (reviewed in Greig *et al*, 2013); indeed deep layers originate first (VI and V) and late-born neurons migrate through early-born layers and sequentially generate more superficial layers (IV, III and II).

Excitatory neurons are not the only component of the brain cortex: indeed, interneurons represent about 20-30% of cortical neurons and modulate the electrical activity of pyramidal cells and other glutamatergic neurons. Interneurons generate in a bilateral compartment of the ventral telencephalon named ganglionic eminence. Once specified in this structure, interneurons migrate tangentially from each ganglionic eminence to the ipsilateral hemisphere. In rodents the earliest migration wave of prospective inhibitory neurons starts from E12.5 and completes at birth (reviewed in Corbin & Butt, 2011).

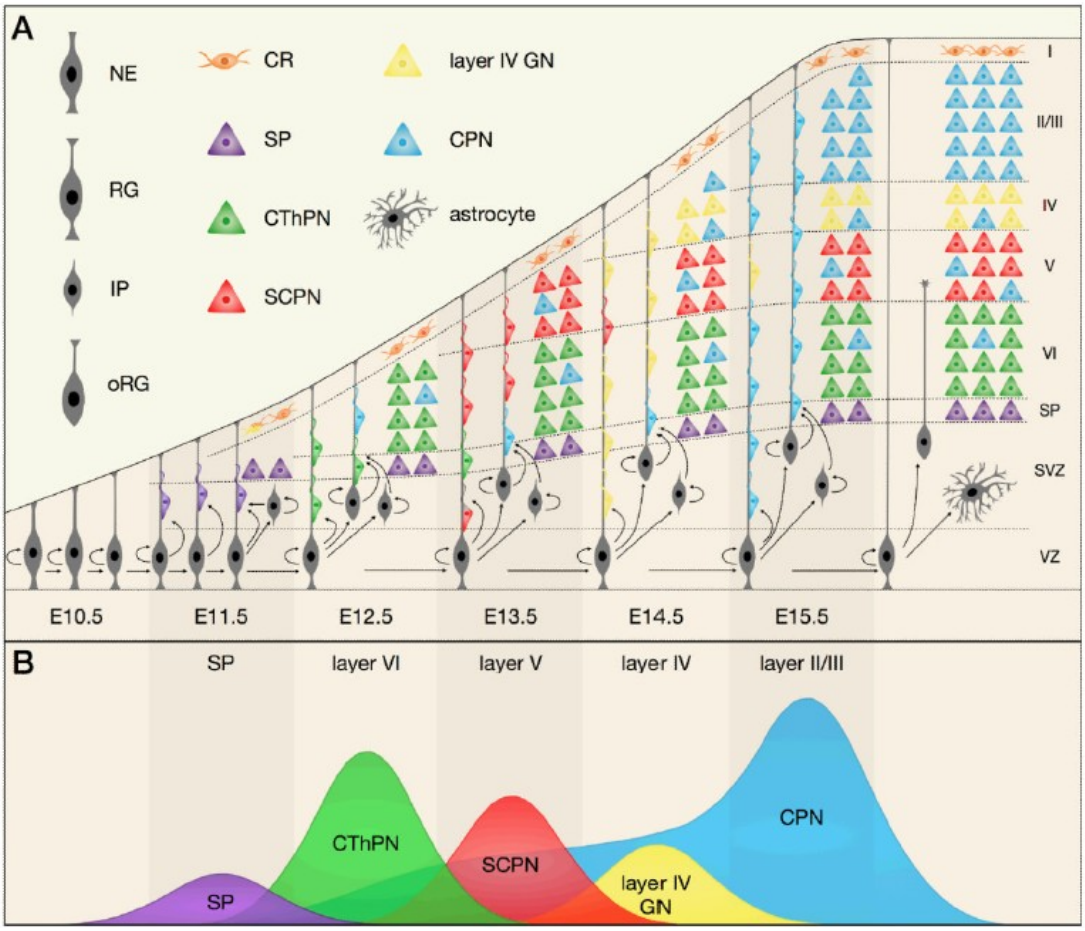


***Figure 3.3. Cortical projection neurons migrate into cortical layers through an "inside-out" mechanism.*** *Schematic representation of the generation and migration of cortical projection neurons during brain cortex development in rodents. Radial glia (RG) starts generating projection neurons at E11.5 in the ventricular zone (VZ). RG divides into intermediate progenitors (IPs) and outer RG (oRG) which generate the subventricular zone (SVZ). Cortical projection neurons of each layer cortex generate by and inside-out mechanism, starting from the deepest layers: subplate neurons (SP) around E11.5, corticothalamic neurons (CthPN) of layer VI around E12.5, subcerebral neurons (SCPN) of layer V at E13.5, granular neurons (GN) of layer IV at E14.5 and callosal projection neurons (CPN) of the superficial layers at E15.5 (from Greig et al., 2013). Reprinted by permission from Copyright Clearance Center (license number: 5235231435684) Springer Nature, Nature Reviews Neuroscience, "Molecular logic of neocortical projection neuron specification, development and diversity", Luciano Custo Greig et al. 2013, advance online publication, 9 Oct 2013 (doi: 10.1038/nrn3586).*

### *3.1.2 Genetics of ALS*

Ten percent of ALS cases show familial inheritance (familial ALS or fALS), while the majority of patients, about 90%, have no family history and are classified as sporadic cases (sALS) (reviewed in Hardiman *et al.*, 2017).

Since 1994, several ALS causative genes and risk factors have been discovered. These genes can be grouped in three main categories on the basis of the roles played by the corresponding proteins: genes involved in protein homeostasis, cytoskeletal maintenance and RNA metabolism.

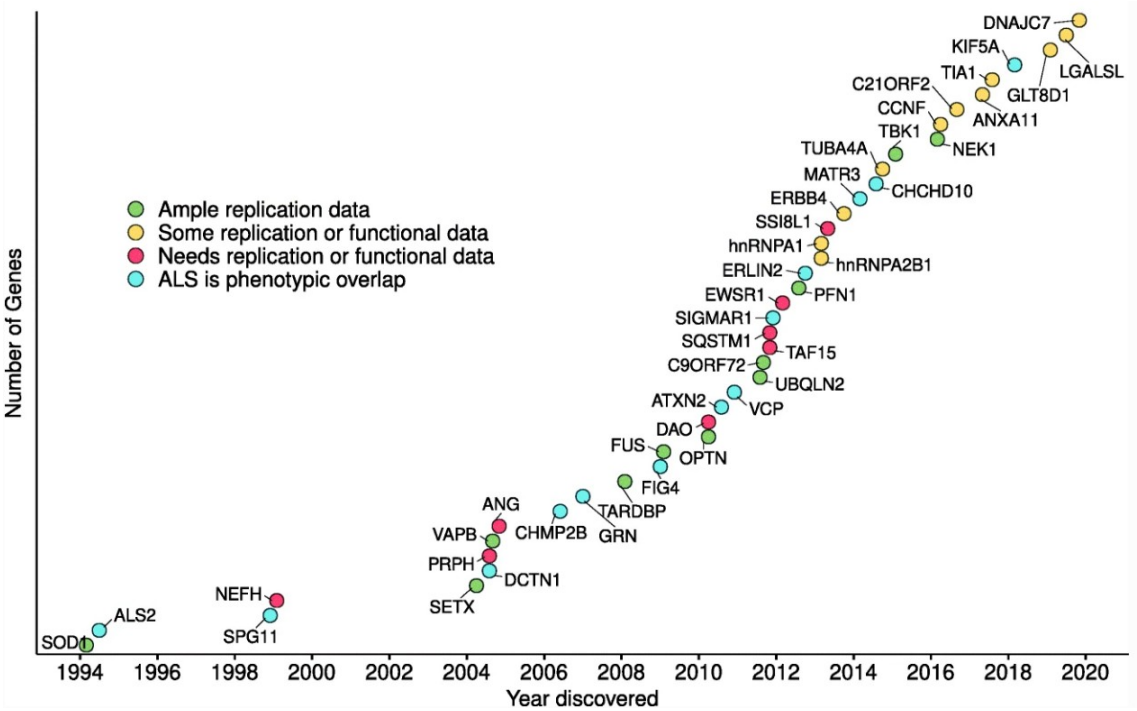


***Figure 3.4. ALS genes discovered from 1994 to date.*** *Representative graph showing ALS genes discovered from 1994 to date. On the y axis it is shown the progressive number of genes, while the x axis displays the year when each gene was discovered. It is worth noticing that the number of discovered genes is very high in recent years. This is due to the establishment of more sophisticated sequencing techniques (i.e. GWAS, genome-wide association studies; WES, whole-exome sequencing; WGS, whole-genome sequencing) and the falling costs of whole-genome sequencing. The color of each circle, as shown in the legend, indicates those genes with variable genetic support in replication and functional studies (from Gregory et al, 2020). Open access, Copyright: http://creativecommons.org/licenses/by/4.0/.*

*Factors involved in protein homeostasis*

The best characterized ALS causative genes involved in protein homeostasis are listed below.

*Superoxide dismutase 1* (*SOD1)* was the first ALS causative gene to be discovered (Rosen *et al*, 1993). It encodes the cytosolic Cu/Zn superoxide dismutase, which catalyzes the dismutation of the toxic superoxide anion ($O_2^-$) to oxygen ($O_2$) and hydrogen peroxide ($H_2O_2$), drawing attention on the potential role of oxygen free radicals in ALS. Mutations in the *SOD1* gene represent about 20% of fALS cases. Typically, patients with *SOD1*

mutations show a pure ALS phenotype with no cognitive disorders, and are characterized by accumulation of SOD1 misfolded aggregates in the central nervous system (CNS) (Shibata *et al*, 1996). Misfolded SOD1 seems to cause cellular damage through a toxic gain of function mechanism; indeed, mutant-SOD1 aggregates trap *Vascular endothelial growth factor (VEGF)* mRNA impairing its stability and downregulating its protein expression (Lu *et al*, 2007). Moreover, misfolded mutant SOD1 inhibits Endoplamic Reticulum Assocated Degradation (ERAD) through interaction with Derlin-1, an integral membrane protein on the cytoplasmic surface of endoplasmic reticulum (ER). This induces ER-stress and pro-apoptotic factor activation (Nishitoh *et al*, 2008).

Transgenic rodents carrying SOD1 mutations, in particular $SOD1^{G93A}$, were the first animal model developed for the study of ALS. Indeed, pathological features of these animal models resemble those of ALS patients, thus mice carrying *SOD1* mutations have been largely used to dissect molecular changes underlying ALS. However, the relevance of these mice for developing clinical trials has been challenged, since trials with factors producing beneficial effects in mouse models have not led to any significant progress in the treatment of ALS in humans (reviewed in Ghasemi & Brown, 2018).

*Ubiquilin2 (UBQLN2).* Mutations of *UBQLN2* gene in fALS patients were discovered in 2011 (Deng *et al*, 2011). UBQLN2 is involved in the ubiquitin-proteasome system (UPS), targeting ubiquitinated proteins to the proteasome. Moreover UBQLN2 colocalizes with TDP-43 aggregates in the spinal cord of ALS patients with or without UBQLN2 mutations (Deng *et al.*, 2011). In addition, it has been demonstrated that overexpression of wt or mutant UBQLN2 causes the aggregation of TDP-43 in Neuro2a cells (Picher-Martel *et al*, 2015). Mutations of UBQLN2 lead to inefficient degradation of ubiquitinated proteins (Deng *et al.*, 2011) and this may cause accumulation of misfolded or redundant polypeptides, impairing neuronal homeostasis and leading to neurodegeneration (reviewed in Renaud *et al*, 2019).

*Valosin-containing protein (VCP).* Mutations of the *VCP* gene are found in 1-2% of familial cases of ALS (Johnson *et al*, 2010). VCP is a hexameric protein involved in the UPS that recycles ubiquitinated proteins and mediates their proteasome-mediated degradation (reviewed in Meyer *et al*, 2012). Mutations of *VCP* in motor neuron-derived

induced pluripotent stem cells (IPSCs) lead to delocalization of TDP-43 and FUS mediated by the ATPase domain, although the underlying mechanism is still uncharacterized (Harley *et al*, 2021).

*Factors involved in cytoskeletal maintenance*

The next category of ALS causative genes and risk factors includes proteins that participate in cytoskeletal dynamics and maintenance. A subset of these genes are listed below.

*Profilin1 (PFN1)* allows the conversion of monomeric G-actin to filamentous F-actin. Mutations of *PFN1* lead to accumulation of ubiquitinated TDP-43-positive aggregates in primary cortical neurons (Wu *et al*, 2012).

*Dynactin (DCN1)* encodes an accessory protein involved in retrograde axonal transport and underlies the role of impaired axonal transport in ALS (Munch *et al*, 2005).

*Tubulin alpha 4A (TUBA4A)* encodes a microtubule subunit. Mutations in TUB4A alter microtubule dynamics and stability through a dominant negative mechanism in primary motor neurons (Smith *et al*, 2014).

*Kinesin family member 5A (KIF5A)* encodes a component of a microtubule motor complex that directionally transport various cargos, including membranous organelles, protein complexes and mRNAs (Hirokawa *et al*, 2009). Mutations in the *KIF5A* gene, contributing to ALS, were identified in 2018. These mutations localize predominantly in the C-terminal cargo-binding region of KIF5A, leading to its loss-of-function (Nicolas *et al*, 2018). Moreover, ALS patients with KIF5A mutations display earlier age of onset and longer survival (Nicolas *et al.*, 2018).

*Proteins involved in RNA metabolism*

Some ALS causative genes encode RNA-binding proteins (RBP) thus highlighting the role of altered RNA metabolism in ALS. The most common ALS genes encoding RBPs are listed below.

*Transactive Response DNA Binding Protein-43.* The *TARDBP* gene encodes the TDP-43 protein. Mutations in *TARDBP* account for about 5-10% of all forms of fALS (Sreedharan *et al*, 2008). TDP-43 is an RBP which is expressed in all tissues in mammals and invertebrates. TDP-43 has several functions: it is involved in gene transcription, splicing, RNA stability and translation (reviewed in Cohen *et al*, 2011). Although mutations of this gene are less frequent relative to other RBP gene mutations predisposing to ALS, TDP-43 has been widely studied since it has been identified as the main component of ubiquitinated inclusions found in the cytoplasm of motor neurons in 97% of ALS patients, both sporadic and familial, known as TDP-43 proteinopathy (Neumann *et al*, 2006). The role of TDP-43 in ALS will be examined in detail in section 3.2.

*Fused in sarcoma (FUS).* Mutations in the *FUS* gene, also known as translocated in liposarcoma (TLS), account for 3.2% of familial ALS (Blair *et al*, 2010). Similarly to TDP-43, FUS is a DNA/RNA binding protein involved in RNA metabolism. Several mutations occur in the C-terminal domain of *FUS,* disrupting its nuclear localization sequence, causing its delocalization from the nucleus to the cytoplasm and the formation of cytoplasmic aggregates (reviewed in Butti & Patten, 2018). However, wild type FUS aggregates have been found also in three different forms of sporadic FTLD (i.e. atypical FTLD-U, neuronal intermediate filament inclusion disease and basophilic inclusion body disease); consequently, these diseases were named FUS/TLS proteinopathies. Interestingly in the majority of cases the presence of TDP-43- or FUS/TLS-positive inclusions is mutually exclusive (reviewed in Lagier-Tourenne *et al*, 2010). FUS delocalization leads to nuclear loss of function, in particular FUS is involved in splicing of minor introns, those introns processed by U12-dependent spliceosomes. Interestingly, HeLa cells transfected with mutated FUS show reduced splicing activity of minor introns and mislocalization of U11 and U12 small nucleolar mRNAs in the cytoplasm (Reber *et al*, 2016). In addition, FUS regulates the splicing of several transcripts, including its own, exerting an autoregulation mechanism. Indeed, FUS promotes the retention of introns 6 and 7 of its own transcript. FUS transcript containing introns 6/7 is retained in the nucleus, preventing its translation in the cytoplasm. Mutated FUS, which accumulates in the cytoplasm, cannot regulate its own transcript in the nucleus and this may result in increased cytoplasmic levels through a feed-forward mechanism (Humphrey *et al*, 2020).

As other RBPs, FUS has a role in RNA translation; indeed, a mouse model carrying FUS mutation show decreased axonal translation (Lopez-Erauskin *et al*, 2018). In addition, recently, Birsa et al. found that mutated FUS sequesters another RBP, namely fragile X mental retardation 1 (FMRP), into cytoplasmic condensates, inhibiting the translation of FMRP-target mRNAs in spinal motor neurons (Birsa *et al*, 2021). This evidence supports the hypothesis of a toxic gain of function of cytoplasmic FUS.

*The case of C9orf72*

In 2011, it has been found that expansions of a hexanucleotide repeat (GGGGCC) within the first intron of the C9ORF72 gene, located on chromosome 9p21, was the most common cause of fALS and FTD (DeJesus-Hernandez et al, 2011; Renton et al, 2011). Indeed, hexanucleotide repeat expansions in C9ORF72 account for ~ 40% familial cases and ~ 7% sporadic cases of ALS in the European population (Iacoangeli et al, 2019). The number of repeats in healthy individuals ranges between 2 to 23 units however, the majority of healthy individuals present ≤11 copies of the repeat (reviewed in Balendra & Isaacs, 2018; Iacoangeli et al., 2019). Conversely, ALS and FTD patients have anything between 30 to thousands of repeat expansions (reviewed in Balendra & Isaacs, 2018; Iacoangeli et al., 2019). C9ORF72 has three variants: these repeat expansions occur in the first intron of variant 1 and 3 and in the promoter of variant 2 (reviewed in Balendra & Isaacs, 2018). The protein C9ORF72 is predicted to act as a guanidine exchange factor that interacts with RAB GTPase to regulate membrane trafficking. C9ORF72 repeat expansions may lead to ALS pathology through loss and gain of function. C9ORF72 transcript variants 1 and 2 are downregulated in the frontal cortex and cerebellum of C9ORF72 expansion carriers relative to controls (van Blitterswijk et al, 2015). Moreover C9ORF72 promotes autophagy initiation by mediating interaction between Rab1a and the ULK1 initiation complex, which regulates initiation of autophagosome formation. Accordingly, IPSC-derived motor neurons from C9ALS/FTD patients exhibit autophagy deficits (Webster et al, 2016). Concerning gain of function mechanisms, C9ORF72 repeat expansions can be bidirectionally transcribed generating sense and antisense RNAs, which cluster in nuclear foci in the brain of C9ALS/FTD patients (reviewed in Balendra & Isaacs, 2018) (Zu et al, 2013). C9ORF72 RNA foci can trap other proteins inhibiting their function, for example they trap RanGAP, a protein involved in

nucleocytoplasmic transport, thus impairing nuclear import in a Drosophila model expressing 30G4C2 repeats (Zhang et al, 2015). Furthermore, repeat expansions undergo a non-canonical form of ATG-independent translation, named RAN-translation, that may occur from both sense and antisense expansion transcripts, resulting in the expression of five RAN dipeptides (antisense: Pro-Arg, Pro-Ala, Gly-Pro; and sense: Gly-Ala, Gly-Arg, Gly-Pro). These proteins accumulate in cytoplasmic aggregates in brain and spinal cord neurons of C9ALS/FTD patients and they are highly toxic for cells (Zu et al., 2013).

Notably, the neurons of patients carrying C9ORF72 hexanucleotide repeat expansion display TDP-43 proteinopathy (Scaber & Talbot, 2016). Indeed, in a Drosophila model of C9ORF72 mutation, the overexpression of dipeptide repeats (DPRs) leads to TDP-43 accumulation in the cytoplasm, leading to sequestration of kariopheryns (KPNAs), a family of proteins involved in nuclear import. This translates into a further nucleocytoplasmic transport impairment, which increases TDP-43 mislocalization and promotes neurodegeneration (Solomon et al, 2018).

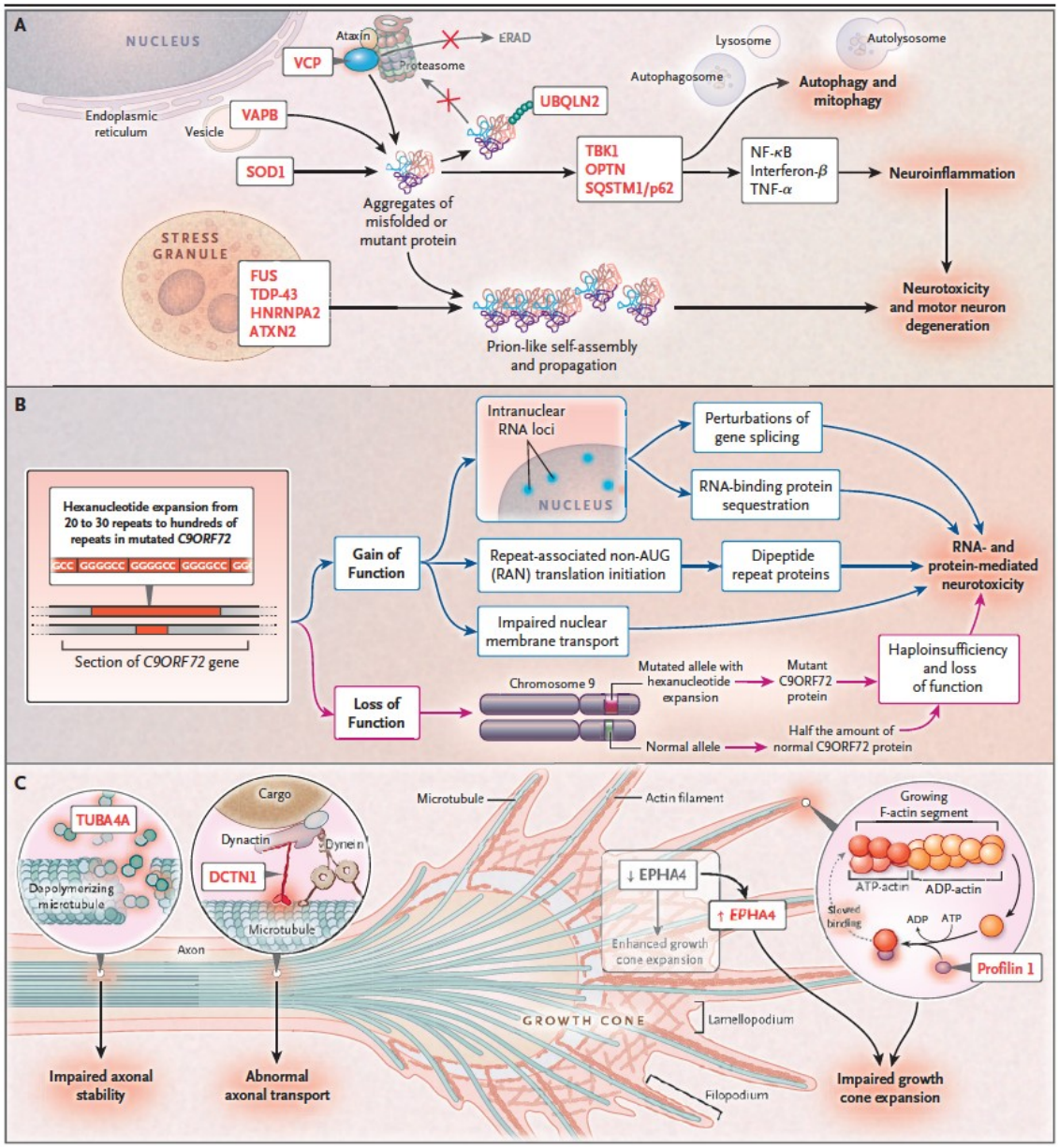


***Figure 3.5. Pathological features of the major ALS mutated genes.*** *(A) Several ALS genes are involved in protein degradation: proteasome degradation, ER-associated degradation and autophagy. Thus, mutations of these genes may impact these functions and consequently protein homeostasis. Genes encoding RBPs represent another important category of ALS genes. Misfolded or mutated RBPs may trap mRNAs and other RBPs inhibiting their function. (B) C9ORF72 repeat expansions are the most common genetic cause of ALS and have a pathological effect in ALS through gain and loss of function mechanisms (see text for mechanisms). (C) Some ALS causative genes and risk factors encode protein involved in axonal transport (e.g. DCTN1, KIF5A) or cytoskeleton maintenance (e.g. TUBA4A, PFN1); thus, mutations of these genes may alter axonal maintenance. Reproduced with permission (from Brown & Al-Chalabi, 2017), Copyright Massachusetts Medical Society.*

### *3.1.3 Pathophysiological features of ALS*

One of the main features of ALS is glutamate excitotoxicity. Glutamate is the main excitatory neurotransmitter of the CNS and is released by the presynaptic membrane in the synaptic cleft, in response to axonal depolarization. Glutamate interacts with metabotropic and ionotropic receptors localized onto the postsynaptic membrane. Ionotropic receptors can be grouped into α-amino-3-hydroxy-5-methyl-4-isoxazolepropionic acid receptors (AMPA), N-methyl-D-aspartate receptors (NMDA) and kainate receptors. Glutamate excitotoxicity is the hyperactivation of these ionotropic glutamate receptors which results in an increased influx of $Na^+$ and $Ca^{2+}$ ions that activates downstream pathways leading to neuronal degeneration (reviewed in Geevasinga *et al*, 2016). Different mechanisms may underlie glutamate excitotoxicity. Increased glutamate receptor activation may be due to defective glutamate reuptake from the synaptic cleft by neurons and astrocytes. Indeed the excitatory amino acid receptor 2 (EAAT2) is downregulated in in-vivo models of ALS (Howland *et al*, 2002) and in patient tissues (Lin *et al*, 1998). Moreover, increased glutamate response may be due to increased levels of AMPA receptors lacking the GluR2 subunit. This kind of AMPA receptor is more permeable to $Ca^{2+}$ ions and is particularly abundant in motor neurons (reviewed in Grosskreutz *et al*, 2010). The presence of GluR2 is regulated by neurotrophic factors released from astrocytes (e.g. VEGF). GluR2 pre-mRNA undergoes a Q/R RNA editing, resulting in a conversion of glutamine (CAG, encoding a Q) to an arginine (CGG, encoding an R), which is essential for calcium impermeability of the AMPA receptor containing the GluR2 subunit (Sommer *et al*, 1991). Interestingly, GluR2 pre-mRNA editing seems to be defective in spinal cord tissues of sALS patients (reviewed in Grosskreutz *et al.*, 2010).

The exact mechanism by which glutamate excitotoxicity mediates neuron degeneration still needs to be clarified. Increased glutamate receptor activation leads to increased calcium levels which may activate $Ca^{2+}$-dependent enzymatic pathways. To date riluzole, an anti-glutamatergic agent that reduces glutamate excitotoxicity, is the only treatment available for ALS patients. However, this treatment only extends the time before tracheostomy becomes necessary (reviewed in Miller *et al*, 2003).

Another pathological feature of ALS is mitochondrial dysfunction. Altered mitochondrial structure and function have been widely observed in in-vivo models of

ALS and in ALS patients. ALS-affected neurons display shorter and more spherical mitochondria, accompanied by reduced ATP production compared to controls (reviewed in Smith *et al*, 2019). Additionally, mitochondrial transport is altered in an in-vivo model of ALS; this would result in axonal deprivation of energy that is necessary for the maintenance of membrane potential and generation of action potentials (Bilsland *et al*, 2010). Moreover, glutamate excitotoxicity increases intracellular calcium levels and, consequently, leads to excessive calcium accumulation in mitochondria, which causes an increased release of free radicals, promoting neurotoxicity (reviewed in Geevasinga *et al.*, 2016).

Oxidative stress is another hallmark of ALS motor neurons. Indeed increased reactive oxygen species (ROS) levels and ROS associated damage have been reported in ALS (reviewed in Barber & Shaw, 2010). ROS are natural products of oxidative phosphorylation, which are generally processed by several enzymes, including superoxide dismutase 1 (SOD1), one of the main genes mutated in ALS (Rosen *et al.*, 1993). However, dysfunctional mitochondria produce excessive ROS levels that may damage DNA, protein, lipids and even mitochondria producing a feed-forward loop (reviewed in Smith *et al.*, 2019). In addition, oxidative stress promotes the release of cytokines, thus triggering a pro-inflammatory response. Several lines of evidence show that non-autonomous mechanisms drive neuronal toxicity in ALS; indeed microglia and astrocytes play an important role in the pathogenesis of this disease (reviewed in Liu & Wang, 2017). Interestingly, the replacement of $SOD1^{G93A}$ microglia with wild-type microglia in $SOD1^{G93A}$ transgenic mice slows down motor neuron loss and extends their survival (Beers *et al*, 2006). However, the microglial contribution could be either beneficial or detrimental for motor neurons depending on the stage of the disease. During the initial phase of the disease, microglial cells display an M2 phenotype, positive for CD206 and Ym1, promoting neuronal regeneration and repair. Instead, at later stages of the disease, microglia show an M1 phenotype, secreting ROS, NOX2 and proinflammatory cytokines, i.e. TNF-α, IL-1, IL-6 (reviewed in Liu & Wang, 2017). Indeed, it has been demonstrated that microglia isolated from $SOD1^{G93A}$ transgenic mice at early stages of disease progression are neuroprotective for co-cultured wild-type motor neurons, while M1-microglia isolated from late stage $SOD1^{G93A}$ mice, are neurotoxic

(Liao *et al*, 2012). Even astrocytes contribute to neuronal toxicity: for instance, wild-type motor neurons co-cultured with astrocytes expressing mutated SOD1 show increased toxicity (Marchetto *et al*, 2008) and suppression of mutated SOD1 in astrocytes of $SOD1^{G85R}$ transgenic mice delays disease onset and prolongs the early stages of disease progression (Wang *et al*, 2011). The reasons why astrocytes drive neuronal toxicity could be explained by the decreased re-uptake of glutamate due to decreased levels of the glutamate transporter EAAT2 (as mentioned before), the secretion of pro-inflammatory factors (i.e. prostaglandin E2, nitric oxide, NOX2) or the promotion of necroptosis (Re *et al*, 2014).

Another pathological hallmark of ALS is the alteration of energy metabolism. Many ALS patients show hypermetabolism, body weight loss and abnormal lipid metabolism. Interestingly, reduced glucose uptake has been observed in the brain and spinal cord of ALS patients and in murine models of ALS. Moreover, the activity of enzymes involved in glycolysis and tricarboxylic acid (TCA) cycle seem to be reduced in muscles of $SOD1^{G93A}$ mice (Palamiuc *et al*, 2015; Tefera *et al*, 2016). As mentioned before, mitochondrial dysfunction is another feature of ALS; indeed, it has been found that several genes encoding mitochondrial electron transport chain proteins are dysregulated in ALS, which leads to deficient ATP production (reviewed in Tefera *et al*, 2017). Furthermore, lactate influx from astrocytes and oligodendrocytes to neurons seem to be impaired due to reduced levels of lactate transporters in $SOD1^{G93A}$ mice (the solute carriers Slc16a4 for astrocytes and Slc16a1 for oligodendrocytes) (Ferraiuolo *et al*, 2011; Philips *et al*, 2013). Lactate is a product of glycolysis that is secreted from glial cells to neurons in order to supply the energy demand of axons, especially during intense activity (Martinez, 2012). Thus, motor neurons, which have very long axons that may reach one meter in length, may be particularly sensitive to metabolic dysfunction.

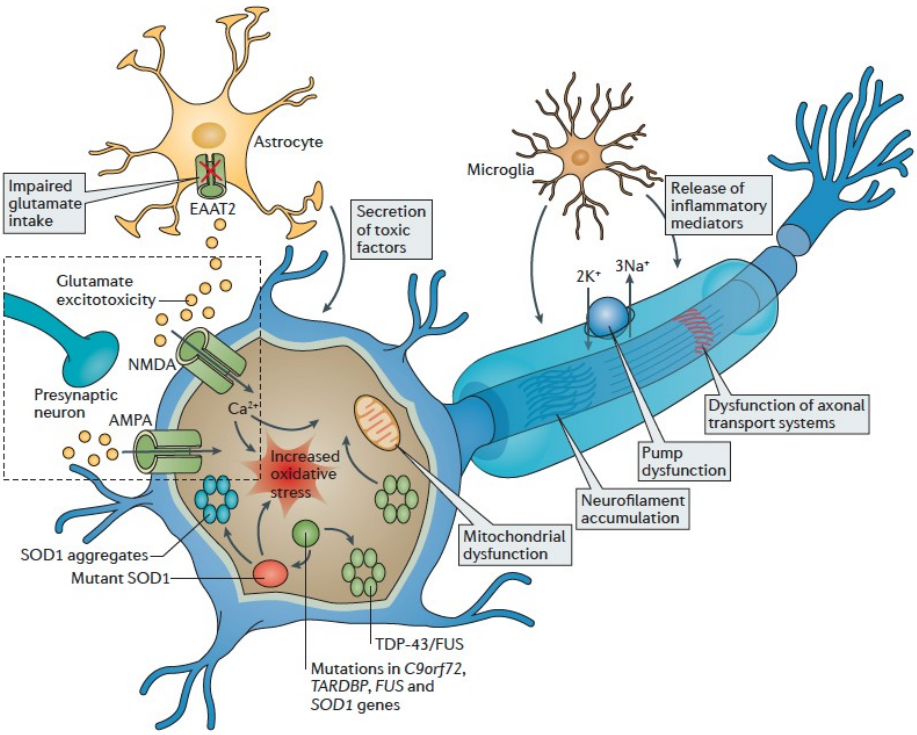


***Figure 3.6. Pathophysiological mechanisms underlying ALS.*** *Schematic representation of an ALS motor neuron showing pathophysiological features correlating with this disease. ALS presents both cell-autonomous mechanisms, as altered RNA metabolism due to mutations of RNA binding proteins, axonal transport defects, oxidative stress and mitochondrial dysfunction, and non-cell autonomous mechanisms due to impaired glutamate re-uptake by astrocytes, leading to excitotoxicity, and activated microglia releasing pro-inflammatory factors, which are neuroprotective at early stages and neurotoxic at later stages. (From Geevasinga et al., 2016). Reprinted by permission from Copyright Clearance Center (license number: 5235280851352) Springer Nature, Nature Reviews Neurology, "Pathophysiological and diagnostic implications of cortical dysfunction in ALS", Nimeshan Geevasinga et al. 2016, advance online publication, 23 Sep 2016 (doi 10.1038/nrneurol.2016.140).*

### *3.2 TDP-43*

TAR DNA-binding protein 43 (TDP-43) is an RNA-binding protein encoded by the gene *TARDBP*. TDP-43 is expressed ubiquitously in all species examined, from invertebrates to mammals.

TDP-43 protein is composed by an N-terminal region containing a nuclear localization sequence, two RNA Recognition Motifs (RRM1 and RRM2), which contain a nuclear export sequence (NES), and a C-terminal domain which is a glycine-enriched region where the majority of ALS-linked mutations are localized (Cohen *et al.*, 2011) (Fig. 3.7).

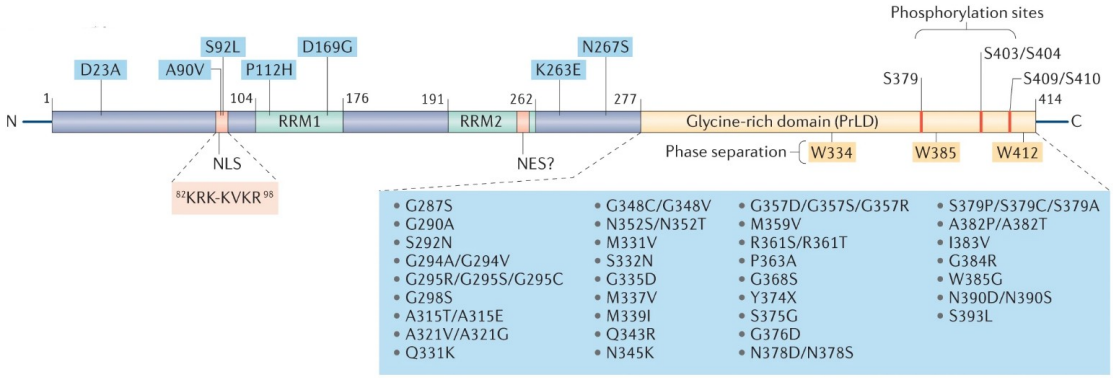


***Figure 3.7. TDP-43 domain structure.*** *Representative scheme showing TDP-43 domains: TDP-43 contain a nuclear localization sequence (NLS), two RNA recognition motifs (RRM1/2) a nuclear export sequence (NES) and a C-terminus glycine-enriched in which the majority of familial mutations occur (Adapted from Tziortzouda et al, 2021). Reprinted by permission from Copyright Clearance Center (license number: 5260241319212) Springer Nature, Nature Reviews Neuroscience, "Triad of TDP43 control in neurodegeneration: autoregulation, localization and aggregation", Paraskevi Tziortzouda et al. 2021, advance online publication, Mar 2, 2021 (doi:10.1038/s41583-021-00431-1).*

TDP-43 is an essential gene, as shown by the fact that TDP-43 KO mice show early embryonic lethality (Kraemer *et al*, 2010). TDP-43 localization is predominantly nuclear; however, thanks to its NES sequences, it is able to shuttle between nucleus and cytoplasm (Ayala *et al*, 2008). This protein binds preferentially UG-enriched region of RNA targets (Ayala *et al*, 2005; Buratti *et al*, 2001), through which it plays several roles in RNA metabolism.

### *3.2.1 Recognized functions of TDP-43 as an RNA binding protein*

**Pre-mRNA splicing.** TDP-43 was implicated in pre-mRNA splicing for the first time in 2001, when Buratti et al. discovered that TDP-43 mediates the skipping of exon 9 in the *CFTR* transcript (Buratti *et al.*, 2001), however CFTR does not appear to play a fundamental role in neuronal biology. iCLIP analysis of the neuroblastoma cell line SH-SY5Y, revealed that TDP-43 regulates the splicing of genes involved in development: neural tube formation and organ morphogenesis (Tollervey *et al*, 2011). This might explain the embryonic lethality of TDP-43 KO mice (Tollervey *et al.*, 2011). Analysis of the mouse brain showed that TDP-43 KD leads to reduced levels of 601 mRNA and altered splicing events of 965 mRNAs. TDP-43 binds long introns in pre-mRNAs, which are particularly abundant in brain tissues (Polymenidou *et al*, 2011). Polymendou et al. hypothesized that TDP-43-binding of long pre-mRNA may inhibit unproductive splicing

events that may introduce premature stop codons, however other mechanisms of regulation cannot be excluded. TDP-43 binds pre-mRNAs of *FUS*, progranulin and of other transcripts involved in neurologic diseases (Polymenidou *et al.*, 2011). Moreover, RNA-immunoprecipitation revealed that TDP-43 binds several mRNAs involved in splicing and RNA processing and maturation, suggesting also an indirect role of TDP-43 in regulating the splicing process (Sephton *et al*, 2011). Interestingly, ALS-associated mutations of TDP-43 impair its splicing activity, thus leading to the insertion of new exons (cryptic exons), or to the exclusion of constitutively inserted exons (skipped exons) (Fratta *et al*, 2018; Watanabe *et al*, 2020).

**RNA stability.** It is known that TDP-43 affects the stability of several mRNAs. Indeed, TDP-43 binds the UG-enriched region of the 3'-UTR of several mRNAs, thus influencing their stability in a positive manner, such as *Nflh* (Strong *et al*, 2007) and *Add2* (Costessi *et al*, 2014), or in a negative one, as is the case of *Vegfa* and *Grn* (Colombrita *et al*, 2012).

Interestingly, TDP-43 regulates the stability of its own transcript to fine tune the total amount of the corresponding protein (Ayala *et al*, 2011). Two models have been proposed for TDP-43 autoregulation (reviewed in Tziortzouda *et al.*, 2021). In the first model, under overexpression conditions, TDP-43 binds a conserved region of its transcript's 3'-UTR, promoting the splicing of intron 7 and the use of an alternative polyadenylation site. The transcript, containing the alternative polyadenylation site, is retained in the nucleus and degraded by RNA exosome complex (Avendano-Vazquez *et al*, 2012; Ayala *et al.*, 2011). However, in the second model, in overexpression conditions TDP-43 binds the 3'-UTR leading to the removal of both intron 6 and 7, which generates a premature stop codon upstream of the last exon-exon junction leading to degradation in the cytoplasm by nonsense-mediated decay (Koyama *et al*, 2016).

**mRNA transport.** Despite its predominantly nuclear localization, TDP-43 is transported in the axon and dendrites of neurons (Fallini *et al*, 2012). Indeed, TDP-43 and its mRNA targets, together with other RBPs, generate RNA granules (mRNP) to drive those mRNAs in the sub-neuronal compartments.

For example Chu et al., demonstrated that TDP-43, together with the RBP FMRP, modulates anterograde transport of dendritic mRNPs, although when it is bound by Staufen, it modulates the retrograde transport (Chu *et al*, 2019). Localization of mRNA in specific subcellular compartments allows proteins to be synthesized locally in appropriate subcellular domains. Interestingly, TDP-43 has been found to mediate the transport of ribosomal protein-coding transcripts (Nagano *et al*, 2020), thus TDP-43 has a key role in mRNA transport and local translation of its mRNA targets but also influences the local translation of other mRNAs. Mutations of TDP-43 leads to defective axonal transport of TDP-43 mRNA granules (Alami *et al*, 2014) pointing out the role of defective axonal transport in ALS.

**mRNA translation.** As mentioned earlier, TDP-43 is also involved in mRNA translation. Not only does TDP-43 mediate transport of its target mRNAs, but it keeps them in an "untranslated state" until they reach dendritic spines (Chu *et al.*, 2019). The importance of local protein synthesis will be further examined in section 3.3. In keeping with the above, Briese et al., demonstrated that TDP-43 KD in cultured motor neurons leads to decreased axonal translation (Briese *et al*, 2020). One possible explanation for the observed decrease in local translation could be the role of TDP-43 in the transport of mRNAs encoding ribosomal proteins (Nagano *et al.*, 2020).

**Stress granules.** In 2009 Colombrita et al. found that TDP-43 is recruited in stress granules (SGs), which are membraneless organelles containing RBPs, polyadenylated mRNAs and stalled ribosomes (Colombrita *et al*, 2009). SGs are highly dynamic structures, which generate under stress conditions in order to maintain mRNAs in an untranslated state until stress relief (reviewed in Wolozin & Ivanov, 2019). Although TDP-43 is not an essential component of SGs (Colombrita *et al.*, 2009), TDP-43 KD has been found to impair stress granule dynamics in cultured cortical neurons (Khalfallah *et al*, 2018). Moreover TDP-43 regulates the protein levels of TIA1 and G3BP1, two key component of SGs (McDonald *et al*, 2011). It has been demonstrated that TDP-43 promotes mRNA stability of a shorter isoform of *G3BP1* transcript, and TDP-43 nuclear delocalization leads to *G3BP1* degradation and reduced protein levels (Sidibe *et al*, 2021). It has been hypothesized that SGs may represent the nucleation site of TDP-43 aggregates in ALS. This will be further examined in section 3.2.3.

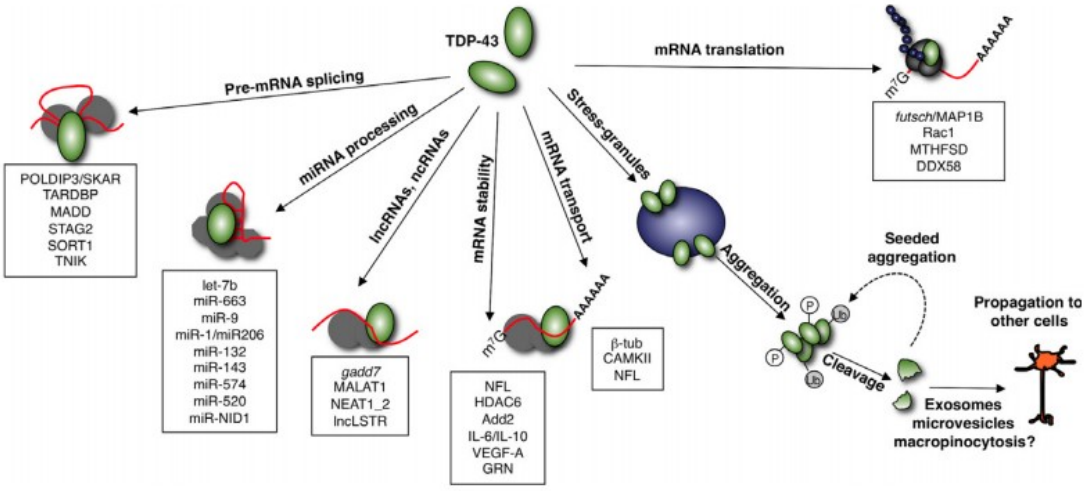


***Figure 3.8. TDP-43 regulates RNA metabolism at multiple levels.*** *TDP-43 is an RBP involved in several functions concerning RNA metabolism: pre-mRNA splicing, miRNA and lncRNA biogenesis, mRNA stability, transport and translation, stress granules dynamics (From Ratti & Buratti, 2016). Reprinted by permission from Copyright Clearance Center (license number: 5235250561860) John Wiley and Sons, Journal of Neurochemistry, "Physiological functions and pathobiology of TDP-43 and FUS/TLS proteins", Emanuele Buratti, Antonia Ratti, advance online publication, 15 Jun 2016 (doi:10.1111/jnc.13625).*

### *3.2.2 TDP-43 post-translational modifications associated with neurodegeneration*

In 2006 Neumann et al. and Arai et al. found that TDP-43 is the main component of ubiquitin-positive aggregates in spinal cord and brain of ALS and FTD patients (Arai *et al*, 2006; Neumann *et al.*, 2006). Indeed, ALS and FTD represent a continuum of the same neurodegenerative disease spectrum (reviewed in Ling *et al*, 2013). ALS motor neurons, but also glial cells and muscles, show TDP-43 aggregates together with its nuclear depletion (reviewed in Saberi *et al*, 2015). Over the last decade, it has been found that several neurodegenerative diseases (e.g. Alzheimer disease, Perry disease, etc) were characterized by TDP-43 nuclear clearance and the presence of cytoplasmic aggregates; for this reason these diseases have been collectively referred to as "TDP-43 proteinopathies" (reviewed in de Boer *et al*, 2020).

TDP-43 undergoes several post-translational modifications associated with neurodegenerative diseases (reviewed in Buratti, 2018). As mentioned before, ubiquitination is one of the main features of TDP-43 aggregates in ALS (Neumann *et al.*, 2006). Mass spectrometry analysis identified Lys49 as the ubiquitination site of TDP-43 in ALS human brain (Kametani *et al*, 2016). However, other several lysines were identified as TDP-43 ubiquitination sites (Lys102, Lys114, Lys145, Lys181), indeed

ubiquitination sites differ on the basis of the cellular context (reviewed in Buratti, 2018). TDP-43 presents both Lys-48 and Lys-63 polyubiquitin chains, suggesting different degradation pathways, in fact Lys-48 is a signal of proteasomal degradation, while Lys-63 is a feature of autophagy-dependent degradation (Seyfried *et al*, 2010). Parkin has been identified as the E3-ubiquitin ligase of TDP-43, however Parkin-mediated ubiquitination promotes the cytoplasmic accumulation of TDP-43 but not its proteasomal degradation. Interestingly, TDP-43 regulates Parkin expression, thus dysregulation of TDP-43 may affect its ubiquitination-mediated cytoplasmic accumulation (Hebron *et al*, 2013).

Phosphorylation is another post-translational modification associated with TDP-43 aggregates in ALS and FTD. Several phosphorylation sites were identified, however the main residues involved in pathological phosphorylation of TDP-43 are Ser 403-404 or Ser 409-410 (Hasegawa *et al*, 2008). Several kinases were found to phosphorylate TDP-43. Inhibition of Cell Division Cycle 7 (CDC7) kinase blocks TDP-43 phosphorylation and reduces neuron loss in a *C. elegans* model of TDP-43$^{M337V}$ mutation (Liachko *et al*, 2013). Another TDP-43 kinase is Tau tubulin kinases 1 and 2 (TTBK1/2) which co-localizes with phosphorylated TDP-43 in tissues from FTLD patients (Taylor *et al*, 2018). Some TDP-43 phosphatases have been identified: for example Protein Phosphatase 1 (or PP1) was described to dephosphorylate TDP-43 Ser403/404 and Ser409/410 in HEK293FT cells overexpressing TDP-43 (Gu *et al*, 2018). However, Choi et al. found that PP1 activity is increased in neurons derived from ALS mouse models, which dephosphorylate and activate Dynamin related protein 1 (Drp1), leading to increased mitochondrial fission (Choi *et al*, 2020). Calcineurin was identified as another TDP-43 phosphatases. Loss of calcineurin in the *C. elegans* model of TDP-43 ALS exacerbates motor neuron degeneration (Liachko *et al*, 2016).

The pathological consequences of this phosphorylation are still debated (reviewed in Buratti, 2018; reviewed in Hergesheimer *et al*, 2019). For example, Li et al. demonstrated that the overexpression of a TDP-43 C-terminal fragment phosphomimetic mutant shows decreased aggregation in HEK293T and Neuro2a cells (Li *et al*, 2011), while Kim et al., demonstrated that the TDP-43 phosphomimetic mutant leads to increased cytotoxicity in Neuro2a cells (Kim *et al*, 2015).

To date, phosphorylated TDP-43 has emerged as a potential biomarker of the disease, since increased levels of phosphorylated TDP-43 have been found in the plasma of ALS and FTD patients (Ren *et al*, 2021; Suarez-Calvet *et al*, 2014).

The presence of C-terminal TDP-43 protein fragments (CTFs) is a hallmark of TDP-43 positive aggregates associated with ALS and FTD (Neumann *et al.*, 2006). The main C-terminal TDP-43 fragments are 25 and 35kDa fragments that are likely generated by proteolytic cleavage. Caspase-3 and -7 generate 25 and 35kDa fragments, while asparaginyl endopeptidase mainly generates 35kDa fragments. Calpain-I and II are able to cleave TDP-43 in a widespread range of fragments. Moreover, some fragments may be generated also by alternative splicing and by alternative translation start sites. Interestingly, N-terminal fragments do not seem to be detected, probably because they are quickly degraded (reviewed in Buratti, 2018). A common feature of these CTFs is the absence of the NLS, which leads to the cytoplasmic accumulation of these fragments.

The role of CTFs in the pathogenesis of ALS still needs to be clarified. Overexpression of TDP-43 CTFs in neuroblastoma-derived cell lines leads to the formation of cytoplasmic phosphorylated and ubiquitinated aggregates resembling those of ALS and FTD (Igaz *et al*, 2009; Nonaka *et al*, 2009).

TDP-43 CTF overexpression results in increased cytotoxicity in vitro (Zhang *et al*, 2009). Moreover, 25kDa TDP-43 CTFs seem to weakly bind endogenous full length TDP-43 (Zhang *et al.*, 2009), while 35kDa TDP-43 CTFs bind endogenous full length TDP-43 through RNA binding mediated by the RRM1 domain (Che *et al*, 2015).

While in-vitro studies seem to show the link between pathological aggregates and TDP-43 CTFs, in mouse models the overexpression of TDP-43 CTF does not fully recapitulate TDP-43 modifications observed in the human disease. Indeed, transgenic rodents overexpressing TDP-43 CTFs, display motor and cognitive impairments resembling those of ALS and FTD, however they do not show ubiquitin-positive inclusions and motor neuron loss (Caccamo *et al*, 2012; Dayton *et al*, 2013; Tsuiji *et al*, 2017). Some transgenic mouse models, overexpressing wt or mutated human full-length TDP-43, show the presence of CTFs (Stallings *et al*, 2010; Wegorzewska *et al*, 2009). However, the inducible mouse model produced by Virginia Lee's lab, which overexpresses human wt TDP-43 or a mutant protein lacking the NLS signature, does not produce TDP-43 CTFs despite showing motor neuron loss and ubiquitin-positive

inclusions (Igaz *et al*, 2011). Thus, TDP-43 CTFs are a hallmark of, yet not a requirement for TDP-43 mediated toxicity (reviewed in Buratti, 2018).

Other less characterized post-translational modifications of TDP-43 are lysine acetylation and cysteine oxidation. In Cohen et al., 2015 two TDP-43 acetylation sites were discovered: Lys145, in the RRM1 domain, and Lys192, adjacent to the RRM2 domain. TDP-43 acetylation is mediated by the acetyltransferase known as Creb-binding protein (CBP). Overexpression of an acetylation-mimic TDP-43 mutant lacking the NLS leads to the formation of ubiquitinated and phosphorylated cytoplasmic aggregates in QBI293 and Neuro2a cells. Moreover, in this paper they show the presence of TDP-43 acetylated in Lys145 in the spinal cord of sALS patients, an event not detected in FTD human brains. This group explains that this discrepancy may be due to increased accumulation in FTD brain tissues of 25kDa fragments, which lack of the acetylation sites (Cohen *et al*, 2015). TDP-43 acetylation seems to impair the RNA regulatory function of this protein. Interestingly, acetylated TDP-43 has been shown to generate shell-like structures in the nucleus (see section 3.2.3) (Yu *et al*, 2021).

Virginia Lee's lab found that oxidative stress promotes TDP-43 cross-linking by cysteine oxidation and disulfide bond formation, which leads to decreased TDP-43 solubility. Moreover, increases in cross-linked TDP-43 species were found in FTD human brains (Cohen *et al*, 2012).

Another emerging TDP-43 post-translational modification is SUMOylation. SUMOylation consists in the conjugation of small ubiquitin-related modifiers (SUMO-1, 2/3 and 4) to specific lysines. TDP-43 SUMOylation was first identified by proteomic analyses in HeLa cells after heat shock (Golebiowski *et al*, 2009). Recently, Maraschi et al. found a TDP-43 SUMOylation site in Lys163 (Maraschi *et al*, 2021). In neuroblastoma SK-N-BE cells, the SUMO-resistant mutant TDP-43 K163R, which however shows a slight reduced RNA-binding activity, displays reduced exon skipping capability but unaltered exon inclusions of some of its known mRNA targets (e.g. reduced skipping of exon 9 of *CFTR* and of exon 15 of *TNIK*, unaltered inclusion of exon 30 of *MADD*). TDP-43 K163R mutant also shows impaired recruitment into SGs. SUMOylation seems to impact TDP-43 cytoplasmic localization. Moreover, deSUMOylation promotes formation of small cytoplasmic aggregates of exogenous 35kDa-TDP-43 but has no effect on the already formed 25kDa-TDP-43 aggregates (Maraschi *et al.*, 2021). This may be

due to the fact that the 35kD C-terminal fragment still contains the Lys163. However, an indirect effect mediated by other pathways dependent on SUMOylation cannot be excluded (Maraschi *et al.*, 2021).

In conclusion, TDP-43 post-translational modifications have a key role in TDP-43 proteinopathy; however the role of these modifications in the formation of pathological inclusions still awaits elucidation.

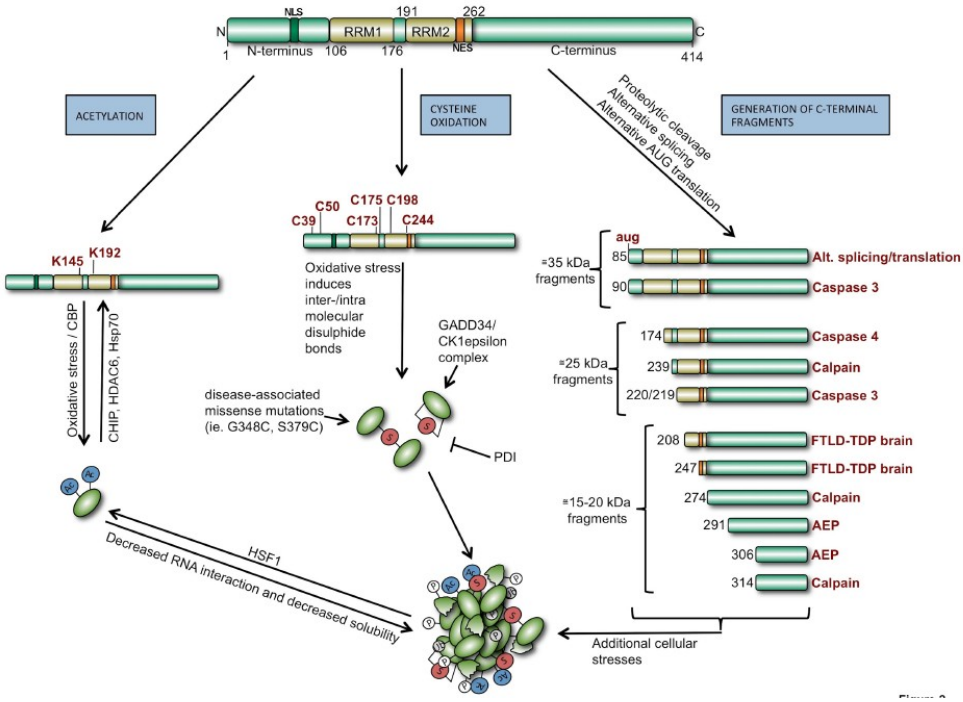


***Figure 3.9. Post-translational modifications of TDP-43.*** *Schematic representation of TDP-43 post-translational modifications: TDP-43 may be cleaved in 35-20kDa fragments by caspase3/7, calpain and asparaginyl endo-peptidase (AEP) (on the right). TDP-43 may undergo phosphorylation, ubiquitination, cysteine oxidation (in the middle), acetylation (on the left) and sumoylation. Free to use for thesis or dissertation (From Buratti, 2018), Copyright Taylor & Francis.*

### *3.2.3 TDP-43 liquid-liquid phase separation properties*

The C-terminal domain (CTD) of TDP-43 has been widely studied over the past few years. TDP-43 CTD contains an intrinsically disordered protein region named low complexity domain (LCD). Weak interactions between LCDs (hydrogen bonds, electrostatic interactions, etc) promote the process of liquid-liquid phase separation (LLPS), which leads to the formation of liquid droplets. This process also underlies the

formation of RNA granules (reviewed in Harrison & Shorter, 2017), (reviewed in Wolozin & Ivanov, 2019). The main feature of these liquid droplets is their highly dynamic properties. Interestingly, the majority of ALS-mutations localize in the C-terminal domain (reviewed in Buratti, 2015; reviewed in Prasad *et al*, 2019) and these mutations affect the ability of TDP-43 to give rise to LLPS (Conicella *et al*, 2016) and may promote aggregation. Moreover, it has been found that the TDP-43 N-terminal domain promotes its oligomerization. Within TDP-43 oligomers the LCDs are separated, thus preventing its aggregation. This findings may explain the high content of CTFs in TDP-43 insoluble inclusions (Afroz *et al*, 2017).

As mentioned above, TDP-43 is recruited to SGs and affects their dynamics (Khalfallah *et al.*, 2018). SGs, like other RNA granules, coalesce through LLPS. Thus, SGs are highly dynamic structures that disassemble after stress relief. For several years it was hypotesized that prolonged stress or repetitive LLPS might promote the conversion of SGs from highly dynamic liquid structures to non-functional solid-like amyloid aggregates that would promote the generation of TDP-43 cytoplasmic inclusions (Dewey *et al*, 2012; reviewed in Wolozin & Ivanov, 2019). This hypothesis was corroborated by some findings showing that TDP-43 inclusions colocalize with SG makers, such as TIA-1 and eIF3 in both cellular model and ALS patient brains (Liu-Yesucevitz *et al*, 2010). However this is in contrast with the findings by Colombrita et al., 2009, which show no colocalization between TDP-43 inclusions and SG markers in spinal cord tissue of ALS patients (Colombrita *et al.*, 2009). However, recent findings show that prolonged stress promotes the generation of TDP-43 insoluble inclusions, which do not colocalize with SGs markers (Gasset-Rosa *et al*, 2019; Mann *et al*, 2019). Interestingly, Mann et al. found that RNA binding, mediated by the RRM domain of TDP-43, reduces the production of insoluble cytoplasmic inclusions. Mann et al., conclude that TDP-43 recruitment to SGs requires RNA binding and makes this protein soluble, whereas TDP-43 outside these RNA compartments is insoluble (Mann *et al.*, 2019). Recently, Ratti et al. found that chronic stress induces SGs formation in IPSCs-derived motor neurons and that TDP-43 is recruited into SGs. However, chronic stress promotes formation of p-TDP-43 aggregates which do not colocalize with SGs (Ratti *et al*, 2020).

Overall, to date it is unclear whether SG assembly is necessary for TDP-43 aggregation, since we cannot rule out the possibility that SGs may represent transient

nucleation sites for TDP-43 aggregation (reviewed in Fernandes *et al*, 2018), (reviewed in Wolozin & Ivanov, 2019). Recent findings by the Cleveland lab have shown that acetylated TDP-43, or TDP-43 carrying mutations in RRMs, generate liquid spherical shell-like structure in the nucleus named anisosome. These anisosomes do not contain RNA, but contain the heat shock protein HSP70, which maintains them in a liquid state. Indeed, in the absence of ATP they collapse into gel-like structures. They hypothesized that these anisosomes may be the precursors of intranuclear and cytoplasmic aggregates of TDP-43 (Yu *et al.*, 2021).

### *3.2.4 TDP-43 gain- and loss of function in ALS*

To date, the mechanism through which TDP-43 mutation or aggregation results in the ALS phenotype has not been completely understood. However, TDP-43 mislocalization seems to play a key role in the cellular toxicity of ALS neurons, through gain and loss-of-function mechanisms (reviewed in Suk & Rousseaux, 2020). As mentioned above, TDP-43 is a predominantly nuclear RBP, which can shuttle between the nucleus and cytoplasm. In the nucleus, TDP-43 is involved in transcription and splicing. TDP-43 binds long clusters of UG-rich introns (Tollervey *et al.*, 2011) and represses the splicing of non-conserved cryptic exons, which otherwise may introduce frameshifts or premature stop codons, leading to nonsense mediated decay. Indeed post-mortem brain tissues of ALS and FTD patients show an impairment in the suppression of these cryptic exons indicating that TDP-43 proteinopathy leads to the loss of its splicing function (Ling *et al*, 2015). Moreover, TDP-43 roles in RNA metabolism are strictly interconnected. For example TDP-43 regulates the splicing of the ribosomal protein S6 kinase 1 (S6K1) Aly/REF-like target (SKAR) which is a component of the exon junction complex and recruits S6K1, thereby facilitating the pioneer round of translation. TDP-43 KD leads to an alternative splice variant of SKAR which is more active, thus increasing the general translation levels (Fiesel *et al*, 2012). Additionally, it has been found that TDP-43 binds preferentially promoters of short genes, regulating their transcription levels (Morera *et al*, 2019). TDP-43 KD promotes chromatin relaxation and increased retrotransposon expression (Liu *et al*, 2019; Morera *et al.*, 2019).

Nuclear loss-of-function is accompanied by TDP-43 cytoplasmic gain-of-function. For example, cytoplasmic accumulation of TDP-43 in a murine model of TDP-FTD leads to

cytoplasmic mislocalization of Histone Deacetylase 1 (HDAC1), a protein involved, among other functions, in DNA repair and neuroprotection. This results in the accumulation of DNA damage during disease progression (Wu *et al*, 2020). Moreover, TDP-43 inclusions seem to trap other mRNAs, thus preventing their translation. Lehmkuhl et al., found that several mRNAs co-immunoprecipitate with TDP-43 and are less associated with ribosomes in a Drosophila model of TDP-43 proteinopathy relative to control. Among these mRNAs they found glypican Dally-like protein (Dlp)/GPC6, which is involved in Wnt signaling. Overexpression of Dlp ameliorated the motor phenotype of a Drosophila model of TDP-43 proteinopathy (Lehmkuhl *et al*, 2021). In a previous work of Zarnescu's group, they showed that TDP-43, irrespective of whether it was wt or mutant retained *futsch* mRNA (the Drosophila ortholog of MAP1B) in a Drosophila model of TDP-43 proteinopathy, thus preventing its axonal localization and translation (Coyne *et al*, 2014).

Interestingly, TDP-43 aggregates can recruit nuclear TDP-43. Indeed, in hippocampal cultured neurons, overexpression of a TDP-43 carrying a mutation of the NLS, generates aggregates in the cytoplasm that sequester endogenous TDP-43 from the nucleus (Winton *et al*, 2008). Similarly, Buratti's lab developed a construct expressing TDP-43 with 12 tandem repeats of the Q/N region of its prion-like domain (namely TDP-12xQ/N). This exogenous protein generates aggregates in the cytoplasm and is able to sequester endogenous TDP-43 causing TDP-43 nuclear clearance (Budini *et al*, 2015; Prpar Mihevc *et al*, 2016).

Moreover, it has been shown that TDP-43 also localizes to the inner mitochondrial membrane and that its mitochondrial localization is increased in transgenic TDP-43 mouse models. There, TDP-43 binds to mRNAs encoding ND3 and ND6, two subunits of the mitochondrial complex I, inhibiting their translation. Thus, increased TDP-43 mitochondrial localization leads to reduced complex I functionality and assembly, thereby promoting mitochondrial dysfunction (Wang *et al*, 2016).

Overall, we can conclude that TDP-43 proteinopathy exerts its pathogenic effect through a combination of nuclear loss-of-function and cytoplasmic gain-of-function. Thus, targeting TDP-43 mislocalization may rescue the ALS phenotype. Walker et al., developed a suppressible mouse model, characterized by overexpression of a mutant TDP-43 lacking the nuclear localization signal (ΔNLS). This line

exhibits TDP-43 cytoplasmic inclusions and a motor phenotype inclusive of neurodegeneration and motor neuron loss in both brain and spinal cord. Interestingly, suppression of the tet-off transgene by doxycycline addition resulted in complete clearing of TDP-43 accumulation in the cytoplasm, promoting its nuclear localization, improving the motor phenotype and stopping the progression of motor neuron loss. These results suggest that the clearance of TDP-43 in the cytoplasm and the increased nuclear localization of TDP-43 allow the CNS to restore its functionality even at an advanced stage of the disease (Walker *et al*, 2015).

However, how to target TDP-43 mislocalization in ALS is a complex issue that still needs to be investigated.

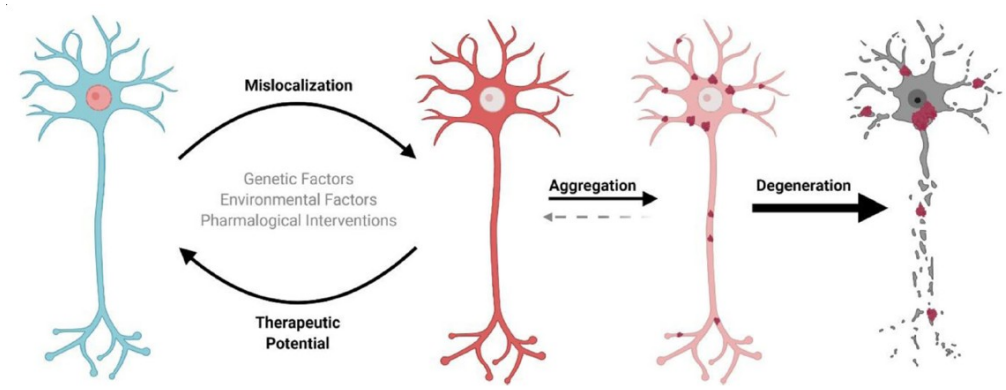


***Figure 3.10. TDP-43 mislocalization promotes neuronal toxicity and degeneration.*** *Representative scheme showing that TDP-43 localizes predominantly in the nucleus of motor neurons in homeostatic conditions. TDP-43 mutations or other environmental factors promote its mislocalization in the cytoplasm and nuclear clearance leading to cytoplasmic inclusions and neuronal degeneration. (From Suk & Rousseaux, 2020). Open access, Copyright: http://creativecommons.org/licenses/by/4.0/.*

### *3.2.5 TDP-43 prion-like transmission*

Recent findings show that pathological TDP-43 inclusions spread within cells through a prion-like transmission in TDP-43 proteinopathies. This mechanism has been widely studied in other neurodegenerative diseases (i.e. α-amyloid and tau in Alzheimer disease and α-synuclein in Parkinson's disease). Indeed, both ALS and FTD have a focal onset that spreads over time. Brettschneider et al. has subdivided the spread of ALS-related damage in 4 stages according to the distribution of phosphorylated TDP-43: in stage 1 pTDP-43 is mainly localized in the primary motor cortex and somatomotor neurons of the brainstem and spinal cord; in stage 2 it localizes also in the reticular formation and

precerebellar nuclei; in stage 3 in the prefrontal neocortex and basal ganglia, and in stage 4 in anteromedial areas of the temporal lobe and hippocampus (Brettschneider *et al*, 2013).

Abundant in-vitro and in-vivo evidence suggests that TDP-43 inclusions may spread from cell to cell, likely explaining the dissemination of damage and clinical signs observed during ALS progression.

Feiler et al., showed that cortical neurons cultured in microfluidic chambers, to separate axons from somata, can spread exogenous luciferase-TDP-43 into H4 human neuroglioma cells co-cultured in the axonal compartment. Moreover cortical neurons in microfluidic chambers show luciferase activity in the soma, when axons were cultured with conditioned medium obtained from HEK293T transfected with luciferase-TDP-43. This demonstrated the cellular uptake of TDP-43 from the conditioned medium. Additionally, they developed two constructs to detect TDP-43 oligomerization: exogenous TDP-43 fused to the N-terminal half of luciferase (TDP-L1) and exogenous TDP-43 fused to the C-terminal half of luciferase (TDP-L2). Once TDP-L1 and TDP-L2 interact, the luciferase activity is reconstituted, allowing the measurement TDP-43 oligomerization. Cortical neurons transduced with TDP-L1 and TDP-L2, cultured with brain cortex lysate obtained from TDP-43 ALS patients, show increased luciferase activity relative to those cultured with control lysate. Thus, brain cortex lysate obtained from ALS patients triggers TDP-43 oligomerization in this in-vitro assay (Feiler *et al*, 2015).

Recently Ding et al. developed a transgenic mouse line, expressing human TDP-43 (hTDP-43) under the Thy1 promoter, in which they injected TDP-43 preformed fibrils into the left caudal part or the left lateral part of the primary motor cortex. At 6 months post-injection, pTDP-43 pathology invaded into bilateral motor cortex, pyramidal tract, lower motor neuron and developed motor dysfunction (Ding *et al*, 2021). The mechanism by which TDP-43 inclusions spread between cells has not been clarified yet; however both exosome and tunneling nanotubes-mediated mechanisms have been hypothesized (Jo *et al*, 2020).

## 3.3 Axonal translation

### *3.3.1 ALS is a distal axonopathy*

Several lines of evidence suggest that ALS is a distal axonopathy, characterized by axonal impairment, which precedes motor neuron degeneration and the onset of clinical symptoms (Moloney *et al*, 2014). Fischer et al. have shown that the $SOD1^{G93A}$ transgenic mouse displays denervation of neuromuscular junctions (NMJ)s and reduced fibers in the ventral roots earlier than loss of motor neuron cell bodies in the lumbar spinal cord (Fischer *et al*, 2004). Interestingly, Gould et al., found that the progeny of the $SOD1^{G93A}$ transgenic mouse bred with the Bax KO mouse, nullisomic for the BAX apoptotic activator, does not show motor neuron loss relative to $SOD1^{G93A}$; Bax $^{+/+}$. However, Bax deletion delays neuromuscular degeneration (Gould *et al*, 2006), while falling short of arresting it. Upper and lower motor neurons, which are the neurons stricken hardest by ALS, have a very long axon that in some cases reaches about 1 meter in length. Under such circumstances the axon accounts for well over 99% of the total neuronal volume (reviewed in Ragagnin *et al*, 2019); for this reason, among others, it is worth considering the key role played by this subcellular compartment in ALS.

### *3.3.2 Axonal transport*

Neurons have a highly polarized morphology, for this reason axonal transport plays a key role on neuronal maintenance by transporting the required cargoes from the soma to the axon terminal. Axonal transport occurs thanks to microtubules, which extend along the axon; to motor proteins, which transport cargoes anterogradely (kinesins) or retrogradely (dyneins); and to cargoes (reviewed in Guo *et al*, 2020).

Radiolabeling pulse chase experiments have demonstrated the presence of two kinds of axonal transport:

- Fast axonal transport, with a speed rate of 50-200 mm/day, which transports membranous organelles as well as transmembrane and secreted proteins.
- Slow axonal transport, with a speed rate of 0.2-10mm/day, which transports cytoskeletal proteins and cytosolic soluble proteins.

Cargoes that use slow axonal transport comprise a slower component, or slow component a (SCa), which consists of cytoskeletal proteins (speed rate: 0.2-1 mm/day) and a slightly

faster slow component, which consists of cytosolic proteins (speed rate: 2-8mm/day) (reviewed in Roy, 2020).

However, published evidence suggest that cytoskeletal proteins of SCa, would be transported as motile polymers in the axons, together with other molecules associated with the cytoskeleton, including microtubule associated proteins. Likewise, cytosolic proteins of SCb may be transported as multiprotein complexes (reviewed in Roy, 2020). Interestingly, it has been found that some cytosolic proteins may be also partially transported by fast axonal transport. For example Tang et al. found that inhibiting the fast axonal transport by treatment with Brefeldin A, which blocks the trafficking between ER and Golgi, affects the anterograde transport of the cytosolic protein synapsin. They propose a model in which synapsin stochastically associates with vesicles and a small fraction of this cytosolic protein remains attached to vesicles and is transported by fast axonal transport (Tang *et al*, 2013).

Axonal transport defects are a common feature of many neurodegenerative disorders; indeed, several genes involved in this process are mutated in neurodegenerative diseases (reviewed in Guo *et al.*, 2020). In particular, mutations of *Profilin-1*, *Tubulin alpha 4A Dynactin-1* and *Kinesin Family Member 5A*, genes involved in cytoskeleton maintenance, have been observed in ALS patients (see section 3.1.2). Defects of axonal transport have been reported in both in-vitro (Alami *et al.*, 2014) and in mouse models of ALS (Bilsland *et al.*, 2010).

However, axonal transport does not only allow the localization of transmembrane and cytosolic proteins in the axon terminal. Indeed, mRNAs and the translation machinery (ribosomal subunits and whole ribosomes) are transported along the axon to translate selected proteins locally, in response to stimuli arising around the axon and presynaptic terminal, as detailed below.

### *3.3.3 RNA localization in the axon*

To date it is well established that mRNAs localize in specific subcellular compartments to compartmentalize gene expression in response to the specific needs of these compartments. It has been found that axons are sites of local translation (reviewed in Jung *et al*, 2012) and that axonal RNA content is different from that of cell bodies (Rotem *et al*, 2017). Briese et al. found that lower motor neuron axons contain both coding and non-

coding RNAs, in particular these axons contain mRNAs encoding proteins involved in translation (i.e translation initiation factors, ribosomes) and actin binding (Briese *et al*, 2016). Even considering the key role played by axonal transport in transferring the majority of proteins that play roles in the axon, local mRNA translation can be highly beneficial for several reasons, among which:

- Functionally related mRNAs may be spatially restricted to an appropriate subcellular location.
- It ensures a fast regulation of on-site translation, in response to local stimuli, instead of signaling a given requirement to the nucleus, sometimes at considerable distances, and then relying on the transport of newly synthesized proteins to the subcellular compartment of choice.
- It allows energy saving since mRNAs can be translated multiple times, generating several proteins, which is more efficient than transporting each copy of the protein individually (reviewed in Martin & Ephrussi, 2009).

How these mRNAs localize in the axon is an intriguing question that still needs to be further addressed. Several lines of evidence suggest that compartmentalized transcripts contain cis-actin elements mainly localized in the 3'UTR (reviewed in Turner-Bridger *et al*, 2020). For example *Importin β1* has got two isoforms which generate by alternative polyadenylation site: one with a short 3'UTR, mainly localized in the cell body, and one with a long 3'UTR, localized in the axon; the latter is involved in the retrograde response to axonal injury (Perry *et al*, 2012).

Messenger RNA localization is mediated by RBPs, which recognize the nucleotide sequence and/or the secondary structure of the cis-acting elements. A consensus motif has yet to be identified in axonal mRNAs: Martinez et al. have analyzed both cell body and axonal transcriptome of rat embryonic dorsal root ganglia (DRG) to identify consensus motifs among cell body-specific transcripts and axonal ones. They found that cell body transcripts contain a motif recognized by the RBP Pumilio2 (Pum2) but they did not find any consensus motif among axonal transcripts. They demonstrated that Pum2 modulates the axonal transcriptome, during development, by retaining mRNAs containing Pum2 binding elements in the soma (Martinez *et al*, 2019).

As mentioned before, mRNAs and RBPs generate complexes named messenger ribonucleoprotein particles (mRNPs) (reviewed in Turner-Bridger *et al.*, 2020). mRNPs

are membraneless organelles that assemble through LLPS, a process that consists of demixing of soluble components from the cytoplasm and generation of complexes with liquid-like properties. These complexes, indeed, are highly dynamic, as they can recover after FRAP photobleaching, and they are spherical at rest but undergo deformation when subjected to fast axonal transport, compatible with the effect of superficial tension (reviewed in Formicola *et al*, 2019).

Messenger RNP composition is very heterogeneous and the majority of mRNPs are translationally inactive; however translation can be inactivated at a stage preceding the recruitment of the pre-initiation complex, as shown by the interaction with the cap-binding complex, or during elongation, by the presence of stalled ribosomes (reviewed in Formicola *et al.*, 2019). Moreover, several lines of evidence suggest that mRNAs are associated with RBPs generating "RNA regulons", consisting of cohorts of mRNAs regulated by the same RBPs, encoding functionally related proteins, e.g. factors involved in axonal growth (Lee *et al*, 2018) or axonal viability (Cosker *et al*, 2016). In this way axons are able to functionally organize mRNA transport and translation in response to external stimuli or physiological conditions. However we cannot exclude that any given mRNA be recruited as part of different RNA regulons, being transported in different ways depending on the function it serves (reviewed in Dalla Costa *et al*, 2021).

Messenger RNPs travel along the axon through microtubule-mediated transport. In fact nocodazole treatment, a microtubule depolymerizing agent, dramatically disrupts the transport of fluorescently-tagged *β-Actin* in the axon of *Xenopus* retinal ganglion cells (RGC) (Leung *et al*, 2018). The transport along microtubules is mediated by microtubule-associated motor proteins: kinesin moves its cargo towards the plus-end and dynein towards the minus-end. However, recent findings indicate that mRNP transport along microtubules may be also mediated by hitchhiking on intracellular organelles. Cioni et al. found that many mRNPs associate with endosomes positive for Rab7a, a marker of late-endosomes, in the axons of *Xenopus* RGCs. They showed that these mRNP granules are larger and more intense than those not associated with endosomes, suggesting they contain a heavier mRNA cargo. However the majority of mRNPs move towards the axon in an endosomal-independent manner. Rab7a-positive endosomes colocalize with puromycin, an aminoacyl-tRNA analog used to detect actively translated polypeptides, suggesting that late-endosomes are sites of intra-axonal protein synthesis. Moreover these

intra-axonal protein synthesis sites often colocalize with mitochondria, which may sustain translation of mRNAs involved in mitochondrial maintenance (Cioni *et al*, 2019).

Endosomes are not the only intracellular organelles capable of transporting mRNPs along the axon. In fact Liao et al. found that lysosomes are also able to hitchhike mRNPs along the axons of rat cortical neurons and neurons derived from human IPSCs. Annexin A11 (ANXA11) tethers mRNPs to lysosomes allowing their transport (Liao *et al*, 2019). Interestingly ANXA11 mutations have been found in familial cases of ALS (Zhang *et al*, 2018) and expression of ANXA11 carrying ALS-linked mutations disrupt mRNP hitchhiking on lysosomes in rat cortical neurons (Liao *et al.*, 2019).

Furthermore, also pre-miRNAs hitchhike on late-endosomes and lysosomes to reach the axon tip, where they may be processed to generate miRNAs. Accordingly, pre-miRNAs processing machinery components (i.e. Dicer, Ago2) were detected in axonal tips, where they are ready to generate mature miRNAs in response to stimuli (Corradi *et al*, 2020).

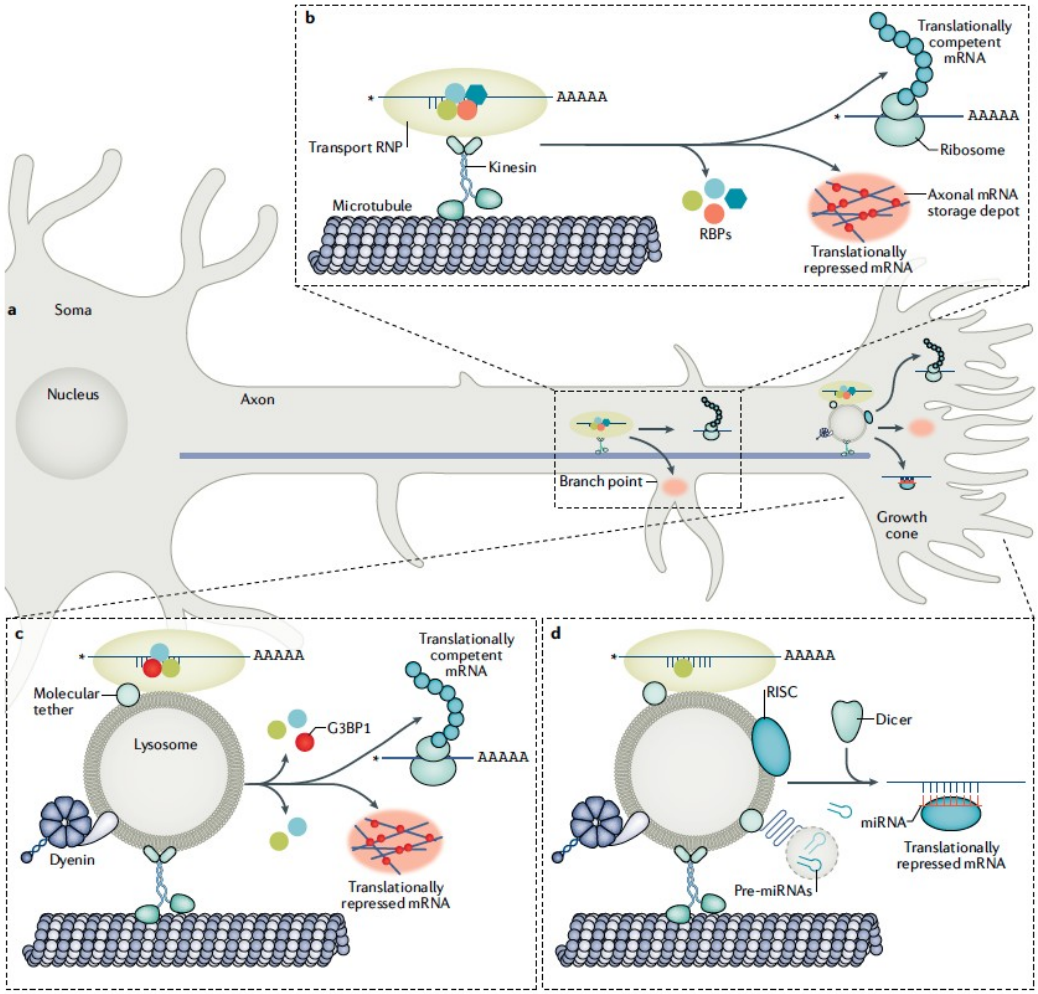


***Figure 3.11. mRNA transport along the axon.*** *Schematic representation of the mechanisms that mediate mRNA transport along the axons. mRNAs interact with RBPs generating mRNP granules(a). These mRNP granules may be transported directly by motor proteins (b) or through association with intracellular organelles, i.e, lysosomes or late-endosomes (c). Furthermore, pre-miRNAs are also transported by lysosome hitchhiking together with the pre-miRNA processing machinery (d). (From Dalla Costa et al., 2021). Reprinted by permission from Copyright Clearance Center (license number: 5235290907672) Springer Nature, Nature Reviews Neuroscience, "The functional organization of axonal mRNA transport and translation", Irene Dalla Costa et al. 2020, advance online publication, 7 Dec 2020 (doi: 10.1038/s41583-020-00407-7).*

Interestingly, several transcripts encoding transmembrane and secreted proteins were identified in the axons, suggesting the presence of a peculiar secretory pathway (reviewed in Gonzalez *et al*, 2018). Whereas smooth endoplasmic reticulum (SER) is found in the axon (Wu *et al*, 2017), no axonal Golgi structures have been identified there, however, despite the presence of Golgi markers (Merianda *et al*, 2009). The current hypothesis is

that mixed-identity organelles and ER-endosomal pathway may support the secretory pathway in the axon (reviewed in Gonzalez *et al.*, 2018).

### *3.3.4 Axonal protein synthesis in ALS*

For several years axonal translation has been considered an exceptional process restricted to developing or regenerating axons. However, neurons live for decades in the human brain and some project very long axons. For this reason, axonal proteins need to be replenished throughout a neuron's lifetime (reviewed in Kim & Jung, 2020) and even considering the well-established role of axonal transport in this process, local protein synthesis exhibits many advantages, as detailed above. Recent evidence suggests that axonal translation has a fundamental role also in mature axons (Ostroff *et al*, 2019; Shigeoka *et al*, 2016). Shigeoka et al., used a knock-in mouse model expressing a ribosomal protein of the large subunit (Rpl22) fused to a hemagglutinin (HA) tag. The expression of this tagged ribosome is mediated by a Cre-recombinase. This mouse model allows the immunoprecipitation of tagged-ribosomes with bound mRNAs from a specific compartment; this procedure is named translating ribosome affinity purification (TRAP) (Sanz *et al*, 2009). Through this model they analyzed the axonal translatome (i.e. transcripts associated with tagged ribosomes) in developing and mature RGC axons. They found that ribosome-engaged transcripts are more abundant in developing axons than mature axons, suggesting that axonal mRNA translation decreases during neuronal maturation. As expected, developing axons mainly contain translated transcripts involved in neuron axonogenesis and growth, while mature axons are enriched for transcripts involved in synaptic transmission. Mitochondrial-related transcripts are abundant at both stages (Shigeoka *et al.*, 2016). Also Ostroff et al., used TRAP assay to identify the axonal translatome of cortical axons projecting into the amygdala in adult rats, further demonstrating that axonal translation occurs in mature axons and is regulated by neuroplasticity: in fact, they found that axonal translatome changes occur in response to learning (Ostroff *et al.*, 2019).

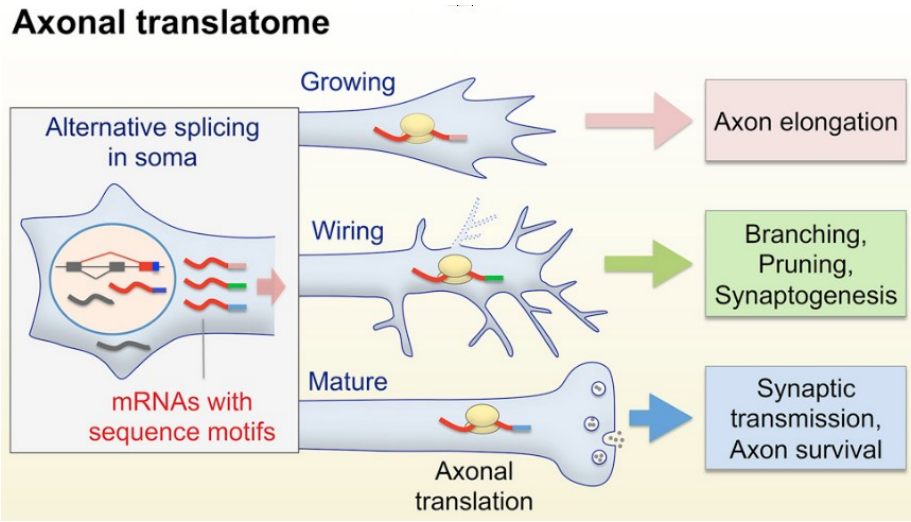


***Figure 3.12. Axonal translation occurs in both developing and mature axons.*** *Representative scheme showing that axonal translation occurs in developing axons, wiring and mature axons and the axonal translatome changes in response to the specific needs of this compartment: axonal elongation, branching and axonal maintenance respectively. (Adapted from Shigeoka et al., 2016). Open access article distributed under the terms of the Creative Commons CC-BY license.*

Considering the role of axonal translation in mature axonal maintenance and that a wide number of ALS-related genes encode RBPs, it is worth considering altered axonal translation as an emerging pathophysiological mechanism. Briese et al., found that TDP-43 loss of functions leads to decreased axonal translation in cultured spinal motor neurons (Briese *et al.*, 2020). Moreover, Lopez-Erauskin et al., showed that axonal translation is downregulated in the sciatic nerve of a FUS-mutated mouse model (Lopez-Erauskin *et al.*, 2018).

As mentioned in section 3.2.1, TDP-43 loss of function impairs the transport of mRNAs encoding ribosomal proteins (Nagano *et al.*, 2020). Indeed, recent findings showed that ribosomal proteins are translated in the axon and incorporated in pre-existing ribosomes, in particular those mRNAs encoding proteins exposed on the ribosomal surface (Fusco *et al*, 2021; Shigeoka *et al*, 2019). In addition, as mentioned in section 3.2.4, Zarnescu's lab demonstrated that, in a *Drosophila* model of TDP-43 proteinopathy, TDP-43 sequesters many of its mRNA targets in insoluble aggregates, thus preventing their translation and leading to reduced levels of the corresponding proteins at NMJ (Coyne *et al*, 2017; Coyne *et al.*, 2014; Lehmkuhl *et al.*, 2021).

Thus, altered axonal translation in ALS may be the result of defective axonal localization of mRNAs due to RBP aggregates, and ribosomal dysfunction may be due to

reduced transport of ribosomal protein mRNAs that normally ensure ribosomal turnover (reviewed in Nagano & Araki, 2021).

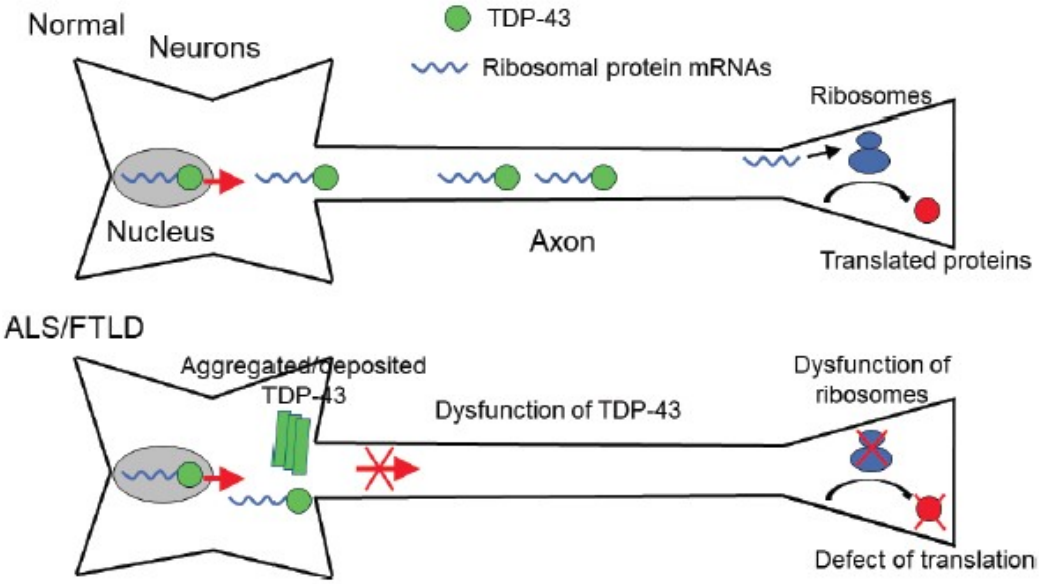


***Figure 3.13. ALS affects axonal localization of mRNAs in the axons.*** *Representative scheme showing that in healthy neurons TDP-43 mediates axonal transport of its mRNA targets allowing their axonal translation. Instead in ALS motor neurons insoluble aggregates of TDP-43 impairs the axonal localization of these targets, including those encoding ribosomal protein, thus preventing their axonal translation and the turnover of axonal ribosomes. (From Nagano & Araki, 2021). Free to use for non-commercial purpose, Copyright Creative Commons AttributionNonCommercial 4.0 International (CC BY-NC 4.0). https://creativecommons.org/licenses/by-nc/4.0/.*

## 4. Aim of the work

Amyotrophic lateral sclerosis is a neurodegenerative disease that leads to progressive paralysis and death. To date, no effective treatment is available for these patients, mainly due to our sketchy grasp of the mechanisms underlying this disorder. Since several ALS-related genes encode RNA binding proteins (RBP), altered RNA metabolism seems to play a key role in this disorder. Several lines of evidence suggest that ALS is a distal axonopathy; because mRNA localization and translation in the axon are involved in the development, function and maintenance of the axon and presynaptic terminal, we hypothesize that defects of RNA metabolism in the axon may at least partially explain the distal axonopathy observed in ALS.

The aim of our project was to identify mRNAs whose axonal levels are altered in an in-vitro model of ALS-related neuronal damage. First, we have developed an in-vitro model of upper motor neurons, a less intensively unexplored field in ALS research, since most studies have focused on lower motor neurons. Our model consists of cortical neuron primary cultures overexpressing the RBP, TDP-43 (wt or carrying a familial ALS mutation, A315T). Our cellular models have been assessed for features of ALS neuronal damage, such as the presence of TDP-43 cytoplasmic aggregates, proteolytic fragments, TDP-43 ubiquitination and phosphorylation and mRNA granule formation, comparing these findings with a mouse model of TDP-43 proteinopathy. Next, thanks to a collaboration with Gabriella Viero's lab in Trento, we have analyzed the results of RNA-sequencing of polysome-engaged and sub-polysomal mRNAs in the axon of overexpressing neurons and controls. This was achieved by physically separating axons from cell bodies in microfluidic chambers. Polysome-engaged mRNAs and mRNAs not associated to polysomes (sub-polysomal), from both axonal and whole-cell compartment, were separated by a miniaturized sucrose gradient protocol and sequenced. Our analysis has focused especially on differentially expressed axonal mRNAs important for axonal maintenance and function. Our results lay a foundation for the study of early stages of ALS neuronal damage and will be exploited to develop novel therapeutic strategies for the early treatment of ALS.

# 5. Results

## 5.1 Functional and molecular characterization of an in-vitro model of ALS neuronal damage

### *5.1.1 Cortical neuron primary cultures established from E14.5 mouse embryos do not contain glial cells*

As mentioned in the Introduction, ALS mainly affects upper and lower motor neurons. To generate an appropriate in-vitro model to study ALS-related neuronal damage in upper motor neurons, we established primary cultures of mouse cortical neurons enriched in glutamatergic neurons of layers V and VI of the brain cortex. For this reason, we cultured neurons isolated from the cerebral cortex of mouse embryos harvested at 14.5 days post conception (E14.5), from here on referred to as E14.5 CN cultures. Glial cells appear after E14 embryonic stage, with a peak after birth, and continues until 14 days after birth (Sauvageot & Stiles, 2002). To verify the absence of glial cells in E14.5 cortical neuron primary cultures, we performed immunofluorescent staining on neurons after 3 days-in-vitro (3 DIV) with the following glia specific antibodies:

- Glial fibrillary acidic protein (GFAP), a marker of astrocytes.
- Oligodendrocyte Marker O4 (O4), a marker of oligodendrocyte precursors.
- Ionized calcium binding adaptor molecule 1 (IBA1), a marker of microglia.

Neurons were immunostained with a TuJ1 antibody to visualize β3-tubulin, which is a neuronal-specific protein of the cytoskeleton, and with DAPI, to detect nuclei.

Sagittal sections of mouse cerebellum 8 days postnatal (P8) and frontal sections of E18.5 mouse mesencephalon were used as positive controls for the above antibodies.

Immunostaining with anti-GFAP shows that GFAP-positive cells are not detectable in E14.5 CN cultures (Fig. 5.1A), while they are present in the P8 mouse cerebellum (Fig. 5.1A').

Likewise, these E14.5 CN cultures do not contain O4-positive cells (Fig. 5.1B) nor IBA1-positive cells (Fig. 5.1C), thus confirming the absence of oligodendrocyte precursors and microglial cells, respectively.

These results confirmed that cortical neuron primary cultures established from E14.5 mouse embryos contain a negligible contribution of glial cells.

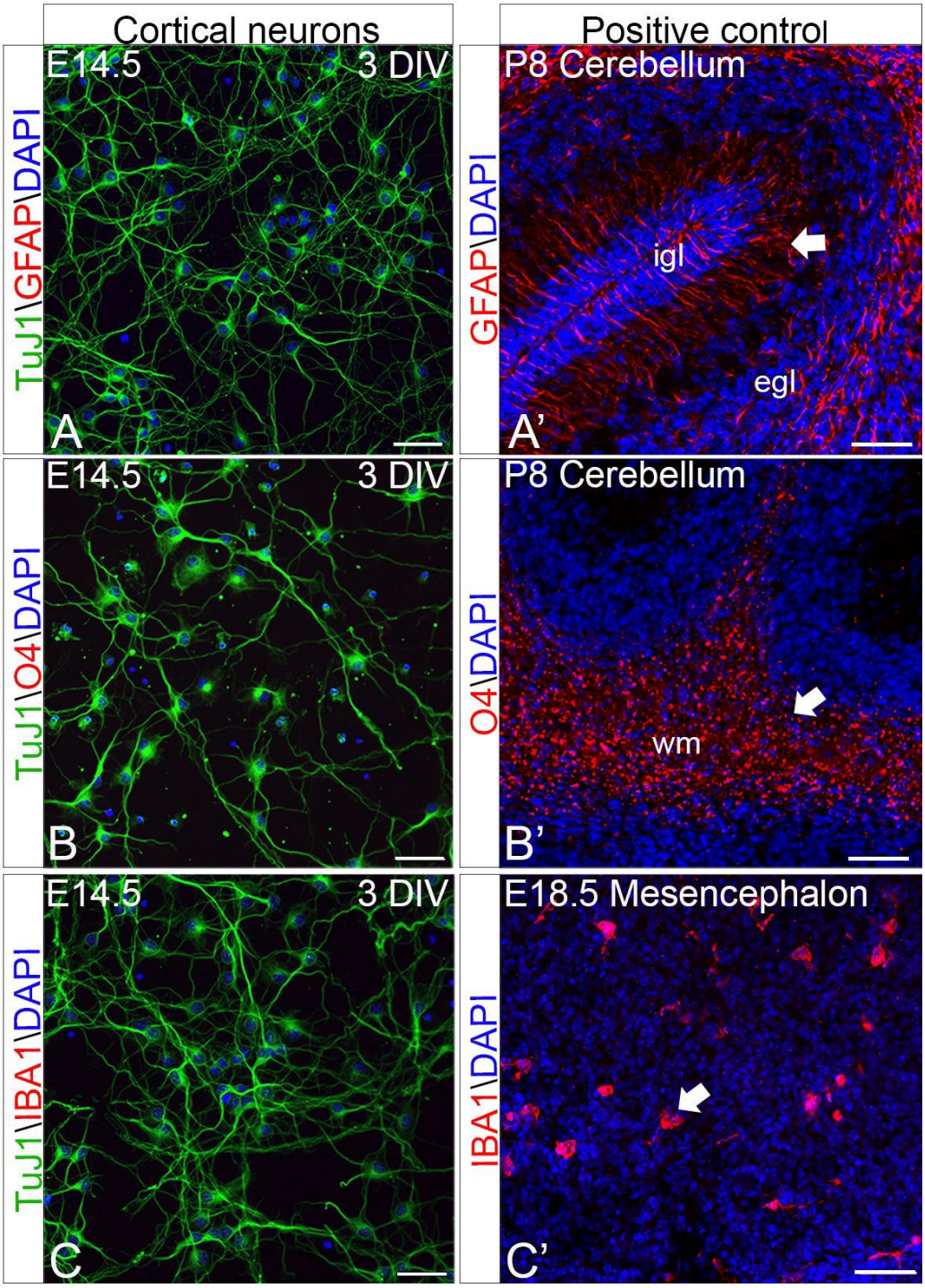


***Figure 5.1. E14.5 CN cultures do not contain glial cells.*** *(A,B,C) Immunofluorescence of E14.5 CN cultures. Glial markers such as GFAP(A), O4(B) and IBA1(C) (in red) are not present in these primary cultures. Green: TuJ1; blue: DAPI. (A',B',C') Immunofluorescence of cerebellar or mesencephalic sections as positive controls of the antibodies used on cell cultures. Sagittal sections of P8 mouse cerebellum show GFAP-positive signals in radial glia (A', white arrow) and O4-positive cells in white matter (B', white arrow). A coronal section of E18.5 mouse*

*mesencephalon shows IBA1-positive microglial cells (C', white arrow). (igl: internal granular layer; egl: external granular layer; wm: white matter) (Size bar: 50 μm).*

### *5.1.2 E14.5 CN cultures are enriched in glutamatergic neurons of V and VI layers of brain cortex and contain a minimal amount of GABAergic neurons*

As mentioned in section 3.1.1, during brain development the deepest layers of the cortex (V-VI) are generated earlier than superficial ones, thus E14.5 CN cultures are expected to be enriched in glutamatergic neurons of neocortical layer V (Fig. 3.3). To this end, we immunostained E14.5 CN cultures with anti-T-Box Brain Transcription Factor 1 (Tbr1) antibody, which is an early marker of glutamatergic neurons (Fig. 5.2A) and anti-COUP-TF-interacting protein 2 (CTIP2) antibody, which is a transient marker of cortical neurons of the V and VI layer of the cortex (Fig. 5.2B). Then we counted Tbr1-positive cells and CTIP2-positive cells relative to total cell number.

As shown in the graph in Fig. 5.2C, Tbr1-positive cells represent about 90% of total cells and CTIP2-positive cells amount to 60% of total cells in our primary cultures.

GABAergic neurons start their tangential migration at E12 and complete it after birth (reviewed in Corbin & Butt, 2011). To assess the GABAergic component of these cultures, we immunostained neuronal cultures with an antibody specific for glutamic acid decarboxylase-65 (GAD65), a marker of GABAergic neurons. Cortical neurons, established from mouse embryos at a later developmental stage (E17.5), were used as positive control of GAD65 antibody.

As shown in Fig. 5.2D, E14.5 CN cultures contain few if any GAD65-positive cells, while these cells are present in E17.5 mouse cortical neurons (Fig. 5.2E).

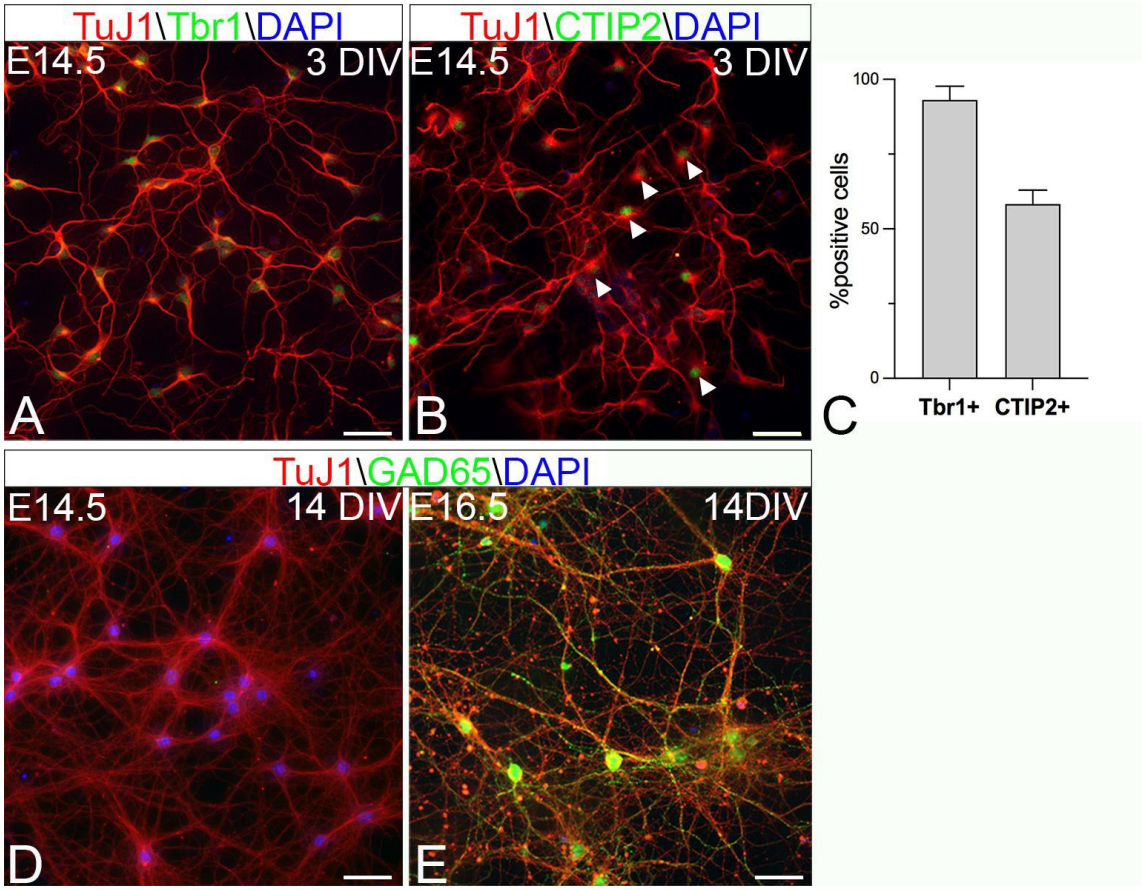


***Figure 5.2. E14.5 CN cultures are strongly enriched in glutamatergic cells of the V layer of the brain cortex and do not contain any GABAergic cells.*** *(A,B,D) Immunofluorescence of E14.5 CN cultures show the presence of Tbr1-positive glutamatergic cells (A, green) and of CTIP2-positive neurons of the V layer of the cortex (B, green, white arrowheads) and the absence of GAD65-positive GABAergic neurons (D, lack of green signal). (E) Immunofluorescence of E17.5 cortical neurons shows the presence of GAD65-positive cells as a positive control of GAD65 antibody (in green). TuJ1: in red; DAPI: in blue. (Size bar: 50µm).(C) The graph shows the percentage of Tbr1-positive cells, which is about 90% of total cells (first column), and the percentage of CTIP2-positive cells, which is about 60% of total cells (second column) (Mean ±SEM, n=3).*

In summary, E14.5 CN cultures are strongly enriched in glutamatergic neurons of the V layer of the brain cortex and contain a negligible percentage of glial cells and GABAergic neurons. Carefully selecting a homogeneous population of cortical neurons is a requisite for the success of transcriptomic analyses described later. While cortical neurons of cortical layer V are present even earlier than E14.5, we chose to establish E14.5 primary cultures as a tradeoff between the ease of establishing primary cultures from the murine telencephalic cortex and the goal of enriching our cultures in glutamatergic cells. All experiments described in the following sections made use of neuronal cultures established at E14.5.

### *5.1.3 Cortical neuron overexpressing tRFP-TDP-43 (wt or A315T) show cytoplasmic accumulation of the exogenous protein*

In order to develop an in-vitro model of ALS-related neuronal damage, we transduced these neurons with lentiviral particles in order to overexpress a recombinant protein consisting of human TDP-43, wild type or carrying an ALS-mutation (A315T (Gitcho *et al*, 2008)) fused at N-terminal with turbo Red Fluorescent Protein (tRFP). Neurons overexpressing tRFP only were used as control cells. Hereon, these neurons will be named as following:

- ctrl: control neurons overexpressing tRFP or transduced with a nonrecombinant lentivirus.
- wtTDP: neurons overexpressing tRFP-hTDP-43 wt.
- mutTDP: neurons overexpressing tRFP-hTDP-43 (A315T).

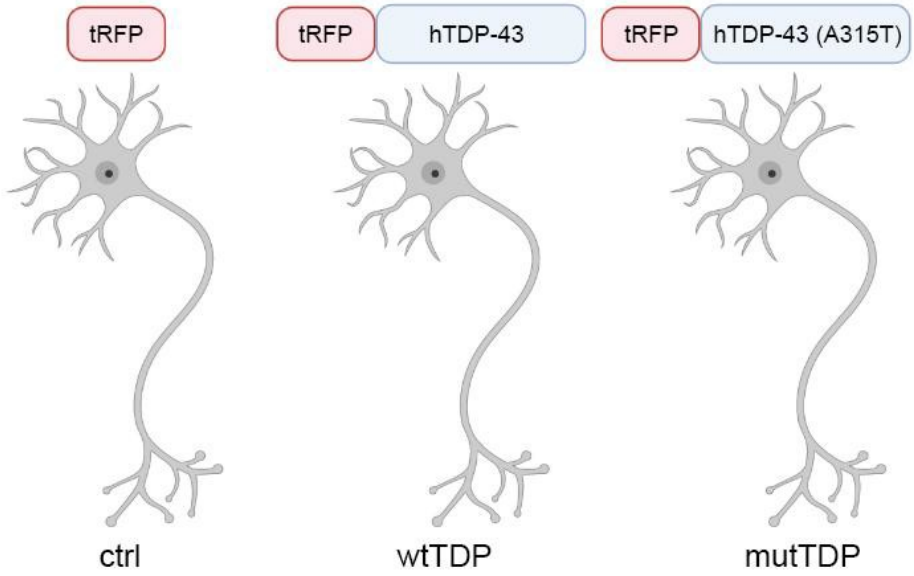


***Figure 5.3. In-vitro model of ALS-related neuronal damage.*** *Representative scheme showing the three neuronal populations, obtained by lentiviral transduction, that will be analyzed in this project: control neurons overexpressing tRFP only (named as "ctrl", on the left); neurons overexpressing human wt TDP-43 N-terminally fused with tRFP (named as "wtTDP", in the middle) and neurons overexpressing hTDP-43 carrying a mutation found in familial cases of ALS (A315T) fused at N-terminal with tRFP (named as "mutTDP", on the right). Created with BioRender.com.*

First, to characterize this in-vitro model, we quantified the level of TDP-43 by western blotting with proteins extracted from primary neuronal cultures transduced with ctrl, wtTDP and mutTDP lentiviruses. The membrane was incubated with a TDP-43 antibody

reactive with human and murine TDP-43, to detect both endogenous and exogenous TDP-43; the anti-Calnexin antibody was used as a loading control.

As shown in Fig. 5.4A, anti-TDP-43 antibodies recognize a 48kDa band, which consists of the endogenous murine TDP-43 (mTDP-43) presents in all three neuronal populations, and a 75kDa band in wtTDP and mutTDP neurons, which represents the exogenous TDP-43(tRFP-hTDP-43).

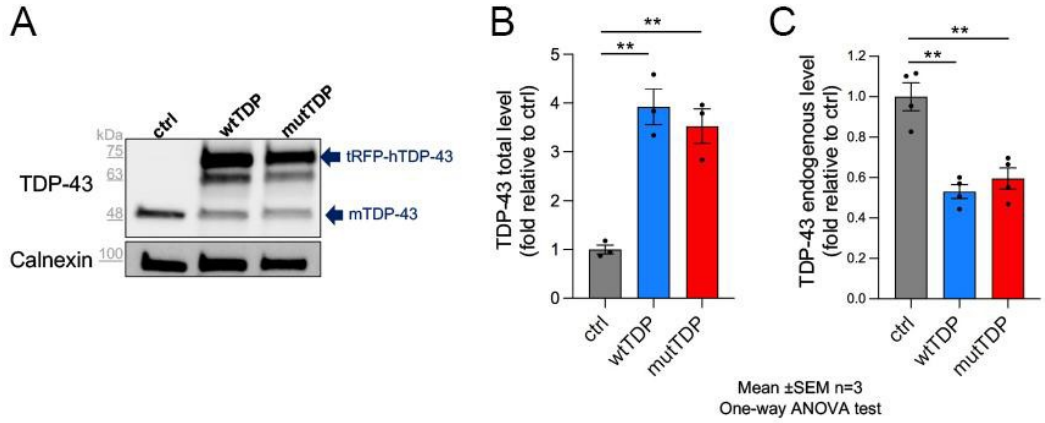


***Figure 5.4. wtTDP and mutTDP neurons have TDP-43 levels 4 times higher than control neuron.*** *(A) Western blot of protein extracts from wtTDP, mutTDP and ctrl neurons. The 48kDa band is the TDP-43 endogenous protein (mTDP-43), which is present in all three cellular populations, while the 75 kDa band, present in wtTDP and mutTDP protein extracts, represents the exogenous TDP-43 (tRFP-hTDP-43). The picture also shows the levels of Calnexin used as loading control. (B) Western blot quantification of total levels of TDP-43, both endogenous and exogenous, in wtTDP (in blue) and mutTDP (in red) relative to ctrl neurons (in gray). In both wtTDP and mutTDP neurons, TDP-43 total levels are about 4 times higher than ctrl neurons. (C) Western blot quantification of endogenous levels of TDP-43, in wtTDP (in blue) and mutTDP (in red) relative to ctrl neurons (in gray). Levels of endogenous TDP-43 in wtTDP and mutTDP neurons are half than ctrl, maybe due to TDP-43 autoregulation mechanisms (Mean ±SEM, n=3, One-way Anova test, **p-value <0.01).*

We quantified the total TDP-43 protein levels considering the sum of endogenous and exogenous TDP-43 for wtTDP and mutTDP neurons and endogenous only for ctrl neurons, and normalized it to Calnexin protein levels. Then we calculated the fold change of TDP-43 protein levels relative to ctrl (Fig. 5.4B). We observed that TDP-43 protein levels in wtTDP and mutTDP neurons are 4 times higher than in ctrl neurons (Fig. 5.4B).

It is worth noting that the levels of endogenous TDP-43 in wtTDP and mutTDP neurons are lower than those of ctrl (Fig 5.4C). This can be explained by the autoregulation mechanism described for TDP-43 (Avendano-Vazquez *et al.*, 2012; Ayala *et al.*, 2011), see section 3.2.1 of the Introduction).

As mentioned in the Introduction, under physiological conditions TDP-43 is predominantly nuclear, however, since it has some fundamental cytoplasmic functions, it shuttles between nucleus and cytoplasm (Ayala *et al.*, 2008). TDP-43 nuclear delocalization and its cytoplasmic accumulation are key pathological features of ALS neurons in 97% of patients, both sporadic and familial, except for familial cases carrying SOD1 or FUS mutations (reviewed in Suk & Rousseaux, 2020).

Thus, since TDP-43 mislocalization is a hallmark of ALS neurons, we assessed the localization of exogenous TDP-43 in wtTDP and mutTDP neurons. We performed immunofluorescence on wtTDP and mutTDP neurons, at 14 DIV, with anti-TDP-43 antibody, which is able to detect both human and murine TDP-43, to compare TDP-43 localization in wtTDP and mutTDP neurons relative to ctrl.

As shown in Fig. 5.5, exogenous fluorescent tagged-TDP-43 is mainly localized in the cytoplasm of both wtTDP and mutTDP neurons (Fig. 5.5B-C) generating aggregates, while endogenous TDP-43 localizes predominantly in the nucleus of ctrl neurons (Fig. 5.5A'). This phenotype observed in wtTDP and mutTDP neurons is fully penetrant.

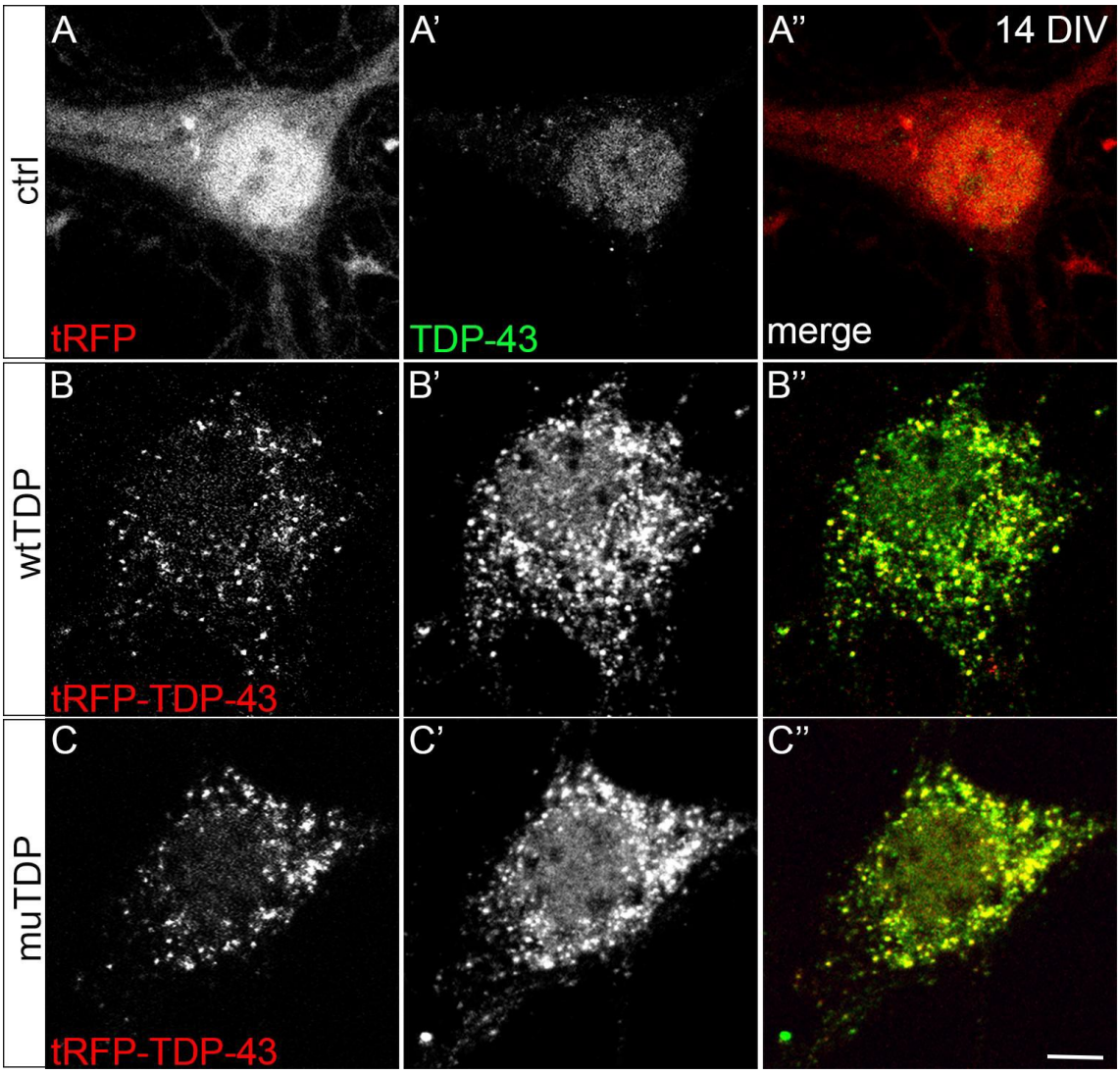


***Figure 5.5. Exogenous TDP-43 mainly localizes in the cytoplasm.*** *(A-C'') Immunofluorescence of ctrl, wtTDP and mutTDP neurons, cultured at 14 DIV reveals that exogenous TDP-43 localizes in the cytoplasm, generating aggregates (B,C). tRFP alone has a diffused pattern in both nucleus and cytoplasm in ctrl neurons (A). Endogenous TDP-43 in ctrl neurons has a predominantly nuclear localization as expected (A'), while the total amount of TDP-43, endogenous and exogenous, has a strong cytoplasmic localization in wtTDP and mutTDP neurons (B',C'). (Size bar: 5µm).*

Overall, we can conclude that wtTDP and mutTDP neurons show TDP-43 expression levels 4-times higher than ctrl cells and that exogenous TDP-43 accumulates in the cytoplasm of those neurons, recapitulating one of the main features of ALS neurons (reviewed in Suk & Rousseaux, 2020).

### *5.1.4 wtTDP and mutTDP neurons display TDP-43 proteolytic fragments, which, together with full-length exogenous TDP-43, localize in the insoluble cytoplasmic fraction*

As mentioned in section 3.2.2 of the Introduction, one of the hallmarks of TDP-43 proteinopathy is the presence of TDP-43 C-terminal fragments (reviewed in Buratti, 2018). The main fragments are about 25 and 35kDa, however their molecular weight can vary since several different mechanisms contribute to the generation of these fragments (reviewed in Buratti, 2018).

Thus, we analyzed whether TDP-43 overexpression generates TDP-43 fragments in wtTDP and mutTDP neurons. To this end, we performed western blot analysis with protein lysates of ctrl, wtTDP and mutTDP neurons, cultured at 14 DIV. The membrane was incubated with an anti-TDP-43 antibody. As shown in Fig. 5.6A, wtTDP and mutTDP neurons produce TDP-43 proteolytic fragments of about 35- and 30kDa, which are not found in ctrl neurons.

Another feature of ALS neurons is the presence of insoluble TDP-43 aggregates, which can be phosphorylated and ubiquitinated (Arai *et al.*, 2006; Neumann *et al.*, 2006). Thus, we asked whether exogenous TDP-43 localizes in the insoluble fraction in wtTDP and mutTDP neurons. To this end, we set up a protein subcellular fractionation protocol, to separate nuclear fraction from soluble and insoluble cytoplasmic fractions, of untransduced neurons cultured at 14 DIV (see Materials and Methods). The proteins extracted from the different fractions were processed for western blotting and the membrane was incubated with the following antibodies (Fig. 5.6B):

- anti-TDP-43, a marker of the nuclear fraction.
- anti-Calnexin, a transmembrane protein of the endoplasmic reticulum, enriched in the insoluble cytoplasmic fraction, which also contains membranes.
- anti-GAPDH, a cytosolic protein which is present in both soluble and insoluble cytoplasmic fractions, thus revealing an incomplete separation of the soluble fraction from the insoluble one.
- anti-Histone H3 which is enriched in the nuclear fraction and insoluble cytoplasmic fraction.

The presence of Histone H3 in the insoluble cytoplasmic fraction can be explained by the presence of insoluble chromatin in this fraction which may co-precipitate with cytoplasmic insoluble pellet and by the fact that histones have a high affinity for common plastic tubes.

Once assessed the adequacy of the subcellular fractionation protocol, we performed it on 14 DIV ctrl, wtTDP and mutTDP neuron extracts. The membrane was incubated with anti-TDP-43 antibody. As shown in Fig. 5.6C, endogenous TDP-43 is localized in all fractions, but exogenous TDP-43 is enriched in the insoluble cytoplasmic fraction. After a long exposure, the 35kDa TDP-43 band appears in the soluble cytoplasmic fraction and, predominantly, in the insoluble fraction.

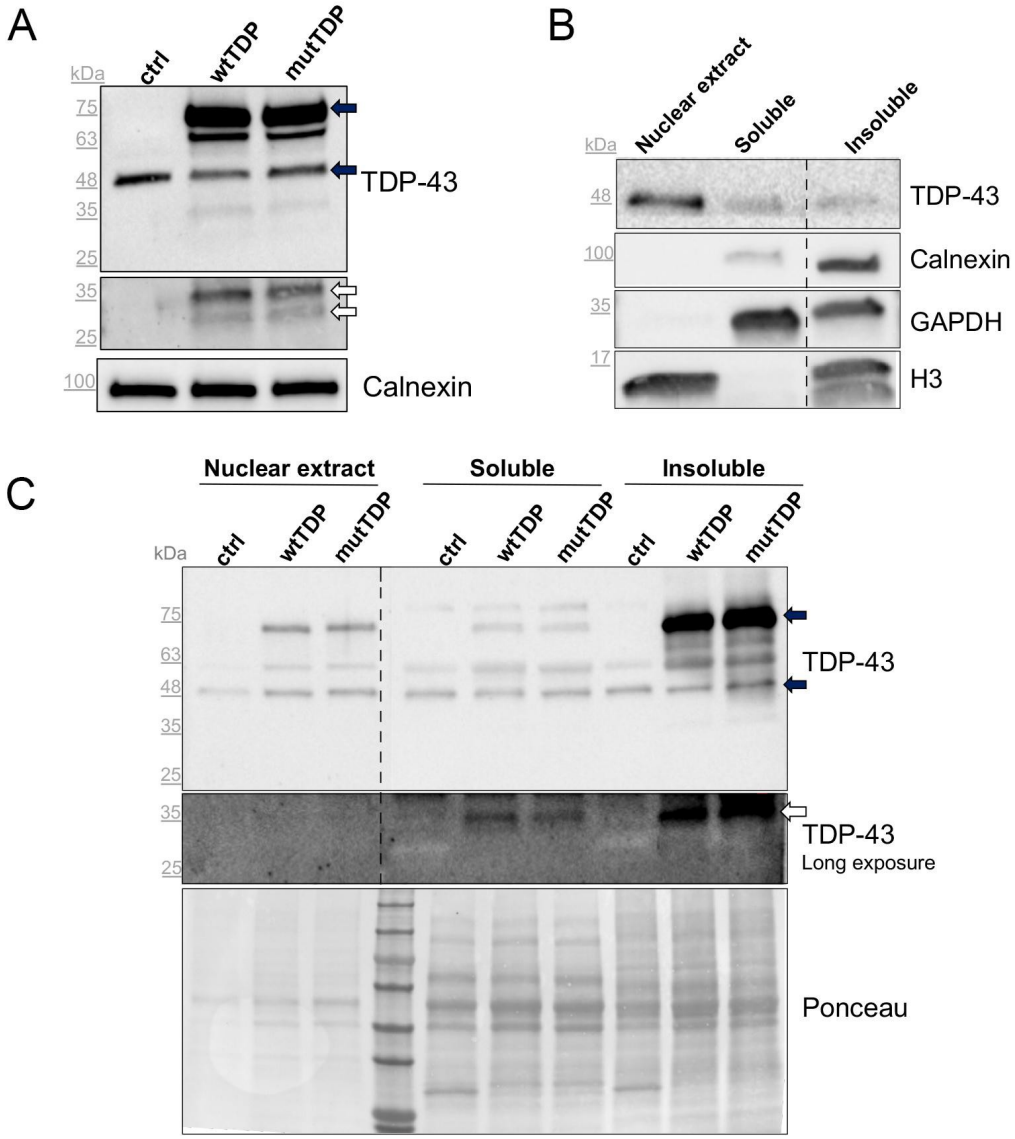

***Figure 5.6. wtTDP and mutTDP neurons produce TDP-43 proteolytic fragments, which, together with full-length exogenous TDP-43, mainly localize to the insoluble cytoplasmic fraction.*** *(A) Western blot of ctrl, wtTDP and mutTDP protein lysates shows the presence of TDP-43 proteolytic fragments, of about 35 and 30kDa, after a long exposure (white arrows). Calnexin was used as loading control. Blue arrows indicate exogenous (75kDa) and endogenous (48kDa) full-lenght TDP-43. (B) Western blot of the subcellular fractions extracted from untransduced cortical neurons at 14 DIV was used as a control of the fractionation protocol. TDP-43 is mainly enriched in the nuclear fraction. Calnexin, a transmembrane protein of the endoplasmic reticulum, is enriched in the insoluble cytoplasmic fraction. The cytoplasmic protein GAPDH mainly localizes in the soluble and insoluble cytoplasmic fractions. Histone H3 is present in both nuclear and insoluble cytoplasmic fraction. (C) Western blot analysis of subcellular fractionation (as in B) performed on neurons at 14 DIV transduced with ctrl, wtTDP and mutTDP. Endogenous TDP-43 (48kDa blue arrow) is detected in all fractions as expected, however exogenous TDP-43 (75kDa blue arrow) is particularly abundant in the cytoplasmic insoluble fraction. 35kDa TDP-43 is present in both cytoplasmic fractions, however it is predominant in the insoluble fraction (white arrow). The less-prominent band of endogenous TDP-43, in the nuclear fraction of ctrl neurons, is explained by the lower total protein amount as shown by the Ponceau staining. Dotted lines indicate image cropping to remove unrelated lanes.*

Thus, TDP-43 overexpression of both wt and mutant TDP-43 recapitulates some features of TDP-43 proteinopathy: the presence of TDP-43 proteolytic fragments and its accumulation in the insoluble fraction. It is worth considering that the anti-TDP-43 antibody used for this assay reacts with aa 1-260 of the protein. Considering that Asp174 has been reported as the main cleavage site to generate TDP-43 25kDa fragment (Li *et al*, 2015), there is a likelihood that this antibody reacts more efficiently with the 35kDa band than with lower MW ones. Incubation with a C-terminal specific antibody should be performed to visualize whether other lower MW bands are present.

### *5.1.5 Exogenous TDP-43 granules partially colocalize with HuC/D*

Considering the pattern of exogenous TDP-43 distribution, we questioned the nature of the observed cytoplasmic granules. TDP-43 in known to bind other RBPs (e.g. FMRP, HuD) generating granules, to transport mRNAs along neurites (Fallini *et al.*, 2012). For this reason, we asked whether exogenous TDP-43 colocalizes with two members of the ELAV family, HuC and HuD, which are neuronal specific. HuC and D are RNA binding proteins involved in RNA transport and translation (Bronicki & Jasmin, 2013).

We immunostained wtTDP and mutTDP cortical neurons at 14 DIV with an antibody that reacts with both HuC and HuD, to determine whether exogenous TDP-43 and HuC/D colocalize. As shown in Fig. 5.7 exogenous TDP-43 partially colocalizes with HuC/D in the cytoplasm of both wtTDP and mutTDP neurons, suggesting that exogenous TDP-43 recruits other RBPs, as previously described for TDP-43 aggregates. (Fallini *et al.*, 2012).

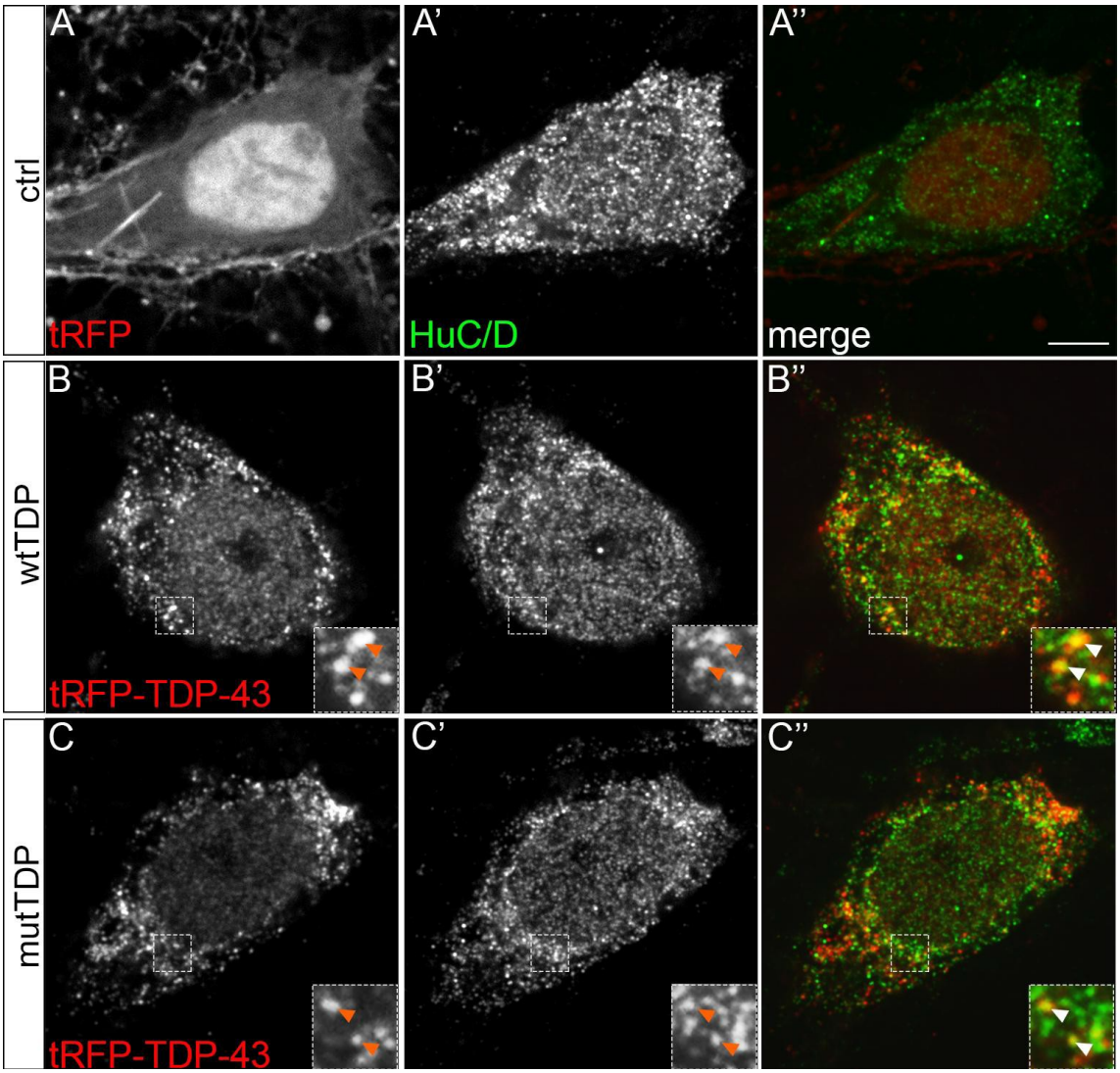


***Figure 5.7. Exogenous TDP-43 granules partially colocalize with HuC/D.*** *(A-C'') Immunofluorescence of ctrl, wtTDP and mutTDP neurons, cultured at 14 DIV, reveals that exogenous TDP-43 cytoplasmic granules partially colocalizes with HuC/D. HuC/D localizes in both nucleus and cytoplasm of ctrl, wtTDP and mutTDP neurons (A',B',C'). In the cytoplasm, exogenous TDP-43 (in red) partially colocalizes with HuC/D (in green), in both wtTDP and mutTDP (see arrowheads in insets, B'' and C''). (Size bar: 5µm).*

### *5.1.6 TDP-43 overexpression is not sufficient per se to induce stress granules, however exogenous TDP-43 is recruited in stress granules under stress conditions*

To further investigate the nature of these granules, we asked whether exogenous TDP-43 aggregates may be stress granules. To answer this question, we immunostained ctrl, wtTDP and mutTDP neurons, cultured at 14 DIV with an antibody specific for anti-RasGAP SH3 domain binding protein 1 (G3BP1), which is one of the main component of stress granules (reviewed in Wolozin & Ivanov, 2019).

As shown in Fig. 5.8, under basal conditions G3BP1 has a diffuse pattern in wtTDP and mutTDP (Fig. 5.8B',C') as in ctrl neurons (Fig. 5.8A'), thus suggesting that TDP-43 overexpression alone is not able to induce large stress granules. This is in agreement with the fact that stress granules accumulation is generally induced after acute stress (e.g. osmotic stress, heat shock, sodium arsenite treatment), while in neurodegenerative conditions neurons undergoes chronic stress, which takes years of time to develop (reviewed in Wolozin & Ivanov, 2019).

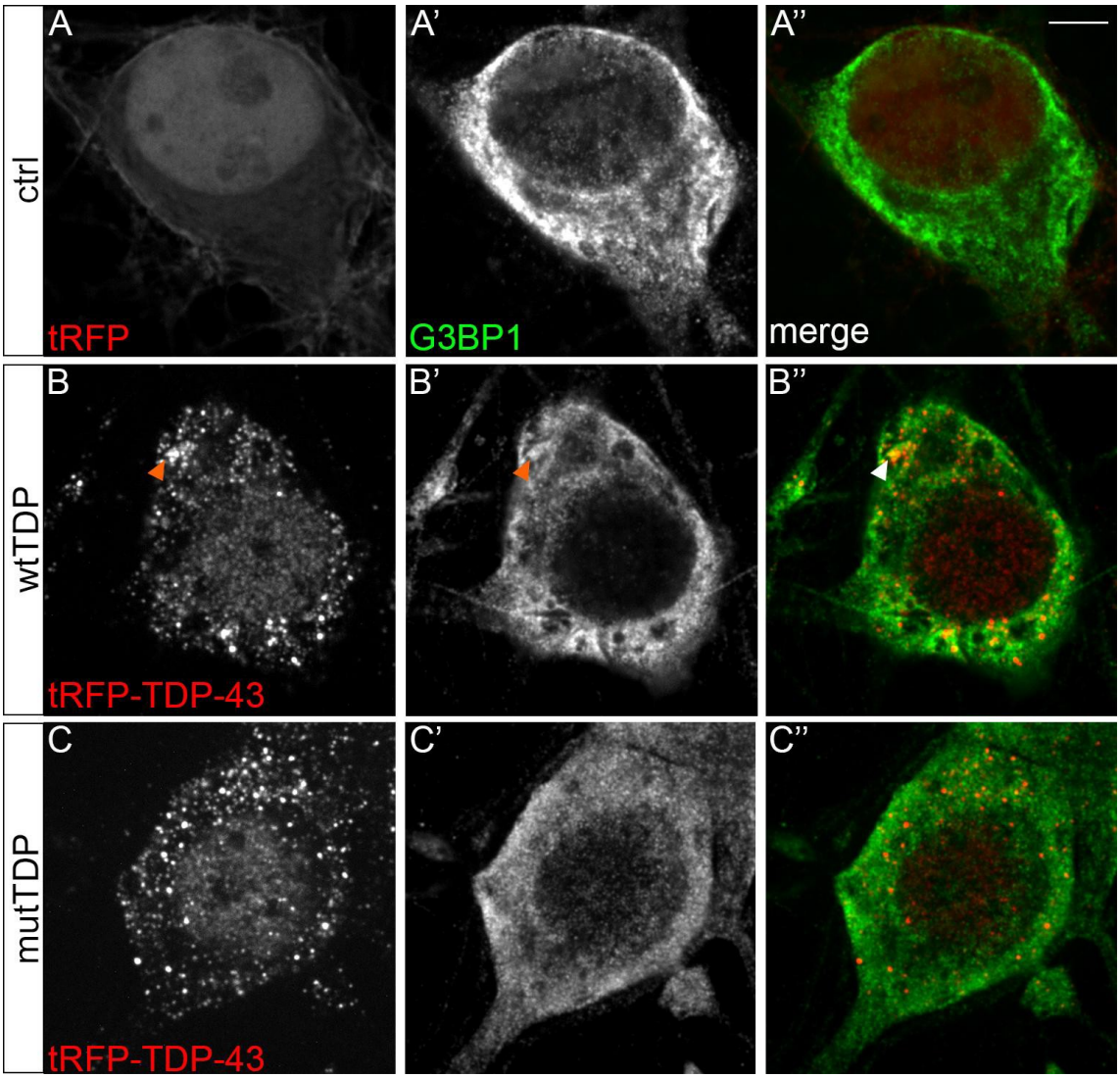


***Figure 5.8. TDP-43 overexpression is not sufficient per se to induce large stress granules under basal conditions.*** *(A-C'') Immunofluorescence of ctrl, wtTDP and mutTDP neurons, cultured at 14 DIV, reveals that TDP-43 overexpression is not able to induce large stress granules under basal conditions. Indeed G3BP1 shows a diffuse pattern in wtTDP (B') and mutTDP (C') like in ctrl neurons (A'). However, few G3BP1 and tRFP-TDP-43 double positive granules appear (see arrowheads in B-B''). (Size bar: 5µm).*

Since TDP-43 is an established component of stress granules (Khalfallah *et al.*, 2018), we asked whether exogenous TDP-43 is recruited in stress granules under cellular stress conditions (e.g. heat shock). To assess this, ctrl, wtTDP and mutTDP neurons were incubated at 43°C for 60 min, then fixed and immunostained with anti-G3BP1 antibody.

As shown in Fig 5.9 wtTDP and mutTDP neurons, after heat shock, exhibit massive stress granule accumulations in the cytoplasm, comparable to the pattern observed in ctrl neurons. These granules recruit exogenous TDP-43 (Fig 5.9B'',C'').

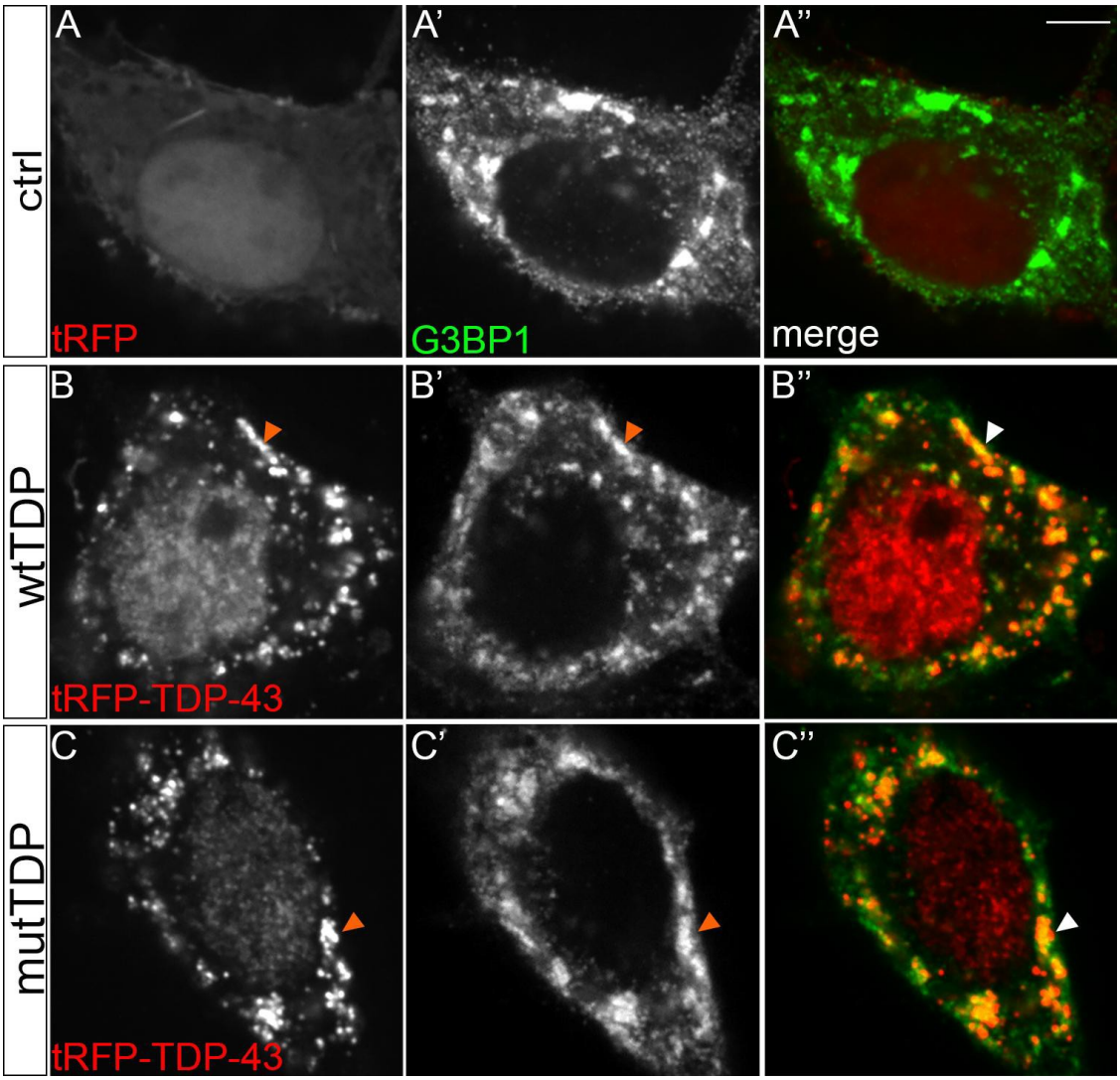


***Figure 5.9. Exogenous TDP-43 is recruited to stress granules under stress conditions.*** *(A-C'') Immunofluorescence of ctrl, wtTDP and mutTDP neurons, cultured at 14 DIV and incubated at 43°C for 60 min, indicates that exogenous TDP-43 is recruited to stress granules under stress conditions. After heat shock, G3BP1 generates large granules in the cytoplasm of wtTDP (B') and mutTDP (C') similar to ctrl neurons (A'). Exogenous TDP-43 (in red) mostly colocalizes with G3BP1 positive granules (in green) in both wtTDP and mutTDP neurons (see arrowheads in B'',C'') (Size bar: 5μm).*

Overall these results show that under basal conditions TDP-43 overexpression is not sufficient to induce large stress granule accumulation, as expected since ALS-related neuronal damage is a chronic condition. However, under acute stress, as heat shock, exogenous TDP-43 maintains its ability to be recruited to stress granules.

### *5.1.7 Exogenous TDP-43 colocalizes very weakly with RPL26 and more frequently with RPS6*

To further analyze the composition of these granules generated by exogenous TDP-43, we asked whether they colocalize with ribosomal particles. Whether TDP-43 associates with ribosomal particles is not fully understood. Higashi et al. found that, in HeLa cells, TDP-43 associates with stalled ribosomes only in stress conditions (Higashi *et al*, 2013), while Russo et al. found that in SH-SY5Y cells TDP-43 associates with ribosomes by binding with Receptor Activated C Kinase 1 protein (RACK1) (Russo *et al*, 2017).

First, we assessed the localization of exogenous TDP-43 with a ribosomal protein of the large subunit: RPL26. To this end, we immunostained wtTDP and mutTDP cortical neurons cultured at 14 DIV with an anti-RPL26 antibody.

As shown in Fig. 5.10, hardly any colocalization was detected between exogenous TDP-43 and RPL26 in both wtTDP and mutTDP neurons. Several sparse colocalization dots are shown in insets of Fig. 5.10A'', B''.

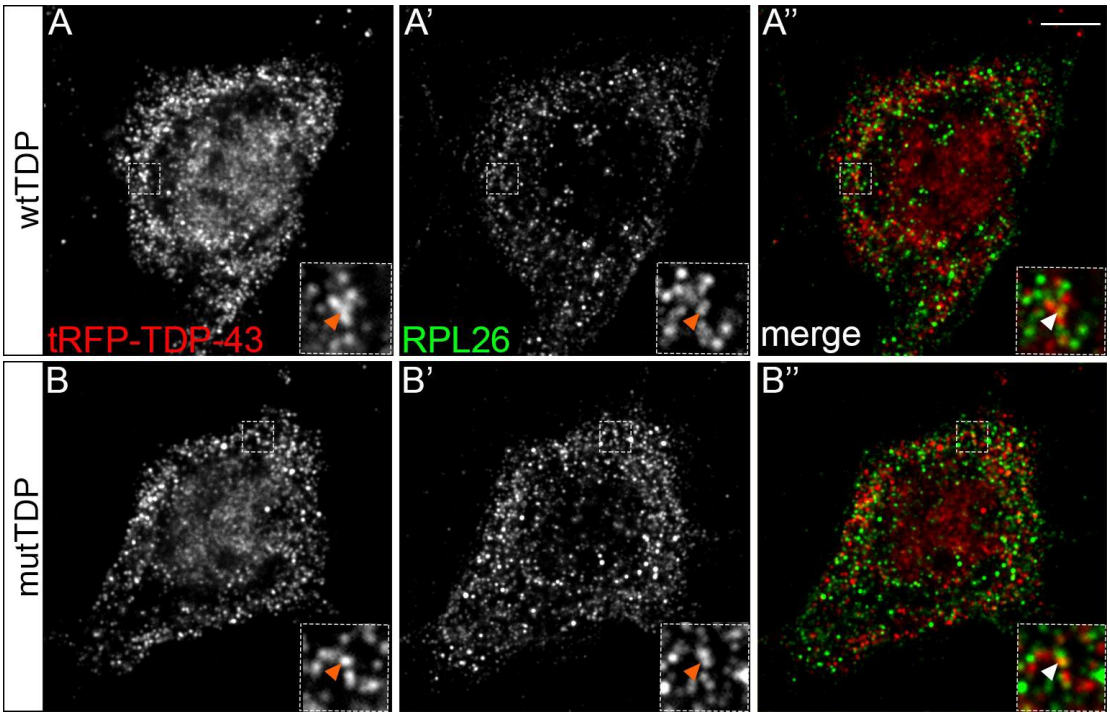


***Figure 5.10. Exogenous TDP-43 does not significantly colocalize with RPL26.*** *(A-B'') Immunofluorescence of wtTDP and mutTDP neurons, cultured at 14 DIV, reveals that exogenous TDP-43 cytoplasmic granules (in red) infrequently colocalize with RPL26 (in green) (see white arrowheads in insets in A'',B''). (Size bar: 5µm).*

Based on this evidence we can conclude that exogenous TDP-43 colocalizes very weakly with the large subunit protein RPL26. The most likely explanation is that these fluorescently tagged granules do not colocalize with assembled ribosomes.

Next, we investigated whether these TDP-43 granules colocalize with a ribosomal protein of the small subunit: RPS6. Indeed, 40S ribosomal proteins are among the core proteins of untranslating granules, such as stress granules (reviewed in Wolozin & Ivanov, 2019). To assess this, we performed immunofluorescence of wtTDP and mutTDP, cultured at 14 DIV, with an anti-RPS6 antibody.

As shown in Fig. 5.11 exogenous TDP-43 granules partially colocalize with RPS6 in both wtTDP and mutTDP neurons.

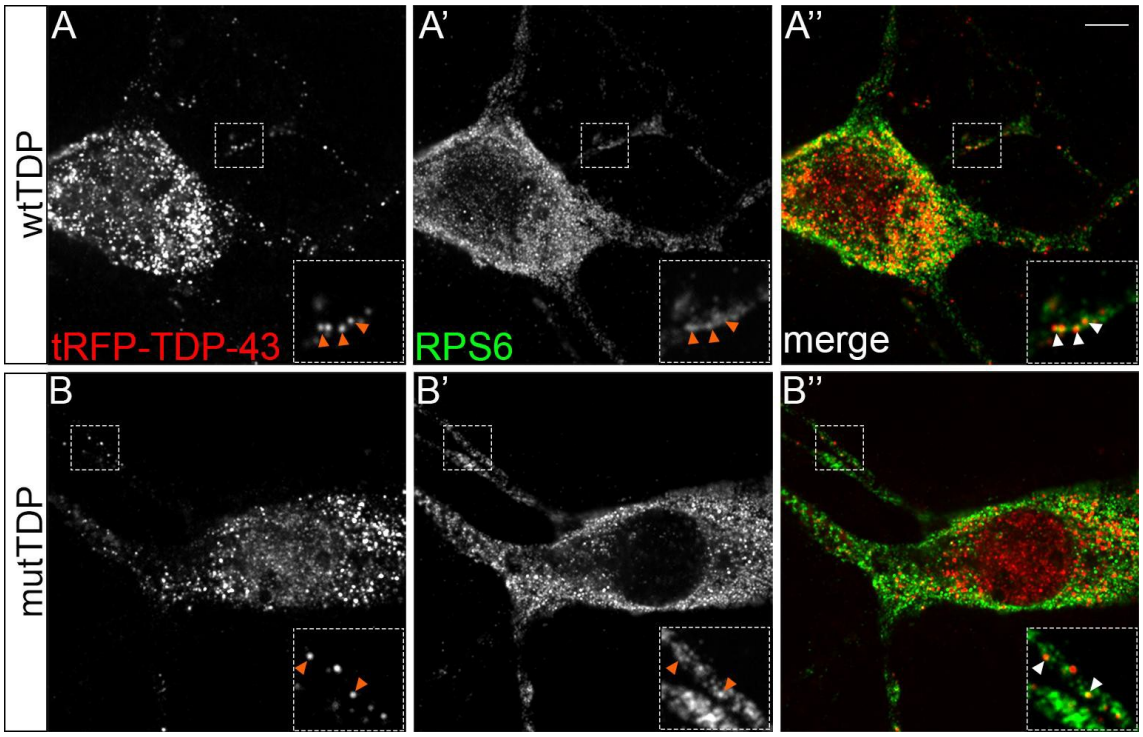


***Figure 5.11. Exogenous TDP-43 partially colocalizes with RPS6.*** *(A-B'') Immunofluorescence of wtTDP and mutTDP neurons, cultured at 14 DIV, reveals that exogenous TDP-43 cytoplasmic granules (in red) partially colocalize with RPS6 (in green) (A'',B''). This is shown best in primary neurites (see arrowheads in insets, A'', B''). (Size bar: 5μm).*

These findings indicate that in our in-vitro model fluorescently tagged TDP-43 granules, which colocalize very weakly with the 60S protein RPL26, recruit 40S ribosomal small subunits, which contain the RPS6 protein. This evidence supports the notion that these exogenous TDP-43 granules may be untranslating granules.

### *5.1.8 wtTDP and mutTDP cultures show a slight increase in cell death*

We investigated whether TDP-43 overexpression might cause apoptotic cell death on these neurons relative to ctrl. For this reason, we counted the number of cells with active Caspase-3 signal, which is produced at early stages of apoptosis, in wtTDP, mutTDP and ctrl. To this end, wtTDP, mutTDP and ctrl neurons were immunostained with anti-active Caspase-3 antibody and the number of positive cells was counted.

As shown in the graph of Fig. 5.12B, wtTDP and mutTDP neurons show a significant slight increase of active caspase-3-positive cells, particularly in mutTDP.

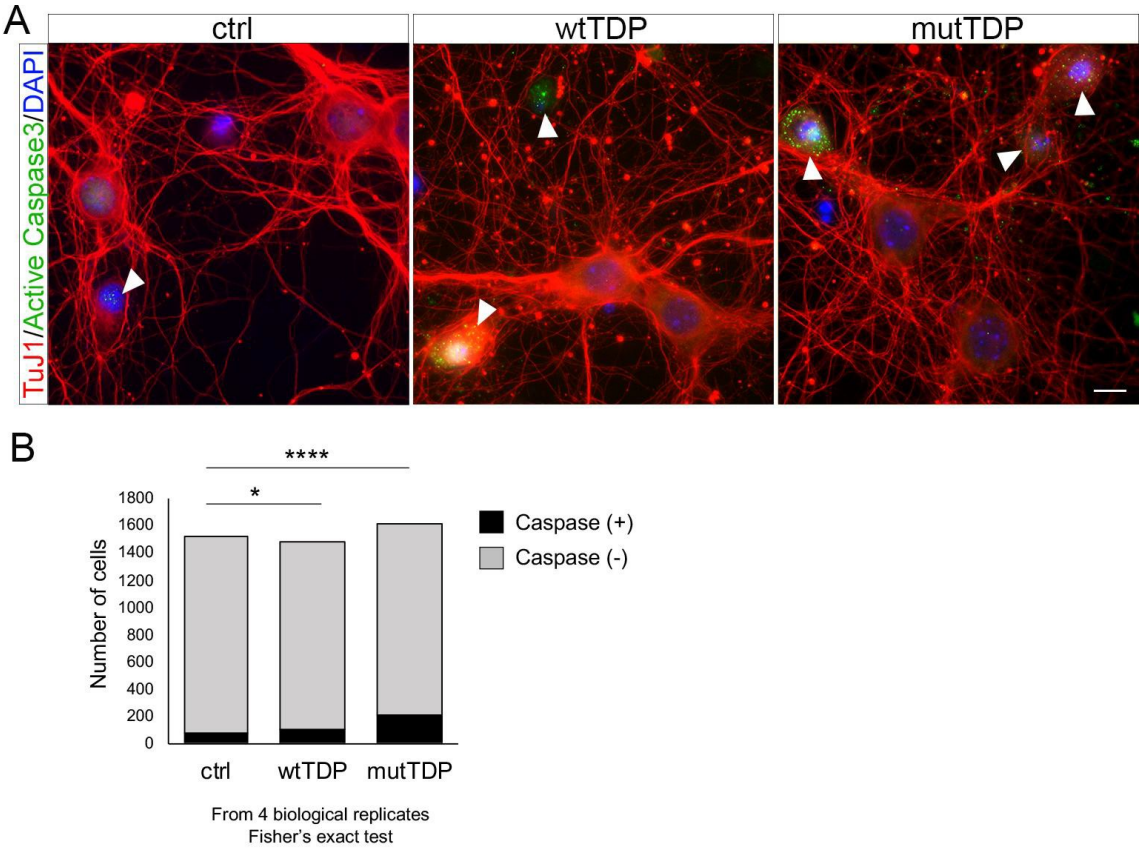


***Figure 5.12. wtTDP and mutTDP neurons a slight increase in cell death.*** *(A) Immunofluorescence of ctrl, wtTDP and mutTDP neurons, cultured at 14 DIV, with anti-active Caspase-3 antibody (in green) and anti-TuJ1 (in red). DAPI: in blue. White arrows indicate active Caspase-3 positive cells. (Size bar: 10µm). (B) Histogram showing the number of active Caspase-3 positive cells (in black) and negative cells (in gray) in ctrl, wtTDP, mutTDP. The graph shows that wtTDP and mutTDP neurons show a significant slight increased cell death, particularly in mutTDP. (n=4, Fisher's exact test, *p-value<0.05, ****p-value<0.0001).*

### *5.1.9 Characterization of a mouse model of TDP-43 proteinopathy*

To validate the features of ALS-related damage in the in-vitro model, we compared it with a mouse model of TDP-43 proteinopathy. This model (Stallings *et al.*, 2010) is a transgenic mouse expressing wild-type human TDP-43 under the prion gene promoter (PrP), which is mainly expressed in the nervous system but also blood, kidney, skin, heart and muscle (https://www.genecards.org/cgi-bin/carddisp.pl?gene=PRNP&keywords=PRNP#protein_expression). The transgene is integrated in the X chromosome; thus, only male mice were analyzed.

This mouse line has been characterized only in skeletal muscles (Stallings *et al.*, 2010). Thus, first, we analyzed TDP-43 overexpression levels in the mouse brain cortex. To this end, we performed western blot analysis of protein lysates obtained from the brain cortex of transgenic mice and control littermates at 1, 4 and 9 months of age. The membrane was incubated with an anti-TDP-43 antibody, which reacts with both human and murine protein. As shown in Fig. 5.13A, transgenic mice show that TDP-43 levels are significantly higher than control mice in the brain cortex at all stages analyzed.

Furthermore, we asked whether neurons of the motor brain cortex show signs of TDP-43 proteinopathy: TDP-43 nuclear depletion and cytoplasmic accumulation. For this reason we immunostained frontal cortex sections of transgenic mice and control littermates with an anti-TDP-43 antibody. As shown in Fig. 5.13B, transgenic mice show early signs of TDP-43 accumulation in the cytoplasm at 4 months of age. These abnormalities are further exacerbated at 9 months, when cytoplasmic TDP-43-positive aggregates are present.

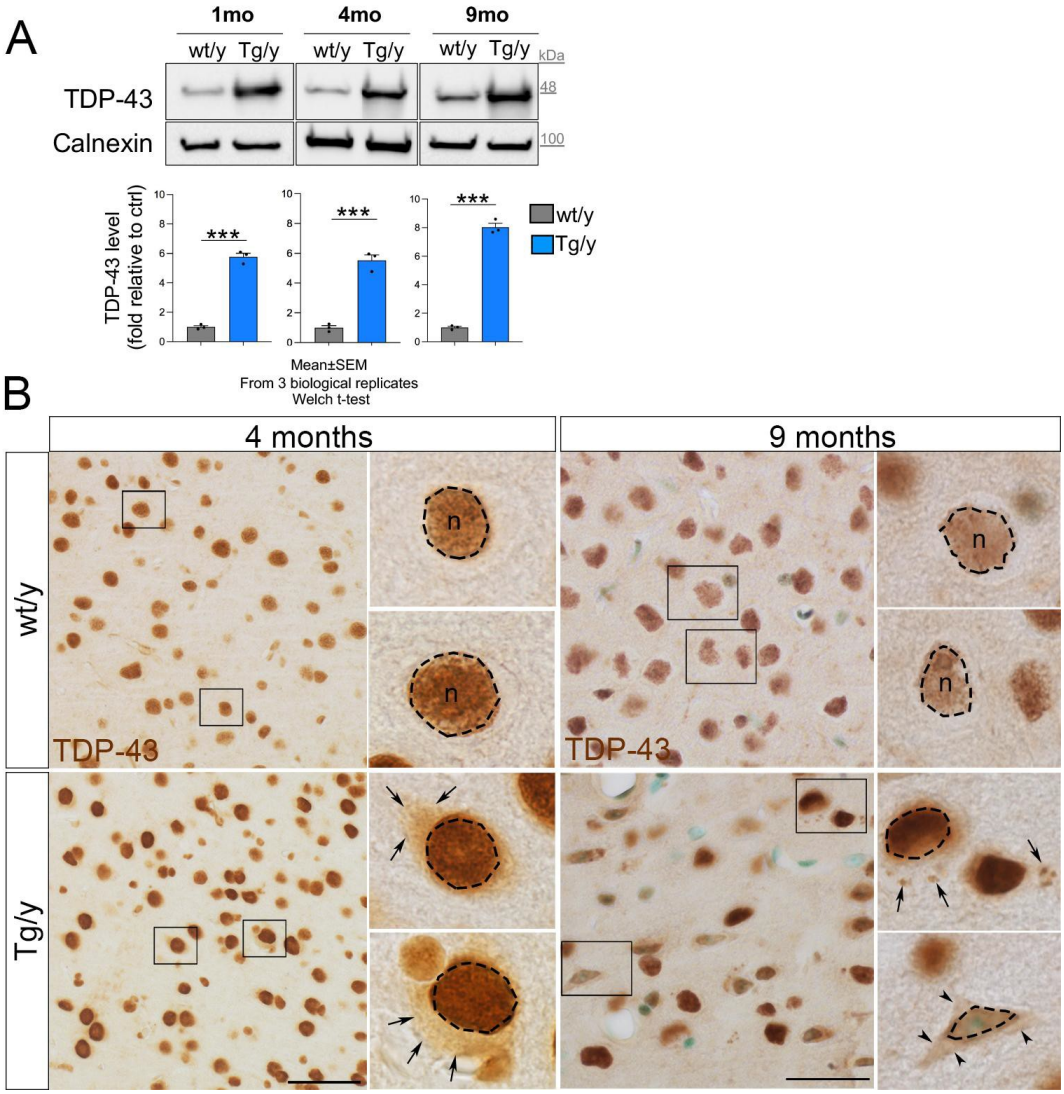


***Figure 5.13. TDP-43 transgenic mice show increased TDP-43 protein levels accompanied by cytoplasmic accumulation and aggregate formation.*** *(A) Western blot of protein lysates obtained from the brain cortex of transgenic mice (Tg/y) and control littermates (wt/y) at 1 month (1mo), 4 months (4mo), and 9 months (9mo) of age. The membrane was incubated with anti-TDP-43 and anti-Calnexin antibody as loading control. On the bottom, graphs show western blot quantification of TDP-43 levels in transgenic mice (in blue) relative to ctrl (in gray). TDP-43 levels are significantly higher in transgenic mice than controls. (Mean ±SEM, n=3, Welch t-test, **p-value<0.001). (B) Immunohistochemical analysis of frontal brain sections of transgenic mice (Tg/y) and control littermates (wt/y) at 4 months (on the left) and 9 months of age (on the right) with anti-TDP-43 antibody. At 4 months TDP-43 accumulates in the cytoplasm of neurons of the motor cortex (black arrows in insets) and at 9 months it generates cytoplasmic aggregates (black arrows in insets). Dotted lines indicate nucleus border. (Size bar: 50μm for 4 months and 25 μm for 9 months).(n: nucleus).*

In addition, we assessed whether mutant mice showed microgliosis and astrocytosis in the brain motor cortex since astrocytes and microglia activation are two pathological signs of ALS (Lee *et al*, 2016). Thus, immunohistochemical analysis of frontal cortex sections of transgenic mice and control littermates was performed using an anti-IBA1 antibody, to detect microglia, and an anti-GFAP to decorate astrocytes. As shown in Fig. 5.14 no macroscopic signs of microgliosis and astrocytosis were found at either stage. Higher magnification of brain cortex at 9 months of age displays no morphological changes in astrocytes, while IBA1-positive cells have reduced ramifications and shortened cellular processes, which are hallmarks of microglia activation (reviewed in Anttila *et al*, 2017). This suggests a moderate activation of microglia at 9 months of age in these mice, however an in-depth analysis with specific markers of activated microglia (e.g. CD86, CD11b (reviewed in Zheng & Wong, 2019)) should be performed to confirm this data.

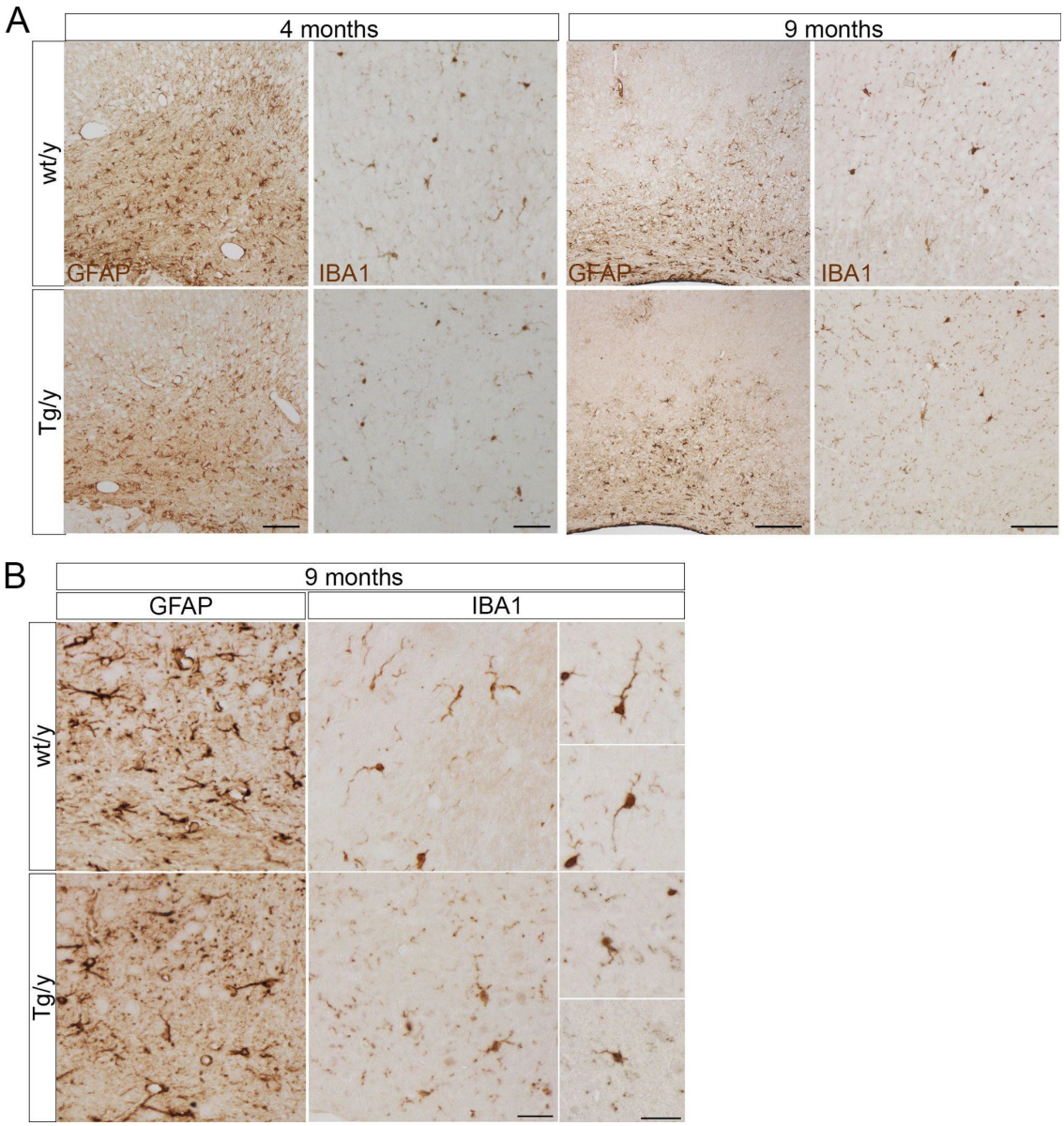


***Figure 5.14. TDP-43 transgenic mice show no obvious signs of microgliosis and astrocytosis but show preliminary evidence of microglia activation.*** *(A)Immunohistochemical analysis of frontal brain sections of transgenic mice (Tg/y) and control littermates (wt/y) at 4 months and 9 months of age with anti-IBA1 and anti-GFAP antibodies. No increased density of astrocytes and microglia was found in transgenic mice relative to control littermates at both 4 and 9 months of age. (Size bar:50μm for GFAP pictures and 100μm for IBA1 pictures). (B) Higher magnification of pictures in A at 9 months of age. GFAP-positive cells do not show morphological changes while IBA1-positive cells show shortened processes in transgenic brain cortex, suggesting a moderate microglia activation. (Size bar:20μm on the left and 25μm on the right).*

Afterwards, we investigated whether TDP-43 transgenic mice show a pathological motor phenotype. Indeed, the transgenic mouse shows moderate levels of hindlimb clasping at 4 and 9 months of age. Hindlimb clasping is a distinctive sign of defective

hindlimb functionality in murine models of ALS (Fig. 5.15A) (Igaz *et al.*, 2011; Walker *et al.*, 2015). Moreover, transgenic mice and control littermates were subjected to the catwalk test (see Materials and Methods), which shows reduced stride length for all paws (i.e. RF: right front; RH: right hind; LF: left front; LH: left hind) of transgenic mice at both 3.5 and 6 months of age compared to control littermates, suggesting that these mice have a gait abnormality. Furthermore, transgenic mice show a reduced performance in the rotarod test (see Materials and Methods) at both 3.5 and 8 months of age relative to control littermates. The result of the rotarod test highlights a reduced motor coordination in transgenic mice relative to controls.

In addition, transgenic mice were also assayed using the grip strength test and hanging wire test at 3.5 months of age (Fig. 5.15D). However, no statistically significant differences were found suggesting that these mice display no major defects in muscle strength until 3.5 months of age.

Overall, we can conclude that moderate levels of hindlimb clasping and other motor abnormalities make this mouse a legitimate model of pre- and pauci-symptomatic early stages of ALS. *Bona fide*, this model is well suited for comparative analyses *in vivo* of events observed in our *in vitro* model of TDP-43 proteinopathy.

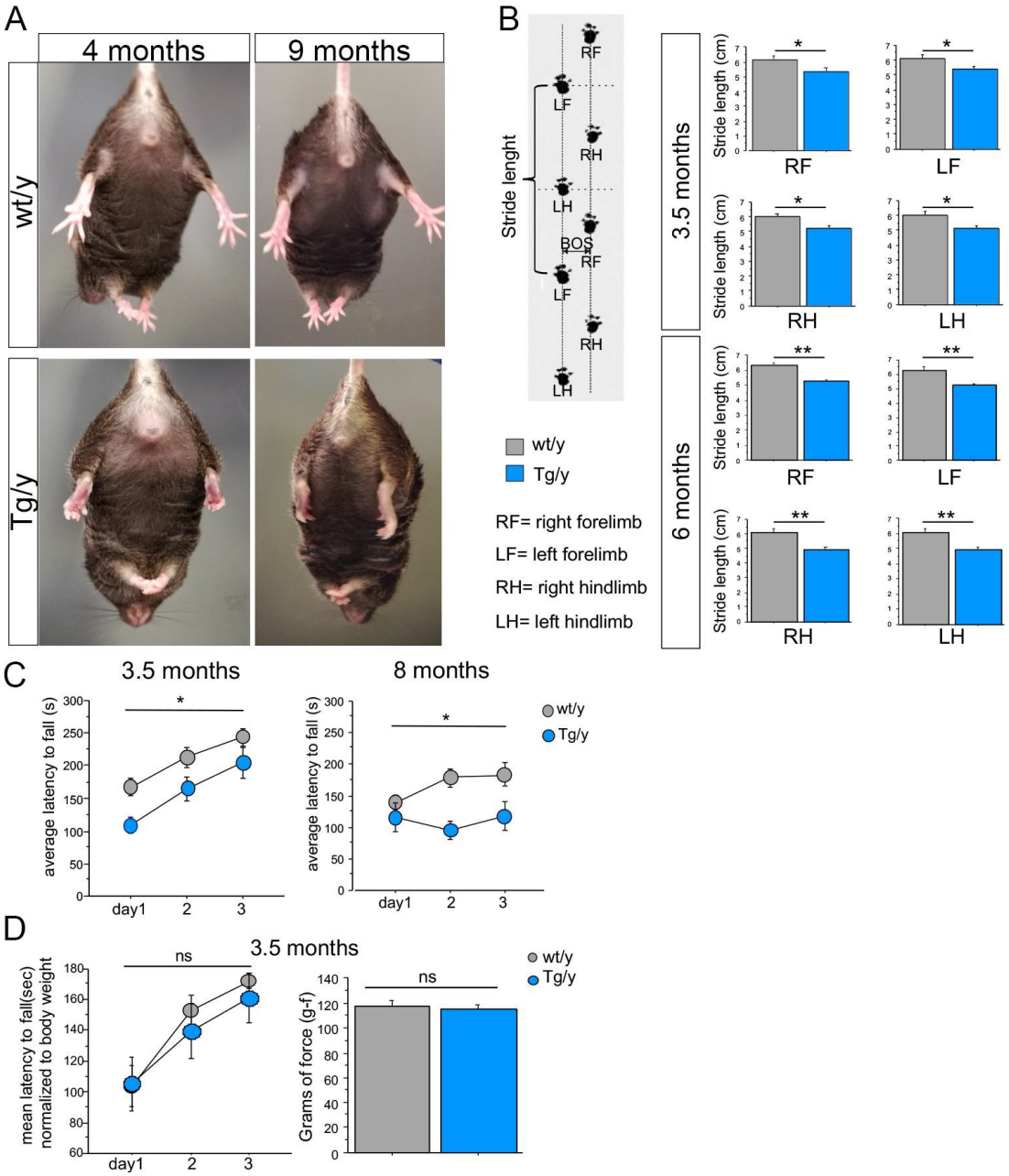


***Figure 5.15. TDP-43 transgenic mice show defective motor performance.*** *(A) Representative pictures showing hindlimb clasping in transgenic mice (Tg/y, bottom row) at 4 and 9 months of age, compared to control littermates (wt/y upper row). (B) The schematic on the left shows the parameters measured in the catwalk test: stride length between right forelimbs (RF), left forelimbs (LF), right hindlimbs (RH) and left hindlimbs (LH). On the right, graphs showing RF, LF, RH and LH stride length in transgenic mice (blue) relative to control littermates (gray) at 3.5 months (top) and 6 months of age (bottom). The graphs show that transgenic mice display a significantly shorter stride length. (C) Graphs showing average latency to fall at rotarod test in transgenic mice (in blue) and control littermates (in gray) at 3.5 months (graph on the left) and 8 months (graph on the right). Transgenic mice have a reduced motor performance in the rotarod test compared to controls. (D). Graphs showing average latency to fall at hanging wire test (on the left) and maximal strength applied by forelimbs at grip test (on the right) at 3.5 months of transgenic mice and control littermates. (Mean±SEM, number of mice: Tg/y: 11, wt/y: 13 at 3.5*

*and 6 months; Tg/y: 8, wt/y: 11 at 8 months; ANOVA repeated measures for genotype effect, ns=p>0.05, *p-value<0.05, **p-value<0.01).*

### *5.1.10 wtTDP and mutTDP neurons show weak TDP-43 phosphorylation and no TDP-43 ubiquitination*

As mentioned above TDP-43 phosphorylation and ubiquitination are two post-translational modifications associated with ALS. For this reason, we tested them in wtTDP and mutTDP neurons.

To detect whether wtTDP and mutTDP neurons show increased TDP-43 phosphorylation, we performed western blot analysis of protein lysates obtained from ctrl, wtTDP and mutTDP neurons at 14 DIV. The membrane was incubated with an anti-phosphoTDP-43 (Ser 409-410). Preliminary data (Fig. 5.16A) show that exogenous TDP-43 is weakly phosphorylated (see blue arrow). TDP-43 phosphorylation is also increased in the transgenic mouse model, however the ratio of phosphorylated to total TDP-43 amount does not change between transgenic and control mice (Fig. 5.16B).

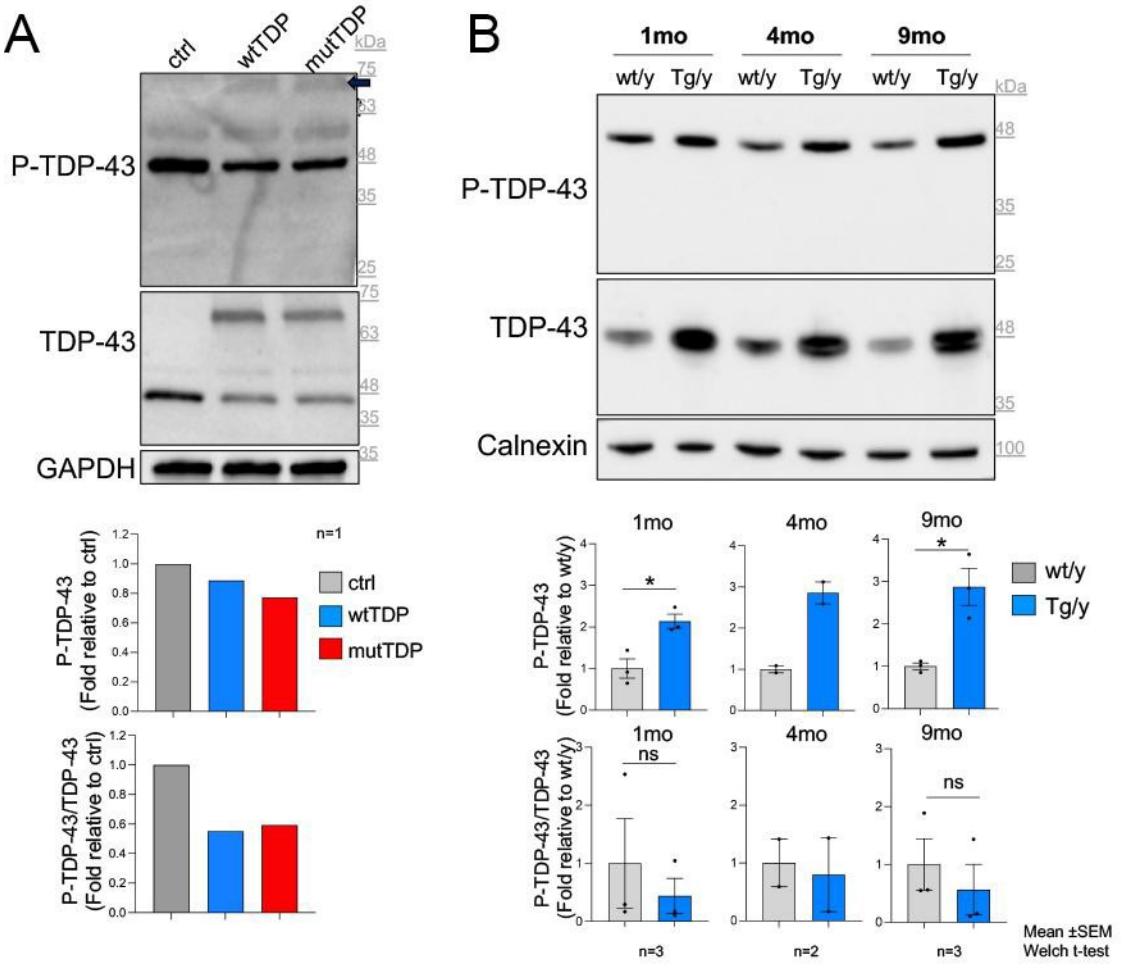


***Figure 5.16. Exogenous TDP-43 is weakly phosphorylated.*** *(A) Western blot of protein lysates obtained from ctrl, wtTDP and mutTDP neurons cultured at 14 DIV. The membrane was incubated with antibodies to phosphoTDP-43 (Ser 409-410, P-TDP-43), TDP-43 and GAPDH as a loading control. The western blot shows a faint band corresponding to exogenous TDP-43 (blue arrow). In the middle, a graph showing western blot quantification of phosphorylated TDP-43 relative to ctrl. On the bottom, western blot quantification expressed as the ratio of phosphorylated to total TDP-43 (n=1). (B) Western blot of protein lysates obtained from the brain cortex of our transgenic mouse model (Tg/y) and wild type littermates (wt/y) at 1 month (1mo), 4 months (4mo) and 9 months (9 mo) of age. The membrane was incubated with anti-P-TDP-43, anti-TDP-43 and anti-Calnexin, as a loading control. In the middle, a graph showing western blot quantification of phosphorylated TDP-43 relative to non-transgenic control. On the bottom, western blot quantification expresses the ratio of phosphorylated to total TDP-43 (Mean±SEM, n=3 or 2, Welch t-test, ns=p-value>0.05, *p-value<0.05).*

First, we immunoprecipitated TDP-43 from protein lysates derived from ctrl, wtTDP and mutTDP neurons cultured at 14 DIV. Then the membrane was incubated with anti-ubiquitin antibody and anti-TDP-43 to light up the immunoprecipitation product. Immunoprecipitation with an anti-IgG unspecific was also performed as a negative

control. As shown in Fig. 5.17A, no specific ubiquitination signal was detected. In fact, the pattern observed in the TDP-43 immunoprecipitation products is also present in the negative control. Moreover, it should be noted that the endogenous TDP-43 was immunoprecipitated very weakly, probably due to the low amount of total protein lysate obtained from these cortical neurons. Thus, we can conclude that the exogenous TDP-43 protein is not significantly ubiquitinated.

Since ubiquitinated TDP-43 is often present in insoluble aggregates in ALS neurons (Neumann *et al.*, 2006) we carried out a subcellular fractionation as in section 5.1.4; the membrane was incubated with an anti-Ubiquitin antibody. However, as shown in Fig. 5.17B no increased ubiquitination signal was detected in wtTDP and mutTDP neurons relative to ctrl ones.

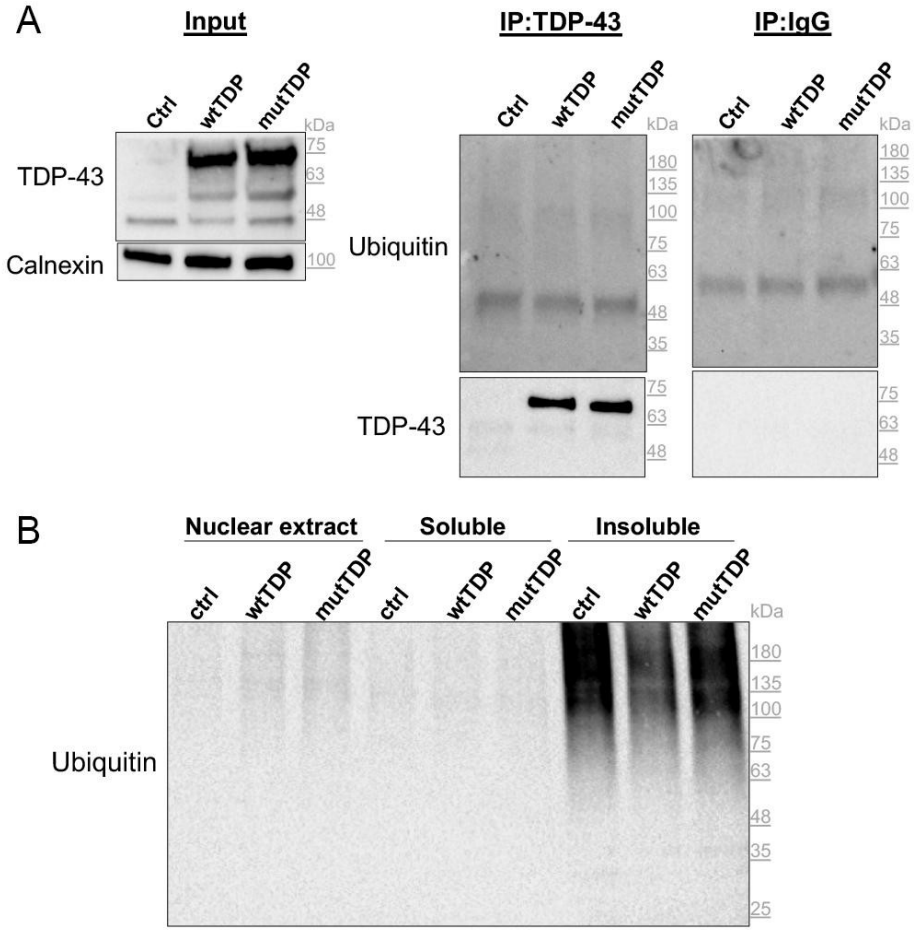


***Figure 5.17. wtTDP and mutTDP show no TDP-43 ubiquitination.*** Western blot of protein lysates from ctrl, wtTDP and mutTDP neurons. (A) On the left, the membrane is incubated with anti-TDP-43. A 48kDa band, corresponding to endogenous TDP-43, is detected in all samples, while a 75kDa band, corresponding to exogenous TDP-43, is present in wtTDP and mutTDP neurons. In the middle, immunoprecipitation products obtained with anti-TDP-43 antibody and,

on the right, with a non-specific anti-IgG used as a negative control. The membrane was incubated with anti-ubiquitin and anti-TDP-43 antibodies. No ubiquitin specific signal was detected since the pattern observed after TDP-43 immunoprecipitation is also present in the negative control. Endogenous TDP-43 has been weakly immunoprecipitated, maybe due to the low total protein amount obtained from protein lysates of cortical neurons. (B) Subcellular fractionation as in Fig. 5.6C, incubated with anti-ubiquitin antibody. No increased ubiquitination signal has been detected in wtTDP and mutTDP neurons.

Overall, we can conclude that exogenous TDP-43 is not ubiquitinated and that no specific ubiquitinated insoluble proteins have been detected in wtTDP and mutTDP relative to ctrl neurons. One possible explanation is that TDP-43 ubiquitination is a late event of ALS-disease. Indeed, as shown in Fig. 5.18, in our transgenic mouse model of TDP-43 proteinopathy, ubiquitination of cortical neurons in the motor cortex is hardly detectable at 4 months of age (Fig. 5.18A) and TDP-43 is not ubiquitinated, as shown by TDP-43 immunoprecipitation (Fig. 5.18B). However, ubiquitination levels are sharply increased at 9 months of age (Fig. 5.18C), although immunoprecipitation with anti-TDP-43 has yet to be performed to assess whether TDP-43 is ubiquitinated. Based on our results, it is unsurprising that ubiquitination is undetectable in embryonic cortical neurons maintained in culture for two weeks.

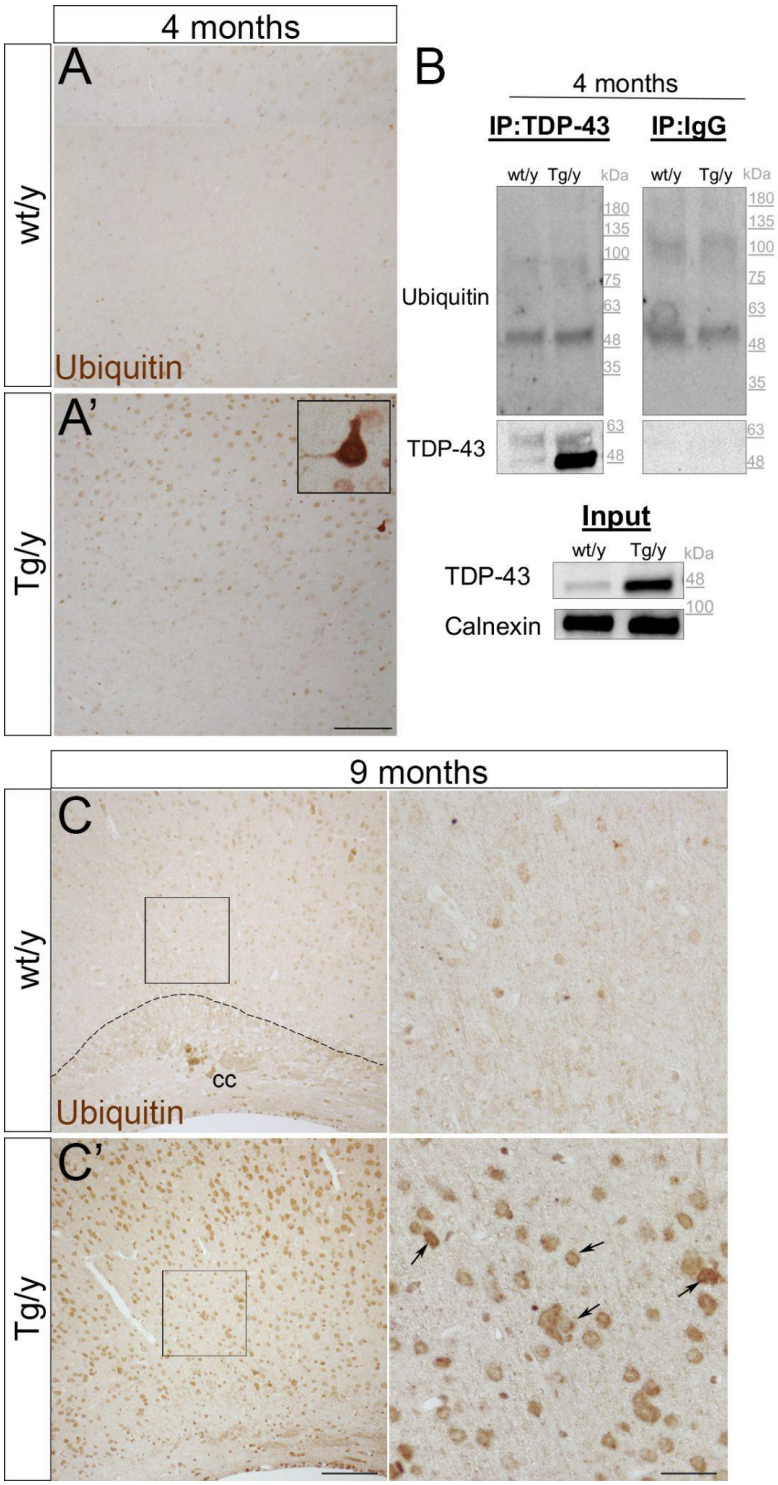


***Figure 5.18. TDP-43 transgenic mice show mildly increased ubiquitination at 4 months of age and, more markedly, at 9 months of age.*** *(A,A') Immunohistochemical analysis of frontal brain sections of transgenic mice (Tg/y) and control littermates (wt/y) at 4 months of age with anti-ubiquitin antibody. Ubiquitination is hardly detectable at 4 months of age however few neurons with strong ubiquitin signal are present (see inset in A'). (B) Western blot of immunoprecipitation products obtained with anti-TDP-43 antibody and non-specific anti-IgG as a negative control from protein lysates of brain cortices of Tg/y and relative control. The membrane was incubated with anti-ubiquitin and anti-TDP-43 antibodies. No ubiquitin specific signal was detected since the pattern observed in the TDP-43 immunoprecipitate products is also present in the negative*

*control. (C-C') At 9 months of age, transgenic mice show markedly increased ubiquitination (C' and inset on the right) relative to controls (C and inset on the right), with presence of ubiquitin-positive aggregates in the cytoplasm (black arrows in C' inset). Black box indicates insets border (Size bar:100μm for A,A',C,C' and 25μm for inset in C,C'). (cc: corpus callosum).*

Overall, these data show that wtTDP and mutTDP neurons show weak phosphorylation and no ubiquitination. Considering that in the mouse model of TDP-43 overexpression these phenotypes appear strongly at 9 months of age, we can *bona fide* assume that our in-vitro model is a model of the early stages of ALS neuronal damage.

## 5.2 Transcriptome and translatome analysis of wtTDP and mutTDP neurons, relative to ctrl in the cell body and axonal compartment

Once assessed that our in-vitro system is a model of early stages of ALS neuronal damage, we analyzed the transcriptome and translatome of cell body and axonal compartments of wtTDP and mutTDP neurons relative to ctrl neurons.

### *5.2.1 Cortical neuron primary cultures were grown in microfluidic chambers to separate axons from cell bodies and dendrites*

To isolate the axonal compartment from cell bodies and dendrites, cortical neurons were plated in microfluidic chambers, which consist of two main channels separated by 450 µm long microgrooves (see Materials and methods). The width of these microgrooves does not allow cell bodies to enter them, while dendrites do and yet they are too short to extend throughout their length. However, to further verify that these microfluidic chambers allow the specific separation of axons from cell bodies and dendrites, untrasduced neurons cultured at 9 DIV were plated in microfluidic chambers and immunostained with anti-Microtubule Associated Protein 2 (MAP2), a dendrite-specific marker, and with anti-TuJ1, which detects both axons and dendrites.

As shown in Fig. 5.19 MAP2-positive dendrites are present in the left channel, together with cell bodies, detected by DAPI staining. However, only axons extend into the right-hand channel and are labeled by TuJ1.

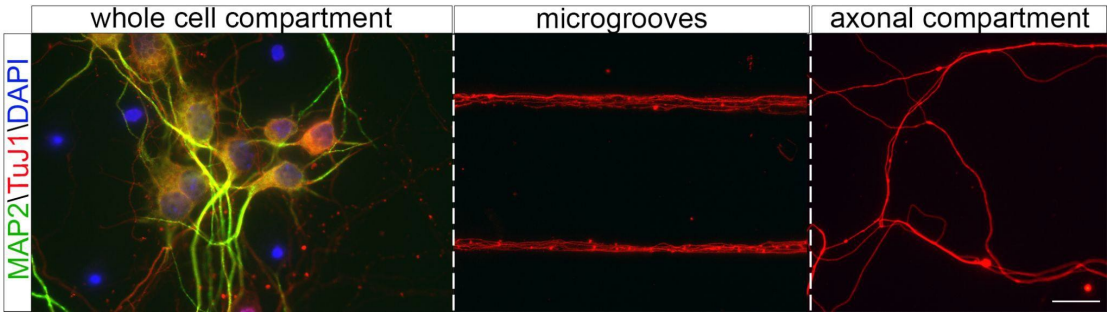


***Figure 5.19. Microfluidic chambers allow the physical separation of axons from cell bodies and dendrites.*** *Immunofluorescence of cortical neurons, cultured at 9 DIV, with anti-MAP2 (green) and anti-TuJ1 (red) antibodies. Blue: DAPI. MAP2 positive dendrites and cell bodies are present only in the left compartment (whole-cell compartment), while axons grow beyond microgrooves (in the middle) and reach the compartment on the right (axonal compartment) (Size bar: 20µm).*

### *5.2.2 Analysis of the axonal transcriptome and translatome of wtTDP, mutTDP and ctrl neurons*

The allied laboratory of Gabriella Viero performed an RNA-sequencing analysis of the axon- and cell-body-specific transcriptome and translatome of wtTDP and mutTDP neurons, cultured at 9 DIV, relative to ctrl, by tag-free polysome isolation (Negro *et al*, 2018). Here, by the term transcriptome I indicate the results of an RNA-seq analysis of sub-polysomal mRNAs; instead, the term translatome indicates the results of an RNA-seq analysis of polysomal-engaged mRNAs.

This approach consists of the following steps (sketched in Fig. 5.20):

1. wtTDP, mutTDP and ctrl neurons are plated in microfluidic chambers until 9 DIV.
2. Axonal and cell body compartments of these neurons are lysed and loaded onto a miniaturized sucrose gradient to separate polysome-engaged mRNAs from sub-polysomal mRNAs.
3. Polysomal mRNAs and sub-polysomal mRNA fractions are isolated through polysome profiling.
4. mRNAs are extracted from these fractions and sequenced.

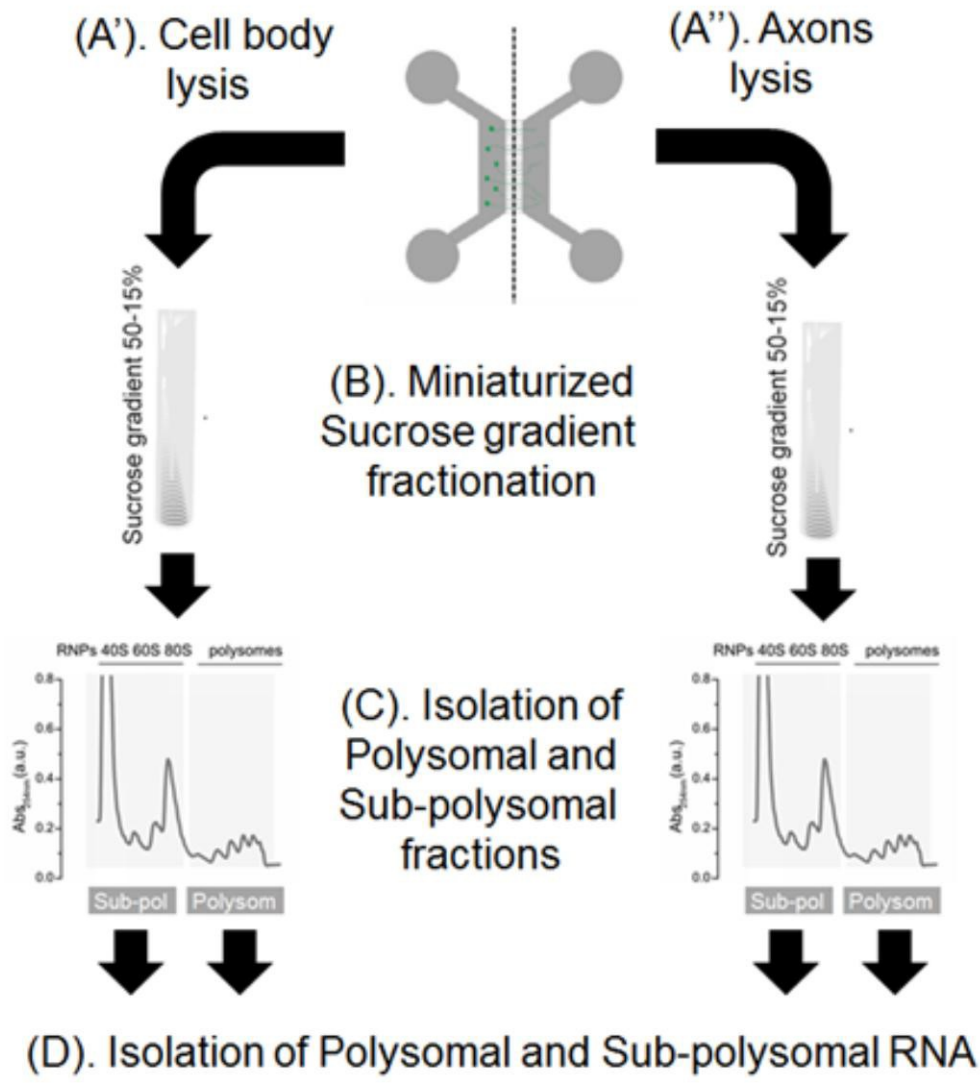


***Figure 5.20. Polysomal and sub-polysomal mRNAs were extracted from the axonal and cell body compartments of wtTDP, mutTDP and control neurons.*** *Representative scheme showing the experimental procedure for transcriptome and translatome analysis: wtTDP, mutTDP and ctrl neurons were grown in microfluidic chambers until 9 DIV. Then, cell body and axonal compartments were lysed (A'-A'') and the lysates were loaded onto a miniaturize sucrose gradient (B) to separate polysomal mRNAs and sub-polysomal mRNAs by polysome profiling (C). Then those mRNAs were isolated and sequenced (D).*

An initial bioinformatic analysis, performed by G. Viero's group, was conducted to

1) generate a collection of soma- and axon-specific differentially expressed genes (DEGs) displaying different levels in a comparison between ctrl somata and TDP-43-overexpressing somata, as well as between ctrl axons and the axon of TDP-43-overexpressing neurons. This differential expression analysis was conducted for both sub-polysomal and polysomal mRNAs.

2) compare the cell-body and axonal transcriptome and translatome within the same cell population (ctrl, wt TDP or mutTDP). This may be regarded as an indirect measure of cell-body-to-axon mRNA transport efficiency.

3) perform comparisons between polysomal and sub-polysomal fractions within each cell population (ctrl, wtTDP or mutTDP) and subcellular compartment (soma or axon). This may be regarded as an indirect measure of mRNA translation efficiency.

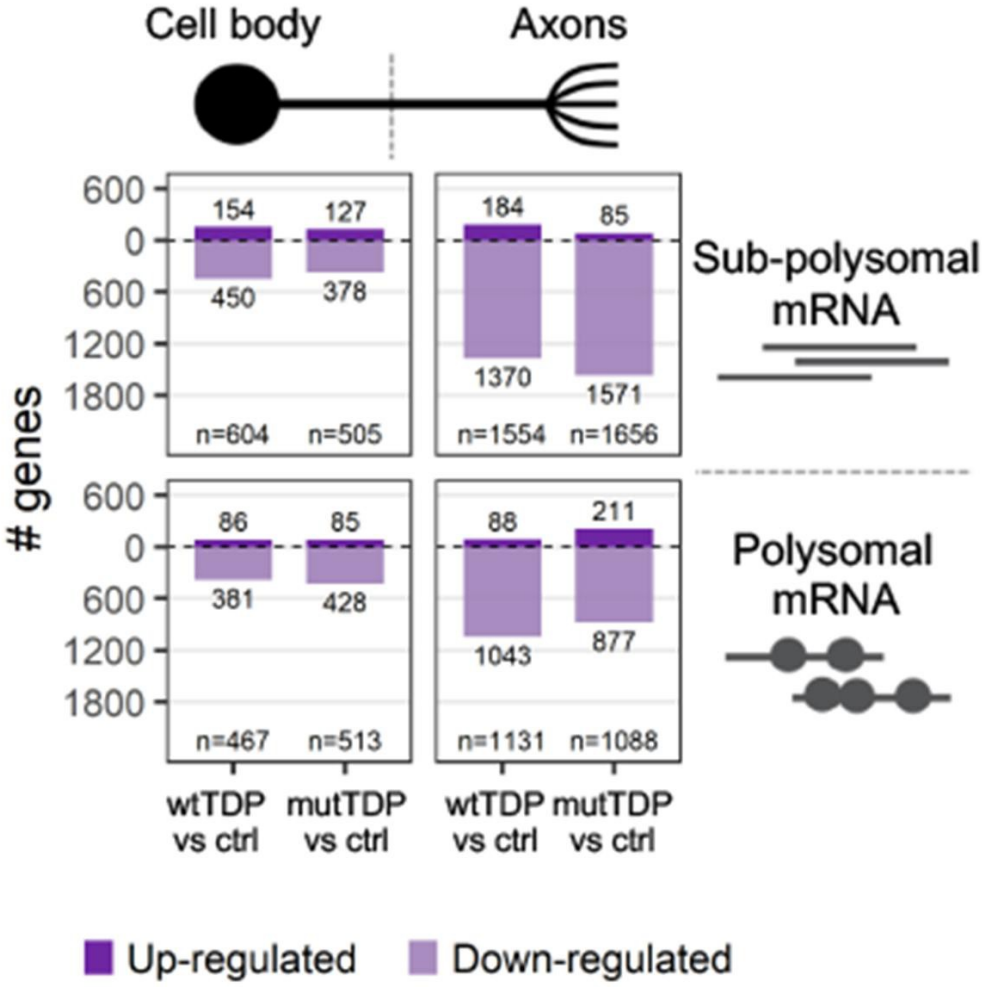


***Figure 5.21. wtTDP and mutTDP show several polysomal and sub-polysomal mRNAs downregulated in the axonal compartment relative to ctrl.*** *Graph showing number of genes differentially expressed in wtTDP and mutTDP neurons in cell body (on the left) and axonal compartment (on the right). The upper row shows sub-polysomal mRNAs, while the bottom row shows polysomal mRNAs. Purple: upregulated genes, light purple: downregulated genes. The number of genes differentially expressed in each compartment is shown close to each column. It is worth noticing that the number of downregulated genes, in the axonal compartment of both wtTDP and mutTDP relative to control (both polysomal and sub-polysomal), is 3-4 times higher than downregulated genes in the cell body compartment.*

In this thesis, I have focused my attention on the simplest of these comparisons, namely the first one, and have extended the analysis generated by the Viero lab focusing on differentially expressed genes connected to the functional analyses described below (Sections 5.2.4-10). The results of this comparison revealed that numerous mRNAs (particularly polysomal mRNAs) are differentially expressed in wtTDP and mutTDP neurons relative to ctrl, both in the cell body compartment and in the axon. Most differences were observed in the axonal compartment that exhibits a downregulation of both polysomal and sub-polysomal mRNAs in wtTDP and mutTDP neurons, relative to ctrls.

It is important to explain the reasons underlying our decision to focus our attention especially on polysomal RNAs rather than on the sub-polysomal fraction. In fact, while it would be inaccurate to assume that all polysomal mRNAs are being actively expressed - published data indicate that polysomes may be associated to RNA granules and maintained in a translationally silent status (reviewed in Richter & Coller, 2015) - we safely assume that the polysomal fraction is strongly enriched in mature, protein-coding mRNAs, as opposed to noncoding splicing variants. In fact, the latter are likely eliminated from the polysomal fraction by RNA mediated decay. This is particularly relevant for a TDP-43 overexpressing neuron, considering that TDP-43, among other functions, heavily regulates mRNA splicing.

Overall, this analysis revealed that the axonal levels of sub-polysomal and polysomal mRNAs are strongly affected by the cytoplasmic accumulation and aggregation of wt and mutated TDP-43 in these neurons.

Because the association of mRNA with polysomes does not necessarily imply that these transcripts are being actively translated, for these reasons from now on we will refer to these mRNAs more generally as polysome-engaged mRNA.

### *5.2.3 Numerous DEGs in the axonal compartment of wtTDP and mutTDP neurons encode ribosomal proteins and proteins involved in exo/endocytosis*

Our transcriptome and translatome analysis revealed that most differences observed between wtTDP and mutTDP neurons relative to ctrl occur in the axonal compartment. Moreover, since published evidence suggests that ALS is a distal axonopathy (inter alia Fischer *et al.*, 2004), we decided to focus on gene ontology (GO) terms relative to factors involved in axonal maintenance and function.

As shown in Fig. 5.22, many downregulated genes belong to GO categories related to synapses, endocytosis and RNA-binding in wtTDP axons, in both polysomal and sub-polysomal mRNAs. Similarly, in mutTDP axons a large share of downregulated genes belong to categories related to ribosomes, RNA binding and synapses.

A

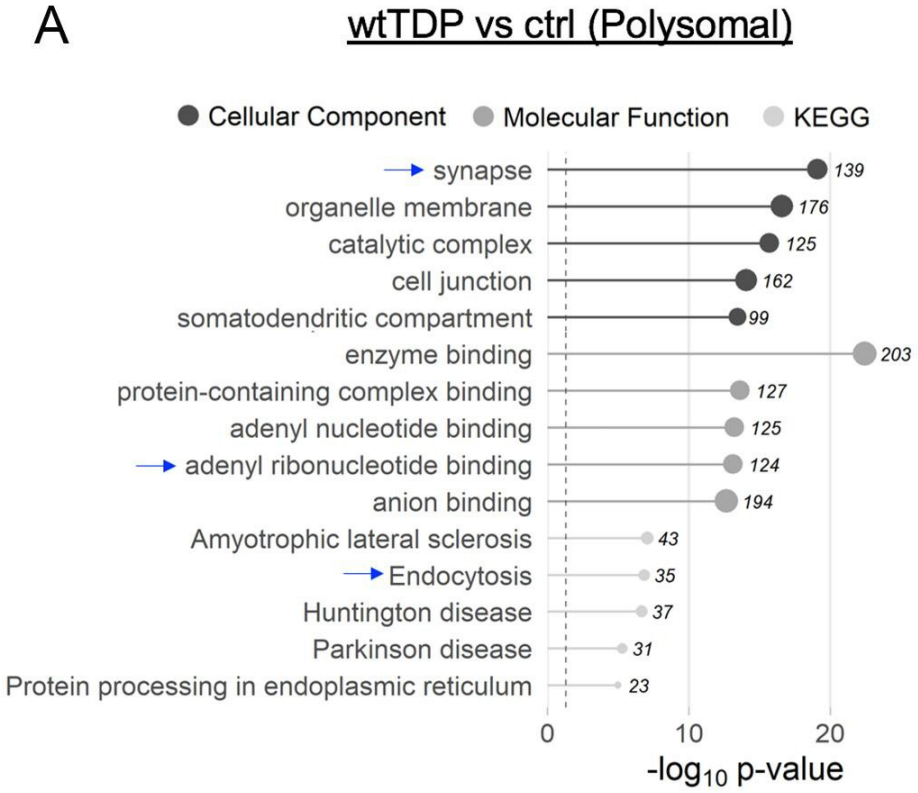
wtTDP vs ctrl (Polysomal)
Cellular Component
Molecular Function
KEGG
synapse
organelle membrane
catalytic complex
cell junction
somatodendritic compartment
enzyme binding
protein-containing complex binding
adenyl nucleotide binding
adenyl ribonucleotide binding
anion binding
Amyotrophic lateral sclerosis
Endocytosis
Huntington disease
Parkinson disease
Protein processing in endoplasmic reticulum
139
176
125
162
99
203
127
125
124
194
43
35
37
31
23
0
10
20
-log10 p-value

A'

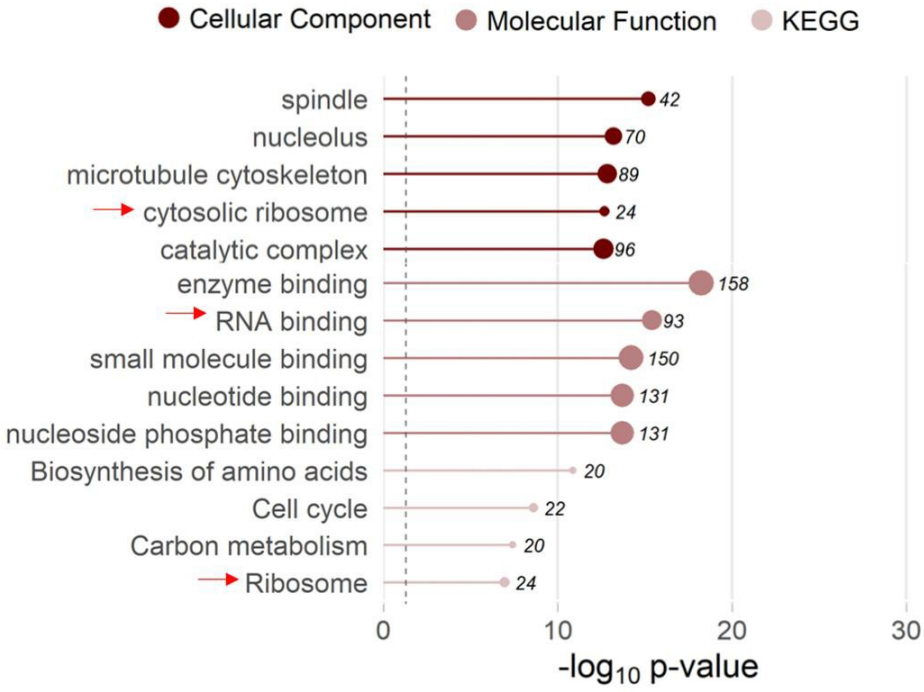
mutTDP vs ctrl (Polysomal)
Cellular Component
Molecular Function
KEGG
spindle
nucleolus
microtubule cytoskeleton
cytosolic ribosome
catalytic complex
enzyme binding
RNA binding
small molecule binding
nucleotide binding
nucleoside phosphate binding
Biosynthesis of amino acids
Cell cycle
Carbon metabolism
Ribosome
42
70
89
24
96
158
93
150
131
131
20
22
20
24
0
10
20
30
-log10 p-value

B

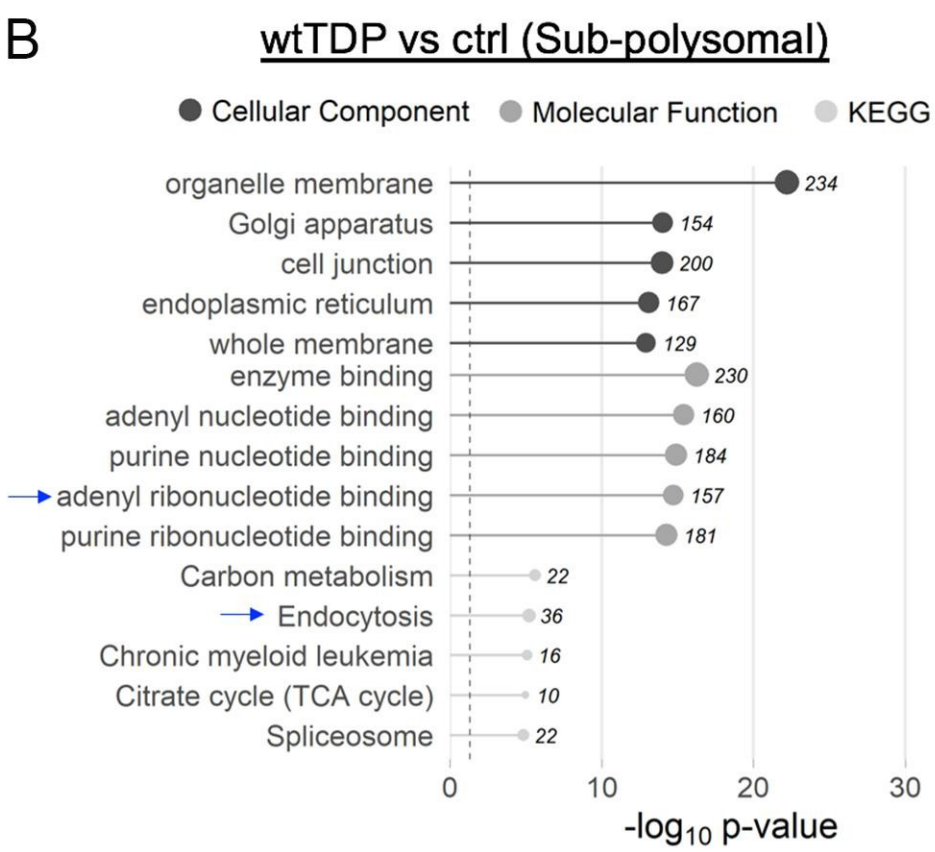
wtTDP vs ctrl (Sub-polysomal)
Cellular Component
Molecular Function
KEGG
organelle membrane 234
Golgi apparatus 154
cell junction 200
endoplasmic reticulum 167
whole membrane 129
enzyme binding 230
adenyl nucleotide binding 160
purine nucleotide binding 184
adenyl ribonucleotide binding 157
purine ribonucleotide binding 181
Carbon metabolism 22
Endocytosis 36
Chronic myeloid leukemia 16
Citrate cycle (TCA cycle) 10
Spliceosome 22
0
10
20
30
-log10 p-value

B'

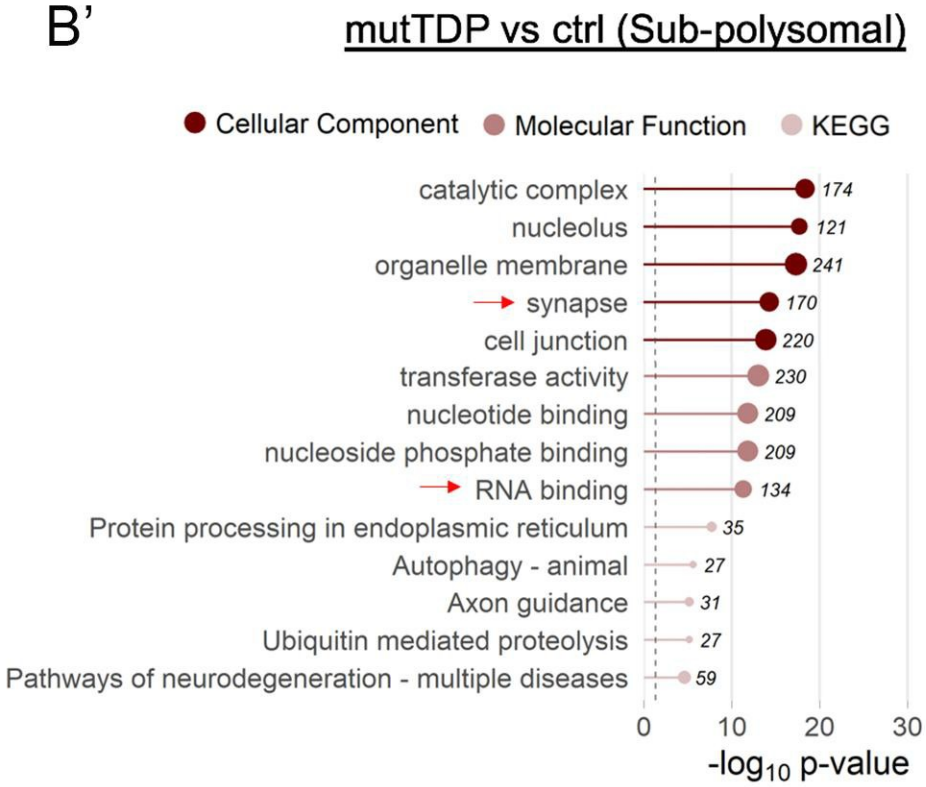
mutTDP vs ctrl (Sub-polysomal)
Cellular Component
Molecular Function
KEGG
catalytic complex 174
nucleolus 121
organelle membrane 241
synapse 170
cell junction 220
transferase activity 230
nucleotide binding 209
nucleoside phosphate binding 209
RNA binding 134
Protein processing in endoplasmic reticulum 35
Autophagy - animal 27
Axon guidance 31
Ubiquitin mediated proteolysis 27
Pathways of neurodegeneration - multiple diseases 59
0
10
20
30
-log10 p-value

***Figure 5.22. A summary of the most abundant GO categories downregulated in wtTDP and mutTDP axons relative to ctrl.*** *(A, A') Graphs showing the most abundant GO categories downregulated in the axon of wtTDP (A) and mutTDP (A') relative to ctrl of polysomal mRNA. (B, B') Graphs showing the most numerous GO categories downregulated in the axon of wtTDP (B) and mutTDP (B') relative to ctrl of sub-polysomal mRNA. Blue arrows show that many downregulated genes in wtTDP axons belong to GO categories relevant to RNA binding, synapses and endocytosis. Red arrows show that many downregulated genes in mutTDP axons belong to RNA binding, ribosomes and synapse categories. The length of each bar represents the -$log_{10}$ p-value. The width of each circle, at the top of each bar, is proportional to the number of genes present in each GO category. The number of genes in each GO category is present on the right of each circle.*

In conclusion, many genes belonging to synaptic processes and translation-related GO categories are significantly downregulated in the axonal compartment of wtTDP and mutTDP neurons.

### *5.2.4 wtTDP and mutTDP neurons show decreased levels of RPL26 in the axon and cell body*

As shown above, the abundance of ribosome-encoding mRNAs is sharply reduced in the axon of mutTDP neurons. This observation prompted questions as to whether ribosomal proteins are comparably downregulated in TDP-43-overexpressing vs. ctrl neurons. We investigated whether wtTDP and mutTDP neurons show decreased levels of the ribosomal protein RPL26 in the axon, relative to ctrl.

To this end, we immunostained wtTDP, mutTDP and ctrl neurons, grown in microfluidic chambers at 9 DIV, with antibodies to RPL26 and the axonal marker TuJ1 (the latter permits an easy localization of axons in microfluidic chambers). RPL26 signal was then quantified in the axon and cell body. As shown in Fig. 5.23, RPL26 protein levels are downregulated in both axons and cell bodies of wtTDP and mutTDP neurons relative to ctrl neurons.

In conclusion, the levels of the 60S ribosomal subunit RPL26 are downregulated in wtTDP and mutTDP axons and cell bodies relative to ctrl cells. However, under these experimental conditions, we cannot distinguish between cytosolic ribosomal proteins and assembled ribosomes or polysomes.

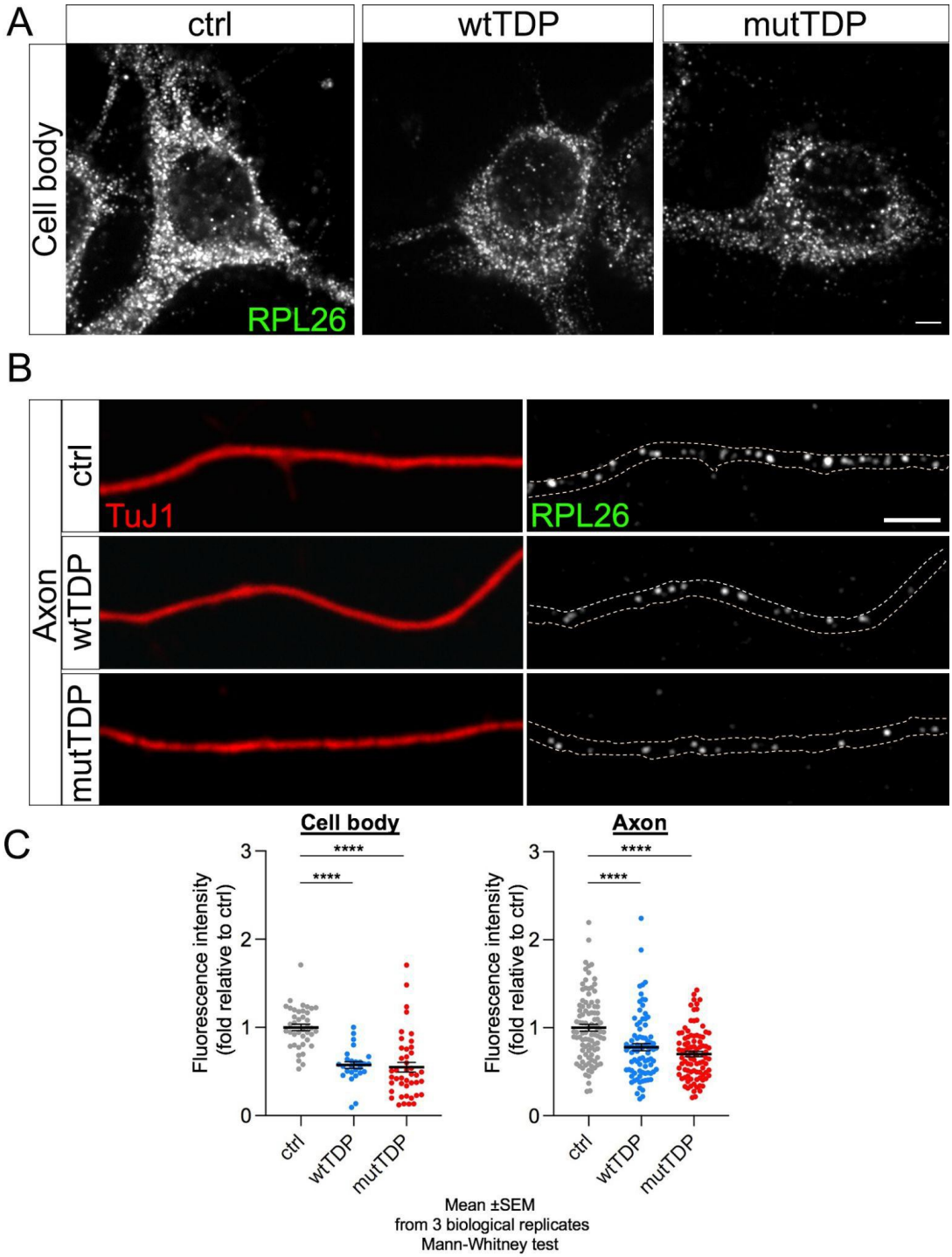


***Figure 5.23. RPL26 levels are downregulated in the axon and cell body of wtTDP and mutTDP neurons relative to ctrl.*** *(A-B) Immunofluorescence of cell bodies (A) and axons (B) of ctrl, wtTDP and mutTDP neurons with anti-TuJ1 (in red) and anti-RPL26 (in greyscale) antibodies. Dotted lines indicate axon borders (Size bar: 2.5µm). (C) Graphs showing wtTDP (in blue) and mutTDP (in red) mean fluorescence intensity of RPL26 relative to ctrl (in gray). The graphs show that RPL26 levels are downregulated in both the cell body (graph on the left) and axon (graph on the right). For axons, sections of 50µm length were analyzed. (Mean ±SEM, from 3 biological replicates, Mann-Whitney test, ****p-value<0.0001).*

### *5.2.5 wtTDP and mutTDP neurons show decreased translation in the axon and cell body relative to ctrl*

Since the ribosomal protein RPL26 is downregulated in both wtTDP and mutTDP neurons, we asked if the overall protein synthesis might be defective in these neurons. To assess whether mRNA translation is affected in wtTDP and mutTDP neurons, we carried out a puromycylation assay (see Materials and Methods), performed by incubating neurons with puromycin, an analog of aminoacyl-tRNA, which is incorporated in the polypeptide nascent chain, causing the release of the peptide and the disassembly of the two ribosomal subunits. By quantitative anti-puromycin immunostaining it is possible to quantify its incorporation as a measure of ongoing protein synthesis.

Thus, wtTDP, mutTDP and ctrl neurons, maintained in microfluidic chambers until 9 DIV, were incubated with 2μM puromycin for 5min, then cells were fixed and immunostained with an anti-Puromycin antibody. As shown in Fig. 5.24, in both wtTDP and mutTDP neurons puromycin signal is significantly reduced in the cell body, axon and growth cone.

Taken together, our results indicate that protein synthesis is significantly reduced in the axon of wtTDP and mutTDP neurons.

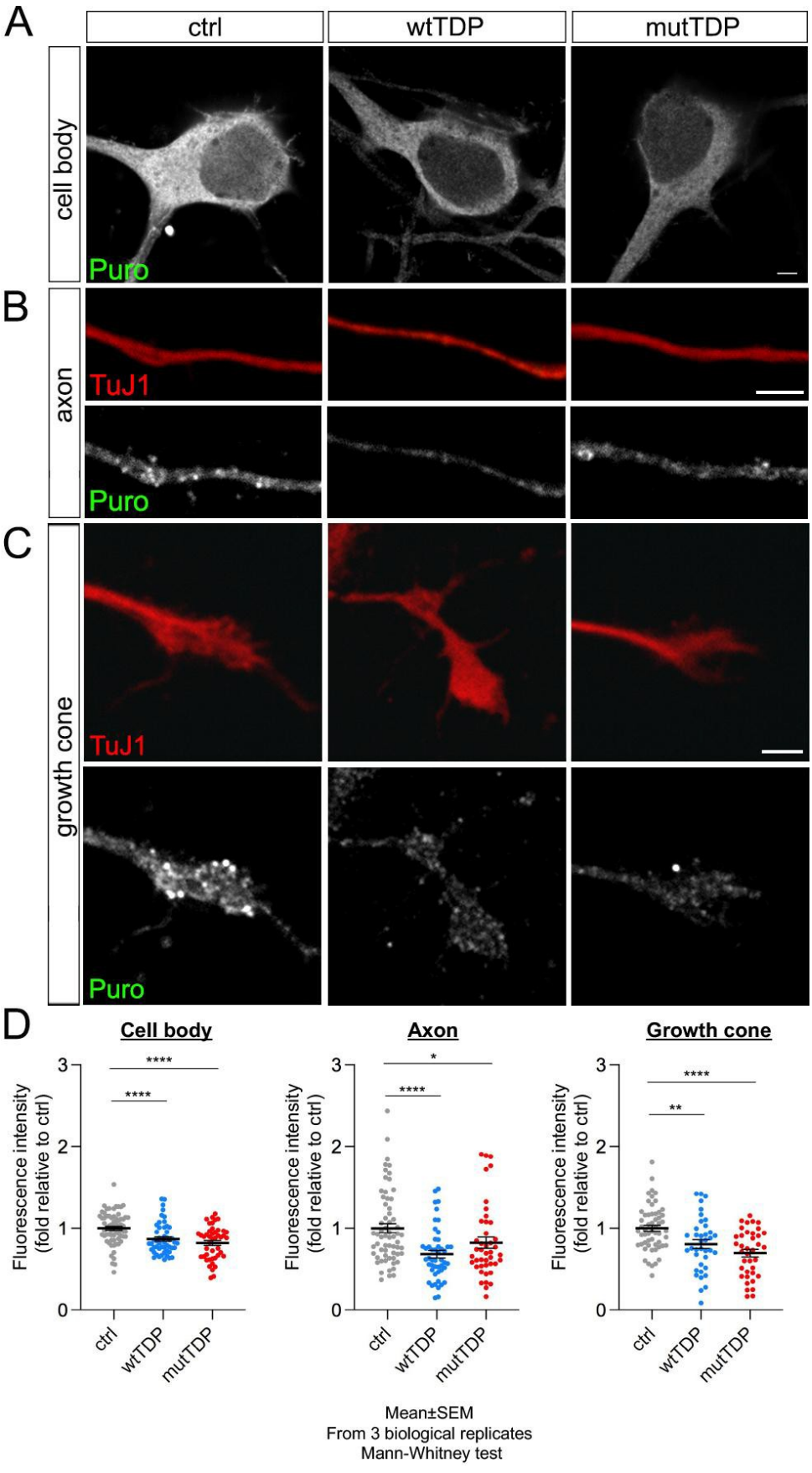
A
ctrl
wtTDP
mutTDP
cell body
Puro
B
axon
TuJ1
Puro
C
growth cone
TuJ1
Puro
D
Cell body
Axon
Growth cone
Fluorescence intensity (fold relative to ctrl)
****
****
*
****
****
**
ctrl
wtTDP
mutTDP
Mean±SEM
From 3 biological replicates
Mann-Whitney test

***Figure 5.24. wtTDP and mutTDP neurons show decreased translation in cell body, axon and growth cone, relative to ctrl.*** *(A-C) Immunofluorescence images of cell bodys (A), axons (B) and growth cones (C) of wtTDP, mutTDP and ctrl neurons, grown in microfluidic chambers until 9 DIV, with anti-TuJ1 (in red) and anti-puromycin (in greyscale). (Size bar: 2.5µm). (D) Graphs showing puromycin fluorescence intensity in cell body (graph on the left), axon (graph in the middle), growth cone (graph on the right) of wtTDP (in blue), mutTDP (in red) relative to ctrl (in gray) neurons. These graphs show that puromycin signal, and consequently translation, is decreased in wtTDP and mutTDP relative to ctrl in cell body, axon and growth cone. (Mean ±SEM, from 3 biological replicates, Mann-Whitney test, *p-value<0.05, **p-value<0.01, ****p-value<0.0001).*

### *5.2.6 wtTDP and mutTDP neurons show several downregulated polysome-engaged mRNAs related to protein synthesis in the axon and cell body*

A bird's eye view of the transcriptome and translatome did not provide a conclusive picture of the transcriptional landscape, so we decided to analyze subsets of differentially expressed axonal mRNAs based on features emerging from our functional analyses of TDP-43-overexpressing neurons. To this end, we interrogated GO term lists containing dysregulated genes subdivided into functional categories, looking for deregulated genes belonging to groups of GO categories related to the changes unveiled by our functional experiments.

Since protein synthesis is impaired in wtTDP and mutTDP neurons, we analyzed the RNA-seq data looking for genes involved in mRNA translation. In particular, we analyzed polysome-engaged mRNAs to focus on protein-encoding mRNAs as opposed to noncoding splicing variants that are enriched in the sub-polysomal fraction.

Interestingly, we found that in wtTDP neurons, relative to controls, 287 genes involved in mRNA translation are downregulated in the axon and 7 in the soma. Of these genes, 5 are shared between axon and soma compartments. Conversely, in mutTDP neurons relative to controls, 119 genes are downregulated in the axon and 207 in the soma, of which 13 are shared between axon and soma.

Moreover, among polysome-engaged mRNAs downregulated specifically in the axonal compartment, 47 are shared between wtTDP and mutTDP axons while 235 are wtTDP- specific and 59 are mutTDP-specific. This suggests that there are many genes downregulated in an allele-specific fashion.

While many mRNAs are underrepresented in the axon of TDP-43 overexpressing neurons, no polysome-engaged mRNA involved in mRNA translation was found upregulated in these neuronal populations compared to controls.

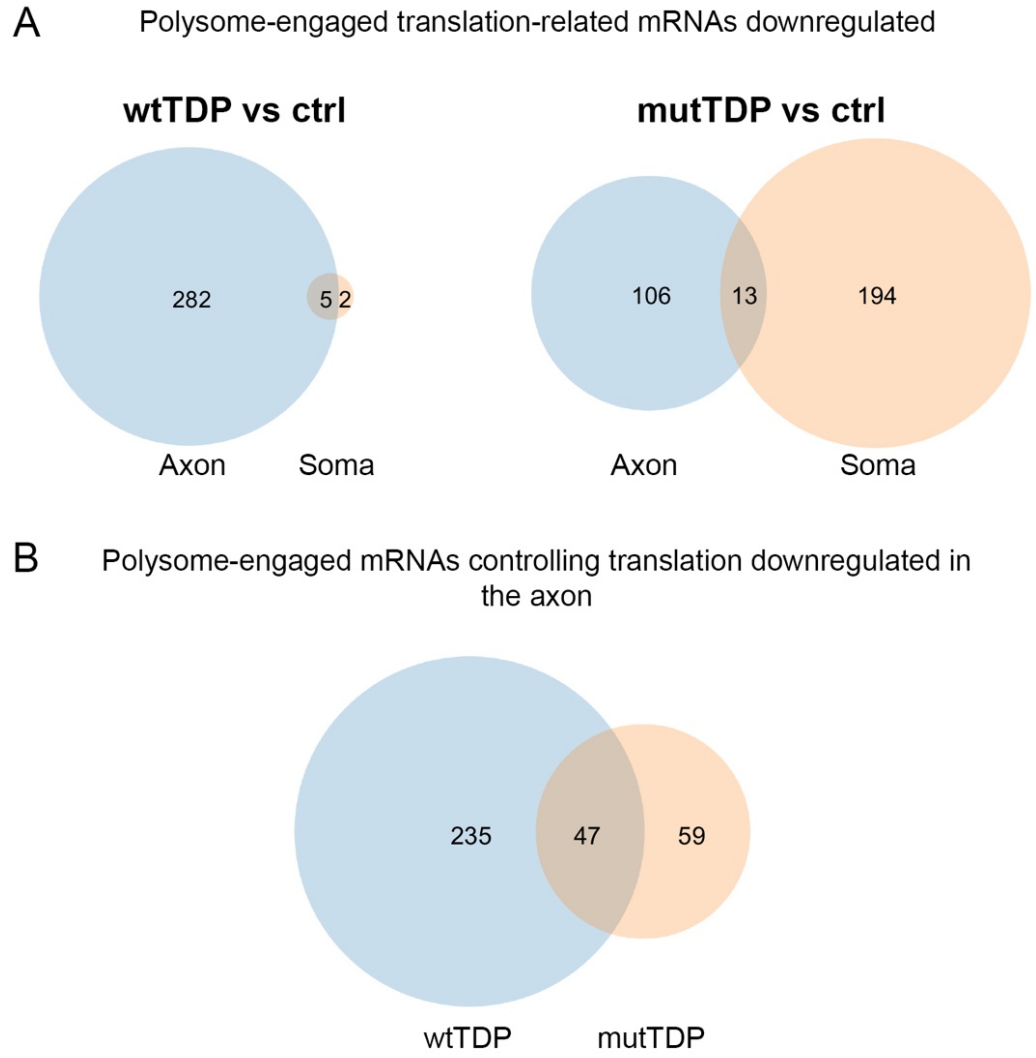


***Figure 5.25. Numerous polysome-engaged mRNAs involved in mRNA translation are downregulated in the axon of wtTDP and mutTDP neurons.*** *(A) Venn diagrams showing the number of downregulated polysome engaged mRNAs involved in mRNA translation in the axon (blue circle) and in the soma (orange circle) in wtTDP relative to ctrl neurons (on the left) and mutTDP relative to controls (on the right). Comparisons of wtTDP vs ctrl neurons show 287 polysome-engaged mRNAs downregulated in the axon and 7 in the soma, 5 of which are shared in both subcellular compartments. Thus, 282 are axon specific and 2 are soma specific. The analysis of mutTDP vs ctrl neurons shows 119 polysome-engaged mRNAs downregulated in the axon and 207 in the soma, 13 of which are reduced in both subcellular compartments. Thus, 106 are axon specific and 194 are soma specific. (B) Venn diagram showing the number of polysome-*

*engaged mRNAs involved in mRNA translation in the axonal compartment of wtTDP (blue circle) and mutTDP (orange circle). This comparison reveals that 47 downregulated genes are shared between wtTDP and mutTDP axons, while 235 are wtTDP-specific and 59 are mutTDP-specific. Query words: translation, ribosom*, polysom*. Created with https://www.meta-chart.com/venn#/.*

### *5.2.7 wtTDP and mutTDP neurons show increased oxidative stress under basal conditions and impaired ROS detoxification under mild chronic oxidative stress conditions*

As mentioned in section 3.1.3 of the Introduction, one of the pathological features of ALS neurons is the presence of high levels of reactive oxygen species (ROS) and ROS-associated damage (reviewed in Barber & Shaw, 2010). For this reason, we asked whether wtTDP and mutTDP neurons exhibit an increase in oxidative stress. To this end, neurons were loaded with the membrane-permeable dye 2',7'-dichlorodihydrofluorescein diacetate (H2DCFDA). Once in contact with intracellular ROS, this dye is oxidized to the highly fluorescent 2',7'-dichlorofluorescein (DCF) (Fig. 5.26A). Thus, fluorescence intensity increases with the intracellular levels of ROS, providing a measure of the level of oxidative stress.

To perform this test, wtTDP, mutTDP and ctrl neurons were incubated with H2DCFDA (Fig. 5.26B) and the intensity of DCF fluorescence was analyzed. Since oxidative stress increases with the days in vitro (Pelizzoni *et al*, 2011), neurons at both 9 DIV and 13 DIV were analyzed. As shown in Fig 5.26C-C', under basal conditions wtTDP and mutTDP neurons show increased oxidative stress relative to controls, at both 9 DIV and 13 DIV.

Subsequently, we analyzed the ability of cells to detoxify ROS in the presence of a mild chronic iron overload (a 2-day treatment with 20μM ferric ammonium citrate). Through the Fenton reaction ($Fe^{2+}+H_2O_2 \rightarrow Fe^{3+} + OH^{\bullet} + OH^-$), iron overload leads to increased ROS levels and, subsequently, to increased oxidative stress. As shown in the histogram in Fig 5.26C'', ROS levels in both wtTDP and mutTDP neurons are 2-fold higher than in ctrl cells after iron treatment.

In conclusion, wtTDP and mutTDP neurons show increased oxidative stress under basal conditions, and an impairment of their antioxidant capability.

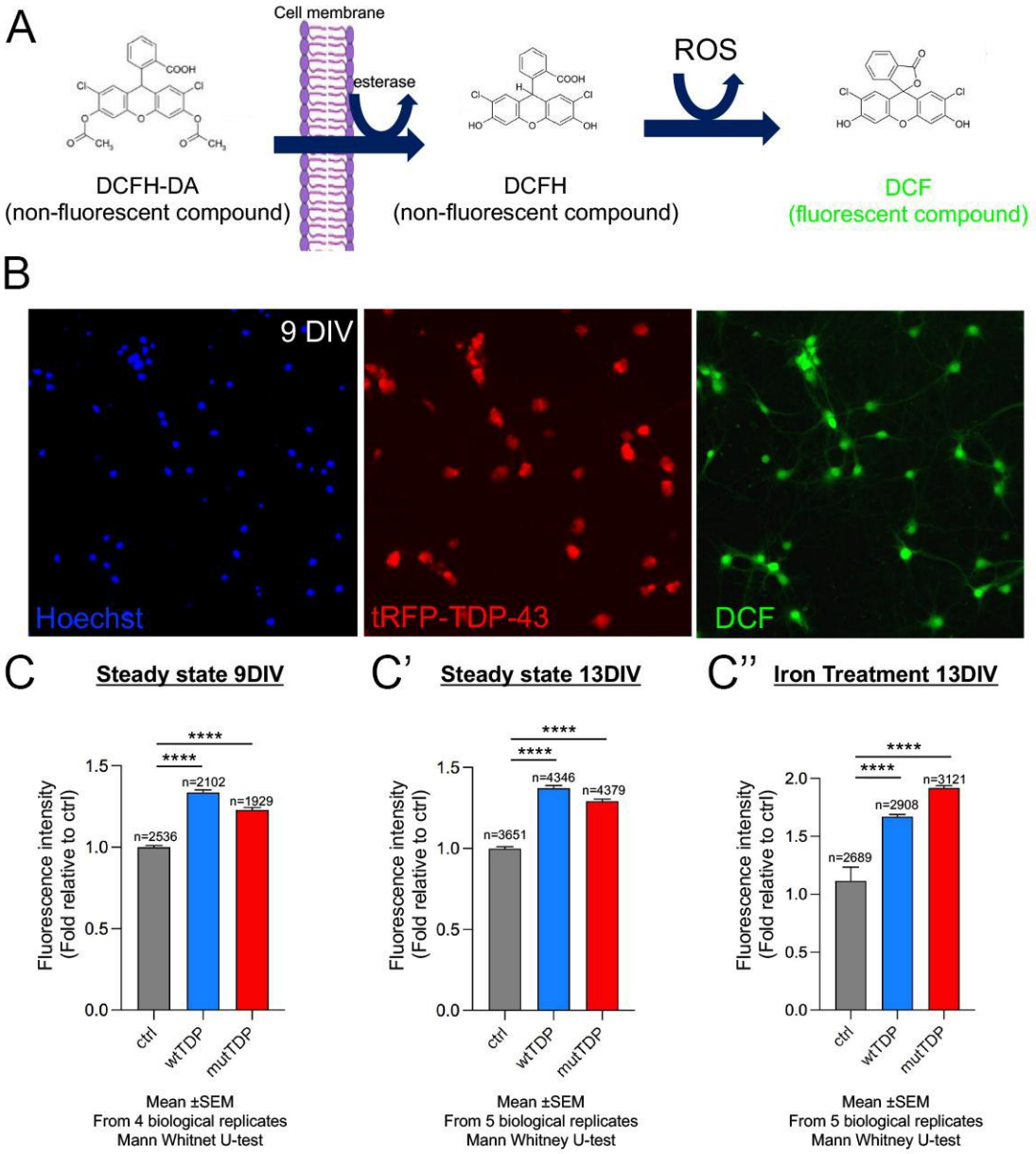


***Figure 5.26. wtTDP and mutTDP neurons show increased oxidative stress compared to ctrl neurons.*** *(A) Scheme illustrating the features of the H2DCFDA dye: the dye crosses the cell membrane where the acetate groups are removed by intracellular esterases. Then, once in contact with ROS, the dye is oxidized (DCF) and becomes fluorescent. (B) Representative results of the experiment sketched in A: neurons were treated with Hoechst to visualize the nuclei (left); transduced cells were detected thanks to tRFP (middle), and cells that have internalized DCF display green fluorescence (right). DCF fluorescence intensity is proportional to the levels of ROS. (C-C') Graphs showing the levels of DCF fluorescence intensity of wtTDP (blue) and mutTDP (red) normalized to ctrl fluorescence signal (gray). wtTDP and mutTDP show increased oxidative stress at steady state at 9 DIV (C) and at 13 DIV (C'). The increased oxidative stress of wtTDP and mutTDP neurons, relative to ctrl, is exacerbated after treatment with ferric ammonium citrate 20μM for 2days (C''). (Mean ±SEM, from 4 or 5 biological replicates, Mann Whitney U-test, ****p-value<0.0001; the number of analyzed cells is indicated above each column).*

### *5.2.8 wtTDP and mutTDP neurons show several downregulated polysome-engaged mRNAs related to the response to oxidative stress in the axon and cell body*

Since oxidative stress is increased in wtTDP and mutTDP neurons, as for translation-related genes, we analyzed the RNA-seq data looking for genes involved in oxidative stress response in the polysome-engaged fraction. We found that, in wtTDP relative to controls, 98 genes are downregulated in the axon and 12 in the soma. Of these genes, 4 are shared between axon and soma compartments. Instead, in mutTDP neurons relative to ctrl, 57 genes are downregulated in the axon and 57 genes in the soma; thirteen DEGs are shared between axon and soma. In this case only 8 downregulated genes are shared between wtTDP axons and mutTDP axons, while 86 are wtTDP-specific and 36 are mutTDP-specific. This suggests that the majority of downregulated genes, involved in oxidative stress response in the axonal compartment of TDP-43-overexpressing neurons, are specific for each allele. Again, we did not find any upregulated polysome-engaged mRNAs involved in oxidative stress, in wtTDP and mutTDP neurons alike, relative to ctrl neurons.

Our results strongly suggest that axonal mRNA translation may contribute importantly in the response to oxidative stress (see Discussion).


***Figure 5.27. Several polysome-engaged mRNAs involved in oxidative stress response are downregulated in the axon and cell body of wtTDP and mutTDP neurons.*** *(A) Venn diagrams showing the number of downregulated polysome-engaged mRNAs involved in oxidative stress in the axon (blue circle) and in the soma (orange circle) in wtTDP relative to ctrl neurons (on the left) and mutTDP relative to ctrl (on the right). wtTDP vs ctrl neurons show 98 polysome-engaged mRNAs downregulated in the axon and 12 in the soma, of which 4 genes are shared. Thus, 94 are axon specific and 8 are soma specific. mutTDP vs ctrl neurons show 57 polysome-engaged mRNAs downregulated in the axon and 57 in the soma, of which 13 genes are shared. Thus, 44 are axon specific and other 44 are soma specific. (B) Venn diagram showing the number of polysome-engaged mRNAs involved in the oxidative stress response in the axonal compartment of wtTDP (blue circle) and mutTDP (orange circle). This comparison reveals that 8 downregulated genes are shared between wtTDP and mutTDP axons while 86 are wtTDP-specific and 36 are mutTDP-specific. Query words used: oxidative; peroxid*; reactive oxygen species. Created with https://www.meta-chart.com/venn#/.*

### *5.2.9 wtTDP and mutTDP neurons show impaired exocytosis*

The GO analysis, illustrated in Fig. 5.22, revealed that numerous genes downregulated in the axon belong to synaptic-related GO categories, particularly in wtTDP neurons. For this reason, we decided to analyze the rate of exocytosis of wtTDP and mutTDP neurons, after depolarization stimulus, by means of the FM1-43 assay.

FM1-43 is a steryl dye that binds cell membranes and can be incorporated in vesicles after depolarizing stimulation (we used 30 mM KCl). Once internalized in the vesicles, FM1-43 becomes fluorescent; this fluorescent signal decreases over time when a second depolarization stimulus promotes vesicle exocytosis. The rate of fluorescence decay correlates with the rate of exocytosis.

Wild-type TDP, mutTDP and ctrl neurons were stimulated with high $K^+$ KRH (HK-KRH, see Materials and Methods), added to the medium together with FM1-43. Three to four washes with physiological extracellular KRH buffer were performed to remove non-internalized dye. Then a second stimulation with HK-KRH was performed (Fig. 5.28A-C) and the decay of fluorescence intensity over time was measured. As shown in Fig. 5.28D, mutTDP neurons and, particularly, wtTDP ones show an impairment of exocytosis compared to ctrl neurons.

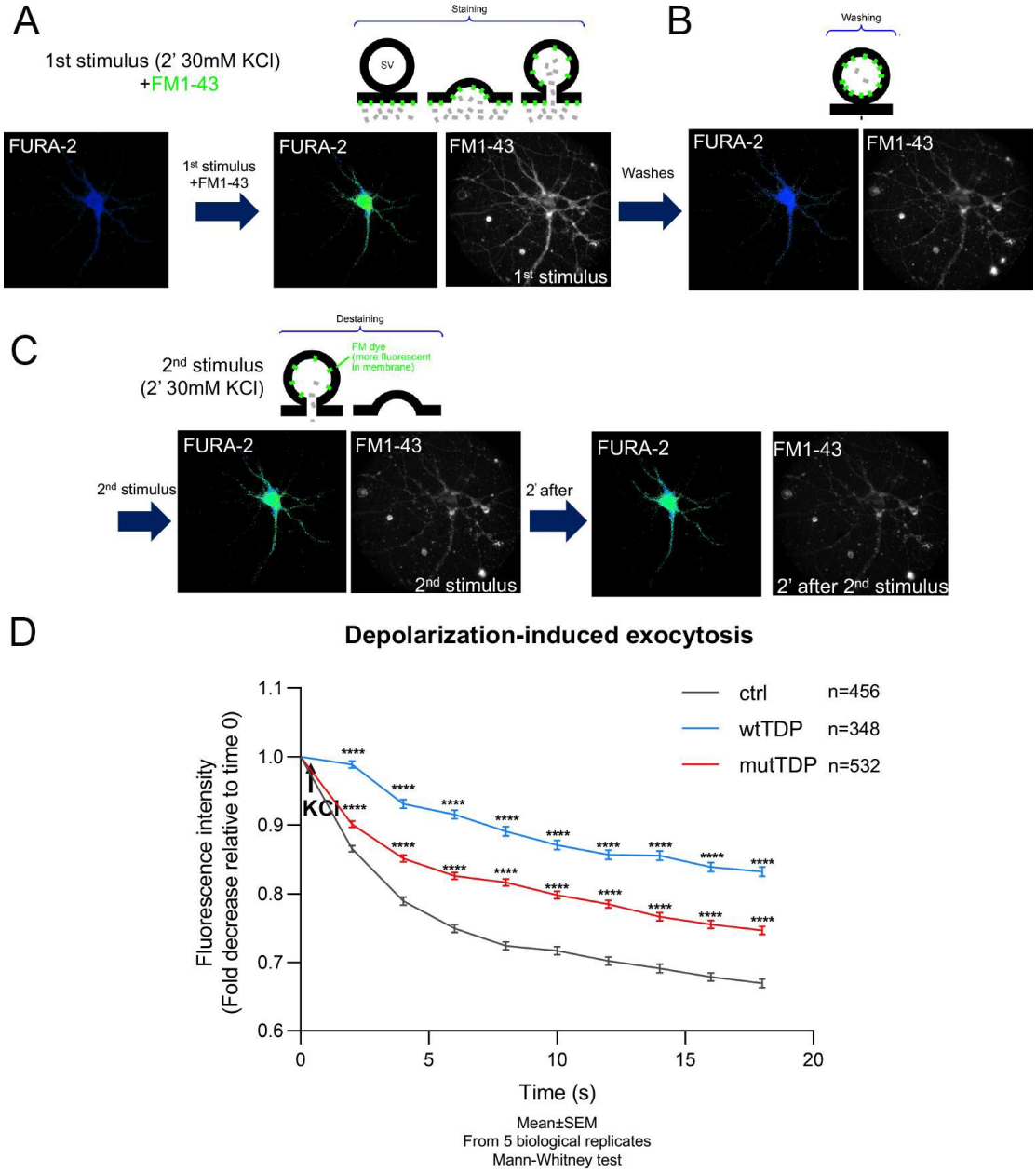


***Figure 5.28. Exocytosis is impaired in wtTDP and mutTDP neurons relative to ctrl.*** *(A-C) Representative images showing the FM1-43 assay steps. Neurons were treated with 10μM FM1-43 and 30mM KCl simultaneously for 2 min to stimulate endocytosis and promote internalization of the dye in the intracellular vesicles (A). 3-4 washes with physiological extracellular buffer (KRH) were performed to remove the excessive dye not internalized in the vesicles (B). A second stimulus with 30mM KCl was added to stimulate exocytosis of fluorescence-loaded vesicles. The decay of fluorescence over time was then measured (C). Fura-2 is a dye whose fluorescence correlates with intracellular calcium levels. Neurons were incubated with the Fura-2 dye 45 min before imaging analysis, as a control of the depolarization induced by KCl. (D) Graph showing the decay of FM1-43 fluorescence relative to time 0, when the second KCl stimulus was added, of wtTDP (blue), mutTDP (red) and ctrl cells (gray). The graph shows that mutTDP and particularly wtTDP neurons exhibit a significantly impaired exocytosis relative to ctrl neurons. (Mean ±SEM, from 5 biological replicates, Mann-Whitney test, ****p-value<0.0001, number of analyzed ROI: ctrl=456, wtTDP=348, mutTDP=532).*

### *5.2.10 wtTDP and mutTDP neurons show several downregulated polysome-engaged mRNAs encoding synaptic proteins in the axon and cell body*

As shown above, exocytosis is impaired in wtTDP and mutTDP neurons, thus we analyzed the RNA-seq data looking for genes encoding synaptic components. Also in this case we focused on polysome-engaged mRNAs.

In wtTDP neurons relative to controls, 441 genes related to synaptic assembly, function and maintenance are downregulated in the axon and 117 in the soma. Of these genes, 46 are shared between axon and soma compartments. However, in mutTDP relative to ctrl neurons, 243 genes are downregulated in the soma and 235 genes in the axon, and only 35 DEGs are shared between axon and soma. Moreover wtTDP and mutTDP share many downregulated genes axon specific encoding synaptic proteins (94 genes), while 301 are wtTDP-specific and 114 are mutTDP-specific. These results indicate that cytoplasmic TDP-43 accumulation affects the expression of distinct genetic regulons in the axon vs. the soma.

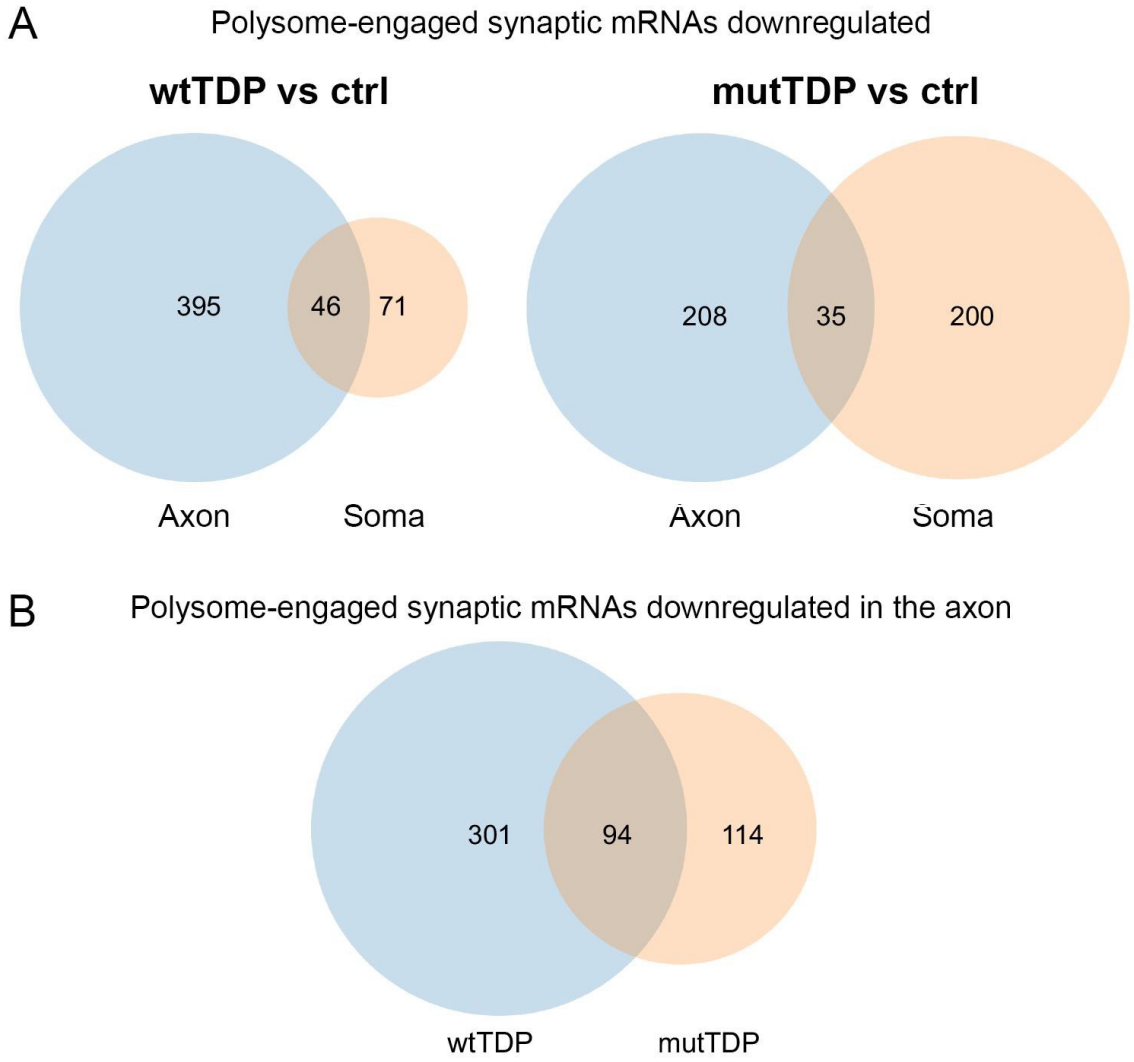


***Figure 5.29. Several polysome-engaged mRNAs encoding synaptic proteins are downregulated in the axon and cell body of wtTDP and mutTDP neurons.*** *(A)Venn diagrams showing the number of downregulated polysome-engaged mRNAs encoding synaptic proteins in the axon (blue circle) and in the soma (orange circle) in wtTDP relative to ctrl neurons (left) and mutTDP relative to ctrl neurons (right). wtTDP vs ctrl neurons show 441 polysome-engaged mRNAs downregulated in the axon and 117 in the soma, of which 46 genes are shared. Thus, 395 genes are axon specific and 71 are soma specific. mutTDP vs ctrl neurons show 243 polysome-engaged mRNAs downregulated in the axon and 235 in the soma, while only 35 DEGs are shared. Thus, 208 DEGs are axon specific and 200 are soma specific. (B) Venn diagram showing that, of the axonal specific genes, wtTDP and mutTDP axons share 94 downregulated genes while 301 are wtTDP-specific and 114 are mutTDP- specific. Query words: synap*; vesicle; exocyt*; endocyt*; neurotransmitter; NOT postsynaptic. Created withhttps://www.meta-chart.com/venn#/.*

Moreover, we found a pool of upregulated genes encoding synaptic proteins in wtTDP and mutTDP neurons relative to controls, of which only one is shared between wtTDP and mutTDP axons (Fig. 5.30).

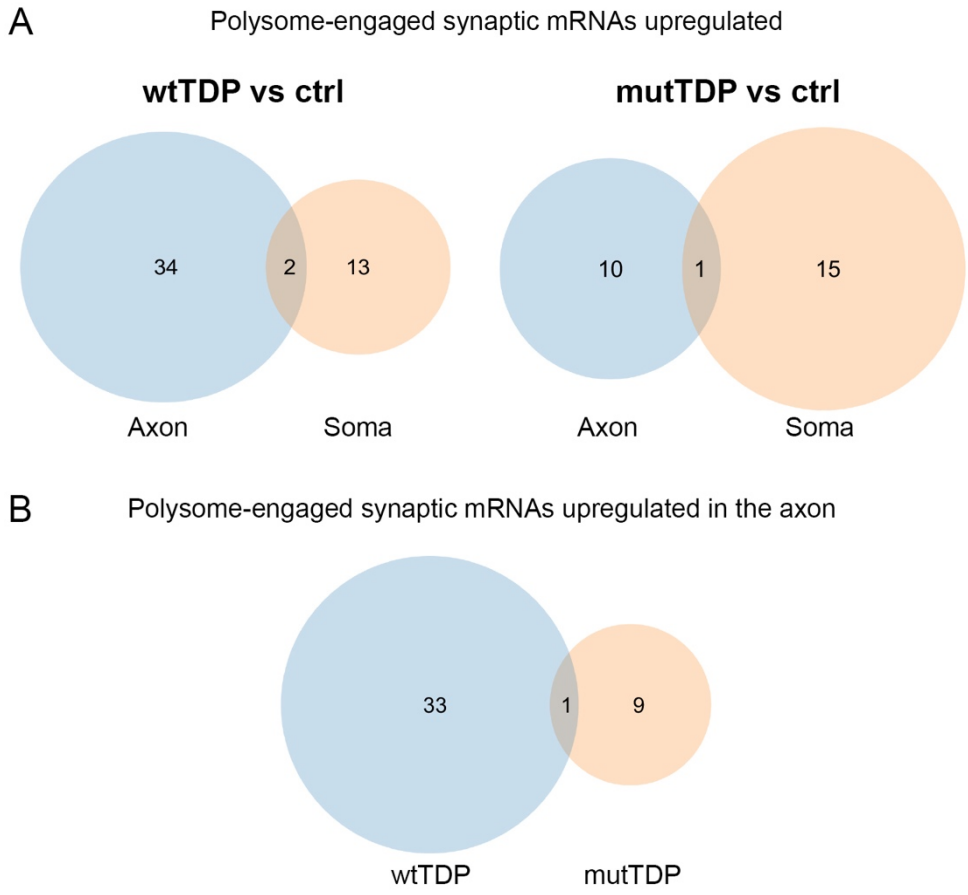


***Figure 5.30. A subset of polysome-engaged mRNAs encoding synaptic proteins are upregulated in the axon and cell body of wtTDP and mutTDP neurons.*** *(A) Venn diagrams showing the number of upregulated polysome-engaged mRNAs encoding synaptic proteins in the axon (blue circle) and in the soma (orange circle) in wtTDP relative to ctrl neurons (on the left) and mutTDP relative to ctrl (on the right). wtTDP vs ctrl neurons show 36 polysome-engaged mRNAs upregulated in the axon and 15 in the soma, of which 2 genes are shared. Thus, 34 genes are axon specific and 13 are soma specific. mutTDP vs ctrl neurons show 11 polysome-engaged mRNAs upregulated in the axon and 16 in the soma, of which one gene is shared. Thus, 10 are axon specific and the other 15 are soma specific. (B) Venn diagram showing that wtTDP and mutTDP share 1 upregulated gene in the axonal compartment while 33 are wtTDP-specific and 9 mutTDP-specific. Query words: synap*; vesicle; exocyt*; endocyt; neurotransmitter; NOT postsynaptic. Created with https://www.meta-chart.com/venn#/.*

Overall we can conclude that several genes encoding synaptic proteins are differentially regulated in wtTDP and mutTDP neurons relative to ctrl.

### *5.2.11 wtTDP and mutTDP neurons show decreased levels of mRNAs mediating the response to oxidative stress*

Our functional analysis revealed that oxidative stress is increased in wtTDP and mutTDP neurons and exocytosis is impaired in these two neuronal populations. For this reason, we decided to validate by RT-qPCR a subset of genes, involved in oxidative stress and synaptic functions, downregulated in the axon of wtTDP and mutTDP neurons.

For consistency, the RT-qPCRs was performed by Gabriella Viero's group starting from RNA extracts obtained from wtTDP and mutTDP neurons after tag-free polysome isolation, as performed for the RNA-sequencing starting materials. Gabriella Viero's lab validated by RT-qPCR the following genes: *Synaptojanin-1 (Synj1),* involved in the recycling of endocytic vesicles, *Mitogen-Activated Protein Kinase Kinase Kinase Kinase 4 (Map4k4), Oxidation Resistance 1 (Oxr1), Parkinsonism Associated Deglycase 7 (Park7), SHC Adaptor Protein 1 (Shc1)* involved in the oxidative stress response. As shown in Fig. 5.31, the RT-qPCR revealed that *Synj1, Park7* and *Shc1* are downregulated in wtTDP and mutTDP axons relative to ctrl in both polysomal and sub-polysomal fractions.

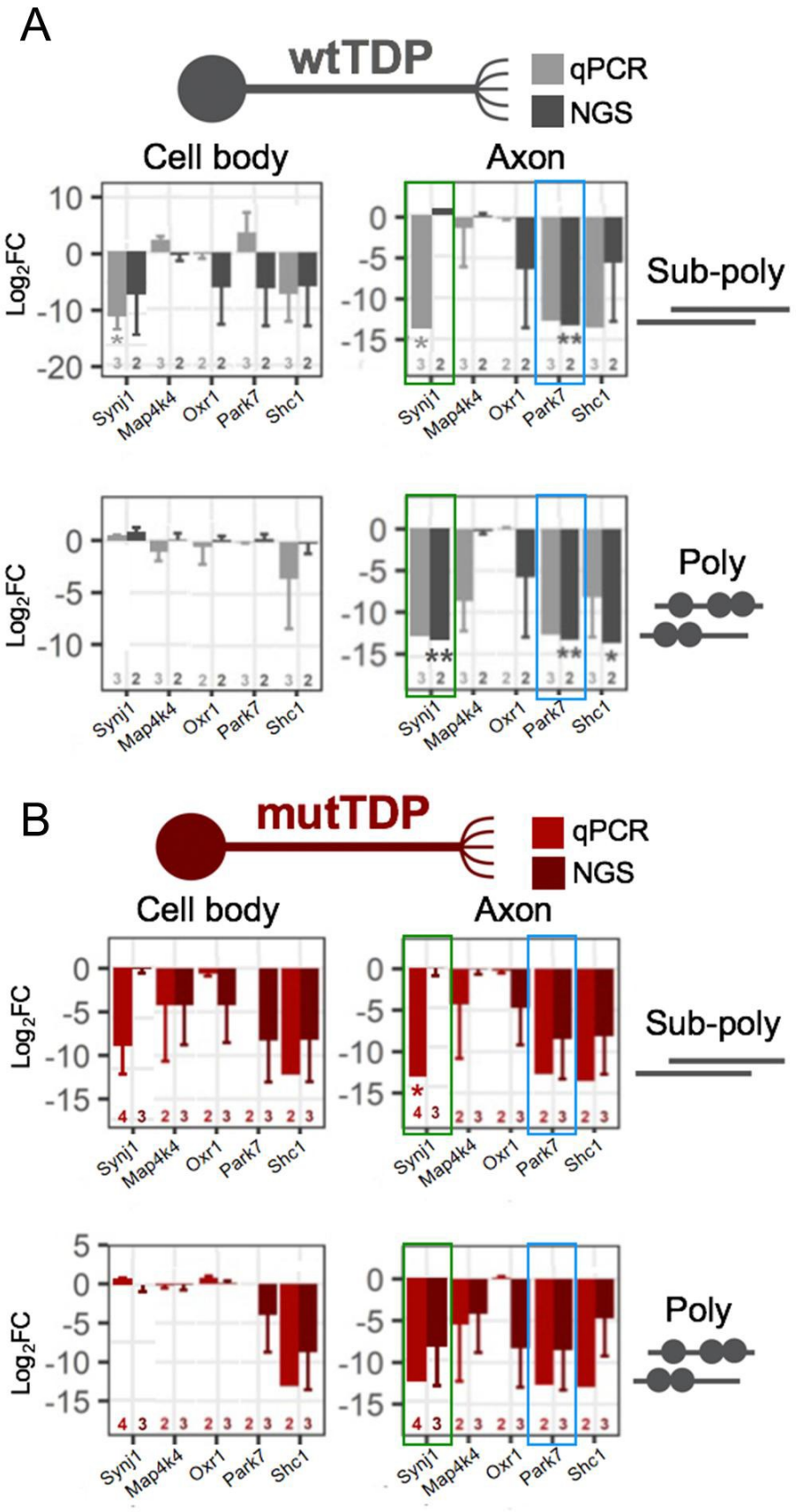
A
wtTDP
qPCR
NGS
Cell body
Axon
Log2FC
Sub-poly
Poly
Synj1
Map4k4
Oxr1
Park7
Shc1
B
mutTDP
qPCR
NGS
Cell body
Axon
Log2FC
Sub-poly
Poly
Synj1
Map4k4
Oxr1
Park7
Shc1

***Figure 5.31. Synj1 and Park7 are downregulated in the axon of wtTDP and mutTDP relative to ctrl in both polysomal and sub-polysomal fractions.*** *(A) Graph showing the $log_2$ fold change ($Log_2FC$) of qPCR (in light gray) and NGS (dark gray) of the indicated genes in wtTDP neurons, relative to ctrl. Values relative to the cell body are shown on the left and those obtained in the axon on the right; the sub-polysomal fraction is shown in the top row and the polysomal fraction in the bottom row. (B) Graph showing the $Log_2FC$ of qPCR (in light red) and NGS (dark red) of the indicated genes in mutTDP neurons, relative to ctrl ones. The cell body is shown on the left and the axon on the right; the sub-polysomal fraction is shown in the top row and the polysomal fraction in the bottom row. Synj1 is downregulated in both sub-polysomal and polysomal compartment of wtTDP and mutTDP axons relative to ctrl axons (green rectangle). Likewise, Park7 is downregulated in the sub-polysomal and polysomal compartment of wtTDP and mutTDP axons relative to ctrl ones (blue rectangle). (Mean ±SD, biological replicates are indicated under each column, t-student test, *p-value<0.05, **p-value<0.01).*

Considering these results, we decided to focus on PARK7, which is a chaperone that has a ROS scavenger function and acts as a sensor of oxidative stress by activating oxidative stress response signaling pathways (reviewed in Huang & Chen, 2021).

Based on the above findings, we extended our characterization to the PARK7 protein in wtTDP and mutTDP neurons. To this end, wtTDP, mutTDP and ctrl neurons, grown in microfluidic chambers until 9 DIV, were immunostained with a PARK7 antibody and while axons were visualized by TuJ1 immunostaining. As shown in Fig. 5.32, wtTDP neurons show a downregulation of PARK7 protein levels in the axonal compartment, while no difference was detected in the cell body. Conversely, in mutTDP neurons, PARK7 protein downregulation is observed in the cell body and axonal compartment alike.

Overall, we can conclude that wtTDP neurons exhibit an axon-specific downregulation of the Park7 transcript and of the corresponding protein.

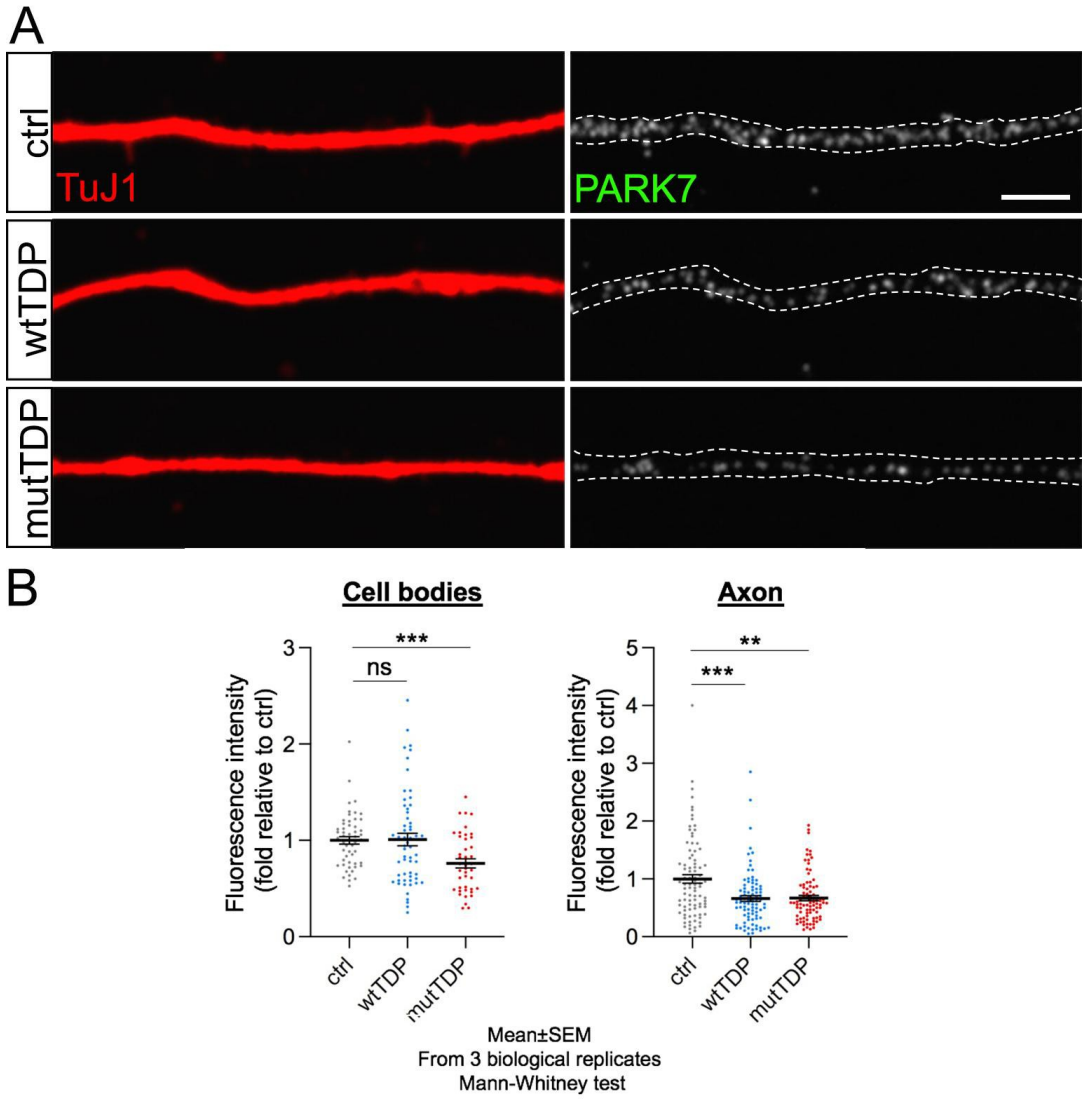


***Figure 5.32. wtTDP and mutTDP neurons show decreased PARK7 levels in the axon.*** *(A) Immunofluorescence of ctrl, wtTDP and mutTDP axons with anti-TuJ1 (in red) and anti-PARK7 (in greyscale) antibodies. Dotted lines indicate axon borders. (Size bar: 2.5µm). (B) Graphs showing wtTDP (in blue) and mutTDP (in red) mean fluorescence intensity of PARK7 relative to ctrl (in gray). The graphs show that PARK7 levels are downregulated in mutTDP cell body but not in wtTDP (graph on the left), while it is downregulated in both mutTDP and wtTDP axons (graph on the right). Thus in wtTDP neurons there is an axonal specific downregulation of PARK7, while in mutTDP neurons there is a general downregulation of PARK7 protein in both cell body and axon. For axons, sections of 30µm length were analyzed. (Mean ±SEM, from 3 biological replicates, Mann-Whitney test, **p-value<0.01, ***p-value<0.001).*

### *5.2.12 mutTDP neurons show decreased levels of SYNJ1 protein in the axon*

As shown above, RT-qPCR confirmed that *Synj1* is downregulated in the axon of wtTDP and mutTDP neurons. SYNJ1 is involved in synaptic vesicle recycling and facilitates the disassembly of the clathrin coating that encloses endocytic vesicles (Cremona *et al*, 1999). Given its key function in synaptic transmission, we investigated whether the SYNJ1 protein is downregulated in wtTDP and mutTDP axons relative to ctrl ones.

To this end, we immunostained wtTDP, mutTDP and ctrl neurons grown in microfluidic chambers, with an anti-SYNJ1 antibody. As shown in Fig. 5.33, mutTDP neurons show reduced levels of SYNJ1 in the axon relative to ctrl one, while there is no difference in the cell body compartment, thus this phenotype is axon specific. wtTDP neurons, instead, show non-significantly reduced levels of SYNJ1 in the axon relative to ctrl, while they show significantly reduced levels in the cell body.

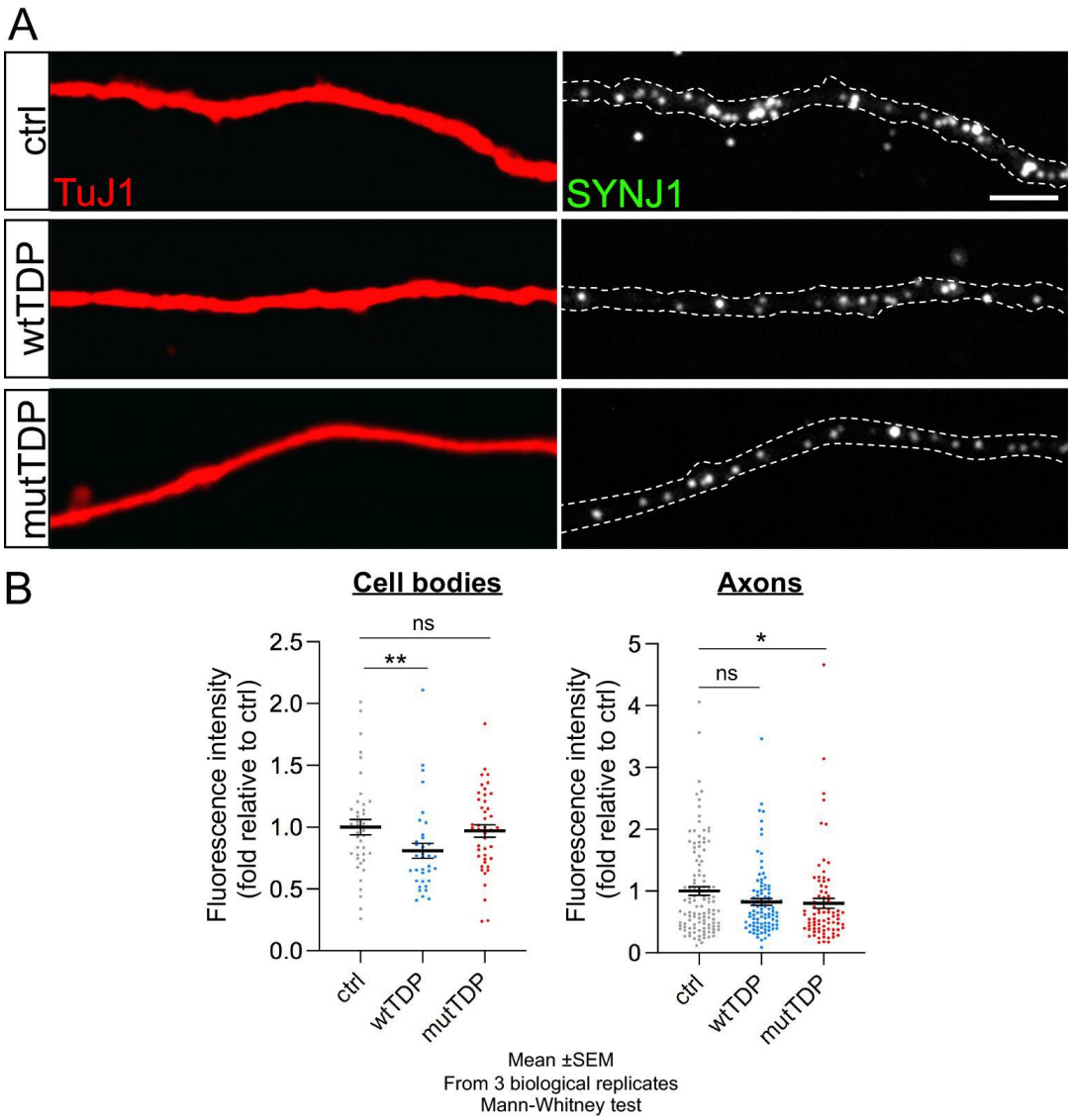


***Figure 5.33. mutTDP neurons show decreased SYNJ1 levels in the axon.*** *(A) Immunofluorescence of ctrl, wtTDP and mutTDP axons with anti-TuJ1 (in red) and anti-SYNJ1 (in greyscale) antibodies. Dotted lines indicate axon borders. (Size bar: 2.5µm). (B) Graphs showing wtTDP (in blue) and mutTDP (in red) mean fluorescence intensity of SYNJ1 relative to ctrl (in gray). The graphs show that SYNJ1 levels are downregulated in wtTDP cell body but not in mutTDP (graph on the left), it is downregulated in mutTDP axons but not in wtTDP ones (graph on the right). Thus, in mutTDP neurons there is an axon- specific downregulation of SYNJ1. For axons, sections of 30µm length were analyzed. (Mean ±SEM, from 3 biological replicates, Mann-Whitney test, *p-value<0.05, **p-value<0.01).*

### *5.2.13 wtTDP and mutTDP neurons show no differences in SNAP25 protein levels in the axon and cell body*

In addition to *Synj1,* Gabriella Viero's group validated, by RT-qPCR, another subset of genes encoding synaptic proteins, which were found downregulated in the axon of wtTDP and mutTDP neurons in RNA-seq analysis. The validated genes are: *Protein Tyrosine Phosphatase Receptor Type D (Ptprd), Regulating Synaptic Membrane Exocytosis 3 (Rims3), SH3GL interacting endocytic adaptor 1 (Sgip1), Synaptosomal-Associated Protein, 25kDa (Snap25), Sorting nexin-2 (Snx2), Syntaxin Binding Protein 1(Stxbp1) and Synaptotagmin-7 (Syt7).*

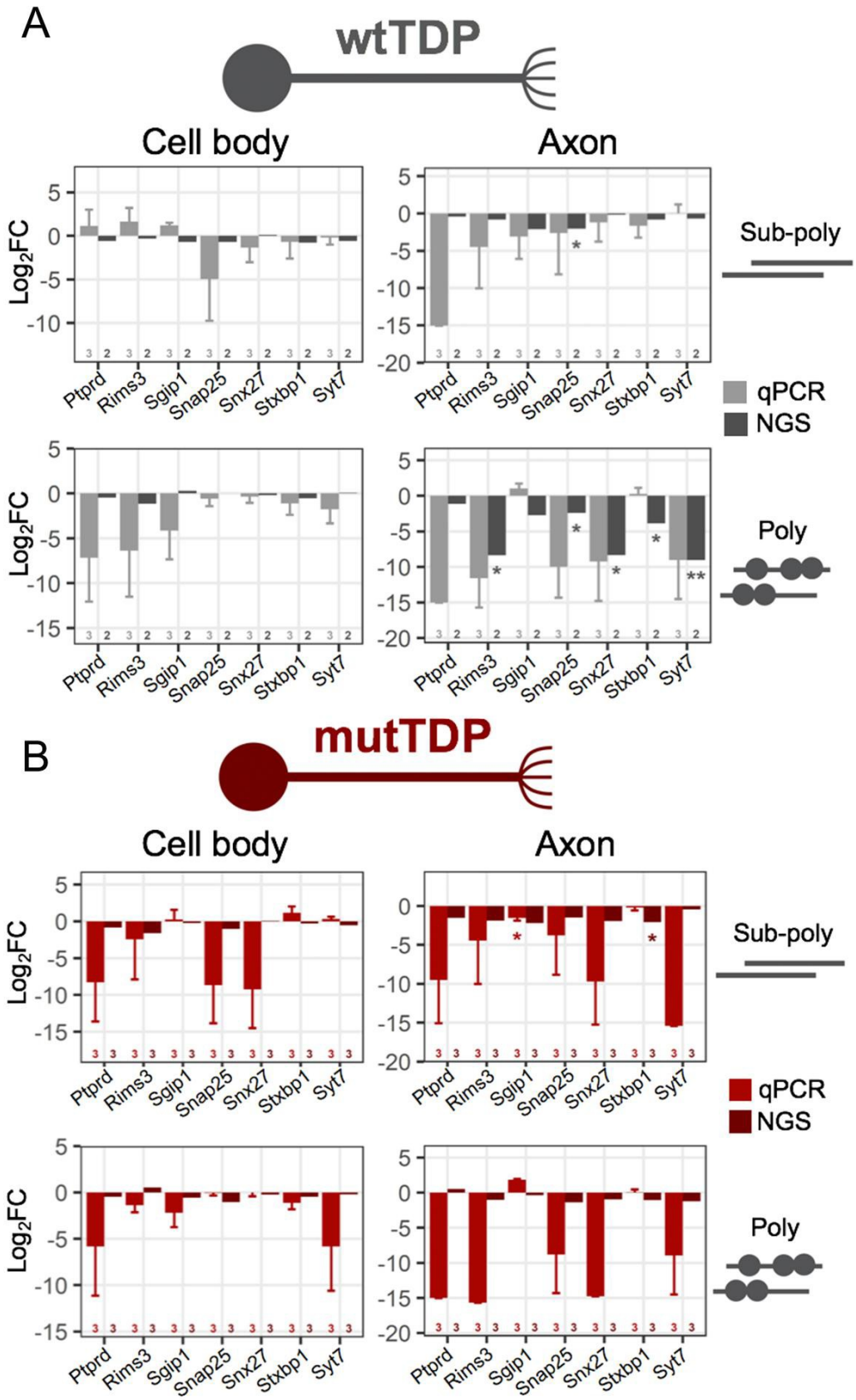


***Figure 5.34. Ptprd, Snap25, Snx27, Rims3 and Syt7 are downregulated in the axon of wtTDP and mutTDP relative to ctrl in both polysomal and sub-polysomal fraction.*** *(A) Graph showing*

*the $Log_2FC$ of qPCR (in light gray) and NGS (dark gray) of the indicated genes in wtTDP neurons, relative to ctrl. The cell body is shown on the left and axon on the right, the sub-polysomal fraction is shown in the upper row and polysomal fraction in the bottom row. (B) Graph showing the $Log_2FC$ of qPCR (in light red) and NGS (dark red) of the indicated genes in mutTDP neurons relative to ctrl. (Mean ±SD, biological replicates are indicated under each column, t-student test, *p-value<0.05, **p-value<0.01).*

As shown in Fig. 5.34, the RT-qPCR revealed that *Ptprd, Snap25, Snx27, Rims3* and *Syt7* mRNAs are strongly downregulated in wtTDP and mutTDP axons in both polysomal and sub-polysomal fractions.

We decided to focus on *Snap25*, which is a t-SNARE protein involved in calcium-triggered exocytosis (Fig. 5.35).

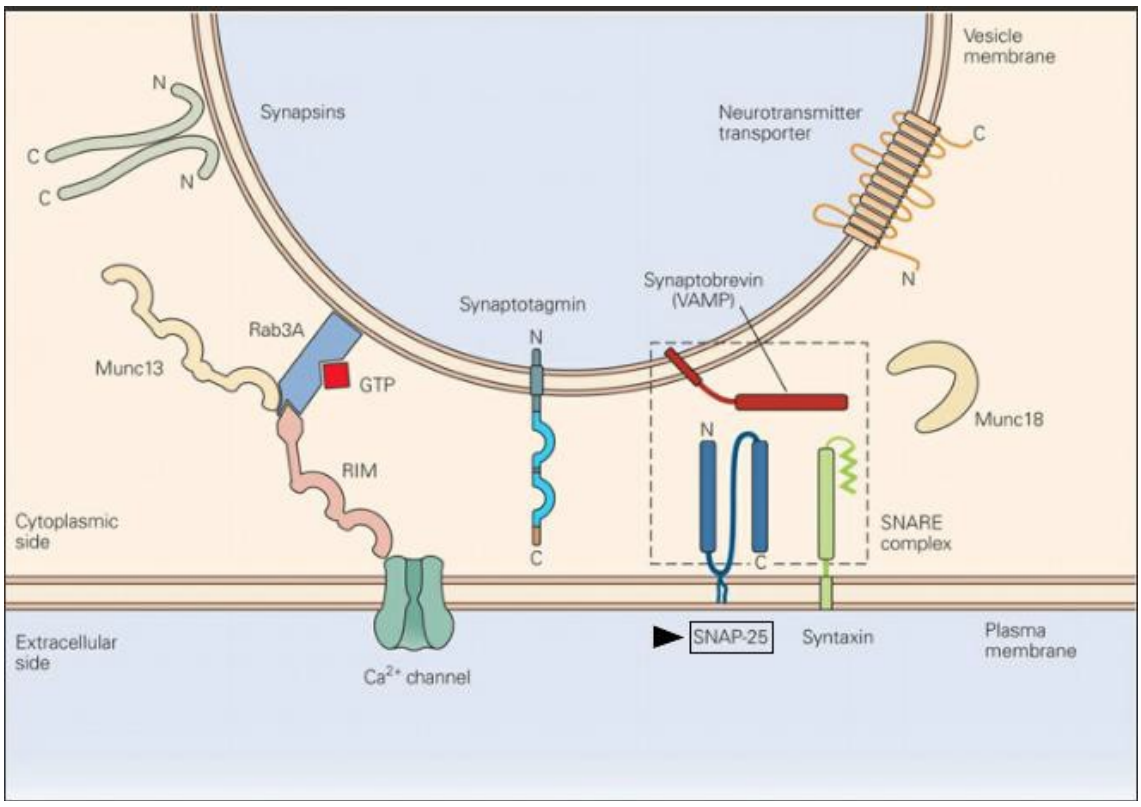


***Figure 5.35. SNAP25 is a t-SNARE involved in synaptic vesicle exocytosis and neurotransmitter release.*** *Representative image showing a synaptic vesicle with its membrane proteins near the presynaptic plasma membrane with its transmembrane proteins and membrane associated proteins, including SNAP25 (black arrowhead). Fair use (from Kandel et al., 2021) according to Italian legislation (legislative decree n. 68 09/04/2003).*

We quantified SNAP25 protein levels in the axon and cell body of wtTDP and mutTDP grown in microfluidic chambers as performed for SYNJ1 and PARK7.

As shown in Fig. 5.35 we do not show any significant differences in protein levels between wtTDP and mutTDP relative to ctrl in either axonal or cell body compartments. Our tentative interpretation is that since SNAP25 is a membrane-associated protein transported through the secretory pathway (Kadkova *et al*, 2019), its protein levels in the axon may be compensated by fast-axonal transport (see section 3.3.2 of the Introduction). Conversely, SYNJ1 and PARK7 are cytosolic proteins that likely move to the axon via slow axonal transport, at rates that are not sufficient to offset the impaired levels of axonal mRNAs and insufficient local synthesis of the corresponding proteins.

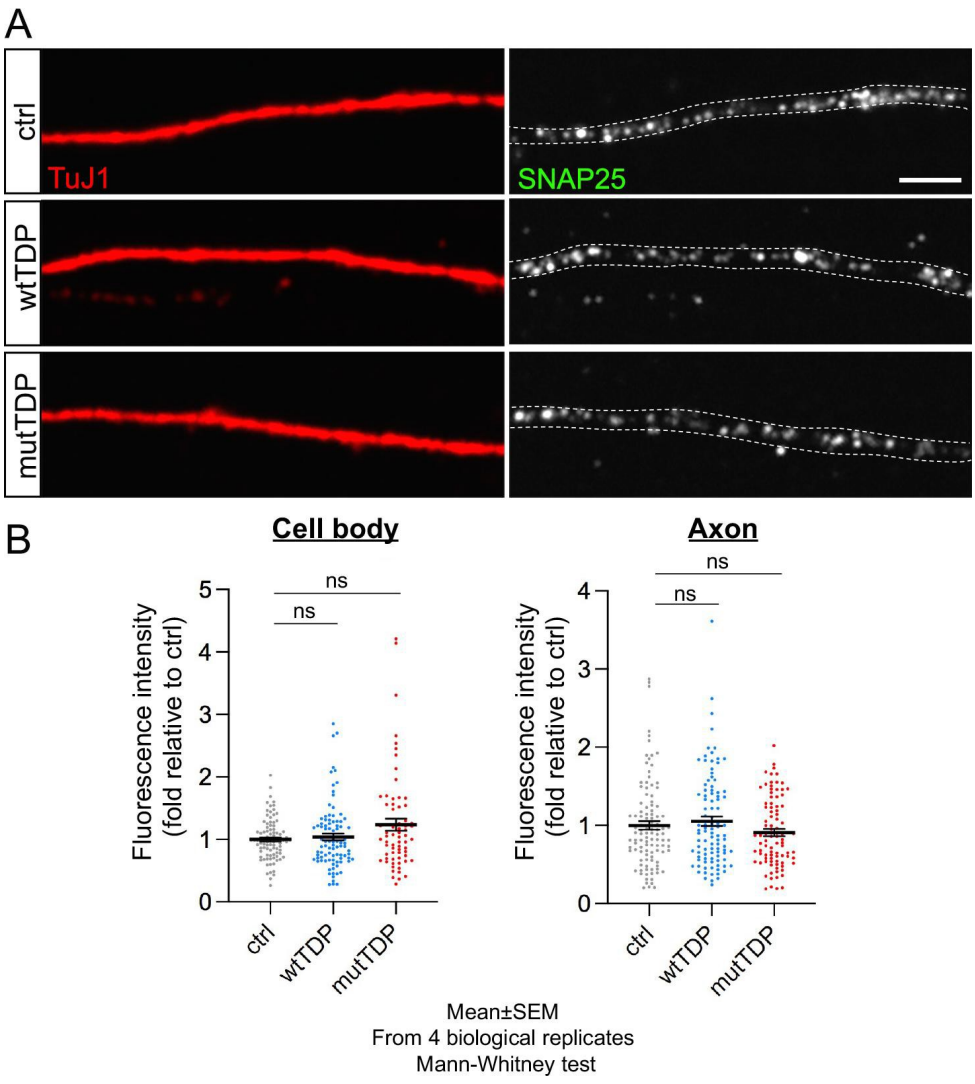


***Figure 5.36. wtTDP and mutTDP neurons show no difference in SNAP25 protein levels.*** *(A) Immunofluorescence of ctrl, wtTDP and mutTDP axons with anti-TuJ1 (red) and anti-SNAP25 (greyscale) antibodies. Dotted lines indicate axon borders. (Size bar: 2.5µm). (B) Graphs showing the distribution of wtTDP (blue) and mutTDP (red) fluorescence intensity of SNAP25 relative to control neurons (gray). The graphs show that SNAP25 levels do not change in wtTDP and mutTDP in either the cell body (graph on the left) or axon (graph on the right). For axons, I*

*analyzed 30µm long segments. (Mean ±SEM, from 3 biological replicates; Mann-Whitney test ns=p>0.05).*

## 5.3 wtTDP and mutTDP neurons show increased gap junction connectivity

### *5.3.1 wtTDP and mutTDP neurons show decreased spontaneous burst frequency*

To investigate whether wtTDP and mutTDP induce changes in the synaptic function of cortical neurons, we first performed whole-cell patch clamp experiments in individual cells to detect spontaneous activity at glutamatergic synapses. AMPA receptor-mediated, action potential-independent spontaneous mini excitatory postsynaptic currents (mEPSCs) were recorded at a holding potential of -70 mV in the presence of the $Na^+$ channel and $GABA_A$ receptor antagonists TTX (1 µM) and gabazine (10 µM), respectively. No significant differences were detected in mEPSC average amplitude, decay time constant, and frequency (Fig. 5.37B-D).

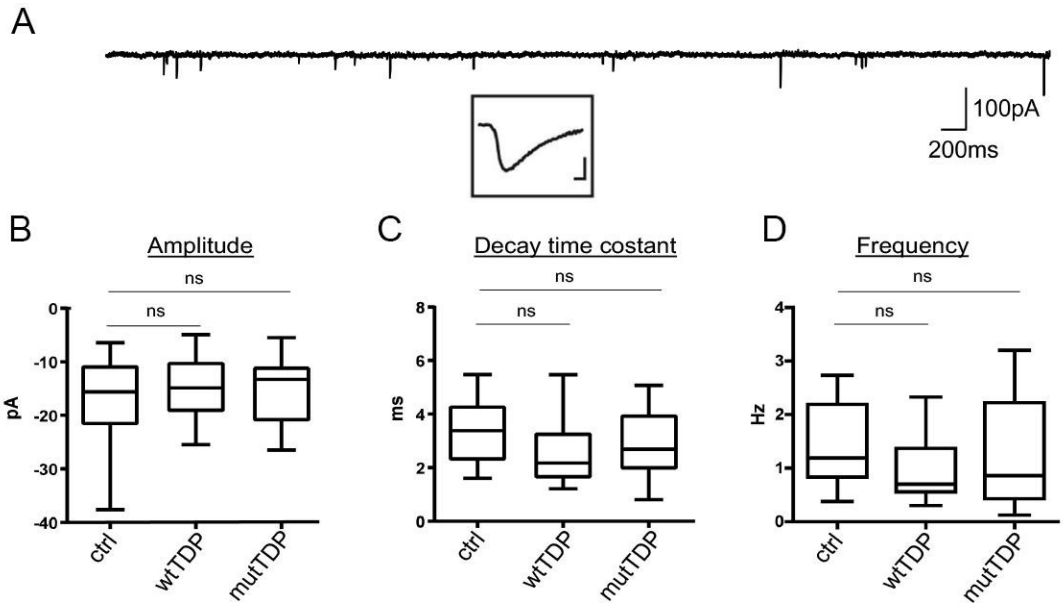


***Figure 5.37. wtTDP and mutTDP neurons show no significant differences in mEPSCs in terms of amplitude, decay time constant and frequency.*** *(A) Example of spontaneous mEPSCs recorded in voltage clamp mode ($V_h$: -70mV) in a cultured cortical cell. The inset shows an enlarged view of an individual mEPSC (scale bar: 10pA, 1ms). (B-D). Summary box plots of peak amplitude, decay time constant, and frequency of mEPSCs recorded in ctrl, wtTDP, and mutTDP cultures (box plots represent medians, 25 and 75 percentiles, and min-max values, from 6 biological replicates, Mann Whitney U-Test, ns=p>0.05).*

However, when TTX and gabazine were omitted from the extracellular solution to record intact (i.e. glutamatergic and GABAergic) action potential-induced spontaneous synaptic activity, we observed recurring bursts of mixed excitatory and inhibitory PSCs (Fig. 5.38A). This pattern of bursty synaptic activity is typical of cortical cultures after

several DIVs and is induced by spontaneous bursts of action potentials fired synchronously by multiple cells (Fig. 5.38B). Interestingly, the average frequency of synaptic bursts was significantly reduced in both wtTDP and mutTDP neurons compared to controls (Fig. 5.38C). Conversely, the average burst duration was not significantly changed (Fig. 5.38D). These data suggest that while the basic function of glutamatergic synapses is overall intact, the ability of wt- and mutTDP cultures to synaptically communicate through burst activity is robustly impaired.

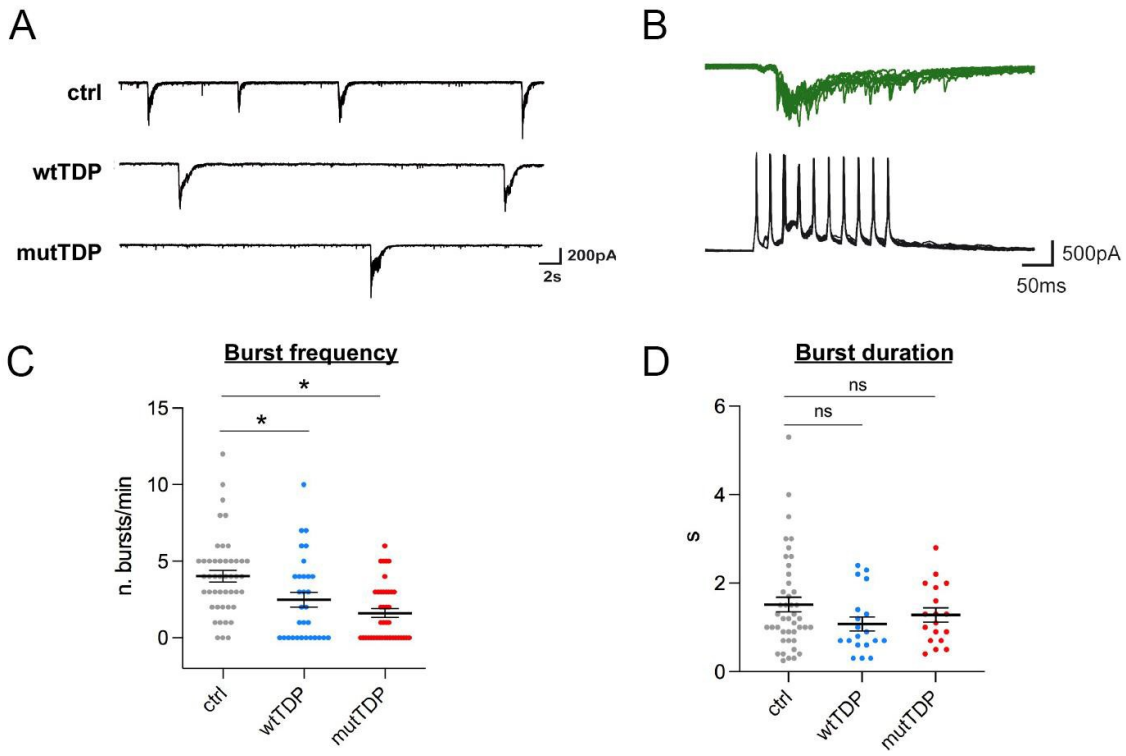


***Figure 5.38. wtTDP and mutTDP neurons show decreased burst frequency.*** *(A) Examples of spontaneous compound PSC bursts recorded in cortical cells from ctrl, wtTDP, and mutTDP cultures. (B) Individual PSC bursts (top) recorded in voltage clamp mode at a Vh of -70 mV correlate with spontaneous action potential bursts (bottom) recorded in current clamp in a different cell. (C,D) Summary plots of average burst frequencies (n. bursts per minute) and average duration of individual bursts. (Mean ±SEM, from 6 biological replicates, Mann Whitney U-Test, ns=p>0.05, *p<0.05).*

### *5.3.2 wtTDP and mutTDP neurons show decreased calcium levels after glutamate stimulus*

Increased calcium levels, due to the influx from extracellular compartment and the release from intracellular deposits, strongly affect neuronal firing activity and synaptic response. Thus, we decided to evaluate calcium levels in wtTDP and mutTDP neurons relative to ctrl, after glutamate stimulation. To this end, wtTDP, mutTDP neurons and ctrl

(ctrl neurons were transduced with empty vector, see Materials and Methods) were loaded with the calcium dye fura-2 (as in Fig. 5.28), and subjected to imaging analysis before and during the stimulation with 100μM glutamate. As shown in Fig. 5.39, wtTDP and mutTDP neurons show reduced calcium levels under basal condition and at the peak of glutamate response relative to ctrl neurons. This is in accordance with the decreased spontaneous burst activity shown above, since the reduced calcium levels in wtTDP and mutTDP neurons may not be sufficient to reach the threshold necessary for spontaneous burst generation.

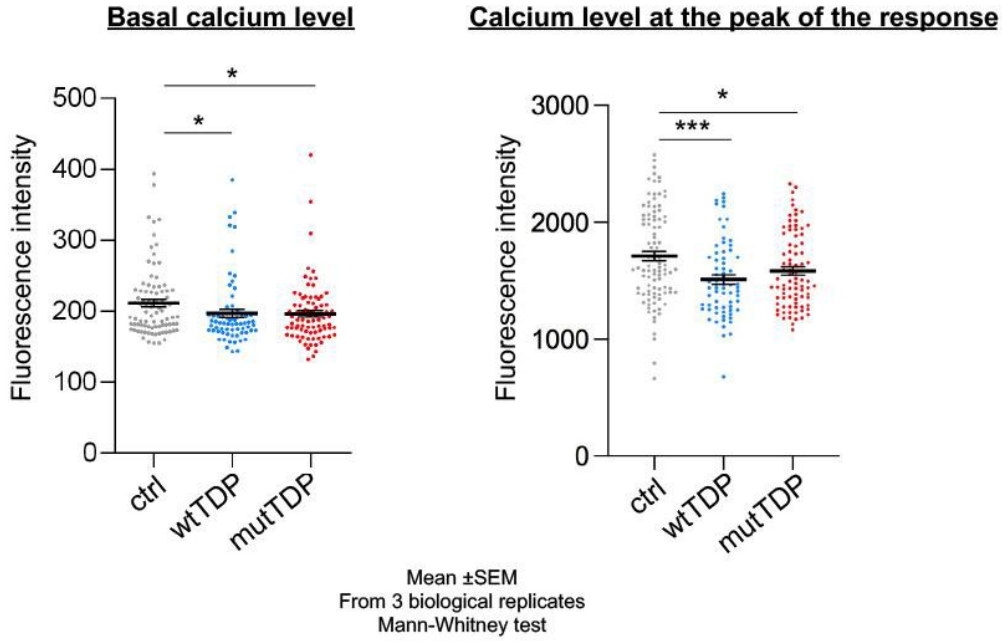


***Figure 5.39. wtTDP and mutTDP neurons show decreased calcium levels under basal conditions and at the peak of the response to glutamate stimulation.*** *Graphs showing fura-2 fluorescence in wtTDP, mutTDP and ctrl neurons under basal condition (graph on the left) and at the peak of response after glutamate stimulation (graph on the right). (Mean ±SEM, from 3 biological replicates, Mann-Whitney test, *p<0.05, ***p<0.01).*

### *5.3.3 Functional electrical synapses are upregulated in wtTDP and mutTDP neurons*

To achieve a more detailed investigation of action potential-dependent cell-to-cell communication between neurons, we performed simultaneous dual patch clamp recordings in pairs of cultured neurons. Trains of action potentials (APs) were elicited by injection of current pulses (5 ms, 800 pA) at a frequency of 40 Hz in one cell while the synaptic response was recorded in the other. A subset of control pairs was connected

through typical AMPA-R mediated glutamatergic synapses, as trains of individual, NBQX-sensitive EPSCs were recorded in correspondence with APs. In all pairs, the EPSC peak amplitude was strongly depressed during trains (Fig. 5.40A), suggesting a progressive depletion of glutamate vesicles. Although the rate of synaptic connectivity between pairs was somewhat higher in both wt-TDP and mutTDP neurons with respect to controls (Fig. 5.40C), these differences did not reach statistical significance.

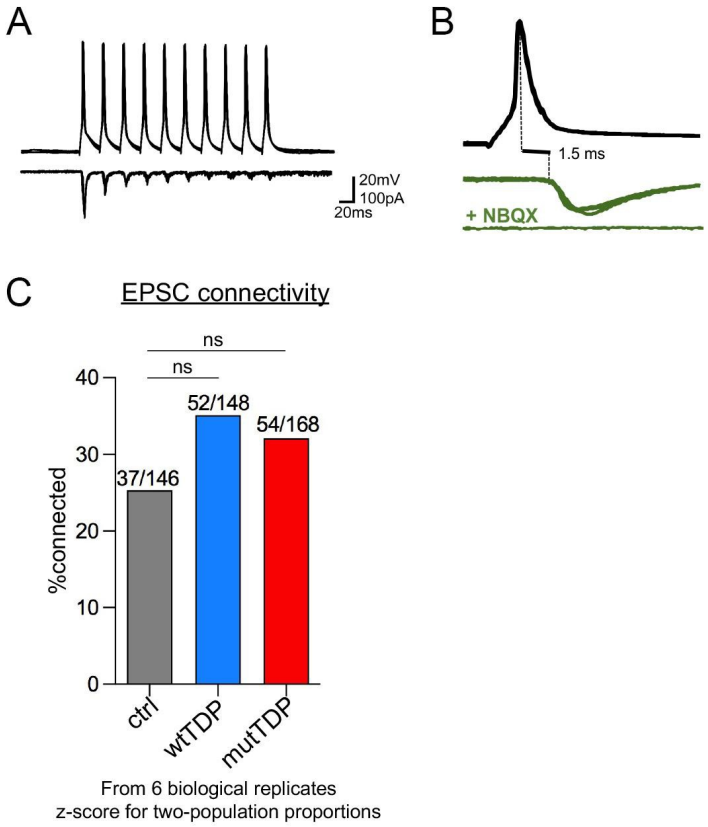


***Figure 5.40. wtTDP and mutTDP neurons show no changes in chemical synapses connectivity.*** *(A) Simultaneous dual patch clamp recordings showing a train of action potentials evoked at a frequency of 40Hz in a presynaptic cell (top) and an array of EPSCs recorded in a synaptically connected cell (bottom). (B). Individual EPSCs were induced by presynaptic spikes with a latency of 1.5 ms. Bottom trace: lack of synaptic response after perfusion with the AMPA-receptor antagonist NBQX (5 μM). (C) Summary plot with AMPA-receptor mediated connectivity percentages (from 6 biological replicates, z-score for two-population proportions test, ns=p-value>0.05).*

Another subset of neurons was reciprocally connected through gap-junctions (GJs, Fig. 5.41). In this type of synaptic communication, electrical signals such as APs are directly conveyed (albeit strongly filtered) to the postsynaptic cell via ionic movements across the pore spanning through GJ functional channels (Fig. 5.41A). GJ-mediated signals induced by presynaptic APs are called spikelets (Fig. 5.41B) and are distinguished

from EPSCs by several features, such as a faster latency, the absence of progressive depression, and a different pharmacological profile. Interestingly, the connectivity rate through GJs was significantly higher in wt- and mutTDP than control pairs (Fig. 5.41C). Since GJs are partly responsible for neuronal electrical synchronization (Bennett & Zukin, 2004), such increased connectivity contrasts with the strongly reduced synchronous activity described above (Fig. 5.38). However, one may speculate that neurons may augment the expression of their functional GJs as a compensatory response to the impaired ability to produce synchronous firing bursts.

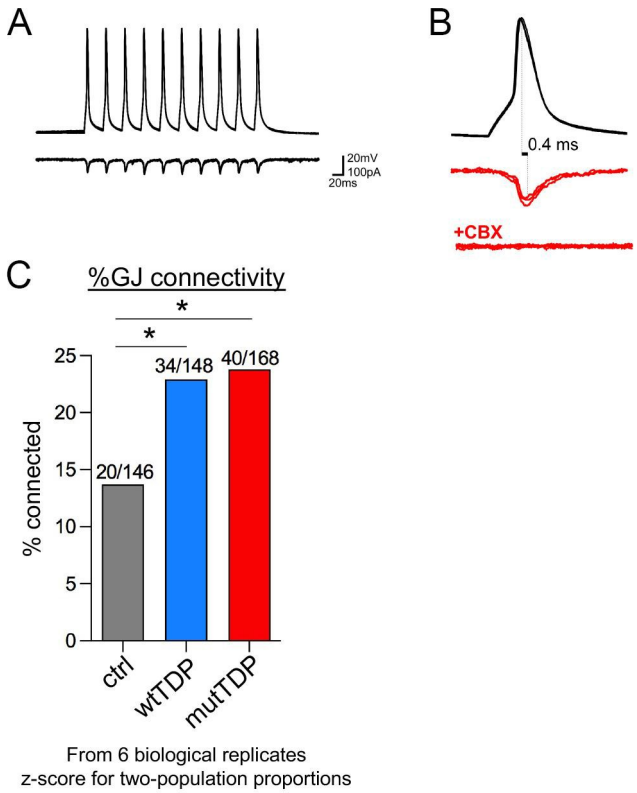


***Figure 5.41. wtTDP and mutTDP neurons show increased gap junction (GJ) connectivity.*** *(A) Simultaneous dual patch clamp recordings showing a train of action potentials evoked at a frequency of 40Hz in a presynaptic cell (top) and an array of GJ-mediated spikelets recorded in an electrically connected cell (bottom). (B) Individual spikelets were induced by presynaptic spikes with a latency of 0.4 ms. Bottom trace: lack of synaptic response after perfusion with the GJ antagonist carbenoxolone (CBX, 100 µM). (C) Summary plot with GJ-mediated connectivity percentages. (Mean ±SEM, from 6 biological replicates, z-score for two-population proportions, *p-value<0.05).*

### *5.3.4 wtTDP and mutTDP neurons show increased Cx36 levels*

Since wtTDP and mutTDP show increased gap junction connectivity relative to ctrl neurons, we asked whether they show increased levels of Connexin-36 (Cx36). Cx36 is the main component of neuronal specific gap junctions (Rash *et al*, 2001).

To address this question, we immunostained western blots obtained from wtTDP, mutTDP and ctrl neurons at 14 DIV. The membrane was incubated with anti-Cx36 antibody. As shown in Fig. 5.42A, A' wtTDP and mutTDP neurons show significantly higher levels of Cx36 compared to controls, which is in agreement with the increased gap junction connectivity observed in these neurons.

Furthermore, we set out to replicate this result in our transgenic mouse model of TDP-43 proteinopathy. Thus, we immunostained western blots obtained from the brain cortex of transgenic mice and control littermates at 1, 4 and 9 months of age. As shown in Fig. 5.42B transgenic mice show increased Cx36 levels at 4 months of age, however no differences were observed at 1 month and 9 months of age. One possible explanation is that increased gap junction connectivity may be a transient attempt to increase connectivity at early-symptomatic stages of the disease.

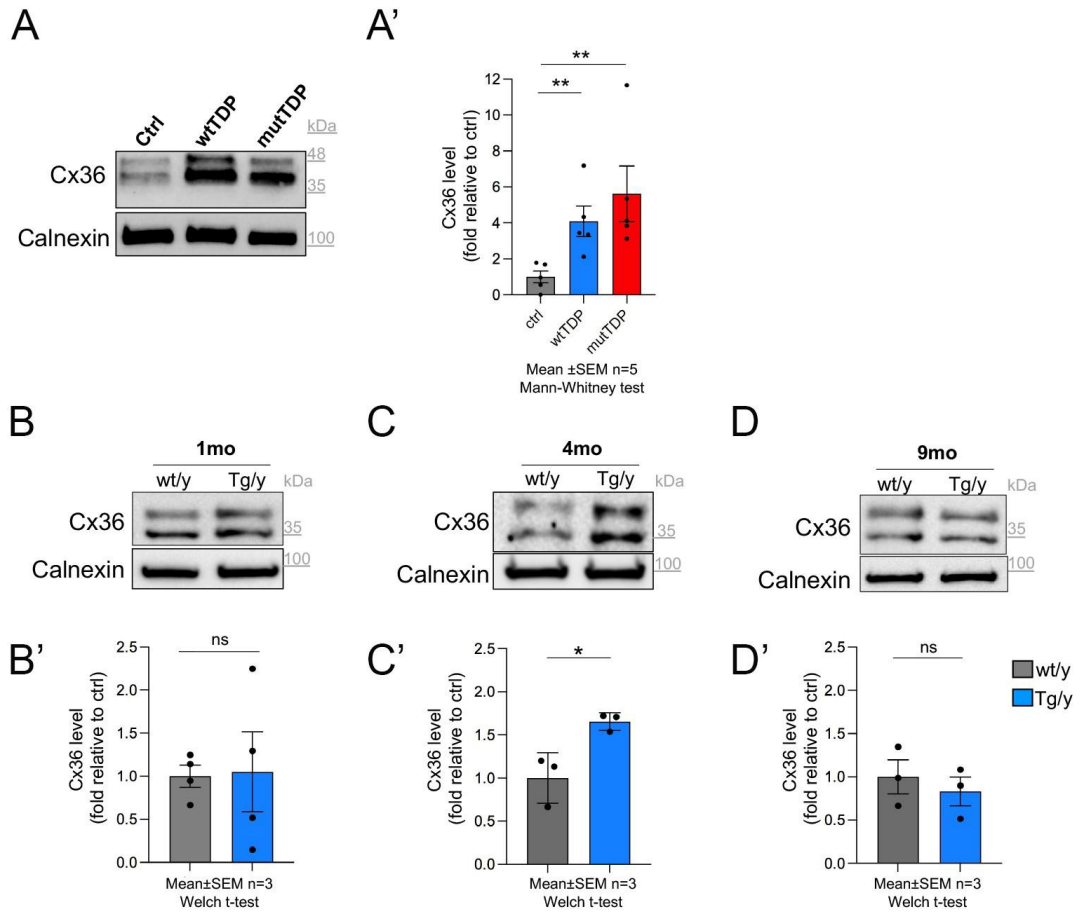


***Figure 5.42. wtTDP and mutTDP neurons show increased Cx36 levels relative to ctrl and the TDP-43 overexpressing transgenic mouse model displays increased Cx36 levels at early symptomatic stages.*** *(A) Western blot analysis of protein lysates obtained from ctrl, wtTDP and mutTDP neurons. The membrane was incubated with anti-Cx36 antibody. Anti-Calnexin antibody was used as a loading control. (A') Graph showing western blot quantification of Cx36 levels in wtTDP (in blue) and mutTDP (in red) relative to ctrl (in gray). Cx36 levels in wtTDP and mutTDP neurons are increased relative to ctrls. (Mean ±SEM, n=5, Mann-Whitney test, **p-value<0.01). (B,C,D) Western blot analysis of protein lysates obtained from the brain cortex of transgenic mice (Tg/y) and control littermates (wt/y) at 1 month (B), 4 months (C), and 9 months (D) of age. (B',C',D') Graph showing western blot quantification of Cx36 levels in transgenic mice (in blue) relative to control littermates (in gray) at 1 month (B'), 4 months (C') and 9 months (D') of age. There is a significant increase of Cx36 levels in transgenic mice at 4 months of age, corresponding to the early-symptomatic stage. (Mean ±SEM, n=3, Welch t-test,*p-value<0.05).*

# 6. Discussion

Amyotrophic lateral sclerosis is a fatal neurodegenerative disease which leads to progressive paralysis and death. To date, only rather ineffectual treatments aimed at slowing clinical progression are available for these patients. This is due to a severe knowledge gap in our understanding of pathogenetic mechanisms that underlie ALS, starting from those that intervene at very early stages of the disease. While only 10% of ALS cases exhibit disease recurrence within the family (fALS), the majority of these patients are sporadic (reviewed in Hardiman *et al.*, 2017). Although the causes, in most sporadic cases, are still unknown, they are characterized by TDP-43 proteinopathy with TDP-43 nuclear depletion and its cytoplasmic accumulation and aggregation (Arai *et al.*, 2006; Neumann *et al.*, 2006). Notably, TDP-43 cytoplasmic inclusions have been found also in other diseases, like Alzheimer's disease, Parkinson's disease and Hungtington's chorea (reviewed in Tziortzouda *et al.*, 2021). Thus, altered TDP-43 pathology may be a common denominator of many neurodegenerative disorders.

During my thesis project, we developed a cellular model of ALS-related neuronal damage in upper motor neurons, which, together with spinal motor neurons, exhibit degeneration specifically in ALS. One reason why we decided to focus on upper motor neurons is the fact that, to date, most studies of ALS have focused on lower motor neurons or cell lines that share many features typical of these neurons. Like any cellular or animal models, these primary cultures have pros and cons. One of the limitations inherent in cortical neuron primary cultures is that they consist of an heterogeneous neuronal population. For this reason, we established cortical neuron primary cultures from E14.5 mouse telencephalic cortex which showed no glial contamination and almost no GAD65-positive neurons. Moreover, our E14.5 derived cultures contain 60% CTIP2 positive cells, which is a marker of layer V of the cortex, while the remaining 40% derived from other layers. However, considering the experimental difficulties of establishing neuronal cultures from earlier developmental stages, we can bona fide assume that these cultures are a population highly enriched in neurons of the fifth neocortical layer. Interestingly, the reason why neurons of the fifth cortical layer are more susceptible to ALS compared to neurons of other cortical layers, has not been clarified yet. Limone et al., in a preprint publication, describe the application of single cell sequencing of brain motor cortex to understand this issue. They found that Thy-positive neurons, which localize in the deepest

layer of the cortex, upregulate several ALS risk factors, including several genes involved in cellular stress. However, further studies should be carried out to decipher the underlying mechanism of motor neuron susceptibility to ALS (Limone *et al*, 2021).

One of the limits of studying TDP-43 pathology is the lack of an appropriate model that fully recapitulates molecular and physiopathological features of TDP-43 proteinopathy. Our cellular model consists of neurons lentivirally transduced with human wild-type TDP-43 or with a mutant form carrying the A315T mutation identified in a fALS family (Gitcho *et al.*, 2008). TDP-43 overexpression models have been widely used to mimic TDP-43 pathology. For example, others have used cellular models overexpressing wild-type TDP-43 or carrying a NLS mutation to induce cytoplasmic accumulation and aggregation (Winton *et al.*, 2008). Regarding in-vivo models, several available transgenic mouse models overexpress wild-type (Stallings *et al.*, 2010) or mutated (Wegorzewska *et al.*, 2009) TDP-43, or carry a modification of this protein that is devoid of the nuclear localization signal (NLS) (Igaz *et al.*, 2011). These transgenic mice show molecular features of TDP-43 proteinopathy with TDP-43 cytoplasmic accumulation, ubiquitination and sometimes motor neuron loss as well as a defective motor performance.

However, TDP-43 levels are tightly controlled in the cells by nucleocytoplasmic shuttling and autoregulation mechanisms (reviewed in Tziortzouda *et al.*, 2021) suggesting that forced overexpression may result in a dose-dependent toxicity. For this reason, leading researchers in the field have redirected their effort towards mouse models with physiological levels of TDP-43 and cultures of neurons derived from IPSC patients. However, these models also show some limitations: for example, neurons derived from IPSCs are established from patients, who have specific mutations and genetic backgrounds. Likewise, most knock-in mouse models show a very mild phenotype that can be properly analyzed only at very late ages. The TDP-43 knock-in mouse model of White et al., carrying the Q331K mutation show almost no motor dysfunction nor TDP-43 pathology, although it exhibits a cognitive phenotype at 12 months of age (White *et al*, 2018). Another knock-in model from Fratta et al., carrying the M323K mutation, shows a mild muscular phenotype with reduced grip strength at 2 years of age and no TDP-43 pathology in spinal cord or brain; however, at the molecular level, these mice show alterations in RNA splicing (Fratta *et al.*, 2018). Nevertheless, recently a new

knock-in mouse model was developed, carrying a mutation found in a patient with sporadic ALS (N390D). This knockin mouse shows a moderate phenotype at 8 months of age, with muscular denervation and reduced motor performance at the rotarod test, and a more severe phenotype at 12 months. However, this mouse only exhibits TDP-43 pathology in the spinal cord, not in the brain cortex (Huang *et al*, 2020). Notably the same group developed a knock-in mouse carrying the A315T mutation, but this line does not show any phenotypic changes relative to the wild type control (Huang *et al.*, 2020). Thus, the N390D mouse model seems to combine physiological levels of TDP-43 protein expression with the development of a disease phenotype at a relatively early age. While this model became available long after the start of my project, I think that an in-depth study of motor cortex pathology should be carried out in this model and may contribute importantly to our understanding of upper motor involvement in ALS. In conclusion, each model has pros and cons. The ideal situation should be to validate one's data in a combination of different models or to choose a model on the basis of the stage of the disease being examined: asymptomatic / early-symptomatic or late symptomatic.

Overall, given these concerns, finding a comprehensive model of TDP-43 proteinopathy ALS still represents a daunting task. For our in-vitro model we decided to lentivirally transduce deep layer cortical neurons with human wt TDP-43 or TDP-43(A315T), leading to a supraphysiological level of TDP-43 expression. The goal ofthis approach was to permit, within the short lifespan of cultured cortical neurons, to analyze events that take decades to manifest in patients.

In our in-vitro model, exogenous tRFP-TDP-43 mainly localizes to the cytoplasm, generating granules. Although the artificial enlargement of the TDP-43 molecule has been reported to impair its nuclear egress (Ederle *et al*, 2018), this does not seem to be the case in our model. Instead we hypothesize that the size of the tRFP fusion protein may impair its nuclear import, generating a model similar to the one produced by Virginia Lee's lab by removing the NLS. However, our fusion protein is expressed in the nucleus and negatively modulates the levels of the endogenous mouse protein, likely due to the well established negative post-transcriptional autoregulation of mRNA stability (Avendano-Vazquez *et al.*, 2012; Ayala *et al.*, 2011). Thus, an alternative possibility is that our fusion protein may exhibit a greater propensity to form cytoplasmic aggregates. Such aggregates

may recruit the endogenous TDP-43 as well as many RNA granule components, possibly leading to nuclear loss of function, mainly in the form of splicing defects (Winton *et al.*, 2008), as well as causing a disruption of mRNA trafficking in the cytoplasm. Interestingly, TDP-43 aggregates have been shown to sequester proteins of the nuclear pore complex, leading to a disruption of the nuclear membrane in both primary neurons and tissues from ALS patients (Chou *et al*, 2018). Moreover, as mentioned in the Introduction, TDP-43 pathology, induced in a *Drosophila* model of C9orf72 repeat expansion, leads to cytoplasmic accumulation of KPNA2/4, involved in TDP-43 nuclear import (Solomon *et al.*, 2018).

Our wtTDP and mutTDP neurons develop cytoplasmic granules whose nature warrants further studies. Our biochemical evidence suggests that they may be insoluble aggregates as TDP-43 mainly precipitate in the cytoplasmic insoluble fraction after subcellular fractionation. These cytoplasmic granules colocalize mainly with RPS6, a protein of the small ribosomal subunit, but weakly with RPL26, a protein of the large subunit. These results suggest that TDP-43 aggregates caused by overexpression of the tRFP-TDP-43 fusion protein may be non-translating granules. However, under stress conditions exogenous TDP-43 can be recruited in G3BP1-positive granules, suggesting that it does not lose its ability to coalesce into stress granules. Thus, further experiments should be performed to better clarify the nature of these granules, including Fluorescence Recovery After Photobleaching (FRAP). Moreover, we found that exogenous TDP-43 mainly colocalizes with HuC/D. However, we do not know whether exogenous TDP-43 recruits HuC/D to generate transport granules or it sequesters it into insoluble aggregates, hampering its function. Interestingly, both HuC and HuD variably colocalize with TDP-43 pathological aggregates in the spinal cord tissues of familial and sporadic ALS patients (Diaz-Garcia *et al*, 2021).

We propose our in-vitro system as a model of early-symptomatic stages of ALS. wtTDP and mutTDP neurons show TDP-43 proteolytic fragments, cytoplasmic accumulation and insoluble granules, but at the same time the exhibit low-level phosphorylation of exogenous TDP-43 in Ser409-410, and no increased TDP-43 ubiquitination. As shown above, the TDP-43-overexpressing transgenic mice available in our lab display increased neuronal ubiquitination at 9 months of age, but no evidence of TDP-43 ubiquitin binding. In light of this in-vivo observation, it is not surprising that

such a late event is not detectable in our in-vitro model after 14 DIV. Regarding TDP-43 phosphorylation, preliminary results show mild phosphorylation of the exogenous protein and no increase in the ratio of phosphorylated to total TDP-43 in the transgenic mouse model. However, it is necessary to analyze other biological replicates for both neuronal cultures and mouse brain cortices, and to perform an immunohistochemical analysis on mouse brain sections. Moreover, it would be interesting to examine whether phosphorylated-TDP-43 is recruited to G3BP1-positive granules in the axon, as previously shown (Altman *et al*, 2021) or if phosphorylation occurs after a stressful stimulus, such as a heat shock.

Once we assessed the fact that our in-vitro model is a model of early stages of ALS we performed a transcriptome and translatome analysis of wtTDP and mutTDP neurons. For the latter, we could rely on a tag-free polysome isolation approach, thanks to our collaboration with the Viero lab. Sub-polysomal and polysomal fractions were isolated by a miniaturized sucrose gradient and polysome profiling. The sub-polysomal mRNA fraction (i.e. transcripts not associated with polysomes) contains both free mRNAs and mRNAs associated with monosomes. Recently published evidence suggests that monosomes play a role in local translation in the axon (Biever *et al*, 2020). In our protocol, mRNAs translated by monosomes could not be examined, as they were pooled with "sub-monosomal" mRNAs enriched in alternatively spliced variants generated by TDP-43 overexpression many of which are noncoding mRNAs. Indeed, TDP-43 also has a role in alternative splicing, thus its experimental manipulation can lead to alternatively noncoding spliced variants liable to be degraded via mRNA decay (Brown *et al*, 2021; Fratta *et al.*, 2018). Thus, while focusing on polysomal mRNAs shifts the balance towards protein-coding transcripts, we cannot exclude that a share of mRNAs associated with polysomes may be translationally stalled transcripts (reviewed in Richter & Coller, 2015). For example, FMRP is known to block ribosomal translocation giving rise to stalled polysomes. Indeed, FMRP co-sediments with the polysomal fraction but is insensitive to the puromycin treatment, which causes the ribosomal release of the two subunits of translocating ribosomes but not of stalled ones (Darnell *et al*, 2011).

Regarding translation, we demonstrated that wtTDP and mutTDP neurons show decreased levels of RPL26 in both the axon and cell body, which correlates with the finding of decreased translation, revealed by the puromycylation assay. If we consider

that the RPL26 levels may reflect the levels of total ribosomes, the decreased levels of RPL26 and other ribosomal mRNAs may explain the decreased translation rate observed in these neurons. Of course, our experimental approach cannot distinguish between cytosolic ribosomal proteins, monosomes and polysomes. We attempted to colocalize RPL26 with markers of the small ribosomal unit to visualize assembled ribosomes, as opposed to cytosolic RPL26; however, this experiment is notoriously difficult, likely due to steric hindrance hampering the simultaneous immunolocalization of two markers within a 20-30nm structure. Indeed, we found that wtTDP and mutTDP neurons show downregulation of several polysomal mRNAs involved in protein synthesis. Several of these genes are downregulated specifically in the axon. In wtTDP neurons 282 genes are downregulated specifically in the axon, of which 14 encode translation initiation factors, 17 encode ribosomal proteins of the large subunit and 13 of the small subunit. Similarly, in mutTDP neurons we found 106 polysomal mRNAs downregulated specifically in the axon. Of these, 8 encode translation initiation factors, 30 encode ribosomal proteins of the large subunit and 18 of the small subunit. Of the 282 translation-related mRNAs downregulated in wtTDP axons and 106 in mutTDP axons, 47 were shared between the two populations.

One important question regards the role of transcripts encoding ribosomal proteins in the axon. As mentioned in the introduction, it has been shown that TDP-43 transports mRNAs encoding ribosomal proteins in the axon (Nagano *et al.*, 2020). Recent evidence suggests that the translation of ribosomal-encoding mRNAs in neuronal processes supports ribosome turnover (Fusco *et al.*, 2021), prompting the hypothesis that in our model the impaired transport or axonal localization of ribosome-encoding mRNAs may lead to reduced turnover –possibly to premature degradation?– of ribosomal proteins and ultimately to defective local translation.

Furthermore, we found that wtTDP and mutTDP neurons display increased oxidative stress levels. Interestingly, although the response to oxidative stress may be considered a prerogative of the cell body, we found that several genes involved in the response to oxidative stress are downregulated in the axon of wtTDP and mutTDP neurons - in fact the number of downregulated axonal mRNAs related to the response to oxidative stress far exceeds the corresponding numbers of deregulated genes in the soma of wtTDP neurons and matches them in the soma of mutTDP neurons (Fig. 5.27). Particularly, in

wtTDP 94 genes are specifically downregulated in the axon, in mutTDP they are 44 and 8 are shared between wtTDP and mutTDP.

A gene downregulated in wtTDP-overexpressing neurons, PARK7 is a sensor of oxidative stress thanks to its cysteine residues. PARK7 promotes the nuclear translocation of the transcription factor Nrf2, thus promoting the transcription of several genes involved in the antioxidant response (Zhang *et al*, 2020). PARK7 also translocates to the nucleus where it contributes to the inhibition of apoptosis (Kim *et al*, 2012). Moreover, PARK7 was found upregulated in the spinal cord of $SOD1^{G93A}$ mice, possibly exerting a compensatory function (Yamashita *et al*, 2010); indeed, $SOD1^{G93A}$ mice null for PARK7 show decreased survival (Lev *et al*, 2015). Interestingly, PARK7 overexpression suppresses TDP-43 aggregation induced by oxidative stress treatment with paraquat in SH-SY5Y cells (Lei *et al*, 2018). Overall we can hypothesize that the downregulation of PARK7 in wtTDP and mutTDP axons might affect the activation of antioxidant pathways, thus leading to increased oxidative stress.

## 6.1 Deregulation of mRNAs encoding synapse and vesicle proteins

The finding emerging from transcription and translatome analysis that both presynaptic and mRNA-translation related mRNAs are strongly affected by TDP-43 overexpression in wtTDP and mutTDP neurons in a way supports the notion that this disease is a distal axonopathy.

With respect to synaptic function, in this project we reveal that numerous mRNAs encoding synaptic proteins are affected by TDP-43 overexpression and their levels are altered both in the axon and cell body.

Out of 395 synaptic mRNAs downregulated in wtTDP axons and 208 in mutTDP axons, 94 were shared between the two populations.

For a small number of downregulated synaptic transcripts we were able to run confirmatory experiments at the protein level. In particular we found that the SYNJ1 protein is downregulated specifically in the axon of mutTDP neurons compared to those scored in ctrl axons. In contrast, the levels of another synaptic protein, SNAP25, do not change significantly although the mRNA levels are downregulated. We hypothesized that the reduced local translation of SNAP25 might be compensated by the fast axonal vesicle transport of this protein, a membrane-associated protein, while factors transported along

the axon via slow axonal transport, as is the case for SYNJ1, may be critically dependent upon axonal and presynaptic mRNA translation.

Although we validated only a small subset of genes involved in the presynaptic compartment, it is worth noting that our RNA-sequencing analysis has revealed that this category of genes is strongly affected by wt or mutant TDP-43 overexpression.

Furthermore, a study by Brown et al. published as a preprint reports that TDP-43 KD leads to the insertion of a cryptic exon in the *UNC13A* mRNA, generating a premature stop codon. This insertion is predicted to promote nonsense mediated decay, causing reduced levels of the *UNC13A* transcript and of the corresponding protein (Brown *et al.*, 2021). Unc13a has a key function in synaptic transmission, namely it promotes vesicle priming. Taken together, these observations suggest that TDP-43 deregulation may have a profound effect on synaptic function.

Our analysis has revealed that in wtTDP neurons a larger number of genes are downregulated in the axon than in the soma, while in mutTDP the numbers of genes downregulated in the axon and soma are comparable. Differences observed between wtTDP and mutTDP neurons may indicate that the A315T mutation causes ulterior disruption in the cell body in comparison to the damage produced by TDP-43 overexpression alone. Based on the distal axonopathy model, mutTDP, damage may have spread retrogradely to the cell body, while in wtTDP neurons it may still be restricted to the axon.

In summary, our unbiased translatome survey of TDP-43 overexpressing neurons compared to controls has also revealed that while many features of ALS-related neuronal and axonal damage are shared between wtTDP and mutTDP neurons (i.e. exocytosis defects, increased oxidative stress and reduced translation), the axonal levels of some mRNAs are regulated in an allele-specific fashion.

## 6.2 wtTDP and mutTDP neurons show an increased electrical synapse connectivity and increased Cx36 levels

By means of electrophysiological recordings, we found that wtTDP and mutTDP neurons show decreased spontaneous burst activity. Accordingly, the calcium response after glutamate stimulation is reduced in wtTDP and mutTDP neurons. It is worth adding that only slight, non-significant differences in chemical synapse activity were observed by

double patch analysis. This is in apparent contrast with the defective exocytosis found by FM1-43 assay but the two experimental conditions are different enough as to be hardly comparable.

Interestingly, during double patch recordings we observed the presence of gap junction connectivity among these neuronal populations. wtTDP and mutTDP neurons show increased Cx36 levels compared to ctrl neurons, in agreement with the increased functional gap junction connectivity exhibited by these neurons. Other authors found that in the anterior horn of the $SOD1^{G93A}$ mouse spinal cord, Cx36-GAD65 double positive synapses are decreased in the presymptomatic stage (Kobayakawa *et al*, 2018). In the rat brain, Cx36 is strongly expressed at 2-weeks after birth only to taper out during the third week, and it is mainly expressed in GABAergic neurons (Belluardo *et al*, 2000). In response to mGluR activation, the coupling of neuronal gap junctions positive Cx36 increases together with Cx36 expression after brain injury, e.g. after an ischemic insult, leading to neuronal cell death (Wang *et al*, 2012). Thus, decreased Cx36 levels in the spinal cord of $SOD1^{G93A}$ may be an attempt to increase neuronal survival.

In our in-vitro model, instead, increased gap-junction connectivity may be an attempt of increasing neuronal connections at the early stage of the disease. A surge in Cx36 levels could be interpreted as an attempt to offset the depression of spontaneous burst firing activity observed in our model. Recent functional neuroimaging studies (Agosta *et al*, 2011) have revealed an increase in brain functional connectivity at early stages of ALS, likely representing a compensatory mechanism in response to neuronal degeneration. In keeping with this, the analysis of our cellular model of early stages of ALS-related neuronal damage has revealed a significant upregulation of connexin 36 (Cx36) and a robust rise in gap junction (GJ)-mediated functional connectivity.

However, a surge in the number of Cx36-containing hemichannels and electrical synapses may be interpreted as a maladaptive response, contributing to the spread of neurotoxic factors and causing an irreversible dissemination of the disease from focal damage to widespread neurodegeneration.

An increase in Cx36 levels was observed in the brain cortex of our transgenic mouse model at an early symptomatic stage and was reverted at later stages. Further analyses will be performed to assess whether the increase of Cx36 promotes the coupling of adjacent corticospinal neurons or establishes anomalous connections with glial cells,

GABAergic neurons or the extracellular matrix, via heterotypic interactions or uncoupled hemichannels.

## 6.3 Conclusion

Overall, we can summarize our data as sketched in Fig. 6.1. In ctrl neurons TDP-43 is localized predominantly in the nucleus and can localize in the cytoplasm to exert its functions. mRNAs transcribed in the nucleus coalesce with RBPs, generating RNP granules that allow their transport along the axon. Messenger RNAs are translated in the axon to support its maintenance. In contrast, in wtTDP and mutTDP neurons, exogenous TDP-43 generates cytoplasmic granules that may trap mRNAs, or other RBPs, inhibiting the axonal localization of these transcripts. This leads to downregulation of subpolysomal and polysomal mRNAs in the axon. These neurons also show reduced protein synthesis, reduced exocytosis and increased oxidative stress. Accordingly, many downregulated polysomal mRNAs encode protein involved in protein synthesis, synaptic function and oxidative stress response. Moreover, these wtTDP and mutTDP neurons show increased GJs, which may spread neurotoxic factors from ailing neurons to their neighbors and to the extracellular environment. Taken together, these alterations may contribute to synaptic failure and subsequent dying-back axonopathy.

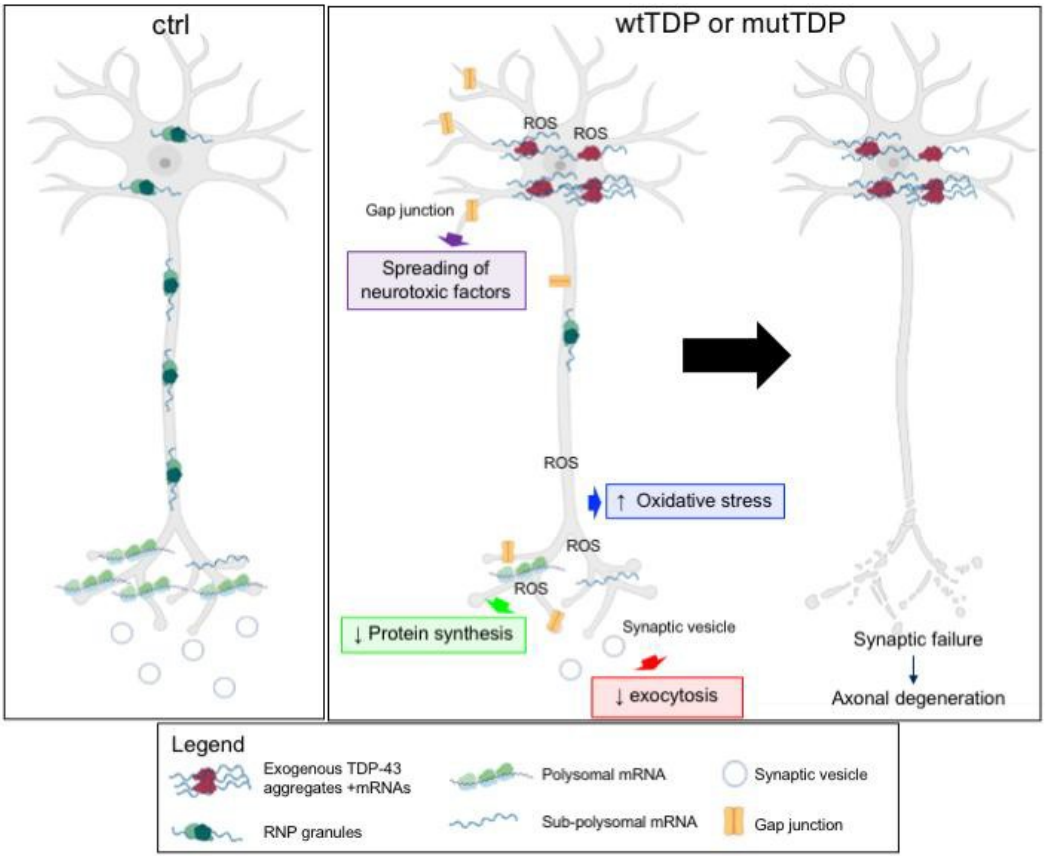


***Figure 6.1. A model of the neuronal damage in wtTDP and mutTDP neurons.*** *Representative scheme of the final model of neuronal damage in wtTDP and mutTDP neurons. On the left, ctrl neurons, with no presence of TDP-43 aggregates, show correct mRNA metabolism and synaptic function. In the middle, wtTDP and mutTDP neurons show the presence of exogenous TDP-43 aggregates that may trap mRNAs and other RBPs. As a result, these neurons display reduced polysomal and sub-polysomal mRNAs. Functionally, wtTDP and mutTDP neurons exhibit a decrease in protein synthesis and exocytosis, and an increase in oxidative stress. Moreover, TDP-43 overexpressing neurons show increased GJs that may lead to the dissemination of neurotoxic factors. This may result in synaptic failure and axonal degeneration as shown on the right. Created with Biorender.com.*

# 7. Materials and Methods

## 7.1 Animal care

All experiments described were performed in agreement with the stipulations of the San Raffaele Scientific Institute Animal Care and Use Committee (I.A.C.U.C.).

## 7.2 Cortical neurons primary culture

Medium composition:

- Dissection medium: 1X Hanks' Balanced Salt Solution (Sigma Aldrich, cat.H6648), 10mM HEPES solution (Sigma Aldrich, cat.H0887), 1X Pen Strep (P/S) (Gibco, cat.15140-122);
- Dissection medium + 0.025% Trypsin (Gibco cat.15090-046);
- First wash medium: Neurobasal Plus™ Medium (Thermo Fisher, cat.A3582901), 10% Fetal Bovine Serum (Euroclone, cat.ECS0180L), 1X P/S;
- Second wash medium: Neurobasal™ Medium, 1X P/S ;
- Neuron culture medium: Neurobasal™ Plus Medium, 1X B-27™ Plus Supplement (Gibco, cat.A35828-01), 1X P/S ;
- Neuron culture medium + Fetal Bovine Serum: Neurobasal™ Plus Medium, 1X B-27™ Plus Supplement, 1X P/S, 10% Fetal Bovine Serum;
- Neuron culture medium for microfluidic chambers: Neurobasal™ Medium, 1X B-27™ Supplement, 1X P/S, 2mM Glutamax (cat.35050061).

C57BL/6N mice were used for cortical neurons primary cultures. Cortical neurons were obtained from the cerebral cortex of mouse embryos at embryonic day 14.5 (E14.5). The collected tissues were dissociated to obtain a single cell suspension according to the following protocol:

- Collected tissues were washed with dissection medium twice, then incubated with Dissection medium + Trypsin at 37°C for 15 minutes.
- Three washing passages were performed: one with First wash medium, and two with Second wash medium.

- The obtained cells were suspended in Neuron culture medium and mechanically dissociated 20 times with a glass Pasteur. Suspension was filtered with 70μm *Cell Strainer* (Falcon, cat.352350).
- Cell concentration was calculated with an automatic *Cell Counter* (Biorad).
- Cortical neurons were plated on plastic or glass slides, previously treated with Poly-D-Lysine (Sigma, cat.P6407) at 100μg/ml for 96, 24 and 6-well plates, and 500μg/ml for chambers, at the following cell densities:

  17.000 cells per well for the 96-well plate

  100.000 cells per well for the 24-well plate

  400.000 cells per well for the 6-well plate

  75.000 cells for chambers

Then, cells were cultured in an incubator at 37°C, 5% CO2 until required days in vitro. For axonal specific experiments, cortical neurons were plated into microfluidic chambers (Xona Microfluidics, cat. SND-450) in Neuron medium indicated above. In the cell body compartment more medium volume was added relative to the axonal compartment to generate hydrostatic pressure. BDNF (Proteintech, cat.450-02-B) was added in the axonal compartment at 2 days in vitro (DIV) (20μg/ml), and at 5 DIV and 7 DIV (10μg/ml).

## 7.3 Cloning of lentiviral vectors and production of lentiviral particles

### *7.3.1 Cloning of human TDP-43 (wt and A315T) in lentiviral vectors*

For the overexpression experiments in cortical neurons we generated constructs encoding for 1) the wt human TDP-43 protein fused at the N-terminal with the turbo-Red Fluorescent Protein (tRFP-hTDP-43 wt); 2) the human TDP-43 protein with A315T mutation fused at the N-terminal with the turbo-Red Fluorescent Protein (tRFP-hTDP-43 (A315T)) 3) the turbo-Red Fluorescent Protein (tRFP), used as a control. Only for calcium assay (section 5.3.2) ctrl neurons were transduced with empty vector p277 instead of tRFP vector due to technical issues of the imaging instrument. The vectors were engineered in the laboratory, starting from the lentiviral vector pLenti277-GFP kindly provided by the group of prof. Naldini.

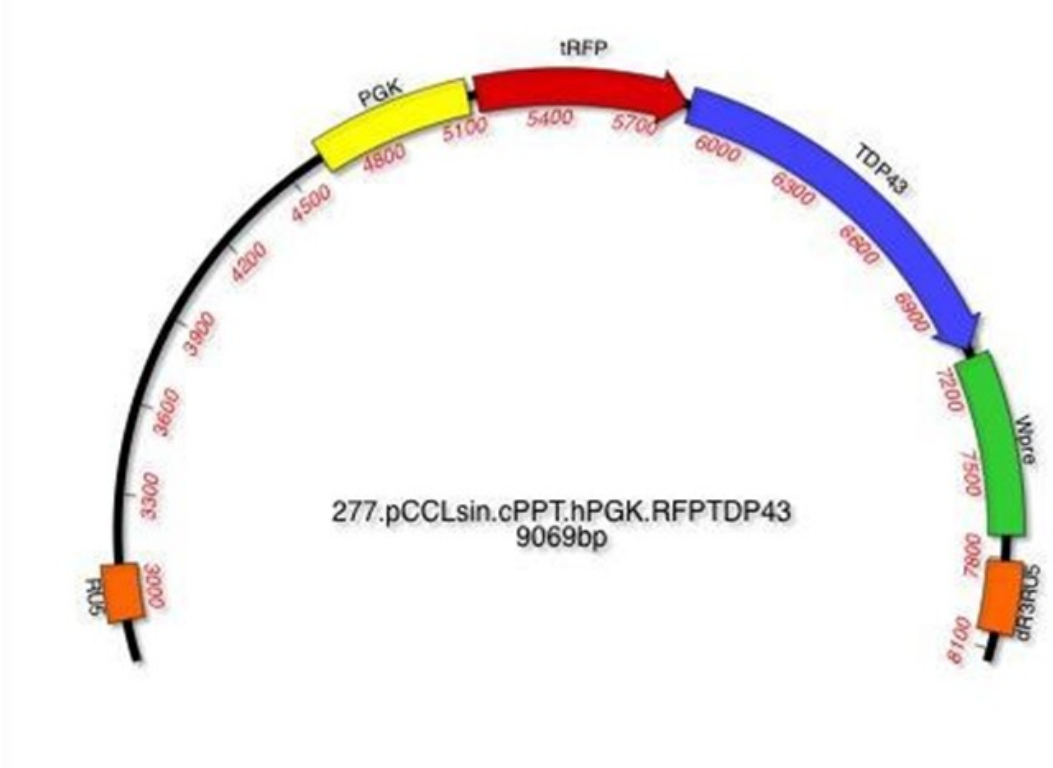


***Figure 7.1. tRFP-hTDP-43 (wt and A315T) vector.*** *Lentiviral vector p277 containing the human protein TDP-43 (in blue) fused at the N-terminal with the red fluorescent turbo-RFP protein (in red). The vectors tRFP-hTDP-43 (wt) and tRFP-hTDP-43 (A315T) are identical, except for the mutation that leads to the replacement of an alanine with a threonine at position 315 of the protein. RU5 and dR3RU5: repeated terminal sequences (long terminal repeats, LTR) that contain signals for regulating the integration of the virus in the host genome. PGK: promoter of the phosphoglycerate kinase enzyme. Wpre: post-transcriptional regulatory element deriving from the woodchuck hepatitis virus.*

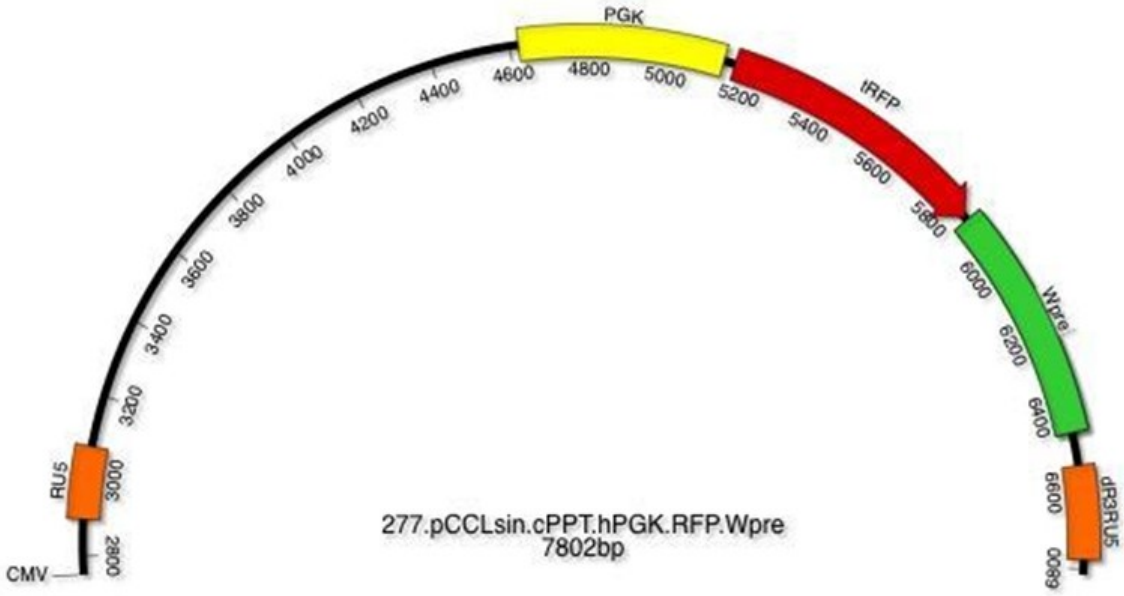


***Figure 7.2. tRFP vector.*** *Lentiviral vector p277 containing the turbo red fluorescent protein RFP (in red).*

### *7.3.2 Production and titration of lentiviral particles for the overexpression of human TDP-43 (wt and A315T)*

For the lentiviral particles production $13x10^6$ low passage (P10-P15) HEK (Human Embryonic Kidney) 293T cells were seeded in 15cm dishes in IMDM medium (Sigma, cat.I6529) with 10% FBS, P/S, Glutamine.

The next day the medium was changed two hours before transfection.

For each dish was prepared a tube containing the following plasmid DNA mix:

- ENV (VSV-G) plasmid DNA 9µg
- -pMDLg/pRRE plasmid DNA 12.5µg
- -REV plasmid DNA 6.25µg
- -Transfer plasmid DNA 32µg

The mix was brought up to a final volume of 1125µl with 0.1X TE/dH2O (2:1), then added with 125µl of 2.5M $CaCl_2$ and vortex.

After 10 minutes each tube was put on a vortex and 1250µl of 2X HBS (pH 7.14) were added drop by drop with a glass pipette.

Finally, this transfection mix was added drop by drop to the cells. After 16 hours the medium was replaced with fresh medium, and the cells were cultured for four days in the incubator. Cell supernatants, containing the lentiviral particles, were collected, filtered

using a stericup (Millipore, cat.S2GPU02RE), and dispensed in ultracentrifuge tubes (Beckman cat. 344058).

The tubes were hooked to a SW32Ti rotor and ultracentrifuged at 20000 rpm for two hours at room temperature. Then, the supernatants were carefully discarded, the tubes were flipped and the excess of liquid along the edges was dried. The pellets were left to dry for 30-40 minutes, resuspended in 70ul 1X D-PBS, and put on a shaker at 4°C for one hour. The viral particles were aliquoted and stored at -80°C.

### *7.3.3 Immunofluorescence to calculate lentiviral particles titer*

To calculate the titer of lentiviral particles, cortical neurons were seeded in a 24-well plate. At 5 DIV neurons were infected with a serial dilution (from $10^{-3}$ to $10^{-7}$) of lentiviral particles overexpressing tRFP-TDP-43 wt, tRFP-TDP-43(A315T) and tRFP. Uninfected cortical neurons were used as control. The experiment was repeated in triplicate for each condition. At 9 DIV cortical neurons were fixed and processed for immunofluorescence as described in Section 4.4, using anti-tRFP and anti-Tubulin beta III (TuJ1) primary antibodies. ArrayScan microscope (Thermo Fisher ArrayScan XTI HCA Reader) was used to acquire 20 random fields per well. For every field the tRFP-positive infected cells (red) and the total number of cells, stained with a nuclear marker (DAPI), were counted. Then, tRFP-positive cells and DAPI-positive cells coming from all fields were summed. A ratio between the number of the total tRFP-positive cells and the total DAPI-positive cells present in each well was made.

To calculate the titer a percentage ratio between tRFP-positive cells and total DAPI-positive cells between 0.1% and 10% (dynamic range) was chosen, and this formula was used: (Infected cells/Total cells)*Dilution factor*Number of seeded cells.

For the lentiviral infection, a multiplicity of infections (MOI) is considered, this corresponds to the ratio between the number of infectious agents and the number of infected cells present in an experimental system. In our experiments a MOI of 4 was used to ensure the infection of almost total cells without inducing cellular toxicity due to excessive lentiviral infection.

### *7.3.4 Infection of cortical neurons with lentiviral particles*

Cortical neurons were infected at 5 DIV with lentiviral particles expressing the cDNA listed in Section 7.3.1; the cells were treated, fixed or lysed at different DIV based on the experimental needs.

## 7.4 Immunofluorescence of cortical neurons

Immunofluorescence was performed on cortical neurons at indicated DIV. Cells were fixed with 4% Paraformaldehyde (PFA)/4% Sucrose in 1X Dulbecco's Phosphate Buffered Saline (D-PBS) for 15 minutes, and then washed 3 times with 1X D-PBS (Euroclone, cat. ECM4004XL). For neurons in microfluidic chambers an additional 5 minutes step of fixation with 4 % PFA/ 4% sucrose was added.

Fixed neurons were treated as following:

- Incubation with primary antibodies in 10% Goat Serum (GS), 0.1% Triton, 0.02% sodium azide in 1X D-PBS overnight (ON) at 4°C. For antibodies directed against nuclear epitopes a previous permeabilization step of 10 minutes with 0.5% Triton in 1X D-PBS was added.
- 3 washes in 1X D-PBS.
- Incubation with Alexa Fluor ™ secondary antibodies (1: 1000) in 10% GS, 1X D-PBS for one hour at room temperature (RT).
- 3 washes in 1X D-PBS.
- Incubation with the nuclear dye 4',6-diamidine-2-phenylindole (DAPI, 1:5000, Roche-Merck, cat.10236276001) in 1X D-PBS for 5 minutes.

Images were acquired using Leica Confocal SP8 (Leica TCS SP8 SMD FLIM Laser Scanning Confocal), Nikon Spinning Disk (Nikon CSU-X1 Spinning Disk, Nikon TE2 inverted microscope), Axio Observer (Zeiss Axio Observer.Z1 with Hamamatsu EM 9100). The quantification of all experiments was performed with ImageJ-Fiji Software.

## 7.5 Puromycylation assay

Neurons grown in microfluidic chambers (9 DIV) were treated with 2μM Puromycin (Sigma, cat.P7255 ) for 5 min in both cell body and axonal compartment. After a wash with PBS + Calcium and Magnesium (150mM NaCl, 50mM Tris, 1mM $MgCl_2$, 0.1mM $CaCl_2$ pH7.4), cells were fixed and processed for immunofluorescence as described in Section 7.4.

## 7.6 Western Blot

Proteins were extracted as follows:

- Cortical neurons were scraped at room temperature using 50µl of Lysis Buffer (5% SDS, 10mM EDTA, 50mM Hepes pH 7.4, in water)
- A brain hemisphere was lysed at 4°C in 1mL of RIPA Buffer (10mM Tris-HCl pH 7.5, 1mM EDTA pH 8, 1% Triton X-100, 0.1% SDS, 0.1% Na-deoxycholate, 140mM NaCl, in water) using a glass tissue potter with a Teflon pestle. After 10 minutes on ice, lysate was centrifuged at 13000 rpm for 30 minutes at 4°C.

A RIPA Buffer with 8M Urea and 10µM Dithiothreitol (DTT, Sigma, cat.D9779) was used for all the experiments that required Cx36 detection.

Protease inhibitors were added fresh to all buffers: 1µg/ml Leupeptin (Sigma, cat., 2µg/ml Aprotinin (Sigma, cat.A1153), 100µg/ml Phenylmethylsulfonyl Fluoride (PMSF, Sigma, cat.P7626), 1µg/ml Pepstatin A (Sigma, cat.P5318), 1mM Sodium Orthovanadate ($Na_3VO_4$, Sigma, cat.S6508), 2.5mM Sodium Pyrophosphate (Sigma, cat.221368), 50mM Sodium Fluoride (NaF, Sigma, cat.S6776), 1mM β-Glycerophosphate (Sigma, cat.G6251) .

All protein extracts were passed through a syringe with a narrow-gauge (No.27) hypodermic needle 5 times, sonicated 3 minutes to disrupt nucleic acids and quantified with Pierce ™ BCA Protein Assay kit (ThermoFisher, cat. 23225). 25µg of protein lysate were resuspended in Laemmli buffer 1X (Sigma, cat.S3401-1VL) or in Laemmli buffer 1X plus 8M urea and 10µM DTT if proteins were extracted with RIPA Buffer 8M Urea, and finally denatured at 95 °C for 5 minutes or at RT for 10 minutes, respectively. Samples were loaded onto a polyacrylamide gel (Mini-PROTEAN® TGX ™ Precast Gels 4-20%, Biorad, cat.456-1094). Protein separation was performed in 1X Running buffer (25mM Tris base, 192mM Glycine, 0.1% SDS), at 100V for about 100 minutes in a vertical electrophoretic apparatus (Biorad).

Proteins were transferred to a nitrocellulose membrane (Biorad, cat.1704159) at 25V for 30 minutes with Trans-Blot® Turbo ™ (Biorad).

Membranes were incubated in blocking buffer, which consists of 5% milk in TTBS (20mM Tris HCl, 150mM NaCl, 0.1% Tween-20) for 1h at RT, and then with primary antibodies diluted in blocking buffer at 4°C overnight.

After 3 washes in TTBS, the membranes were incubated with secondary antibodies in blocking buffer for 1 hour at RT.

After 3 washes in TTBS, the protein signal was revealed using the Clarity ™ Western ECL Substrate (Biorad, cat.170-5061). The images were acquired using the ChemiDoc ™ MP tool (Biorad) and Western blot quantification was performed with Image Lab ™ Software (Biorad).

## 7.7 Immunoprecipitation

To obtain a sufficient amount of protein from cortical neurons we seeded two 6-well plates for each condition (ctrl, wtTDP, mutTDP).

Cortical neurons at 14 DIV and mouse brain cortices at P120 were lysed in RIPA buffer for 30 minutes on ice, and centrifuged at 13000 rpm for 30 minutes at 4°C. The supernatants were quantified with Pierce ™ BCA Protein Assay kit and 1.25mg of protein from each sample were used for immunoprecipitation.

Immunoprecipitation was carried out with magnetic beads following the instructions indicated in the Crosslink Magnetic IP/Co-IP kit (Pierce ™, ThermoFisher, cat. 88805).

## 7.8 Subcellular fractionation

All the procedures described were performed at 4°C.

Cortical neurons were washed in ice-cold 1X PBS and lysed for 10 minutes on ice in Lysis Buffer (50mM Tris–HCl pH 8.0, 10mM NaCl, 5mM MgCl2, 0.3% Nonidet P-40 and protease inhibitors added at the same concentration described in Section 4.6.

Lysate was spin at 1000 x g for 15 minutes to pellet the nuclear fraction (P1), then the supernatant (S1) was collected in an ultracentrifuge Eppendorf (Beckman #357448), while the pellet (P1) was kept on ice waiting to be processed for the isolation of the nuclear fraction.

Supernatant (S1) was centrifuged at 50.000 rpm for 60 minutes in TLA55 rotor (Beckman TLX ultracentrifuge) to yield crude cytosol (S2) and crude membrane pellet (P2).

Pellet (P2) was resuspended in Lysis buffer without Nonidet P-40 (50mM Tris–HCl pH 8.0, 10mM NaCl, 5mM $MgCl_2$ and protease inhibitors) and then was centrifuged again at 50.000 rpm for 60 minutes to yield washed crude membrane pellet (P2').

The nuclear fraction (P1) was washed three times with Lysis buffer without Nonidet P-40 at 1000 x g for 15 minutes.

Pellet was resuspended in a high-salt buffer (20mM HEPES pH 7.5, 0.5M NaCl, 1mM EDTA, 1mM dithiothreitol and protease inhibitors) and rotated for 20 minutes.
Pellet was centrifuged at 17.700 × g for 30 minutes, and the supernatant, the fraction containing the nuclear extracts, was collected.

### 7.9 Treatment of cortical neurons with Dichlorofluorescein Diacetate

Cortical neurons were cultured in a 96-well plate (Greiner Bio-One, cat. 655090) up to 13 DIV, treated with 5μM dichlorofluorescein diacetate (CM-H2DCFDA, Thermofisher, cat.C6827) in KRH-T pH 7.4 buffer (125mM NaCl, 25mM Hepes/NaOH pH 7.4, 5mM KCl, 1.2 mM $MgCl_2$, 2mM $CaCl_2$, 6mM Glucose) for 30 minutes in a incubator at 37 °C. After incubation with 1X Hoechst (Sigma, cat. 33258) in an incubator at 37 °C, 5% $CO_2$ for 10 minutes, neurons were washed with KRH-T.
The images were acquired using ArrayScan (ThermoFisher ArrayScan XTI HCA Reader) and the fluorescence intensity analysis was carried out by the ALEMBIC Facility of the San Raffaele Hospital.
For iron overload, neurons were treated with 20μM ferric ammonium citrate for 2 days before incubation with CM-H2DCFDA.

### 7.10 Heat shock treatment of cortical neurons

Cortical neurons were seeded in 24-well plates and infected as usual. At 14 DIV the plates were incubated in a water bath at 43 °C for 60 minutes, washed in 1X D-PBS and fixed as described in Section 7.4.

### 7.11 Electrophysiology

Individual slides with cortical neuronal cultures were placed in a recording chamber mounted on the stage of an upright BX51WI microscope (Olympus) equipped with differential interference contrast optics (DIC). For EPSC bursts and dual patch recordings, slices were perfused with artificial cerebrospinal fluid (ACSF) containing (in mM): 125 NaCl, 2.5 KCl, 1.25 NaH2PO4, 2 CaCl2, 25 NaHCO3, 1 MgCl2, and 11 D-glucose, saturated with 95% O2 and 5% CO2 (pH 7.3). ACSF was continuously flowing at a rate of 2-3 ml/min at 32 °C. For mEPSC recordings, ACSF was added with the Na+ channel specific blocker tetrodotoxin (TTX, 1μM). Whole-cell patch-clamp recordings

were performed in cortical neurons using pipettes filled with a solution containing the following (in mM): 124 KH2PO4,10 NaCl, 10 HEPES, 0.5 EGTA, 2 MgCl2, 2 Na2-ATP, 0.02 Na-GTP, (pH 7.2, adjusted with KOH; tip resistance: 4-6 MΩ). All recordings were performed using a MultiClamp 700B amplifier interfaced with a computer through a Digidata 1440A (Molecular Devices, Sunnyvale, CA, USA). Traces were sampled at a frequency of 10 kHz and low-pass filtered at 2 kHz. Data were acquired using Clampex software (Molecular Devices) and analyzed with Clampfit and GraphPad Prism applications. Statistical comparisons were obtained using SigmaStat 3.5 (Systat, San Jose, CA).

### 7.12 FM1-43 assay

Neurons were incubated with 4 μM fura-2 acetoxymethyl ester (Calbiochem, cat. CAS 108964-32-5 ) 40 min at 37°C, before FM1-43 assay. Then neurons were treated for 2 minutes with 20μM FM1-43 (Sigma, cat. SCT126) in high K+ containing KRH (HK-KRH; Na+ concentration was adjusted to maintain isotonicity), diluted 1:1 in normal KRH to obtain the required final KCl and FM1-43 concentration (30mM and 10 μM respectively); 3-4 washes with KRH buffer were performed. Additional stimulus with HK-KRH was performed and fluorescence decay over time of FM1-43 was measured. Single-cell videoimaging setup consists of an Axioskope 2 microscope (Zeiss, Oberkochen, Germany) and a Polychrome IV (Till Photonics, GmbH, Martinsried, Germany) light source. Fluorescence images were collected by a cooled CCD video camera (PCO Computer Optics GmbH, Kelheim, Germany). The 'Vision' software (Till Photonics) was used to control the acquisition protocol and to perform data analysis (Codazzi *et al*, 2006).

### 7.13 Fura-2 calcium assay

Neurons were incubated with 4 μM fura-2 acetoxymethyl ester as in section 7.12. Then neurons were subjected to imaging analysis before and during the stimulation with 100μM glutamate. Imaging setup and analysis is the same of FM1-43 assay.

## 7.14 Mouse genetics

### *7.14.1 Transgenic PrP hTDP-43 wt*

The TDP-43 transgenic mouse line was obtained from The Jackson Laboratory (B6SJL-Tg(Prnp-TARDBP)4Jlel/J Strain #016201). Since the transgene integrated in the X chromosome, all experiments were carried out on hemizygous males starting from backcross generation N8, expected to carry 99.6% of the C57BL/6N genetic background.

### *7.14.2 Genotyping*

A small biopsy of the mouse tail was processed for DNA extraction using Xpert directXtract Lysis Buffer Kit (Grisp Research Solutions, Biocell). Genotyping was carried out by PCR with the following primers:

12117 (TDP-43-F): 5'- GGT GGT GGC ATG AAC TTT GG - 3'

12118 (TDP-43-R): 5'- GTG GAT AAC CCC TCC CCC AGC CTA GAC - 3'

| PCR reaction mix composition: | |
|---|---|
| 5X GoTaq® Flexi Buffer | 4µl |
| 2mM dNTPs | 2µl |
| 25mM MgCl2 | 1.2µl |
| 25uM forward primer | 0.4µl |
| 25uM reverse primer | 0.4µl |
| GoTaq® G2 Flexi DNA Polymerase (5u/ul, Promega cat.M7801) | 0.1µl |
| Genomic DNA | 1.5µl |
| Water up to 20µl | |

| PCR conditions | |
|---|---|
| 1 Denaturation: | 95°C, 5 min |
| 2 Denaturation: | 95°C, 30 sec |
| 3 Annealing: | 59°C, 30 sec |
| 4 Extension: | 72°C, 30 sec |
| 5 Go to step 2 | 29 times |
| 6 Extension: | 72°C, 5 min |

The transgene amplification product of 325bp was visualized by electrophoresis on a 1.5% agarose gel.

### *7.14.3 Tissues Preparation*

Postnatal mice were anesthetized with 2,2,2-Tribromoethanol (Sigma, cat.T48402) and perfused with 0.9% NaCl followed by 4% paraformaldehyde (PFA). For Immunohistochemistry tissues were dissected, post-fixed O/N in 4% PFA, dehydrated in an ethanol series and embedded in paraffin. Sections of 3 μm were cut using a microtome (Leica RM2125-RTS). For immunofluorescence tissues were cryoprotected in 30% sucrose, 1X PBS, included in OCT (Bioptica) and stored at –80°C, before sectioning on a cryotome (20 μm).

### *7.14.4 Immunofluorescence (IF) and immunohistochemistry (IHC) on mouse tissues sections*

IF: frontal brain sections were washed in 1X PBS, blocked and permeabilized in 10% normal goat serum, 0,3% Triton X-100 in 1X PBS, incubated in primary antibodies overnight at 4°C. rinsed in 1X PBS, and then incubated for 2 h at room temperature with secondary antibodies (ThermoFisher Alexa Fluor™, 1:1000). The sections were mounted using a fluorescent mounting medium (Dako, cat.S3023).

IHC: for antigen retrieval frontal brain sections were boiled in 10mM citrate buffer for 5 minutes in a microwave, immunostained as recommended (ABC Elite kit, Vector Laboratories, cat.PK-6100), dehydrated and mounted with VectaMount mounting medium (Vector Laboratories, cat.H5000).

## 7.15 Mouse motor test

Motor tests were performed by the Mouse Behavior Facility of the San Raffaele Hospital as follows.

### *7.15.1 Catwalk test*

1 day, before the test, measures the body weight and body length of each mouse. An animal traverses from one side to the other the enclosed glass plate walkway. Paws are captured thanks to the system Illuminated FootprintsTM technology by a high-speed video camera that is positioned underneath the walkway.

Each mouse must complete three runs compliant with the set parameters (run criteria). Not all mice will fulfill the task; in this case at least 15 runs are recorded for such mice.

The stride length for each paw (RF: right front; RH: right hind; LF: left front; LH: left hind) were measured as the distance in cm between successive placements of the same paw. The distance in cm between front and hind paws were measured.

### *7.15.2 Rotarod test*

-Training phase: 3 consecutive trials of 60'' each. In the 1st trial the rod is kept stationary and for the 2nd and 3rd trial the rod is held at 5 RPM. An Inter Trial Interval (ITI)= 10' is maintained between trials.

After 30 min from the 3rd training trial, mice were subjected to the test phase.

-Testing phase: four trials per day with rotation speed accelerated from 5 RPM to 40 RPM in 300'', maximum duration= 300'' per trial, ITI=15 min.

The latency to fall off the rod is the dependent variable analyzed.

### *7.15.3 Grip-Strength Meter*

A newton meter with a T-bar is horizontally fixed. Mouse is held in a horizontal position and lowered towards the T-bar until the animal grasps it. Then it is gently pulled backward until it releases the grid. The force measured when the animal releases the grip is recorded. Six consecutive measures per mouse are done and maximal strength is used as dependent variables (grams of force (g-f)).

### *7.15.4 Hanging wire*

The mouse is placed on the top of the grid, shake it lightly so the mice can hang themselves and then turn the grid upside down, meanwhile activate the timer and record the hanging time (latency to fall, sec is the dependent variable analyzed). The test was performed in 3 consecutive days, 3 trials per day maximum duration 180", inter trial interval 120".

## 7.16 Miniaturize sucrose gradient, polysome profiling, RNA-sequencing, RT-qPCR

Transcriptomic and translatomic analysis was performed by Gabriella Viero's Lab, Institute of Biophysics, National Council Research, Povo, Trento. The protocol of polysome profiling by miniaturized sucrose gradient fractionation was adapted from

Negro et al., 2018 (Negro *et al.*, 2018). GO analysis was performed as in Bernabo et al., 2017(Bernabo *et al*, 2017). RNA-seq and RT-qPCR details will be shown in depth in the dissertation of Gabriella Viero's PhD student. For further details please contact gabriella.viero@gmail.com.

## 7.17 Statistics

All values are expressed as mean ± standard error (SEM) of at least 3 independent experiments. Statistical analysis was performed by GraphPad Prism software.
The statistical test of each experiment is reported in the figure legends. Non significant differences (ns) occur when $p > 0.05$. Significant differences are indicated as follows; *$p < 0.05$, **$p < 0.01$, ***$p < 0.001$ and ****$p < 0.0001$.

## 7.18 Antibodies

| Immunofluorescence | | | |
|---|---|---|---|
| **Primary Antibodies** | | | |
| *Description* | *Brand and Cat.#* | *Host/ isotype* | *Dilution* |
| Rpl26 | BethylLab (A300-686A-T) | Rabbit/IgG | 1:500 |
| Map2 | Millipore (MAB3418) | Mouse/IgG | 1:1000 |
| Synaptojanin1 | Thermo Fisher (711821) | Rabbit/IgG | 1:300 |
| TDP-43 | Proteintech (10782-2-AP) | Rabbit/IgG | 1:500 |
| β-Tubulin ClassIII (TUJ1) | Covance (MMS-435P) | Mouse/IgG2a | 1:1000 |

| | | | |
|---|---|---|---|
| β-Tubulin ClassIII (TUJ1) | BioLegend (802001) | Rabbit/IgG | 1:1000 |
| G3BP1 | Proteintech (13057-2-AP) | Rabbit/IgG | 1:300 |
| HuC/D | Thermo Fisher (A-21271) | Mouse/IgG2b | 1:2000 |
| tRFP | Evrogen (AB233) | Rabbit/IgG | 1:1000 |
| O4 | Sigma (O7139) | Mouse | 1:100 |
| CTIP2 | Abcam (ab18465) | Rat | 1:250 |
| GFAP | DakoCytomation (Z0334) | Rabbit/IgG | 1:500 |
| IBA1 | Wako (01919741) | Rabbit/IgG | 1:500 |
| TBR1 | Abcam (ab31940) | Rabbit/IgG | 1:250 |
| GAD65 | GeneTex (GTX100281) | Rabbit/IgG | 1:100 |
| RPS6 | Cell signaling (mAb#2217) | Rabbit/IgG | 1:500 |
| Active-Caspase-3 | BD PharMingen (559565) | Rabbit/IgG | 1:200 |
| Puromycin | Millipore (MABE343) | Mouse/IgG | 1:100 |
| Park7 | Thermo Fisher (MA5-32297) | Rabbit/IgG | 1:200 |

| Immunofluorescence |
|---|
| **Secondary Antibodies** |

| *Description* | *Brand and Cat.#* | *Dilution, 1h RT* |
|---|---|---|
| Alexa FluorTM 546 Goat anti-mouse (IgG) | Invitrogen (A11003) | 1:1000 |
| AlexaFluor TM 546 Goat anti-mouse (IgG2a) | Invitrogen (A21133) | 1:1000 |
| Alexa FluorTM 488 Goat anti-rabbit (IgG) | Invitrogen (A11034) | 1:1000 |
| Alexa FluorTM 488 Goat anti-mouse (IgG) | Invitrogen (A11001) | 1:1000 |
| Alexa FluorTM 488 Goat anti-mouse (IgG2a) | Invitrogen (A21131) | 1:1000 |
| Alexa FluorTM 647 Goat anti-mouse (IgG) | Invitrogen (A32728) | 1:1000 |
| Alexa FluorTM 647 Goat anti-rabbit (IgG) | Invitrogen (A21244) | 1:1000 |

| Western Blot | | | |
|---|---|---|---|
| **Primary Antibodies** | | | |
| *Description* | *Brand and Cat.#* | *Host/ isotype* | *Dilution* |
| Phospho-TDP-43 (Ser 409-410) | Proteintech (22309-1-AP) | Mouse | 1:500 |
| Ubiquitin | Millipore (MAB1510) | Mouse | 1:500 |

| | | | |
|---|---|---|---|
| TDP-43 | Proteintech (10782-2-AP) | Rabbit | 1:1000 |
| Calnexin | Sigma (C4731) | Rabbit | 1:5000 |
| tRFP | Evrogen (AB233) | Rabbit | 1:5000 |
| GAPDH | Santa Cruz (sc-25778) | Rabbit | 1:2500 |
| Cx36 | Invitrogen (364600) | Rabbit | 1:300 |
| Histone-H3 | Abcam (ab1791) | Rabbit | 1:5000 |

| Western blot | | |
|---|---|---|
| **Secondary Antibodies** | | |
| *Description* | *Brand and Cat.#* | *Dilution, 1.5$^{h}$ RT* |
| Goat anti-mouse IgG (H+L)-HRP Conjugate | Biorad (172-1011) | 1:10000 |
| Goat anti-rabbit IgG (H+L)-HRP Conjugate | Biorad (170-6515) | 1:10000 |

| Immunohistochemistry | | | |
|---|---|---|---|
| **Primary Antibodies** | | | |
| *Description* | *Brand and Cat.#* | *Host/ isotype* | *Dilution Overnight* |
| Ubiquitin | Millipore (MAB1510) | Mouse | 1:40000 |

| | | | |
|---|---|---|---|
| TDP-43 | Proteintech (10782-2-AP) | Rabbit | 1:1000 |
| IBA1 | Wako (01919741) | Rabbit | 1:500 |
| GFAP | DakoCytomation (Z0334) | Rabbit | 1:1000 |

| Immunohistochemistry | | |
|---|---|---|
| **Secondary Antibodies** | | |
| *Description* | *Brand and Cat.#* | *Dilution, $2^h$ RT* |
| Biotinylated anti-mouse IgG (H+L) | Vector Laboratories (BA-9200) | 1:200 |
| Biotinylated anti-rabbit IgG (H+L) | Vector Laboratories (AP-1000) | 1:200 |

## 8. References


Afroz T, Hock EM, Ernst P, Foglieni C, Jambeau M, Gilhespy LAB, Laferriere F, Maniecka Z, Pluckthun A, Mittl P *et al* (2017) Functional and dynamic polymerization of the ALS-linked protein TDP-43 antagonizes its pathologic aggregation. *Nat Commun* 8: 45

Agosta F, Valsasina P, Absinta M, Riva N, Sala S, Prelle A, Copetti M, Comola M, Comi G, Filippi M (2011) Sensorimotor functional connectivity changes in amyotrophic lateral sclerosis. *Cereb Cortex* 21: 2291-2298

Alami NH, Smith RB, Carrasco MA, Williams LA, Winborn CS, Han SS, Kiskinis E, Winborn B, Freibaum BD, Kanagaraj A *et al* (2014) Axonal transport of TDP-43 mRNA granules is impaired by ALS-causing mutations. *Neuron* 81: 536-543

Altman T, Ionescu A, Ibraheem A, Priesmann D, Gradus-Pery T, Farberov L, Alexandra G, Shelestovich N, Dafinca R, Shomron N *et al* (2021) Axonal TDP-43 condensates drive neuromuscular junction disruption through inhibition of local synthesis of nuclear encoded mitochondrial proteins. *Nat Commun* 12: 6914

Anttila JE, Whitaker KW, Wires ES, Harvey BK, Airavaara M (2017) Role of microglia in ischemic focal stroke and recovery: focus on Toll-like receptors. *Prog Neuropsychopharmacol Biol Psychiatry* 79: 3-14

Arai T, Hasegawa M, Akiyama H, Ikeda K, Nonaka T, Mori H, Mann D, Tsuchiya K, Yoshida M, Hashizume Y *et al* (2006) TDP-43 is a component of ubiquitin-positive tau-negative inclusions in frontotemporal lobar degeneration and amyotrophic lateral sclerosis. *Biochem Biophys Res Commun* 351: 602-611

Avendano-Vazquez SE, Dhir A, Bembich S, Buratti E, Proudfoot N, Baralle FE (2012) Autoregulation of TDP-43 mRNA levels involves interplay between transcription, splicing, and alternative polyA site selection. *Genes Dev* 26: 1679-1684

Ayala YM, De Conti L, Avendano-Vazquez SE, Dhir A, Romano M, D'Ambrogio A, Tollervey J, Ule J, Baralle M, Buratti E *et al* (2011) TDP-43 regulates its mRNA levels through a negative feedback loop. *The EMBO journal* 30: 277-288

Ayala YM, Pantano S, D'Ambrogio A, Buratti E, Brindisi A, Marchetti C, Romano M, Baralle FE (2005) Human, Drosophila, and C.elegans TDP43: nucleic acid binding properties and splicing regulatory function. *J Mol Biol* 348: 575-588

Ayala YM, Zago P, D'Ambrogio A, Xu YF, Petrucelli L, Buratti E, Baralle FE (2008) Structural determinants of the cellular localization and shuttling of TDP-43. *Journal of cell science* 121: 3778-3785

Balendra R, Isaacs AM (2018) C9orf72-mediated ALS and FTD: multiple pathways to disease. *Nature reviews Neurology* 14: 544-558

Barber SC, Shaw PJ (2010) Oxidative stress in ALS: key role in motor neuron injury and therapeutic target. *Free Radic Biol Med* 48: 629-641

Beers DR, Henkel JS, Xiao Q, Zhao W, Wang J, Yen AA, Siklos L, McKercher SR, Appel SH (2006) Wild-type microglia extend survival in PU.1 knockout mice with familial amyotrophic lateral sclerosis. *Proc Natl Acad Sci U S A* 103: 16021-16026

Belluardo N, Mudo G, Trovato-Salinaro A, Le Gurun S, Charollais A, Serre-Beinier V, Amato G, Haefliger JA, Meda P, Condorelli DF (2000) Expression of connexin36 in the adult and developing rat brain. *Brain Res* 865: 121-138

Bennett MV, Zukin RS (2004) Electrical coupling and neuronal synchronization in the Mammalian brain. *Neuron* 41: 495-511

Bernabo P, Tebaldi T, Groen EJN, Lane FM, Perenthaler E, Mattedi F, Newbery HJ, Zhou H, Zuccotti P, Potrich V *et al* (2017) In Vivo Translatome Profiling in Spinal Muscular Atrophy Reveals a Role for SMN Protein in Ribosome Biology. *Cell reports* 21: 953-965

Biever A, Glock C, Tushev G, Ciirdaeva E, Dalmay T, Langer JD, Schuman EM (2020) Monosomes actively translate synaptic mRNAs in neuronal processes. *Science* 367

Bilsland LG, Sahai E, Kelly G, Golding M, Greensmith L, Schiavo G (2010) Deficits in axonal transport precede ALS symptoms in vivo. *Proc Natl Acad Sci U S A* 107: 20523-20528

Birsa N, Ule AM, Garone MG, Tsang B, Mattedi F, Chong PA, Humphrey J, Jarvis S, Pisiren M, Wilkins OG *et al* (2021) FUS-ALS mutants alter FMRP phase separation equilibrium and impair protein translation. *Sci Adv* 7

Blair IP, Williams KL, Warraich ST, Durnall JC, Thoeng AD, Manavis J, Blumbergs PC, Vucic S, Kiernan MC, Nicholson GA (2010) FUS mutations in amyotrophic lateral sclerosis: clinical, pathological, neurophysiological and genetic analysis. *J Neurol Neurosurg Psychiatry* 81: 639-645

Brettschneider J, Del Tredici K, Toledo JB, Robinson JL, Irwin DJ, Grossman M, Suh E, Van Deerlin VM, Wood EM, Baek Y *et al* (2013) Stages of pTDP-43 pathology in amyotrophic lateral sclerosis. *Ann Neurol* 74: 20-38

Briese M, Saal L, Appenzeller S, Moradi M, Baluapuri A, Sendtner M (2016) Whole transcriptome profiling reveals the RNA content of motor axons. *Nucleic acids research* 44: e33

Briese M, Saal-Bauernschubert L, Luningschror P, Moradi M, Dombert B, Surrey V, Appenzeller S, Deng C, Jablonka S, Sendtner M (2020) Loss of Tdp-43 disrupts the axonal transcriptome of motoneurons accompanied by impaired axonal translation and mitochondria function. *Acta Neuropathol Commun* 8: 116

Bronicki LM, Jasmin BJ (2013) Emerging complexity of the HuD/ELAVl4 gene; implications for neuronal development, function, and dysfunction. *RNA* 19: 1019-1037

Brown AL, Wilkins OG, Keuss MJ, Hill SE, Zanovello M, Lee WC, Lee FCY, Masino L, Qi YA, Bryce-Smith *et al* (2021) Common ALS/FTD risk variants in UNC13A exacerbate its cryptic splicing and loss upon TDP-43 mislocalization. *bioRxiv*

Brown RH, Jr., Al-Chalabi A (2017) Amyotrophic Lateral Sclerosis. *N Engl J Med* 377: 1602

Budini M, Romano V, Quadri Z, Buratti E, Baralle FE (2015) TDP-43 loss of cellular function through aggregation requires additional structural determinants beyond its C-terminal Q/N prion-like domain. *Hum Mol Genet* 24: 9-20

Buratti E (2015) Functional Significance of TDP-43 Mutations in Disease. *Adv Genet* 91: 1-53

Buratti E (2018) TDP-43 post-translational modifications in health and disease. *Expert Opin Ther Targets* 22: 279-293

Buratti E, Dork T, Zuccato E, Pagani F, Romano M, Baralle FE (2001) Nuclear factor TDP-43 and SR proteins promote in vitro and in vivo CFTR exon 9 skipping. *The EMBO journal* 20: 1774-1784

Butti Z, Patten SA (2018) RNA Dysregulation in Amyotrophic Lateral Sclerosis. *Front Genet* 9: 712

Caccamo A, Majumder S, Oddo S (2012) Cognitive decline typical of frontotemporal lobar degeneration in transgenic mice expressing the 25-kDa C-terminal fragment of TDP-43. *Am J Pathol* 180: 293-302

Che MX, Jiang LL, Li HY, Jiang YJ, Hu HY (2015) TDP-35 sequesters TDP-43 into cytoplasmic inclusions through binding with RNA. *FEBS Lett* 589: 1920-1928

Choi SY, Lee JH, Chung AY, Jo Y, Shin JH, Park HC, Kim H, Lopez-Gonzalez R, Ryu JR, Sun W (2020) Prevention of mitochondrial impairment by inhibition of protein phosphatase 1 activity in amyotrophic lateral sclerosis. *Cell Death Dis* 11: 888

Chou CC, Zhang Y, Umoh ME, Vaughan SW, Lorenzini I, Liu F, Sayegh M, Donlin-Asp PG, Chen YH, Duong DM *et al* (2018) TDP-43 pathology disrupts nuclear pore complexes and nucleocytoplasmic transport in ALS/FTD. *Nature neuroscience* 21: 228-239

Chu JF, Majumder P, Chatterjee B, Huang SL, Shen CJ (2019) TDP-43 Regulates Coupled Dendritic mRNA Transport-Translation Processes in Co-operation with FMRP and Staufen1. *Cell reports* 29: 3118-3133 e3116

Cioni JM, Lin JQ, Holtermann AV, Koppers M, Jakobs MAH, Azizi A, Turner-Bridger B, Shigeoka T, Franze K, Harris WA *et al* (2019) Late Endosomes Act as mRNA Translation Platforms and Sustain Mitochondria in Axons. *Cell* 176: 56-72 e15

Codazzi F, Di Cesare A, Chiulli N, Albanese A, Meyer T, Zacchetti D, Grohovaz F (2006) Synergistic control of protein kinase Cgamma activity by ionotropic and metabotropic glutamate receptor inputs in hippocampal neurons. *The Journal of neuroscience : the official journal of the Society for Neuroscience* 26: 3404-3411

Cohen TJ, Hwang AW, Restrepo CR, Yuan CX, Trojanowski JQ, Lee VM (2015) An acetylation switch controls TDP-43 function and aggregation propensity. *Nat Commun* 6: 5845

Cohen TJ, Hwang AW, Unger T, Trojanowski JQ, Lee VM (2012) Redox signalling directly regulates TDP-43 via cysteine oxidation and disulphide cross-linking. *The EMBO journal* 31: 1241-1252

Cohen TJ, Lee VM, Trojanowski JQ (2011) TDP-43 functions and pathogenic mechanisms implicated in TDP-43 proteinopathies. *Trends Mol Med* 17: 659-667

Colombrita C, Onesto E, Megiorni F, Pizzuti A, Baralle FE, Buratti E, Silani V, Ratti A (2012) TDP-43 and FUS RNA-binding proteins bind distinct sets of cytoplasmic messenger RNAs and differently regulate their post-transcriptional fate in motoneuron-like cells. *The Journal of biological chemistry* 287: 15635-15647

Colombrita C, Zennaro E, Fallini C, Weber M, Sommacal A, Buratti E, Silani V, Ratti A (2009) TDP-43 is recruited to stress granules in conditions of oxidative insult. *Journal of neurochemistry* 111: 1051-1061

Conicella AE, Zerze GH, Mittal J, Fawzi NL (2016) ALS Mutations Disrupt Phase Separation Mediated by alpha-Helical Structure in the TDP-43 Low-Complexity C-Terminal Domain. *Structure* 24: 1537-1549

Corbin JG, Butt SJ (2011) Developmental mechanisms for the generation of telencephalic interneurons. *Developmental neurobiology* 71: 710-732

Corradi E, Dalla Costa I, Gavoci A, Iyer A, Roccuzzo M, Otto TA, Oliani E, Bridi S, Strohbuecker S, Santos-Rodriguez G *et al* (2020) Axonal precursor miRNAs hitchhike on endosomes and locally regulate the development of neural circuits. *The EMBO journal* 39: e102513

Cosker KE, Fenstermacher SJ, Pazyra-Murphy MF, Elliott HL, Segal RA (2016) The RNA-binding protein SFPQ orchestrates an RNA regulon to promote axon viability. *Nature neuroscience* 19: 690-696

Costessi L, Porro F, Iaconcig A, Muro AF (2014) TDP-43 regulates beta-adducin (Add2) transcript stability. *RNA biology* 11: 1280-1290

Coyne AN, Lorenzini I, Chou CC, Torvund M, Rogers RS, Starr A, Zaepfel BL, Levy J, Johannesmeyer J, Schwartz JC *et al* (2017) Post-transcriptional Inhibition of Hsc70-4/HSPA8 Expression Leads to Synaptic Vesicle Cycling Defects in Multiple Models of ALS. *Cell reports* 21: 110-125

Coyne AN, Siddegowda BB, Estes PS, Johannesmeyer J, Kovalik T, Daniel SG, Pearson A, Bowser R, Zarnescu DC (2014) Futsch/MAP1B mRNA is a translational target of TDP-43 and is neuroprotective in a Drosophila model of amyotrophic lateral sclerosis. *The Journal of neuroscience : the official journal of the Society for Neuroscience* 34: 15962-15974

Cremona O, Di Paolo G, Wenk MR, Luthi A, Kim WT, Takei K, Daniell L, Nemoto Y, Shears SB, Flavell RA *et al* (1999) Essential role of phosphoinositide metabolism in synaptic vesicle recycling. *Cell* 99: 179-188

Dalla Costa I, Buchanan CN, Zdradzinski MD, Sahoo PK, Smith TP, Thames E, Kar AN, Twiss JL (2021) The functional organization of axonal mRNA transport and translation. *Nature reviews Neuroscience* 22: 77-91

Darnell JC, Van Driesche SJ, Zhang C, Hung KY, Mele A, Fraser CE, Stone EF, Chen C, Fak JJ, Chi SW *et al* (2011) FMRP stalls ribosomal translocation on mRNAs linked to synaptic function and autism. *Cell* 146: 247-261

Dayton RD, Gitcho MA, Orchard EA, Wilson JD, Wang DB, Cain CD, Johnson JA, Zhang YJ, Petrucelli L, Mathis JM *et al* (2013) Selective forelimb impairment in rats expressing a pathological TDP-43 25 kDa C-terminal fragment to mimic amyotrophic lateral sclerosis. *Mol Ther* 21: 1324-1334

de Boer EMJ, Orie VK, Williams T, Baker MR, De Oliveira HM, Polvikoski T, Silsby M, Menon P, van den Bos M, Halliday GM *et al* (2020) TDP-43 proteinopathies: a new wave of neurodegenerative diseases. *J Neurol Neurosurg Psychiatry*

DeJesus-Hernandez M, Mackenzie IR, Boeve BF, Boxer AL, Baker M, Rutherford NJ, Nicholson AM, Finch NA, Flynn H, Adamson J *et al* (2011) Expanded GGGGCC hexanucleotide repeat in noncoding region of C9ORF72 causes chromosome 9p-linked FTD and ALS. *Neuron* 72: 245-256

Deng HX, Chen W, Hong ST, Boycott KM, Gorrie GH, Siddique N, Yang Y, Fecto F, Shi Y, Zhai H *et al* (2011) Mutations in UBQLN2 cause dominant X-linked juvenile and adult-onset ALS and ALS/dementia. *Nature* 477: 211-215

Dewey CM, Cenik B, Sephton CF, Johnson BA, Herz J, Yu G (2012) TDP-43 aggregation in neurodegeneration: are stress granules the key? *Brain Res* 1462: 16-25

Diaz-Garcia S, Ko VI, Vazquez-Sanchez S, Chia R, Arogundade OA, Rodriguez MJ, Traynor BJ, Cleveland D, Ravits J (2021) Nuclear depletion of RNA-binding protein ELAVL3 (HuC) in sporadic and familial amyotrophic lateral sclerosis. *Acta Neuropathol* 142: 985-1001

Ding X, Xiang Z, Qin C, Chen Y, Tian H, Meng L, Xia D, Liu H, Song J, Fu J *et al* (2021) Spreading of TDP-43 pathology via pyramidal tract induces ALS-like phenotypes in TDP-43 transgenic mice. *Acta Neuropathol Commun* 9: 15

Ederle H, Funk C, Abou-Ajram C, Hutten S, Funk EBE, Kehlenbach RH, Bailer SM, Dormann D (2018) Nuclear egress of TDP-43 and FUS occurs independently of Exportin-1/CRM1. *Scientific reports* 8: 7084

Fallini C, Bassell GJ, Rossoll W (2012) The ALS disease protein TDP-43 is actively transported in motor neuron axons and regulates axon outgrowth. *Hum Mol Genet* 21: 3703-3718

Feiler MS, Strobel B, Freischmidt A, Helferich AM, Kappel J, Brewer BM, Li D, Thal DR, Walther P, Ludolph AC *et al* (2015) TDP-43 is intercellularly transmitted across axon terminals. *J Cell Biol* 211: 897-911

Fernandes N, Eshleman N, Buchan JR (2018) Stress Granules and ALS: A Case of Causation or Correlation? *Adv Neurobiol* 20: 173-212

Ferraiuolo L, Higginbottom A, Heath PR, Barber S, Greenald D, Kirby J, Shaw PJ (2011) Dysregulation of astrocyte-motoneuron cross-talk in mutant superoxide dismutase 1-related amyotrophic lateral sclerosis. *Brain* 134: 2627-2641

Fiesel FC, Weber SS, Supper J, Zell A, Kahle PJ (2012) TDP-43 regulates global translational yield by splicing of exon junction complex component SKAR. *Nucleic acids research* 40: 2668-2682

Fischer LR, Culver DG, Tennant P, Davis AA, Wang M, Castellano-Sanchez A, Khan J, Polak MA, Glass JD (2004) Amyotrophic lateral sclerosis is a distal axonopathy: evidence in mice and man. *Exp Neurol* 185: 232-240

Formicola N, Vijayakumar J, Besse F (2019) Neuronal ribonucleoprotein granules: Dynamic sensors of localized signals. *Traffic* 20: 639-649

Fratta P, Sivakumar P, Humphrey J, Lo K, Ricketts T, Oliveira H, Brito-Armas JM, Kalmar B, Ule A, Yu Y *et al* (2018) Mice with endogenous TDP-43 mutations exhibit gain of splicing function and characteristics of amyotrophic lateral sclerosis. *The EMBO journal* 37

Fusco CM, Desch K, Dorrbaum AR, Wang M, Staab A, Chan ICW, Vail E, Villeri V, Langer JD, Schuman EM (2021) Neuronal ribosomes exhibit dynamic and context-dependent exchange of ribosomal proteins. *Nat Commun* 12: 6127

Gasset-Rosa F, Lu S, Yu H, Chen C, Melamed Z, Guo L, Shorter J, Da Cruz S, Cleveland DW (2019) Cytoplasmic TDP-43 De-mixing Independent of Stress Granules Drives Inhibition of Nuclear Import, Loss of Nuclear TDP-43, and Cell Death. *Neuron* 102: 339-357 e337

Geevasinga N, Menon P, Ozdinler PH, Kiernan MC, Vucic S (2016) Pathophysiological and diagnostic implications of cortical dysfunction in ALS. *Nature reviews Neurology* 12: 651-661

Ghasemi M, Brown RH, Jr. (2018) Genetics of Amyotrophic Lateral Sclerosis. *Cold Spring Harb Perspect Med* 8

Gil J, Funalot B, Verschueren A, Danel-Brunaud V, Camu W, Vandenberghe N, Desnuelle C, Guy N, Camdessanche JP, Cintas P *et al* (2008) Causes of death amongst French patients with amyotrophic lateral sclerosis: a prospective study. *Eur J Neurol* 15: 1245-1251

Gitcho MA, Baloh RH, Chakraverty S, Mayo K, Norton JB, Levitch D, Hatanpaa KJ, White CL, 3rd, Bigio EH, Caselli R *et al* (2008) TDP-43 A315T mutation in familial motor neuron disease. *Ann Neurol* 63: 535-538

Golebiowski F, Matic I, Tatham MH, Cole C, Yin Y, Nakamura A, Cox J, Barton GJ, Mann M, Hay RT (2009) System-wide changes to SUMO modifications in response to heat shock. *Sci Signal* 2: ra24

Gonzalez C, Cornejo VH, Couve A (2018) Golgi bypass for local delivery of axonal proteins, fact or fiction? *Curr Opin Cell Biol* 53: 9-14

Gould TW, Buss RR, Vinsant S, Prevette D, Sun W, Knudson CM, Milligan CE, Oppenheim RW (2006) Complete dissociation of motor neuron death from motor dysfunction by Bax deletion in a mouse model of ALS. *The Journal of neuroscience : the official journal of the Society for Neuroscience* 26: 8774-8786

Gregory JM, Fagegaltier D, Phatnani H, Harms MB (2020) Genetics of Amyotrophic Lateral Sclerosis. *Current Genetic Medicine Reports*

Greig LC, Woodworth MB, Galazo MJ, Padmanabhan H, Macklis JD (2013) Molecular logic of neocortical projection neuron specification, development and diversity. *Nature reviews Neuroscience* 14: 755-769

Grosskreutz J, Van Den Bosch L, Keller BU (2010) Calcium dysregulation in amyotrophic lateral sclerosis. *Cell Calcium* 47: 165-174

Gu J, Wang W, Miao S, Chen F, Wu F, Hu W, Iqbal K, Gong CX, Liu F (2018) Protein Phosphatase 1 dephosphorylates TDP-43 and suppresses its function in tau exon 10 inclusion. *FEBS Lett* 592: 402-410

Guo W, Stoklund Dittlau K, Van Den Bosch L (2020) Axonal transport defects and neurodegeneration: Molecular mechanisms and therapeutic implications. *Semin Cell Dev Biol* 99: 133-150

Hardiman O, Al-Chalabi A, Chio A, Corr EM, Logroscino G, Robberecht W, Shaw PJ, Simmons Z, van den Berg LH (2017) Amyotrophic lateral sclerosis. *Nat Rev Dis Primers* 3: 17085

Harley J, Hagemann C, Serio A, Patani R (2021) TDP-43 and FUS mislocalization in VCP mutant motor neurons is reversed by pharmacological inhibition of the VCP D2 ATPase domain. *Brain Commun* 3: fcab166

Harrison AF, Shorter J (2017) RNA-binding proteins with prion-like domains in health and disease. *Biochem J* 474: 1417-1438

Hasegawa M, Arai T, Nonaka T, Kametani F, Yoshida M, Hashizume Y, Beach TG, Buratti E, Baralle F, Morita M *et al* (2008) Phosphorylated TDP-43 in frontotemporal lobar degeneration and amyotrophic lateral sclerosis. *Ann Neurol* 64: 60-70

Hebron ML, Lonskaya I, Sharpe K, Weerasinghe PP, Algarzae NK, Shekoyan AR, Moussa CE (2013) Parkin ubiquitinates Tar-DNA binding protein-43 (TDP-43) and promotes its cytosolic accumulation via interaction with histone deacetylase 6 (HDAC6). *The Journal of biological chemistry* 288: 4103-4115

Heimer L (1994) *The Human Brain and Spinal Cord: Functional Neuroanatomy and Dissection Guide*. Springer, New York

Hergesheimer RC, Chami AA, de Assis DR, Vourc'h P, Andres CR, Corcia P, Lanznaster D, Blasco H (2019) The debated toxic role of aggregated TDP-43 in amyotrophic lateral sclerosis: a resolution in sight? *Brain* 142: 1176-1194

Higashi S, Kabuta T, Nagai Y, Tsuchiya Y, Akiyama H, Wada K (2013) TDP-43 associates with stalled ribosomes and contributes to cell survival during cellular stress. *Journal of neurochemistry* 126: 288-300

Hirokawa N, Noda Y, Tanaka Y, Niwa S (2009) Kinesin superfamily motor proteins and intracellular transport. *Nat Rev Mol Cell Biol* 10: 682-696

Howland DS, Liu J, She Y, Goad B, Maragakis NJ, Kim B, Erickson J, Kulik J, DeVito L, Psaltis G *et al* (2002) Focal loss of the glutamate transporter EAAT2 in a transgenic rat model of SOD1 mutant-mediated amyotrophic lateral sclerosis (ALS). *Proc Natl Acad Sci U S A* 99: 1604-1609

Huang M, Chen S (2021) DJ-1 in neurodegenerative diseases: Pathogenesis and clinical application. *Prog Neurobiol* 204: 102114

Huang SL, Wu LS, Lee M, Chang CW, Cheng WC, Fang YS, Chen YR, Cheng PL, Shen CJ (2020) A robust TDP-43 knock-in mouse model of ALS. *Acta Neuropathol Commun* 8: 3

Humphrey J, Birsa N, Milioto C, McLaughlin M, Ule AM, Robaldo D, Eberle AB, Krauchi R, Bentham M, Brown AL *et al* (2020) FUS ALS-causative mutations impair FUS autoregulation and splicing factor networks through intron retention. *Nucleic acids research* 48: 6889-6905

Iacoangeli A, Al Khleifat A, Jones AR, Sproviero W, Shatunov A, Opie-Martin S, Alzheimer's Disease Neuroimaging I, Morrison KE, Shaw PJ, Shaw CE *et al* (2019) C9orf72 intermediate expansions of 24-30 repeats are associated with ALS. *Acta Neuropathol Commun* 7: 115

Igaz LM, Kwong LK, Chen-Plotkin A, Winton MJ, Unger TL, Xu Y, Neumann M, Trojanowski JQ, Lee VM (2009) Expression of TDP-43 C-terminal Fragments in Vitro Recapitulates Pathological Features of TDP-43 Proteinopathies. *The Journal of biological chemistry* 284: 8516-8524

Igaz LM, Kwong LK, Lee EB, Chen-Plotkin A, Swanson E, Unger T, Malunda J, Xu Y, Winton MJ, Trojanowski JQ *et al* (2011) Dysregulation of the ALS-associated gene TDP-43 leads to neuronal death and degeneration in mice. *J Clin Invest* 121: 726-738

Jo M, Lee S, Jeon YM, Kim S, Kwon Y, Kim HJ (2020) The role of TDP-43 propagation in neurodegenerative diseases: integrating insights from clinical and experimental studies. *Exp Mol Med* 52: 1652-1662

Johnson JO, Mandrioli J, Benatar M, Abramzon Y, Van Deerlin VM, Trojanowski JQ, Gibbs JR, Brunetti M, Gronka S, Wuu J *et al* (2010) Exome sequencing reveals VCP mutations as a cause of familial ALS. *Neuron* 68: 857-864

Jung H, Yoon BC, Holt CE (2012) Axonal mRNA localization and local protein synthesis in nervous system assembly, maintenance and repair. *Nature reviews Neuroscience* 13: 308-324

Kadkova A, Radecke J, Sorensen JB (2019) The SNAP-25 Protein Family. *Neuroscience* 420: 50-71

Kametani F, Obi T, Shishido T, Akatsu H, Murayama S, Saito Y, Yoshida M, Hasegawa M (2016) Mass spectrometric analysis of accumulated TDP-43 in amyotrophic lateral sclerosis brains. *Scientific reports* 6: 23281

Kandel ER, Koester JD, Mack SH, Siegelbaum SA (2021) *Principles of Neural Science*. MCGraw Hill, New York

Khalfallah Y, Kuta R, Grasmuck C, Prat A, Durham HD, Vande Velde C (2018) TDP-43 regulation of stress granule dynamics in neurodegenerative disease-relevant cell types. *Scientific reports* 8: 7551

Kim E, Jung H (2020) Local mRNA translation in long-term maintenance of axon health and function. *Curr Opin Neurobiol* 63: 15-22

Kim KY, Lee HW, Shim YM, Mook-Jung I, Jeon GS, Sung JJ (2015) A phosphomimetic mutant TDP-43 (S409/410E) induces Drosha instability and cytotoxicity in Neuro 2A cells. *Biochem Biophys Res Commun* 464: 236-243

Kim SJ, Park YJ, Hwang IY, Youdim MB, Park KS, Oh YJ (2012) Nuclear translocation of DJ-1 during oxidative stress-induced neuronal cell death. *Free Radic Biol Med* 53: 936-950

Kobayakawa Y, Masaki K, Yamasaki R, Shiraishi W, Hayashida S, Hayashi S, Okamoto K, Matsushita T, Kira JI (2018) Downregulation of Neuronal and Dendritic Connexin36-Made Electrical Synapses Without Glutamatergic Axon Terminals in Spinal Anterior Horn Cells From the Early Stage of Amyotrophic Lateral Sclerosis. *Front Neurosci* 12: 894

Koyama A, Sugai A, Kato T, Ishihara T, Shiga A, Toyoshima Y, Koyama M, Konno T, Hirokawa S, Yokoseki A *et al* (2016) Increased cytoplasmic TARDBP mRNA in affected spinal motor neurons in ALS caused by abnormal autoregulation of TDP-43. *Nucleic acids research* 44: 5820-5836

Kraemer BC, Schuck T, Wheeler JM, Robinson LC, Trojanowski JQ, Lee VM, Schellenberg GD (2010) Loss of murine TDP-43 disrupts motor function and plays an essential role in embryogenesis. *Acta Neuropathol* 119: 409-419

Lagier-Tourenne C, Polymenidou M, Cleveland DW (2010) TDP-43 and FUS/TLS: emerging roles in RNA processing and neurodegeneration. *Hum Mol Genet* 19: R46-64

Lee J, Hyeon SJ, Im H, Ryu H, Kim Y, Ryu H (2016) Astrocytes and Microglia as Non-cell Autonomous Players in the Pathogenesis of ALS. *Exp Neurobiol* 25: 233-240

Lee SJ, Oses-Prieto JA, Kawaguchi R, Sahoo PK, Kar AN, Rozenbaum M, Oliver D, Chand S, Ji H, Shtutman M *et al* (2018) hnRNPs Interacting with mRNA Localization Motifs Define Axonal RNA Regulons. *Mol Cell Proteomics* 17: 2091-2106

Lehmkuhl EM, Loganathan S, Alsop E, Blythe AD, Kovalik T, Mortimore NP, Barrameda D, Kueth C, Eck RJ, Siddegowda BB *et al* (2021) TDP-43 proteinopathy

alters the ribosome association of multiple mRNAs including the glypican Dally-like protein (Dlp)/GPC6. *Acta Neuropathol Commun* 9: 52

Lei Y, Zhang ZF, Lei RX, Wang S, Zhuang Y, Liu AC, Wu Y, Chen J, Tang JC, Pan MX *et al* (2018) DJ-1 Suppresses Cytoplasmic TDP-43 Aggregation in Oxidative Stress-Induced Cell Injury. *J Alzheimers Dis* 66: 1001-1014

Leung KM, Lu B, Wong HH, Lin JQ, Turner-Bridger B, Holt CE (2018) Cue-Polarized Transport of beta-actin mRNA Depends on 3'UTR and Microtubules in Live Growth Cones. *Front Cell Neurosci* 12: 300

Lev N, Barhum Y, Lotan I, Steiner I, Offen D (2015) DJ-1 knockout augments disease severity and shortens survival in a mouse model of ALS. *PloS one* 10: e0117190

Li HY, Yeh PA, Chiu HC, Tang CY, Tu BP (2011) Hyperphosphorylation as a defense mechanism to reduce TDP-43 aggregation. *PloS one* 6: e23075

Li Q, Yokoshi M, Okada H, Kawahara Y (2015) The cleavage pattern of TDP-43 determines its rate of clearance and cytotoxicity. *Nat Commun* 6: 6183

Liachko NF, McMillan PJ, Guthrie CR, Bird TD, Leverenz JB, Kraemer BC (2013) CDC7 inhibition blocks pathological TDP-43 phosphorylation and neurodegeneration. *Ann Neurol* 74: 39-52

Liachko NF, Saxton AD, McMillan PJ, Strovas TJ, Currey HN, Taylor LM, Wheeler JM, Oblak AL, Ghetti B, Montine TJ *et al* (2016) The phosphatase calcineurin regulates pathological TDP-43 phosphorylation. *Acta Neuropathol* 132: 545-561

Liao B, Zhao W, Beers DR, Henkel JS, Appel SH (2012) Transformation from a neuroprotective to a neurotoxic microglial phenotype in a mouse model of ALS. *Exp Neurol* 237: 147-152

Liao YC, Fernandopulle MS, Wang G, Choi H, Hao L, Drerup CM, Patel R, Qamar S, Nixon-Abell J, Shen Y *et al* (2019) RNA Granules Hitchhike on Lysosomes for Long-Distance Transport, Using Annexin A11 as a Molecular Tether. *Cell* 179: 147-164 e120

Limone F, Mordes D, Couto A, Pietiläinen O, Joseph BJ, Burberry A, Ghosh SD, Meyer D, Goldman M, Bortolin L *et al* (2021) Single-nucleus sequencing reveals enriched expression of genetic risk factors sensitises Motor Neurons to degeneration in ALS. *bioRxiv*: 1-9

Lin CL, Bristol LA, Jin L, Dykes-Hoberg M, Crawford T, Clawson L, Rothstein JD (1998) Aberrant RNA processing in a neurodegenerative disease: the cause for absent EAAT2, a glutamate transporter, in amyotrophic lateral sclerosis. *Neuron* 20: 589-602

Ling JP, Pletnikova O, Troncoso JC, Wong PC (2015) TDP-43 repression of nonconserved cryptic exons is compromised in ALS-FTD. *Science* 349: 650-655

Ling SC, Polymenidou M, Cleveland DW (2013) Converging mechanisms in ALS and FTD: disrupted RNA and protein homeostasis. *Neuron* 79: 416-438

Liu EY, Russ J, Cali CP, Phan JM, Amlie-Wolf A, Lee EB (2019) Loss of Nuclear TDP-43 Is Associated with Decondensation of LINE Retrotransposons. *Cell reports* 27: 1409-1421 e1406

Liu J, Wang F (2017) Role of Neuroinflammation in Amyotrophic Lateral Sclerosis: Cellular Mechanisms and Therapeutic Implications. *Front Immunol* 8: 1005

Liu-Yesucevitz L, Bilgutay A, Zhang YJ, Vanderweyde T, Citro A, Mehta T, Zaarur N, McKee A, Bowser R, Sherman M *et al* (2010) Tar DNA binding protein-43 (TDP-43) associates with stress granules: analysis of cultured cells and pathological brain tissue. *PloS one* 5: e13250

Lopez-Erauskin J, Tadokoro T, Baughn MW, Myers B, McAlonis-Downes M, Chillon-Marinas C, Asiaban JN, Artates J, Bui AT, Vetto AP *et al* (2018) ALS/FTD-Linked Mutation in FUS Suppresses Intra-axonal Protein Synthesis and Drives Disease Without Nuclear Loss-of-Function of FUS. *Neuron* 100: 816-830 e817

Lu L, Zheng L, Viera L, Suswam E, Li Y, Li X, Estevez AG, King PH (2007) Mutant Cu/Zn-superoxide dismutase associated with amyotrophic lateral sclerosis destabilizes vascular endothelial growth factor mRNA and downregulates its expression. *The Journal of neuroscience : the official journal of the Society for Neuroscience* 27: 7929-7938

Mann JR, Gleixner AM, Mauna JC, Gomes E, DeChellis-Marks MR, Needham PG, Copley KE, Hurtle B, Portz B, Pyles NJ *et al* (2019) RNA Binding Antagonizes Neurotoxic Phase Transitions of TDP-43. *Neuron* 102: 321-338 e328

Maraschi A, Gumina V, Dragotto J, Colombrita C, Mompean M, Buratti E, Silani V, Feligioni M, Ratti A (2021) SUMOylation Regulates TDP-43 Splicing Activity and Nucleocytoplasmic Distribution. *Mol Neurobiol* 58: 5682-5702

Marchetto MC, Muotri AR, Mu Y, Smith AM, Cezar GG, Gage FH (2008) Non-cell-autonomous effect of human SOD1 G37R astrocytes on motor neurons derived from human embryonic stem cells. *Cell Stem Cell* 3: 649-657

Martin KC, Ephrussi A (2009) mRNA localization: gene expression in the spatial dimension. *Cell* 136: 719-730

Martinez BA (2012) Lactate-starved neurons in ALS. *Dis Model Mech* 5: 711-712

Martinez JC, Randolph LK, Iascone DM, Pernice HF, Polleux F, Hengst U (2019) Pum2 Shapes the Transcriptome in Developing Axons through Retention of Target mRNAs in the Cell Body. *Neuron* 104: 931-946 e935

McDonald KK, Aulas A, Destroismaisons L, Pickles S, Beleac E, Camu W, Rouleau GA, Vande Velde C (2011) TAR DNA-binding protein 43 (TDP-43) regulates stress granule dynamics via differential regulation of G3BP and TIA-1. *Hum Mol Genet* 20: 1400-1410

Merianda TT, Lin AC, Lam JS, Vuppalanchi D, Willis DE, Karin N, Holt CE, Twiss JL (2009) A functional equivalent of endoplasmic reticulum and Golgi in axons for secretion of locally synthesized proteins. *Mol Cell Neurosci* 40: 128-142

Meyer H, Bug M, Bremer S (2012) Emerging functions of the VCP/p97 AAA-ATPase in the ubiquitin system. *Nat Cell Biol* 14: 117-123

Miller RG, Mitchell JD, Lyon M, Moore DH (2003) Riluzole for amyotrophic lateral sclerosis (ALS)/motor neuron disease (MND). *Amyotroph Lateral Scler Other Motor Neuron Disord* 4: 191-206

Moloney EB, de Winter F, Verhaagen J (2014) ALS as a distal axonopathy: molecular mechanisms affecting neuromuscular junction stability in the presymptomatic stages of the disease. *Front Neurosci* 8: 252

Morera AA, Ahmed NS, Schwartz JC (2019) TDP-43 regulates transcription at protein-coding genes and Alu retrotransposons. *Biochim Biophys Acta Gene Regul Mech* 1862: 194434

Munch C, Rosenbohm A, Sperfeld AD, Uttner I, Reske S, Krause BJ, Sedlmeier R, Meyer T, Hanemann CO, Stumm G *et al* (2005) Heterozygous R1101K mutation of the DCTN1 gene in a family with ALS and FTD. *Ann Neurol* 58: 777-780

Nagano S, Araki T (2021) Axonal Transport and Local Translation of mRNA in Amyotrophic Lateral Sclerosis. In: *Amyotrophic Lateral Sclerosis*, Araki T. (ed.)Brisbane (AU)

Nagano S, Jinno J, Abdelhamid RF, Jin Y, Shibata M, Watanabe S, Hirokawa S, Nishizawa M, Sakimura K, Onodera O *et al* (2020) TDP-43 transports ribosomal protein mRNA to regulate axonal local translation in neuronal axons. *Acta Neuropathol* 140: 695-713

Negro S, Stazi M, Marchioretto M, Tebaldi T, Rodella U, Duregotti E, Gerke V, Quattrone A, Montecucco C, Rigoni M *et al* (2018) Hydrogen peroxide is a neuronal alarmin that triggers specific RNAs, local translation of Annexin A2, and cytoskeletal remodeling in Schwann cells. *RNA* 24: 915-925

Neumann M, Sampathu DM, Kwong LK, Truax AC, Micsenyi MC, Chou TT, Bruce J, Schuck T, Grossman M, Clark CM *et al* (2006) Ubiquitinated TDP-43 in frontotemporal lobar degeneration and amyotrophic lateral sclerosis. *Science* 314: 130-133

Nicolas A, Kenna KP, Renton AE, Ticozzi N, Faghri F, Chia R, Dominov JA, Kenna BJ, Nalls MA, Keagle P *et al* (2018) Genome-wide Analyses Identify KIF5A as a Novel ALS Gene. *Neuron* 97: 1268-1283 e1266

Niedermeyer S, Murn M, Choi PJ (2019) Respiratory Failure in Amyotrophic Lateral Sclerosis. *Chest* 155: 401-408

Nishitoh H, Kadowaki H, Nagai A, Maruyama T, Yokota T, Fukutomi H, Noguchi T, Matsuzawa A, Takeda K, Ichijo H (2008) ALS-linked mutant SOD1 induces ER stress- and ASK1-dependent motor neuron death by targeting Derlin-1. *Genes Dev* 22: 1451-1464

Nonaka T, Kametani F, Arai T, Akiyama H, Hasegawa M (2009) Truncation and pathogenic mutations facilitate the formation of intracellular aggregates of TDP-43. *Hum Mol Genet* 18: 3353-3364

Ostroff LE, Santini E, Sears R, Deane Z, Kanadia RN, LeDoux JE, Lhakhang T, Tsirigos A, Heguy A, Klann E (2019) Axon TRAP reveals learning-associated alterations in cortical axonal mRNAs in the lateral amgydala. *Elife* 8

Palamiuc L, Schlagowski A, Ngo ST, Vernay A, Dirrig-Grosch S, Henriques A, Boutillier AL, Zoll J, Echaniz-Laguna A, Loeffler JP *et al* (2015) A metabolic switch toward lipid

use in glycolytic muscle is an early pathologic event in a mouse model of amyotrophic lateral sclerosis. *EMBO Mol Med* 7: 526-546

Pelizzoni I, Macco R, Morini MF, Zacchetti D, Grohovaz F, Codazzi F (2011) Iron handling in hippocampal neurons: activity-dependent iron entry and mitochondria-mediated neurotoxicity. *Aging Cell* 10: 172-183

Perry RB, Doron-Mandel E, Iavnilovitch E, Rishal I, Dagan SY, Tsoory M, Coppola G, McDonald MK, Gomes C, Geschwind DH *et al* (2012) Subcellular knockout of importin beta1 perturbs axonal retrograde signaling. *Neuron* 75: 294-305

Philips T, Bento-Abreu A, Nonneman A, Haeck W, Staats K, Geelen V, Hersmus N, Kusters B, Van Den Bosch L, Van Damme P *et al* (2013) Oligodendrocyte dysfunction in the pathogenesis of amyotrophic lateral sclerosis. *Brain* 136: 471-482

Picher-Martel V, Dutta K, Phaneuf D, Sobue G, Julien JP (2015) Ubiquilin-2 drives NF-kappaB activity and cytosolic TDP-43 aggregation in neuronal cells. *Mol Brain* 8: 71

Polymenidou M, Lagier-Tourenne C, Hutt KR, Huelga SC, Moran J, Liang TY, Ling SC, Sun E, Wancewicz E, Mazur C *et al* (2011) Long pre-mRNA depletion and RNA missplicing contribute to neuronal vulnerability from loss of TDP-43. *Nature neuroscience* 14: 459-468

Prasad A, Bharathi V, Sivalingam V, Girdhar A, Patel BK (2019) Molecular Mechanisms of TDP-43 Misfolding and Pathology in Amyotrophic Lateral Sclerosis. *Front Mol Neurosci* 12: 25

Prpar Mihevc S, Baralle M, Buratti E, Rogelj B (2016) TDP-43 aggregation mirrors TDP-43 knockdown, affecting the expression levels of a common set of proteins. *Scientific reports* 6: 33996

Ragagnin AMG, Shadfar S, Vidal M, Jamali MS, Atkin JD (2019) Motor Neuron Susceptibility in ALS/FTD. *Front Neurosci* 13: 532

Rash JE, Yasumura T, Davidson KG, Furman CS, Dudek FE, Nagy JI (2001) Identification of cells expressing Cx43, Cx30, Cx26, Cx32 and Cx36 in gap junctions of rat brain and spinal cord. *Cell Commun Adhes* 8: 315-320

Ratti A, Buratti E (2016) Physiological functions and pathobiology of TDP-43 and FUS/TLS proteins. *Journal of neurochemistry* 138 Suppl 1: 95-111

Ratti A, Gumina V, Lenzi P, Bossolasco P, Fulceri F, Volpe C, Bardelli D, Pregnolato F, Maraschi A, Fornai F *et al* (2020) Chronic stress induces formation of stress granules

and pathological TDP-43 aggregates in human ALS fibroblasts and iPSC-motoneurons. *Neurobiol Dis* 145: 105051

Re DB, Le Verche V, Yu C, Amoroso MW, Politi KA, Phani S, Ikiz B, Hoffmann L, Koolen M, Nagata T *et al* (2014) Necroptosis drives motor neuron death in models of both sporadic and familial ALS. *Neuron* 81: 1001-1008

Reber S, Stettler J, Filosa G, Colombo M, Jutzi D, Lenzken SC, Schweingruber C, Bruggmann R, Bachi A, Barabino SM *et al* (2016) Minor intron splicing is regulated by FUS and affected by ALS-associated FUS mutants. *The EMBO journal* 35: 1504-1521

Ren Y, Li S, Chen S, Sun X, Yang F, Wang H, Li M, Cui F, Huang X (2021) TDP-43 and Phosphorylated TDP-43 Levels in Paired Plasma and CSF Samples in Amyotrophic Lateral Sclerosis. *Front Neurol* 12: 663637

Renaud L, Picher-Martel V, Codron P, Julien JP (2019) Key role of UBQLN2 in pathogenesis of amyotrophic lateral sclerosis and frontotemporal dementia. *Acta Neuropathol Commun* 7: 103

Renton AE, Majounie E, Waite A, Simon-Sanchez J, Rollinson S, Gibbs JR, Schymick JC, Laaksovirta H, van Swieten JC, Myllykangas L *et al* (2011) A hexanucleotide repeat expansion in C9ORF72 is the cause of chromosome 9p21-linked ALS-FTD. *Neuron* 72: 257-268

Richter JD, Coller J (2015) Pausing on Polyribosomes: Make Way for Elongation in Translational Control. *Cell* 163: 292-300

Rosen DR, Siddique T, Patterson D, Figlewicz DA, Sapp P, Hentati A, Donaldson D, Goto J, O'Regan JP, Deng HX *et al* (1993) Mutations in Cu/Zn superoxide dismutase gene are associated with familial amyotrophic lateral sclerosis. *Nature* 362: 59-62

Rotem N, Magen I, Ionescu A, Gershoni-Emek N, Altman T, Costa CJ, Gradus T, Pasmanik-Chor M, Willis DE, Ben-Dov IZ *et al* (2017) ALS Along the Axons - Expression of Coding and Noncoding RNA Differs in Axons of ALS models. *Scientific reports* 7: 44500

Roy S (2020) Finding order in slow axonal transport. *Curr Opin Neurobiol* 63: 87-94

Russo A, Scardigli R, La Regina F, Murray ME, Romano N, Dickson DW, Wolozin B, Cattaneo A, Ceci M (2017) Increased cytoplasmic TDP-43 reduces global protein synthesis by interacting with RACK1 on polyribosomes. *Hum Mol Genet* 26: 1407-1418

Saberi S, Stauffer JE, Schulte DJ, Ravits J (2015) Neuropathology of Amyotrophic Lateral Sclerosis and Its Variants. *Neurol Clin* 33: 855-876

Sanz E, Yang L, Su T, Morris DR, McKnight GS, Amieux PS (2009) Cell-type-specific isolation of ribosome-associated mRNA from complex tissues. *Proc Natl Acad Sci U S A* 106: 13939-13944

Sauvageot CM, Stiles CD (2002) Molecular mechanisms controlling cortical gliogenesis. *Curr Opin Neurobiol* 12: 244-249

Scaber J, Talbot K (2016) What is the role of TDP-43 in C9orf72-related amyotrophic lateral sclerosis and frontemporal dementia? *Brain* 139: 3057-3059

Sephton CF, Cenik C, Kucukural A, Dammer EB, Cenik B, Han Y, Dewey CM, Roth FP, Herz J, Peng J *et al* (2011) Identification of neuronal RNA targets of TDP-43-containing ribonucleoprotein complexes. *The Journal of biological chemistry* 286: 1204-1215

Seyfried NT, Gozal YM, Dammer EB, Xia Q, Duong DM, Cheng D, Lah JJ, Levey AI, Peng J (2010) Multiplex SILAC analysis of a cellular TDP-43 proteinopathy model reveals protein inclusions associated with SUMOylation and diverse polyubiquitin chains. *Mol Cell Proteomics* 9: 705-718

Shibata N, Asayama K, Hirano A, Kobayashi M (1996) Immunohistochemical study on superoxide dismutases in spinal cords from autopsied patients with amyotrophic lateral sclerosis. *Dev Neurosci* 18: 492-498

Shigeoka T, Jung H, Jung J, Turner-Bridger B, Ohk J, Lin J, Amieux P, Holt C (2016) Dynamic Axonal Translation in Developing and Mature Visual Circuits. *Cell* 166: 181-192

Shigeoka T, Koppers M, Wong HH, Lin JQ, Cagnetta R, Dwivedy A, de Freitas Nascimento J, van Tartwijk FW, Strohl F, Cioni JM *et al* (2019) On-Site Ribosome Remodeling by Locally Synthesized Ribosomal Proteins in Axons. *Cell reports* 29: 3605-3619 e3610

Sidibe H, Khalfallah Y, Xiao S, Gomez NB, Fakim H, Tank EMH, Tomasso GD, Bareke E, Aulas A, McKeever PM *et al* (2021) TDP-43 stabilizes G3BP1 mRNA: relevance to amyotrophic lateral sclerosis/frontotemporal dementia. *Brain*

Smith BN, Ticozzi N, Fallini C, Gkazi AS, Topp S, Kenna KP, Scotter EL, Kost J, Keagle P, Miller JW *et al* (2014) Exome-wide rare variant analysis identifies TUBA4A mutations associated with familial ALS. *Neuron* 84: 324-331

Smith EF, Shaw PJ, De Vos KJ (2019) The role of mitochondria in amyotrophic lateral sclerosis. *Neurosci Lett* 710: 132933

Solomon DA, Stepto A, Au WH, Adachi Y, Diaper DC, Hall R, Rekhi A, Boudi A, Tziortzouda P, Lee YB *et al* (2018) A feedback loop between dipeptide-repeat protein, TDP-43 and karyopherin-alpha mediates C9orf72-related neurodegeneration. *Brain* 141: 2908-2924

Sommer B, Kohler M, Sprengel R, Seeburg PH (1991) RNA editing in brain controls a determinant of ion flow in glutamate-gated channels. *Cell* 67: 11-19

Sreedharan J, Blair IP, Tripathi VB, Hu X, Vance C, Rogelj B, Ackerley S, Durnall JC, Williams KL, Buratti E *et al* (2008) TDP-43 mutations in familial and sporadic amyotrophic lateral sclerosis. *Science* 319: 1668-1672

Stallings NR, Puttaparthi K, Luther CM, Burns DK, Elliott JL (2010) Progressive motor weakness in transgenic mice expressing human TDP-43. *Neurobiol Dis* 40: 404-414

Strong MJ, Volkening K, Hammond R, Yang W, Strong W, Leystra-Lantz C, Shoesmith C (2007) TDP43 is a human low molecular weight neurofilament (hNFL) mRNA-binding protein. *Mol Cell Neurosci* 35: 320-327

Suarez-Calvet M, Dols-Icardo O, Llado A, Sanchez-Valle R, Hernandez I, Amer G, Anton-Aguirre S, Alcolea D, Fortea J, Ferrer I *et al* (2014) Plasma phosphorylated TDP-43 levels are elevated in patients with frontotemporal dementia carrying a C9orf72 repeat expansion or a GRN mutation. *J Neurol Neurosurg Psychiatry* 85: 684-691

Suk TR, Rousseaux MWC (2020) The role of TDP-43 mislocalization in amyotrophic lateral sclerosis. *Mol Neurodegener* 15: 45

Tang Y, Scott D, Das U, Gitler D, Ganguly A, Roy S (2013) Fast vesicle transport is required for the slow axonal transport of synapsin. *The Journal of neuroscience : the official journal of the Society for Neuroscience* 33: 15362-15375

Taylor LM, McMillan PJ, Liachko NF, Strovas TJ, Ghetti B, Bird TD, Keene CD, Kraemer BC (2018) Pathological phosphorylation of tau and TDP-43 by TTBK1 and TTBK2 drives neurodegeneration. *Mol Neurodegener* 13: 7

Tefera TW, Tan KN, McDonald TS, Borges K (2017) Alternative Fuels in Epilepsy and Amyotrophic Lateral Sclerosis. *Neurochem Res* 42: 1610-1620

Tefera TW, Wong Y, Barkl-Luke ME, Ngo ST, Thomas NK, McDonald TS, Borges K (2016) Triheptanoin Protects Motor Neurons and Delays the Onset of Motor Symptoms in a Mouse Model of Amyotrophic Lateral Sclerosis. *PloS one* 11: e0161816

Tollervey JR, Curk T, Rogelj B, Briese M, Cereda M, Kayikci M, Konig J, Hortobagyi T, Nishimura AL, Zupunski V *et al* (2011) Characterizing the RNA targets and position-dependent splicing regulation by TDP-43. *Nature neuroscience* 14: 452-458

Tsuiji H, Inoue I, Takeuchi M, Furuya A, Yamakage Y, Watanabe S, Koike M, Hattori M, Yamanaka K (2017) TDP-43 accelerates age-dependent degeneration of interneurons. *Scientific reports* 7: 14972

Turner-Bridger B, Caterino C, Cioni JM (2020) Molecular mechanisms behind mRNA localization in axons. *Open Biol* 10: 200177

Tziortzouda P, Van Den Bosch L, Hirth F (2021) Triad of TDP43 control in neurodegeneration: autoregulation, localization and aggregation. *Nature reviews Neuroscience* 22: 197-208

van Blitterswijk M, Gendron TF, Baker MC, DeJesus-Hernandez M, Finch NA, Brown PH, Daughrity LM, Murray ME, Heckman MG, Jiang J *et al* (2015) Novel clinical associations with specific C9ORF72 transcripts in patients with repeat expansions in C9ORF72. *Acta Neuropathol* 130: 863-876

Walker AK, Spiller KJ, Ge G, Zheng A, Xu Y, Zhou M, Tripathy K, Kwong LK, Trojanowski JQ, Lee VM (2015) Functional recovery in new mouse models of ALS/FTLD after clearance of pathological cytoplasmic TDP-43. *Acta Neuropathol* 130: 643-660

Wang L, Gutmann DH, Roos RP (2011) Astrocyte loss of mutant SOD1 delays ALS disease onset and progression in G85R transgenic mice. *Hum Mol Genet* 20: 286-293

Wang W, Wang L, Lu J, Siedlak SL, Fujioka H, Liang J, Jiang S, Ma X, Jiang Z, da Rocha EL *et al* (2016) The inhibition of TDP-43 mitochondrial localization blocks its neuronal toxicity. *Nat Med* 22: 869-878

Wang Y, Song JH, Denisova JV, Park WM, Fontes JD, Belousov AB (2012) Neuronal gap junction coupling is regulated by glutamate and plays critical role in cell death during neuronal injury. *The Journal of neuroscience : the official journal of the Society for Neuroscience* 32: 713-725

Watanabe S, Oiwa K, Murata Y, Komine O, Sobue A, Endo F, Takahashi E, Yamanaka K (2020) ALS-linked TDP-43(M337V) knock-in mice exhibit splicing deregulation without neurodegeneration. *Mol Brain* 13: 8

Webster CP, Smith EF, Bauer CS, Moller A, Hautbergue GM, Ferraiuolo L, Myszczynska MA, Higginbottom A, Walsh MJ, Whitworth AJ *et al* (2016) The C9orf72 protein interacts with Rab1a and the ULK1 complex to regulate initiation of autophagy. *The EMBO journal* 35: 1656-1676

Wegorzewska I, Bell S, Cairns NJ, Miller TM, Baloh RH (2009) TDP-43 mutant transgenic mice develop features of ALS and frontotemporal lobar degeneration. *Proc Natl Acad Sci U S A* 106: 18809-18814

White MA, Kim E, Duffy A, Adalbert R, Phillips BU, Peters OM, Stephenson J, Yang S, Massenzio F, Lin Z *et al* (2018) TDP-43 gains function due to perturbed autoregulation in a Tardbp knock-in mouse model of ALS-FTD. *Nature neuroscience* 21: 552-563

Winton MJ, Igaz LM, Wong MM, Kwong LK, Trojanowski JQ, Lee VM (2008) Disturbance of nuclear and cytoplasmic TAR DNA-binding protein (TDP-43) induces disease-like redistribution, sequestration, and aggregate formation. *The Journal of biological chemistry* 283: 13302-13309

Wolozin B, Ivanov P (2019) Stress granules and neurodegeneration. *Nature reviews Neuroscience* 20: 649-666

Wu CC, Jin LW, Wang IF, Wei WY, Ho PC, Liu YC, Tsai KJ (2020) HDAC1 dysregulation induces aberrant cell cycle and DNA damage in progress of TDP-43 proteinopathies. *EMBO Mol Med* 12: e10622

Wu CH, Fallini C, Ticozzi N, Keagle PJ, Sapp PC, Piotrowska K, Lowe P, Koppers M, McKenna-Yasek D, Baron DM *et al* (2012) Mutations in the profilin 1 gene cause familial amyotrophic lateral sclerosis. *Nature* 488: 499-503

Wu Y, Whiteus C, Xu CS, Hayworth KJ, Weinberg RJ, Hess HF, De Camilli P (2017) Contacts between the endoplasmic reticulum and other membranes in neurons. *Proc Natl Acad Sci U S A* 114: E4859-E4867

Yamashita S, Mori A, Kimura E, Mita S, Maeda Y, Hirano T, Uchino M (2010) DJ-1 forms complexes with mutant SOD1 and ameliorates its toxicity. *Journal of neurochemistry* 113: 860-870

Yu H, Lu S, Gasior K, Singh D, Vazquez-Sanchez S, Tapia 0, Toprani D, Beccari MS, Yates JR, 3rd, Da Cruz S *et al* (2021) HSP70 chaperones RNA-free TDP-43 into anisotropic intranuclear liquid spherical shells. *Science* 371

Zhang K, Donnelly CJ, Haeusler AR, Grima JC, Machamer JB, Steinwald P, Daley EL, Miller SJ, Cunningham KM, Vidensky *S et al* (2015) The C9orf72 repeat expansion disrupts nucleocytoplasmic transport. *Nature* 525: 56-61

Zhang K, Liu Q, Liu K, Shen **D,** Tai H, Shu S, Ding Q, Fu **H,** Liu S, Wang Z *et al* (2018) ANXAll mutations prevail in Chinese ALS patients with and without cognitive dementia. *Neural Genet* 4: e237

Zhang L, Wang J, Wang J, Yang B, He Q, Weng Q (2020) Role of DJ-I in Immune and Inflammatory Diseases. *Front Immunol* 11: 994

Zhang YJ, Xu YF, Cook C, Gendron TF, Roettges P, Link CD, Lin WL, Tong J, Castanedes-Casey M, Ash P *et al* (2009) Aberrant cleavage of TDP-43 enhances aggregation and cellular toxicity. *Proc Natl Acad Sci US A* 106: 7607-7612

Zheng ZV, Wong KCG (2019) Microglial activation and polarization after subarachnoid hemorrhage. *Neuroimmunology and Neuroinjlammation*

Zu T, Liu Y, Banez-Coronel M, Reid T, Pletnikova 0, Lewis J, Miller TM, Harms MB, Falchook AE, Subramony SH *etal* (2013) RAN proteins and RNA foci from antisense transcripts in C90RF72 ALS and frontotemporal dementia. *Proc Natl Acad Sci U S A* 110: E4968-4977